



Aalborg Universitet

AALBORG UNIVERSITY
DENMARK

System Identification and Robust Control

A Synergistic Approach

Tøffner-Clausen, S.

Publication date:
1995

Document Version
Acceperet manuscript, peer-review version

[Link to publication from Aalborg University](#)

Citation for published version (APA):
Tøffner-Clausen, S. (1995). *System Identification and Robust Control: A Synergistic Approach*. Aalborg Universitetsforlag.

General rights

Copyright and moral rights for the publications made accessible in the public portal are retained by the authors and/or other copyright owners and it is a condition of accessing publications that users recognise and abide by the legal requirements associated with these rights.

- Users may download and print one copy of any publication from the public portal for the purpose of private study or research.
- You may not further distribute the material or use it for any profit-making activity or commercial gain
- You may freely distribute the URL identifying the publication in the public portal -

Take down policy

If you believe that this document breaches copyright please contact us at vbn@aub.aau.dk providing details, and we will remove access to the work immediately and investigate your claim.

System Identification
and
Robust Control
A Synergistic Approach

A thesis submitted in partial fulfillment of the requirements
for the degree of Doctor of Philosophy in Electronics and
Electrical Engineering

by

Steen Tøffner-Clausen

Department of Control Engineering
Aalborg University
Fredrik Bajers Vej 7, DK-9220 Aalborg Ø, Denmark.

ISSN 0908-1208
AUC-CONTROL-D95-4102
Oktober 1995

Copyright © by Steen Tøffner-Clausen.

Typeset using L^AT_EX_{2 ϵ} in `report` document class using packages `lcaption`, `epsf`, `ifthen`, `theorem`, `fancyheadings`, `varioref`, `amstex`, `bibunits`, `longtable`, `rotating`, `wrapfigure` and `minitoc`.

Main typeface is *Computer Modern* supplemented with fonts from American Mathematical Society.

Pictures were generated using T_EX_{CaD} and MATLABTM from The MathWorks Inc. Numerical analysis and designs were performed in MATLAB with aid of various toolboxes, in particular the *μ -Analysis and Synthesis ToolBox* [BDG⁺93].

Trademark notice

MATLABTM is a trademark of The MathWorks Inc.

T_EX is a trademark of the American Mathematical Society.

To Else and Nikolaj

Preface

This thesis is presented to the Faculty of Technology and Science at Aalborg University in partial fulfillment of the requirements for the Degree of Doctor of Philosophy. The work has been carried out at the Department of Control Engineering, Institute of Electronic Systems, Aalborg University during a three year period from October 1992 until September 1995.

The main effort in this work has been on bridging *system identification* and *robust control*. In the early 1990'ies a growing awareness developed within the automatic control community that the necessary information on model quality needed in robust control could not be supplied by existing system identification methodologies. This spurred a renewed interest in methods for estimating models and model uncertainty from plant measurements. However, no concurrent treatment of the results of this research has been presented in connection with their application in robust control. Such a treatment is the main theme of this thesis.

In order to present our results in a known framework an introduction to “classical” results within both system identification and robust control will be given. The emphasis will be on both theory and applications. However, mathematical subtleties will be kept to a minimum whenever possible with references to more complete mathematical descriptions.

Related Presentations and Publications

Parts of the work documented in this thesis has been presented at the following conferences or workshops:

SYSID'94, the 10th IFAC Symposium on System Identification, 1994 in Copenhagen.

CCA'94, the 3rd IEEE Conference on Control Applications, 1994 in Glasgow.

EURACO YRW'94, the EURACO¹ Young Researchers Week on Robust and Adaptive Control, 1994 in Dublin.

YAC'95, the IFAC Youth Automation Conference, 1995 in Beijing.

ECC'95, the 3rd European Control Conference, 1995 in Rome.

EURACO Workshop 1995, the EURACO Workshop on Recent Results in Robust and Adaptive Control, 1995 in Florence.

Generally the thesis comprises the majority of information in the following publications:

- [ATCP94] P. Andersen, S. Tøffner-Clausen, and T.S. Pedersen. Estimation of frequency domain model uncertainties with application to robust controller design. In *Proc. SYSID'94*, volume 3, pages 603–608, Copenhagen, Denmark, July 1994.
- [BATC94] M. Blanke, P. Andersen, and S. Tøffner-Clausen. Modelling and uncertainty. Lecture Note for EURACO Young Researchers Week, Dublin. R94-4064, Dept. of Control Engineering, Aalborg University, Frederik Bajers Vej 7, DK-9220 Aalborg Ø, Denmark, Aug. 1994.
- [TC95] S. Tøffner-Clausen. Identification for control: Quantification of uncertainty. In *Proc. Youth Automation Conference*, pages 155–159, Beijing, China, 1995. IFAC.
- [TCA93] S. Tøffner-Clausen and P. Andersen. Quantifying frequency domain model uncertainty in estimated transfer functions using a stochastic embedding approach. Research Report W1D-06-001, Reliability and Robustness in Industrial Process Control, Feb. 1993.
- [TCA94] S. Tøffner-Clausen and P. Andersen. Identification for control: Estimation of frequency domain model uncertainty. Research Report R94-4054, Aalborg University, Dept. of Control Eng., Frederik Bajers Vej 7, DK-9220 Aalborg, Denmark, Aug. 1994.
- [TCA95] S. Tøffner-Clausen and P. Andersen. μ -synthesis – a non-conservative methodology for design of controllers with robustness towards dynamic and parametric uncertainty. In *Proc. EURACO Workshop on Recent Results in Robust and Adaptive Control*, pages 269–303, Florence, Italy, September 1995.
- [TCABG95] S. Tøffner-Clausen, P. Andersen, S.G. Breslin, and M.J. Grimble. The application of μ -analysis and synthesis to the control of an ASTOVL aircraft. In *Proc. EURACO Workshop on Recent Results in Robust and Adaptive Control*, pages 304–322, Florence, Italy, September 1995.

¹European Network on Robust and Adaptive Control.

- [TCASN94a] S. Tøffner-Clausen, P. Andersen, J. Stoustrup, and H.H. Niemann. Estimated frequency domain model uncertainties used in robust controller design — a μ -approach. In *Proc. 3rd IEEE Conf. on Control Applications*, volume 3, pages 1585–1590, Glasgow, Scotland, Aug. 1994.
- [TCASN94b] S. Tøffner-Clausen, P. Andersen, J. Stoustrup, and H.H. Niemann. Estimated frequency domain model uncertainties used in robust controller design — a μ -approach. Poster Session, EURACO Young Researchers Week, Dublin, Aug. 1994.
- [TCASN95] S. Tøffner-Clausen, P. Andersen, J. Stoustrup, and H.H. Niemann. A new approach to μ -synthesis for mixed perturbation sets. In *Proc. 3rd European Control Conf.*, pages 147–152, Rome, Italy, 1995.
- [TCB95] S. Tøffner-Clausen and S.G. Breslin. Classical versus modern control design methods for safety critical control engineering practice. Technical Report ACT/CS08/95, Industrial Control Center, University of Strathclyde, 50 George Street, Glasgow G1 1QE, 1995.

Acknowledgements

Many people have contributed to the enjoyment and productivity of my research at the Department of Control Engineering. Firstly, I would like to thank my supervisor, Palle Andersen, for his enthusiastic support and guidance in this research. He is a very dedicated teacher and we have spend hundreds of hours discussing control design methodologies. These discussions have been invaluable for this work. Palle is a co-author on most of the publications which have stemmed from my research.

Furthermore I would like to thank all other colleagues at the Department of Control Engineering who has contributed or helped in various ways, in particular Torben Knudsen and Morten Knudsen for discussions in connection with system identification, Carsten H. Kristensen for providing many hints and macros for $\text{\LaTeX}2_{\epsilon}$ and last but not least our wonderful secretary Karen Drescher for invaluable general assistance.

Also I would like to thank Jakob Stoustrup and Hans H. Niemann from the Technical University of Denmark for their collaboration on mixed μ synthesis. They have provided much insight in μ methods.

A sincere thank goes to Professor Michael Grimble and the staff at the Industrial Control Center, University of Strathclyde in Glasgow for inviting me to stay with them for a three months period in the autumn 1994. My visit there was a very pleasant and rewarding one. Especially I would like to thank Stephen Breslin for

being a good friend as well as a fine colleague. The flight control case study in Chapter 7 is the result of a joint effort by Stephen and myself.

Mostly, however, I am indebted to my wife Else and my son Nikolaj. Without their understanding, support and love this thesis would never have been written.

Aalborg, October 1995.

Steen Tøffner-Clausen.

Abstract

The main purpose of this work is to develop a coherent system identification based robust control design methodology by combining recent results from system identification and robust control. In order to accomplish this task new theoretical results will be given in both fields.

Firstly, however, an introduction to modern robust control design analysis and synthesis will be given. It will be shown how the classical frequency domain techniques can be extended to multivariable systems using the singular value decomposition. An introduction to norms and spaces frequently used in modern control theory will be given. However, the main emphasis in this thesis will *not* be on mathematics. Proofs are given only when there are interesting in their own right and we will try to avoid messy mathematical derivations. Rather we will concentrate on interpretations and practical design issues.

A review of the classical \mathcal{H}_∞ theory will be given. Most of the stability results from modern control theory can be traced back to the multivariable generalization of the famous Nyquist stability criterion. We will show how the generalized Nyquist criterion is used to establish some of the classical singular value robust stability results. Furthermore it will be shown how a performance specification may be cast into the same framework. The main limitation in the standard \mathcal{H}_∞ theory is that it can only handle unstructured complex full block perturbations to the nominal plant. However, often much more detailed perturbation models are available, e.g. from physical modeling. Such structured perturbation models cannot be handled well in the \mathcal{H}_∞ framework.

Fortunately theory exists which *can* do this. The structured singular value μ is an extension of the singular value which explicitly takes into account the structure of the perturbations. In this thesis we will present a thorough introduction to the μ framework. A central result is that if performance is measured in terms of the ∞ -norm and model uncertainty is bounded in the same manner, then, using μ it is possible to pose one necessary and sufficient condition for both robust stability and robust performance. The uncertainty is restricted to block-structured norm-bounded perturbations which enter the nominal model in a linear fractional

manner. This is, however, a very general perturbation set which includes a large variety of uncertainty such as unstructured and structured dynamic uncertainty (complex perturbations) and parameter variations (real perturbations). The uncertainty structures permitted by μ is definitely much more flexible than those used in \mathcal{H}_∞ .

Unfortunately μ synthesis is a very difficult mathematical problem which is only well developed for purely complex perturbation sets. In order to develop our main result we will unfortunately need to synthesize μ controllers for mixed real and complex perturbation sets. A novel method, denoted *μ -K iteration*, has been developed to solve the mixed μ problem.

A general feature of all robust control design methods is the need for specifying not only a nominal model but also some kind of quantification of the quality of that model. In this work we will restrict ourselves to block-structured norm-bounded perturbations as described above. The specification of the uncertainty is, however, a non-trivial problem which to some extent has been neglected by the theoreticians of robust control. An uncertainty specification has simply been assumed given.

One way of obtaining a perturbation model is by physical modeling. Application of the fundamental laws of thermodynamics, mechanics, physics etc. will generally yield a set of coupled non-linear partial differential equations. These equations can then be linearized (in time and position) around a suitable working point and Laplace transformed for linear control design. The linearized differential equations will typically involve physical quantities like masses, inertias, etc. which are only known with a certain degree of accuracy. This will give rise to real scalar perturbations to the nominal model. Furthermore working point deviations may also be addressed with real perturbations.

However, accurate physical modeling may be a complicated and time consuming task even for relatively simple systems. An appealing alternative to physical modeling for assessment of model uncertainty is system identification where input/output measurements are used to estimate a, typically, linear model of the true system. From the covariance of the parameter estimate frequency domain uncertainty estimates may be obtained.

In classical (i.e. Ljungian) system identification, model quality has been assessed under the assumption that the only source of uncertainty is noisy measurements. Thus the structure of the model is assumed to be correct. This is, however, often an inadequate assumption in connection with control design.

Recently, system identification techniques for estimating model uncertainty have gained renewed interest in the automatic control community. In this thesis, a quick survey of these results will be given together with their Ljungian counterparts. Unlike the classical identification methods these new techniques enables

the inclusion of both structural model errors (bias) and noise (variance) in the estimated uncertainty bounds. However, in order to accomplish this, some prior knowledge of the model error must be available. In general, this prior information is non-trivial to obtain. Fortunately one of these new techniques, denoted *the stochastic embedding approach*, provides the possibility to estimate, given a parametric structure of certain covariance matrices, the required a priori information from the model residuals. Thus the a priori knowledge is reduced from a quantitative measure to a qualitative measure. We believe that this makes the stochastic embedding approach superior to the other new techniques for estimating model uncertainty. In this work, new parameterizations of the undermodeling (bias) and the noise are investigated. Currently, the stochastic embedding approach is only well developed for scalar systems. Thus some work is needed to extend it to multivariable systems. This will, however, be beyond the scope of this work.

Using the stochastic embedding approach it is possible to estimate a nominal model and frequency domain uncertainty ellipses around this model. It will then be shown how these uncertainty ellipses may be represented or, more correct, approximated with a mixed complex and real perturbation set. This is the link needed to combine the results in robust control and system identification into a step-by-step design philosophy for synthesis of robust control systems for scalar plant which is the main result presented in this thesis.

Throughout the thesis, the presented results will be illustrated by practical design examples. Some of these examples are quite simple, but a few are much more complex. The point of view taken is that the theories presented should be applicable to practical control systems design. The given examples thus represent a major part of the work behind this thesis. They consequently serve not just as illustrations but introduce many new ideas and should be interesting in their own right.

Dansk Sammenfatning

Hovedformålet med dette arbejde er at udvikle en metode til sammenhængende system identifikation baseret robust reguleringsdesign ved at kombinere nylige resultater fra system identifikation og robust regulerings-teori. I forbindelse med udviklingen af denne designmetodik er der udviklet nye teoretiske resultater indenfor begge områder.

Først vil der imidlertid gives en introduktion til moderne robust reguleringsanalyse og -design. Det vil vises, hvorledes de klassiske frekvens domæne teknikker kan udvides til multivariable systemer ved hjælp af singulær værdi opspaltningen. En introduktion til normer og rum, der ofte anvendes i moderne robust regulerings-teori, vil blive givet. Hovedvægten i denne afhandling vil imidlertid ikke blive lagt på matematikken. Beviser vil kun blive medtaget, når de i sig selv er interessante. Vi vil istedet koncentrere os om fortolkninger samt praktiske design spørgsmål.

Der vil blive givet en gennemgang af den klassiske \mathcal{H}_∞ teori. De fleste stabilitetsresultater fra moderne regulerings-teori kan føres tilbage til den multivariable generalisering af det berømte Nyquist stabilitets kriterie. Vi vil vise, hvorledes det generaliserede Nyquist kriterie kan bruges til at udlede nogle af de klassiske singulær værdi robust stabilitets resultater. Desuden vil vi vise, hvordan performance specifikationer kan blive givet indenfor de samme teoretiske rammer. Hovedbegrænsningen i standard \mathcal{H}_∞ teori er, at det kun kan anvendes i forbindelse med ustrukturerede komplekse fuld blok perturbationer på det nominelle system. Imidlertid har vi ofte adgang til lange mere detaljerede usikkerhedsmodeller, for eksempel fra fysisk modellering. Sådanne perturbations modeller kan ikke behandles naturligt indenfor \mathcal{H}_∞ .

Heldigvis eksisterer der teori, som kan gøre dette. Den strukturerede singulær værdi μ er en generalisering af den singulær værdi, som direkte tager højde for strukturen af perturbationerne. I denne afhandling vil vi give en grundig introduktion til μ . Et centralt resultat er, at hvis vi måler performance ved hjælp af ∞ -normen og beskriver model usikkerheden på samme vis kan vi ved μ give en nødvendig og tilstrækkelig betingelse for robust performance. Usikkerheden er

begrænset til blok-strukturerede norm-begrænsede perturbationer, som påvirker den nominelle model lineært. Dette er, til gengæld en meget general usikkerhedsstruktur, som inkluderer mange forskellige usikkerheder såsom ustruktureret og struktureret dynamisk usikkerhed (komplekse perturbationer) samt parameter variationer (reelle perturbationer). De usikkerhedsstrukturer, der tillades ved μ er bestemt meget mere genrelle end dem, der tillades ved \mathcal{H}_∞ .

Desværre er μ synthese et meget vanskeligt matematisk problem, hvor design strategier kun er veludviklede for udelukkende komplekse perturbationer. For at kunne udvikle vores centrale resultat i afhandlingen er vi desværre nødt til at kunne designe regulatorer for blandede perturbation set. En ny metode kaldt μ - K iteration er blevet udviklet for at klare dette problem.

En generel egenskab ved alle robust reguleringsmetoder er, at man skal bruge ikke bare en nominel model men også en kvantificering af kvaliteten af den model. I denne afhandling har vi afgrænset os til blok-struktureret norm-begrænset usikkerhed som ovenfor beskrevet. Det er imidlertid ikke trivielt at skulle specificere model usikkerheden på denne måde. Dette har til en vis grad været overset af teoretikerne indenfor robust regulering. Usikkerhedsspecifikationen har simpelthen være givet på forhånd.

En perturbationsmodel kan for eksempel bestemmes ved fysisk modellering. Ved at anvende de fundamentale ligninger fra termodynamikken, mekanikken, fysikken osv. kan man generelt opstille et sammenhørende sæt af ulineære partielle differential-ligninger, der beskriver den fysiske proces. Disse differential-ligninger kan så lineariseres (i tid og sted) omkring et passende arbejds punkt og Laplace transformeres for regulator design. De lineariserede differential-ligninger vil typisk indeholde udtryk, hvori masse, inertie osv. indgår. Disse fysiske størrelser vil normalt kun være kendt med en vis usikkerhed. Dette vil give anledning til reelle skalare perturbationer til den nominelle model. Desuden kan arbejds punktvariationer også beskrives ved reelle perturbationer.

Imidlertid kan fysisk modellering være kompliceret og tidskrævende, selv for ret simple systemer. Et tiltrækkende alternativ til fysisk modellering er system identifikation, hvor input/output målinger bruges til at estimere en, typisk, lineær model af det virkelige system. Fra kovariansen på parameterestimatet kan man herefter opnå et estimat af frekvens domæne usikkerheder.

I klassisk system identifikation er model usikkerheden beregnet under den antagelse at den eneste kilde til usikkerhed er støjfyldte målinger. Med andre ord, det antages at modelstrukturen er korrekt. Dette er imidlertid ofte en urealistisk antagelse i forbindelse med reguleringsdesign.

Fornyligt er interessen for system identifikations metoder til estimering af model usikkerhed atter vokset indenfor automatisk regulerings samfundet. I denne afhandling vil vi give en hurtig oversigt over disse resultater og en sammen-

ligning med de klassiske metoder vil blive givet. I modsætning til de klassiske metoder giver disse nye metoder mulighed for at inkludere både strukturfejl and støjfejl i de estimerede usikkerhedsgrænser. For at kunne opnå dette må vi imidlertid have en vis a priori viden om systemet. Denne a priori viden er generelt vanskelig at få fat på. Heldigvis giver en af de nye metoder, nemlig *the stochastic embedding approach* mulighed for, givet en parametrisk struktur på visse covarians matrices, at estimere the nødvendige a priori viden fra residualerne. Således kan den nødvendige a priori viden reduceres fra en kvantitativ til en kvalitativ. Vi mener, at dette gør the stochastic embedding approach mere anvendelig til estimering af modelusikkerheder end de andre ny teknikker. I denne afhandling vil vi foreslå nye parameteriseringer for covariansmatricerne for støjen og undermodelleringen. For nuværende er the stochastic embedding approach kun udviklet for skalare systemer. Det bør undersøges, om det er muligt at udvide den til multivariable systemer. Dette er imidlertid for omfangsrigt et emne til at det vil blive behandlet i denne afhandling.

Ved hjælp af the stochastic embedding approach kan vi estimere en nominel model and frekvens domæne usikkerhedsellipser omkring denne model. Det vil så blive vist, hvorledes disse ellipser kan repræsenteres eller rettere approksimeres ved et blandet reelt og komplekst perturbations set. Denne repræsentation er det nødvendige bindeled til at kombinere resultaterne fra robust reguleringsteori og system identifikation til en skridt-for-skridt design filosofi til syntese af robust regulerings systemer for skalare systemer. Denne design filosofi er hovedresultatet i afhandlingen.

Igennem hele afhandlingen vil de præsenterede teoretiske resultater blive illustreret med praktiske design eksemple. Nogle af disse eksempler er ret simple, men et par stykker er langt mere involverede. Vi mener, at de givne teoretiske metoder skal være anvendelige i forbindelse med praktisk regulator design. De præsenterede eksempler er således en væsentlig del af det arbejde, der ligger bag denne afhandling. De virker ikke bare som illustrationer, men introducerer mange nye ideer og skulle være interessante i sig selv.

Contents

1	Introduction	1
1.1	The Organization of the Thesis	6
1.1.1	Part I, Robust Control – Theory and Design	6
1.1.2	Part II, System Identification and Estimation of Model Error Bounds	7
1.1.3	Part III, A Synergistic Control Systems Design Philosophy	8
1.1.4	Part VI, Conclusions	8
I	Robust Control – Theory and Design	9
2	Introduction to Robust Control	11
2.1	μ Theory	12
2.1.1	μ Synthesis	12
2.2	An Overview	13
3	Spaces and Norms in Robust Control Theory	15
3.1	Normed Spaces	16
3.1.1	Vector and Matrix Norms	16
3.1.2	Singular Values	18
3.2	Banach and Hilbert Spaces	23
3.2.1	Convergence and Completeness	23
3.3	Lebesgue and Hardy Spaces	24
3.3.1	Time Domain Spaces	24
3.3.2	Frequency Domain Spaces	27

3.3.3	Transfer Function Norms	29
3.4	Summary	31
4	Robust Control Design using Singular Values	33
4.1	Nominal Stability	35
4.2	Nominal performance	36
4.3	Robust Stability	42
4.3.1	The Small Gain Theorem	43
4.4	Robust Performance	49
4.5	Computing the \mathcal{H}_∞ Optimal Controller	55
4.5.1	Remarks on the \mathcal{H}_∞ Solution	58
4.6	Discrete-Time Results	61
4.7	Summary	61
5	Robust Control Design using Structured Singular Values	63
5.1	μ Analysis	64
5.1.1	Robust Stability	64
5.1.2	Robust Performance	71
5.1.3	Computation of μ	74
5.2	μ Synthesis	78
5.2.1	Complex μ Synthesis – D - K Iteration	78
5.2.2	Mixed μ Synthesis – D, G - K Iteration	80
5.2.3	Mixed μ Synthesis – μ - K Iteration	85
5.3	Summary	90
6	Mixed μ Control of a Compact Disc Servo Drive	93
6.1	Complex μ Design	95
6.2	Mixed μ Design	96
6.3	Summary	102
7	μ Control of an Ill-Conditioned ASTOVL Aircraft	105
7.1	The Aircraft Model	106
7.1.1	Plant Scaling	107
7.1.2	Dynamics of the Scaled Aircraft Model	108
7.2	Control Objectives	110

7.2.1	Robustness	111
7.2.2	Performance	115
7.3	Formulation of Control Problem	117
7.4	Evaluation of Classical Control Design	119
7.5	Controller Design using μ	123
7.6	Summary	129

II System Identification and Estimation of Model Error Bounds 131

8	Introduction to Estimation Theory	133
8.1	Soft versus Hard Uncertainty Bounds	135
8.2	An Overview	137
8.3	Remarks	137
9	Classical System Identification	139
9.1	The Cramér-Rao Inequality for any Unbiased Estimator	141
9.2	Time Domain Asymptotic Variance Expressions	142
9.3	Frequency Domain Asymptotic Variance Expressions	146
9.4	Confidence Intervals for $\hat{\theta}_N$	148
9.5	Frequency Domain Uncertainty Bounds	149
9.6	A Numerical Example	150
9.6.1	Choosing the Model Structure	152
9.6.2	Estimation and Model Validation	155
9.6.3	Results	157
9.7	Summary	163
10	Orthonormal Filters in System Identification	165
10.1	ARX Models	166
10.1.1	Variance of ARX Parameter Estimate	167
10.2	Output Error Models	169
10.2.1	Variance of OE Parameter Estimate	170
10.3	Fixed Denominator Models	171
10.3.1	Variance of Fixed Denominator Parameter Estimate	172

10.3.2	FIR Models	174
10.3.3	Laguerre Models	176
10.3.4	Kautz Models	179
10.4	Combined Laguerre and Kautz Structures	181
10.5	Summary	181
11	The Stochastic Embedding Approach	183
11.1	The Methodology	184
11.1.1	Necessary Assumptions	184
11.1.2	Model Formulation	185
11.1.3	Computing the Parameter Estimate	187
11.1.4	Variance of Parameter Estimate	188
11.1.5	Estimating the Model Error	189
11.1.6	Recapitulation	193
11.2	Estimating the Parameterizations of f_Δ and f_ν	194
11.2.1	Estimation Techniques	195
11.2.2	Choosing the Probability Distributions	196
11.2.3	Maximum Likelihood Estimation of ζ	197
11.3	Parameterizing the Covariances	198
11.3.1	Parameterizing the Noise Covariance C_ν	198
11.3.2	Parameterizing the Undermodeling Covariance C_η	199
11.3.3	Combined Covariance Structures	204
11.4	Summary	204
11.4.1	Remarks	205
12	Estimating Uncertainty using Stochastic Embedding	207
12.1	The True System	208
12.2	Error Bounds with a Classical Approach	210
12.3	Error bounds with Stochastic Embedding Approach	211
12.3.1	Case 1, A Constant Undermodeling Impulse Response	212
12.3.2	Case 2: An Exponentially Decaying Undermodeling Impulse Response	215
12.3.3	Case 3: A First Order Decaying Undermodeling Impulse Response.	219
12.4	Summary	222

III A Synergistic Control Systems Design Philosophy 223

13 Combining System Identification and Robust Control	225
13.1 System Identification for Robust Control	226
13.1.1 Bias and Variance Errors	227
13.1.2 What Can We Do with Classical Techniques	227
13.1.3 The Stochastic Embedding Approach	230
13.1.4 Proposed Approach	231
13.2 Robust Control from System Identification	231
13.2.1 The \mathcal{H}_∞ Approach	232
13.2.2 The Complex μ Approach	235
13.2.3 The Mixed μ Approach	236
13.3 A Synergistic Approach to Identification Based Control	239
13.4 Summary	241
14 Control of a Water Pump	243
14.1 Identification Procedure	244
14.1.1 Estimation of Model Uncertainty	246
14.1.2 Constructing A Norm Bounded Perturbation	249
14.2 Robust Control Design	252
14.2.1 Performance Specification	252
14.2.2 \mathcal{H}_∞ Design	254
14.2.3 Mixed μ Design	256
14.3 Summary	259

IV Conclusions 261

15 Conclusions	263
15.1 Part I, Robust Control – Theory and Design	263
15.2 Part II, System Identification and Estimation of Model Error Bounds	268
15.3 Part III, A Synergistic Control Systems Design Methodology	269
15.4 Future Research	270

V	Appendices	285
A	Scaling and Loop Shifting for \mathcal{H}_∞	287
B	Convergence of μ-K Iteration	293
C	Rigid Body Model of ASTOVL Aircraft	297
C.1	Flight Control Computer Hardware $G_c(s)$	297
C.2	Engine and Actuation Model $G_E(s)$	298
C.3	Force Transformation Matrix F_{mat}	299
C.4	Rigid Aircraft Frame $G_A(s)$	300
C.5	Sensor Transfer Matrix $G_S(s)$	300
D	Computing the Parameter Estimate $\hat{\theta}_N$	303
D.1	Computation of $\phi(k, \theta)$ and $\psi(k, \theta)$	305
E	A MATLAB Function for Computing $\Phi(\theta)$ and $\Psi(\theta)$	311
F	Computing the θ Estimate through QR Factorization	313
F.1	Transforming the Residuals	314
G	First and Second Order Derivatives of $\ell(\varpi U, \zeta)$	317
G.1	Partial First Order Derivatives of $\ell(\varpi U, \zeta)$	318
G.2	Partial Second Order Derivatives of $\ell(\varpi U, \zeta)$	319
H	Partial Derivatives of the Noise Covariance	321
I	Partial Derivatives of the Undermodeling Covariance	323
J	ARMA(1) Noise Covariance Matrix	325
K	Extracting Principal Axis from Form Matrix	329
L	Determining Open Loop Uncertainty Ellipses	333

List of Figures

3.1	Singular value decomposition of a real matrix	21
3.2	The functions $f_1(t)$ and $f_2(t)$	26
4.1	General feedback control configuration	34
4.2	The eigenvalues and singular values of $G(j\omega)$	38
4.3	Output sensitivity $S_o(s)$ with input weight $W_{p1}(s)$ and output weight $W_{p2}(s)$	39
4.4	Nominal performance problem	42
4.5	Closed loop system with additive perturbation	45
4.6	Uncertain closed loop system and corresponding 2×2 block problem	48
4.7	Robust performance problem with additive uncertainty	50
4.8	Block diagram structure for robust performance check	51
4.9	Approximating $G(s)$ with its largest singular value in the uncertainty specification	54
4.10	The DGKF parameterization of all stabilizing controllers	56
4.11	\mathcal{H}_∞ suboptimal control configuration	60
5.1	The $N\Delta K$ formulation of robust stability problem	64
5.2	Example 5.1 on page 65: Block diagram of $G(s)$	66
5.3	Transfer function representation of uncertain second order lag	68
5.4	A general framework for analysis and synthesis of linear control systems	72
5.5	K -step of D - K iteration	80
5.6	K -step in D, G - K iteration	84
5.7	K -step in μ - K iteration	89
6.1	Control problem set-up for the compact disc servo drive	94

6.2	Results from D - K iteration on the CD player servo	96
6.3	Results from first iteration on the CD player servo	98
6.4	μ results from first μ - K iteration on the CD servo	99
6.5	Results from μ - K iteration on the C.D. player servo	101
6.6	γ scalings to be fitted in μ - K iteratio and G scalings to be fitted in D , G - K iteration	102
7.1	The rigid-body model of the aircraft $G(s)$	107
7.2	Singular value Bode plot of the plant $G(s)$ (solid) and plant condition number (dashed)	109
7.3	Block diagram of controlled aircraft	111
7.4	Singular value Bode plot of the uncertainty specification $W_u(s) = w_u(s)I$	114
7.5	Singular value Bode plot of the performance weight $W_e(s)$	116
7.6	$N\Delta K$ formulation of aircraft robust performance control problem	117
7.7	Classical controller configuration	119
7.8	Results from applying the classical controller on the aircraft	121
7.9	Transient responses for classical control configuration	122
7.10	Upper bound on the structured singular value $\mu_{\tilde{\Delta}}(F_l(N(j\omega), K(j\omega)))$ in D - K iteration	124
7.11	Results from applying the μ controller on the aircraft	126
7.12	Transient responses for μ control system	127
7.13	Nominal sensitivity and performance bounds for the aircraft design	128
9.1	First period of the signals used for identification of the wind turbine	152
9.2	Simple model of a pitch controlled wind turbine	153
9.3	Residual tests for the wind turbine identification	158
9.4	Pole-zero configuration for the deterministic and stochastic part of the estimated wind turbine model	158
9.5	Bode plot for the deterministic and stochastic part of the estimated wind turbine model	159
9.6	Step response of deterministic part of estimated wind turbine model	159
9.7	Estimated power spectrum for the pitch input signal, a pure square wave with the same amplitude and frequency and the power output	160
9.8	Nominal Nyquist curve with 2 standard deviations uncertainty ellipses	162
9.9	Robustness bound on the complementary sensitivity	162

10.1	A priori information for Laguerre (solid) and Kautz (dashed) models . . .	178
10.2	Laguerre network	179
11.1	A constant diagonal assumption on the undermodeling impulse response	201
11.2	A exponentially decaying assumption on the undermodeling impulse response	202
11.3	A first order decaying assumption on the undermodeling impulse response	203
12.1	Distribution of Laguerre model parameter estimates	209
12.2	Results from classical identification on Rohrs Counterexample	211
12.3	Case 1: Montecarlo testing of the maximum likelihood estimation of ζ	212
12.4	Case 1: Nominal Nyquist with 1 std. deviation error bounds	214
12.5	Case 1: Total model error components and comparison with true model error	215
12.6	Case 2: Montecarlo testing of the maximum likelihood estimation of ζ	216
12.7	Case 2: Nominal Nyquist with 1 std. deviation error bounds	217
12.8	Case 2: Total model error components and comparison with true model error	218
12.9	Case 3: Montecarlo testing of the maximum likelihood estimation of ζ	219
12.10	Case 3: Nominal Nyquist with 1 std. deviation error bounds	220
12.11	Case 3: Total model error components and comparison with true model error	221
13.1	Approximating estimated frequency domain uncertainty ellipses with a norm bounded perturbation set	232
13.2	2×2 block problem used for robust performance with \mathcal{H}_∞ approach . .	234
13.3	$N\Delta K$ framework used for robust performance with complex μ approach	236
13.4	Fitting an uncertainty ellipse with a mixed perturbation set	237
13.5	$N\Delta K$ formulation for robust performance problem with a mixed μ approach	239
14.1	The water supply system	244
14.2	Input/output sequence used for identification of pump system	245
14.3	True and simulated output together with estimated Nyquist and measured discrete frequency points	246
14.4	Results from the maximum likelihood estimation of ζ	248
14.5	Nominal Nyquist with 90% uncertainty ellipses	248

14.6	Comparison of uncertainty ellipses and perturbation model	250
14.7	Fitting weighting functions to the principal axis and angles of the uncertainty ellipses	251
14.8	Comparison of uncertainty ellipses and frequency domain regions described by the weights	251
14.9	Time domain response $\phi_{step}(t)$ corresponding to the chosen performance specification $S_\phi(z)$	253
14.10	\mathcal{H}_∞ approach: Nominal Nyquist with error bounds	254
14.11	\mathcal{H}_∞ approach: Nominal sensitivity with error bounds	255
14.12	Robust performance check for the \mathcal{H}_∞ controller	256
14.13	Result of μ - K iteration on the pump system	257
14.14	μ approach: Nominal Nyquist with error bounds	258
14.15	μ approach: Nominal sensitivity with error bounds	259
14.16	Results from implementing the reduced order mixed μ controller on the pump system	260
A.1	Scaling and loop shifting for \mathcal{H}_∞ suboptimal control	291
C.1	Engine and actuation system	298
K.1	Ellipse with major and minor principal axis a and b respectively and angle A	330
K.2	Rotation of ellipse	331
L.1	Rotating the vector y ϕ degrees	334

List of Tables

1.1	Control theory in this century	2
4.1	Different uncertainty descriptions and their influence on the sensitivity functions	47
6.1	Results from D - K iteration on the CD player servo	97
6.2	Results from μ - K iteration on the C.D. player servo	100
7.1	Expected maximum magnitude for each input/output component	107
7.2	Maximum absolute and relative-to-maximum-step-size deviation on pitch rate $q(t)$, pitch attitude $\theta(t)$, height rate $\dot{h}(t)$ and longitudinal acceleration $a_x(t)$ for each reference step	123
7.3	Maximum upper bound for $\mu_{\Delta}(P_{11}(j\omega))$, $\bar{\sigma}(P_{22}(j\omega))$ and $\mu_{\hat{\Delta}}(P(s))$ in each step of D - K iteration	124
7.4	Maximum absolute and relative-to-maximum-step-size deviation on pitch rate $q(t)$, pitch attitude $\theta(t)$, height rate $\dot{h}(t)$ and longitudinal acceleration $a_x(t)$ for each reference step	125
9.1	Working point values for the signals displayed in Figure 9.1	151
13.1	Some properties of classical system identification techniques	228
14.1	Working point values for the data sequence used for estimation	244
14.2	Results from μ - K iteration on the pump system	258

Nomenclature

Part I, Robust Control – Theory and Design

Symbols

Symbol	Denotes
s/z	S/Z transform complex variable.
ω	Frequency [rad/sec].
$d(s), \delta(s)$	Disturbance.
$d'(s), \delta'(s)$	Normalized disturbance ($d(s) = W_{p1}(s)d'(s)$).
$e(s)$	Control error ($e(s) = r(s) - y(s)$).
$e_0(s)$	Measured control error ($e_0(s) = r(s) - y_m(s)$).
$e'(s)$	Weighted control error ($e'(s) = W_{p2}(s)e(s)$).
$m(s)$	Model output ($m(s) = G(s)u(s)$).
$n(s)$	Sensor noise.
$r(s)$	Reference.
$u(s)$	Input.
$w(s)$	Perturbation.
$y(s)$	Output.
$y_m(s)$	Measured output ($y_m(s) = y(s) + n(s)$).
$z(s)$	Input to perturbation structure ($w(s) = \Delta(s)z(s)$).
$D(\omega), G(\omega)$	Scaling matrices for computation of μ upper bound.
$D(s)$	Scaling used in D - K iteration.
$G(s), G_h(s)$	Additional scalings used in D, G - K iteration.
$\Gamma(s), \gamma(s)$	Additional scalings used in μ - K iteration.
$G(s)$	Plant transfer function matrix.
$G_T(s)$	Perturbed plant transfer function matrix.
$J(s)$	DGKF parameterization.
$K(s)$	Controller transfer function matrix.
$M(s)$	Control sensitivity.
$N(s)$	Generalized plant.
$N_D(s)$	Augmented generalized plant for D - K iteration. $N_D = DND^{-1}$.

continued on next page

<i>continued from previous page</i>	
Symbol	Denotes
$N_{DG}(s)$	Augmented generalized plant for D, G - K iteration. $N_{DG} = (DND^{-1} - \beta^*G)G_h$.
$N_{D\Gamma}(s)$	Augmented generalized plant for μ - K iteration. $N_{D\Gamma} = \Gamma DND^{-1}$.
$P(s)$	Generalized closed loop system.
$Q(s)$	Free stable transfer matrix used in DGKF parameterization.
$S_o(s)/S_i(s)$	Sensitivity evaluated at plant output and input.
$T_o(s)/T_i(s)$	Complementary sensitivity evaluated at plant output and input.
$W_{p1}(s)$	Disturbance weight.
$W_{p2}(s)$	Control error weight.
$W_{u1}(s)$	Perturbation input weight.
$W_{u2}(s)$	Perturbation output weight.
$\hat{\Delta}(s)$	Perturbation, $\bar{\sigma}(\Delta) \leq \ell$.
$\Delta(s)$	Normalized perturbation, $\bar{\sigma}(\Delta) \leq 1$.
$\Delta_p(s)$	Performance block.
$F_l(N(s), K(s))$	Lower LFT ($F_l(N(s), K(s)) = N_{11} + N_{12}K(I - N_{21}K)^{-1}N_{21}$).
$F_u(P(s), \Delta(s))$	Upper LFT ($F_u(P(s), \Delta(s)) = P_{22} + P_{21}\Delta(I - P_{11}\Delta)^{-1}P_{12}$).
A, B, C, D	State space matrices.
T_s	Sampling time [secs].
j	$\sqrt{-1}$, sometimes an index as in x_{ij} .
I_n	$n \times n$ identity matrix.
\mathcal{J}_{np}	Nominal performance cost function.
\mathcal{J}_u	Robust stability cost function.
\mathcal{J}_{rp}	Robust performance cost function.
$\Delta \arg$	Change in argument as s traverses the Nyquist \mathcal{D} contour.
$\det(A)$	Determinant of complex matrix A .
A^T	Transpose of A .
A^*	Complex conjugate transpose of A .
A_{ij}	The (i, j) element of A .
$\text{tr} \{A\}$	Trace of A .
$\lambda_i(A)$	The i 'th eigenvalue of A .
λ_{R_i}	The i 'th real eigenvalue of A .
$\rho(A)$	The spectral radius of A .
$\rho_R(A)$	The real spectral radius of A .
$\mu_{\Delta}(A)$	The structured singular value of A .
$\bar{\mu}_{\Delta}(A)$	Upper bound for $\mu_{\Delta}(A)$.
$\text{Ric}(H)$	The Ricatti solution.

Sets, Norms and Spaces

Symbol	Denotes
$\ \cdot\ $	Norm.
<i>continued on next page</i>	

<i>continued from previous page</i>	
Symbol	Denotes
$\langle \cdot \rangle$	Scalar product.
$A = Y\Sigma U^*$	Singular value decomposition of A .
$\bar{\sigma}(A)$	Maximum singular value of A , $\bar{\sigma}(A) = \sigma_1(A) = \ A\ _2$.
$\underline{\sigma}(A)$	Minimum singular value of A , $\underline{\sigma}(A) = \sigma_k(A)$.
$\sigma_i(A)$	The i 'th singular value of A .
$\kappa(A)$	Condition number of A , $\kappa(A) = \bar{\sigma}(A)/\underline{\sigma}(A)$.
$\ G(s)\ _2$	Transfer 2-norm, $\ G(s)\ _2 = \sqrt{\frac{1}{2\pi} \int_{-\infty}^{\infty} \text{tr} \{G(j\omega)^H G(j\omega)\} d\omega}$.
$\ G(s)\ _{\infty}$	Transfer function ∞ -norm, $\ G(s)\ _{\infty} = \sup_{\omega} \bar{\sigma}(G(j\omega))$.
\mathbf{K}	Field of real or complex numbers.
H	A linear space.
$\mathbf{C}^{n \times m}$	Set of complex $n \times m$ matrices.
$\mathbf{R}^{n \times m}$	Set of real $n \times m$ matrices.
\mathcal{L}	Lebesgue spaces.
\mathcal{H}	Hardy spaces.
\mathcal{K}_S	Set of all stabilizing controllers.
\mathcal{D}'	Set of normalized generic disturbances, $\ \delta'\ _2 \leq 1$.
\mathcal{D}	Set of generic disturbances, $\delta(s) = W_{p1}(s)\delta'(s)$.
Δ	Block diagonal perturbation structure used with μ .
Δ_c	Corresponding complex perturbation set.
$\mathbf{B}\Delta$	Bounded subset of perturbations, $\mathbf{B}\Delta = \{\Delta(s) \in \Delta \bar{\sigma}(\Delta(j\omega)) < 1\}$.
$\mathbf{Q}, \mathbf{D}, \mathbf{G}, \hat{\mathbf{D}}, \hat{\mathbf{G}}$	Sets of scaling matrices used for μ upper and lower bounds.

Abbreviations

Abbreviation	Denotes
ASTOVL	Advanced short take-off and vertical landing.
CD	Compact disc.
DGKF	Doyle, Glover, Khargonekhar and Francis \mathcal{H}_{∞} parameterization.
FDLTI	Finite dimensional linear time invariant.
LFT	Linear fractional transformation.
LHP/RHP	Left/right half plane.
LMI	Linear matrix inequality.
LQ	Linear quadratic.
LQG	Linear quadratic gaussian.
LTR	Loop transfer recovery.
MIMO	Multiple input multiple output.
SISO	Single input single output.
SSV	Structured singular value.

Part II, System Identification and Estimation of Model Error Bounds

Symbols

Symbol	Denotes
\mathcal{S}	Observed system.
$E\{\cdot\}$	Expectation.
$\bar{E}\{\cdot\}$	Statistical expectation.
\mathcal{N}	The normal distribution.
χ^2	The chi-square distribution.
Cov	Covariance.
q	Shift operator.
s, z	S/Z transform complex variable.
ω	Frequency [rad/sec].
μ	Mean value.
σ	Standard deviation.
H	Hessian matrix.
M	Fisher Information matrix.
T_s	Sampling time [sec].
j	$\sqrt{-1}$, sometimes an index like in x_{ij} .
I_N	The N dimensional identity matrix.
p	Number of model parameters.
θ	Parameter vector.
$\hat{\theta}_N$	N measurements parameter estimate.
$\hat{\theta}^*$	∞ measurements parameter estimate.
θ_0	True parameter vector.
N	Number of measurements.
L	Length of FIR model for the undermodeling.
$G_T(z)$	True system discrete-time transfer function.
$G_\Delta(z)$	Undermodeling discrete-time transfer function.
$G(z, \hat{\theta}_N)$	N measurements model estimate.
$H(z)$	Noise discrete-time transfer function filter.
A, B, F, C, D	Black box model polynomials.
$y(k)$	Output.
$\hat{y}(k \theta)$	Predicted output.
$u(k)$	Input.
$e(k)$	Zero mean iid stochastic process.
λ	Variance of $e(k)$.
$\nu(k)$	Process noise.
$\delta(k)$	Undermodeling output.
$\eta(k)$	Undermodeling impulse response.
η	Undermodeling impulse response vector.

continued on next page

<i>continued from previous page</i>	
Symbol	Denotes
$h_\nu(k)$	Process noise impulse response.
f_Δ	Probability density for the undermodeling $\delta(k)$.
f_ν	Probability density for the process noise $\nu(k)$.
β	Parameter vector for the undermodeling impulse response covariance matrix C_η .
γ	Parameter vector for the process noise covariance matrix C_ν .
ζ	Combined parameter vector $[\beta \ \gamma]^T$.
Π	Undermodeling FIR regressor matrix.
ξ	Undermodeling filter $\Pi(q^{-1})u(k)$.
X	Undermodeling filter matrix.
Λ_k	k th fixed denominator model regressor.
Λ	Fixed denominator model regressor matrix.
ϕ	Predictor state vector, $\hat{y}(k \theta) = \phi(k, \theta)\theta$.
Φ	Predictor filter matrix.
$\psi(k, \theta)$	Model gradient $\partial \hat{y}(k \theta)/\partial \theta$.
Ψ	Model gradient filter matrix.
Y	Output vector.
V	Process noise vector.
$V_N(\theta, Z^N)$	Performance function for estimation problem.
$\bar{V}(\theta)$	Limit function for $V_N(\theta, Z^N)$.
$\bar{V}'(\theta)$	Derivative of $V_N(\theta, Z^N)$ with respect to θ .
Q	Variance of $\sqrt{N}V'_N(\theta, Z^N)$.
Ω	$(\Phi^T \Phi)^{-1} \Phi$.
P_θ	Parameter vector covariance matrix.
\hat{P}_N	Data estimate of P_θ .
C_η	Covariance matrix for the undermodeling impulse response.
C_ν	Covariance matrix for the process noise.
a, c, σ_e^2	Noise covariance parameters.
α, λ	Undermodeling covariance parameters.
$\hat{\rho}_N$	$\begin{bmatrix} \hat{\theta}_N & 0 \\ \theta_0 & \eta \end{bmatrix}$
ρ_0	
$\tilde{g}(z)$	Frequency domain model uncertainty.
$\Gamma(z)$	Uncertainty filter, $\tilde{g}(z) = \Gamma(z)(\theta^* - \hat{\theta}_N)$.
$P_{\tilde{g}}$	Covariance matrix for the total model error.
Υ	$E \{ (\rho_0 - \hat{\rho}_N)(\rho_0 - \hat{\rho}_N)^T \}$.
$\epsilon(k, \theta)$	Prediction errors.
$\hat{R}_N(\kappa)$	Data estimate of residual covariance.
$\hat{R}_N^{\epsilon, u}(\kappa)$	Data estimate of residual/input cross-covariance.
ϖ	Transformed residuals vector.
R	Transformation matrix.
P_Φ	$[I - \Phi(\Phi^T \Phi)^{-1} \Phi^T]$.
$\mathcal{L}(\varpi U, \zeta)$	The likelihood of ϖ given U and ζ .

continued on next page

<i>continued from previous page</i>	
Symbol	Denotes
$\ell(\varpi U, \zeta)$	The loglikelihood of ϖ given U and ζ .
$f(\varpi U, \zeta)$	The probability density function for ϖ given U and ζ .
Σ	The covariance for the residuals ϖ .
$d_n(\mathcal{S}, \mathcal{B})$	n -width.
$\delta_{\alpha\beta}$	Kronecker delta.
$L_i(z, a)$	Laguerre filters.
$\Psi_i(z, b, c)$	Kautz filters.

Abbreviations

Abbreviation	Denotes
AR	Auto-regressive.
ARX	Auto-regressive with exogenous input.
FDLTI	Finite dimensional linear time invariant.
FIR	Finite impulse response.
LHP/RHP	Left/right half plane.
MIMO	Multiple input multiple output.
OE	Output error.
PEM	Prediction error methods.
SISO	Single input single output.

Chapter 1

Introduction

Contents

1.1	The Organization of the Thesis	6
1.1.1	Part I, Robust Control – Theory and Design	6
1.1.2	Part II, System Identification and Estimation of Model Error Bounds	7
1.1.3	Part III, A Synergistic Control Systems Design Phi- losophy	8
1.1.4	Part VI, Conclusions	8

Control theory within the 20th century can conveniently be divided into 3 main periods: classical control, optimal control and robust control. In Table 1.1 on the next page some of the key results for each period is given. The period 1930–1960 can be classified as the “Classical Control” period. Here famous pioneers, like Bode and Nyquist, developed control design tools which made it possible to meet standard requirements on stability, robustness and performance for scalar (single-input single-output) systems. These are e.g. Bode and Nyquist plots, Nichols charts and root-locus plots. The chief paradigm for this period was the frequency domain. The results from the classical control period make up the bulk of industrial control practice to this day.

	Classical Control 1930–1960	Optimal Control 1960–1980	Robust Control 1980–present
Analysis	Nyquist plots Bode plots Root-locus Gain/phase margins	State space models Controllability Observability Random processes	Singular value plots μ analysis Balanced realizations Spectral factorizations
Synthesis	PID controllers Lead-lag compensation	LQ state feedback Kalman-Bucy filters LQG control	\mathcal{H}_∞ synthesis μ synthesis LQG/LTR control Youla parameterizations
Chief paradigm	Frequency domain	Time domain	Frequency domain

Table 1.1: *Control theory in this century [Dai90].*

The period from 1960–1980 can be termed “Optimal Control”. In the early 1960’s Kalman and others introduced concepts like controllability, observability, optimal state estimation and optimal state feedback. Concepts which were based on state space matrix equations rather than frequency domain transfer functions. It was shown that using the state space approach one could formulate sensible performance measures and optimize the control scheme with respect to these measures not only for scalar systems but also for multivariable systems. When Kalman in a series of papers, see e.g. [Kal60, KHN62, Kal64], provided a state-space solution to the *Linear Quadratic Gaussian* (LQG) optimal control problem it almost created euphoria within the automatic control community. A multivariable control design method was discovered which was *optimal* for the given design criteria. Furthermore, it was possible to show that the full state feedback linear quadratic (LQ) optimal control law possessed some very strong robustness properties, namely at least 60° phase margin and infinite gain margin *regardless of the choice of performance weights*. Because of duality, the optimal state estimator had similar fine properties.

These and related results shifted the emphasis in control engineering from the frequency domain to the time domain and for 20 years the frequency domain approach was more or less considered to be obsolete.

Unfortunately it turned out that LQG controllers did not always work well in

practice. In fact, poor stability and, in particular, very poor performance was not an uncommon phenomena quite opposed to the theoretical results. However, these practical problem were to a large extent ignored by the theoreticians of automatic control and this created a gab between practitioners and theoreticians in control engineering.

Then in 1979 Doyle & Stein showed in their famous paper [DS79] that even though the control law and the state estimation law are optimal, there is no guarantee that the *combined* LQG scheme possesses equivalent fine properties. Thus the problems encountered by control engineers with LQG in practice had a firm theoretical explanation. Doyle & Stein used standard frequency domain methods to prove their point. The chief paradigm for the automatic control community was beginning to shift once again.

Another key paper from that period is the frequently quoted paper [DS81] also by Doyle & Stein. In this paper singular value sensitivity plots and norm bounded uncertainty descriptions was introduced. The similarities between (multivariable) singular value analysis and classical (scalar) frequency domain analysis was emphasized. The singular value plots represented the extension of the classical scalar Bode plots to multivariable systems. They are thus also frequently termed *singular value Bode plots*.

In both papers [DS79, DS81] a method for regaining the fine loop properties of the LQ state feedback from the LQG implementation is presented. This method, known as *loop transfer recovery* (LTR), works by modifying the intensity of the process noise in the Kalman-Bucy filter. Thus, even though that the main emphasis was on the frequency domain, state space (or time domain) algorithms were used to compute the controller. The papers by Doyle & Stein amongst many others introduced a new period in control engineering. The mixture of frequency domain analysis and state space formulations became symptomatic for the period from 1980 until today. This period is usually termed “Robust Control”.

The next decade witnessed an intensive research in robust control designs. The term robust stressed the importance of developing methods which maintained closed loop stability and performance not only for the nominal model of the control object (plant) but also for a set of plants including the invariable discrepancy between the nominal model and the true plant. The robust control paradigm in fact represented a return to a more physically motivated basis for control design. In order to pose a meaningful problem, the model uncertainty or perturbations are assumed to be norm bounded. For example, a description of the true multivariable plant $G_T(s)$ could be

$$G_T(s) = (I + \Delta(s)) G(s) \quad (1.1)$$

where $G(s)$ is the nominal transfer function matrix and $\Delta(s)$ a multiplicative

perturbation at the plant output. $\Delta(s)$ could then be bounded in magnitude as

$$\|\Delta(j\omega)\|_2 = \bar{\sigma}(\Delta(j\omega)) < \ell(\omega) \quad (1.2)$$

where $\bar{\sigma}$ denotes the *maximum singular value, induced 2-norm or spectral norm* and $\ell(\omega)$ is a frequency dependent scalar. The choice of bounding norm is a compromise between those that best describe the plant perturbations and those that lead to mathematically tractable problems. The spectral norm has been a popular compromise since it describes well the effects of high frequency unmodeled dynamics, non-linearities and time delays and a solution to the corresponding control problem has been found. Using the celebrated *Small Gain Theorem* it is e.g. possible to show that for the perturbation structure in (1.1) on the preceding page with $\Delta(s)$ bounded by (1.2), the stability of the closed loop system is maintained if and only if

$$\bar{\sigma}(T(j\omega)) = \bar{\sigma}(G(j\omega)K(j\omega)(I + G(j\omega)K(j\omega))^{-1}) \leq \ell(\omega) \quad (1.3)$$

If the process noise is assumed to be bounded by the same induced norm a unifying framework can be used for considering both stability and disturbance rejection.

Much of the literature on robust control have focused strongly on the *computational engine* of robust control, namely the \mathcal{H}_∞ optimization algorithm. This has, unfortunately, in some sense hampered the application of robust control in practice since many practical issues have been left unattended. In fact, it turns out that the standard state space \mathcal{H}_∞ framework is not very suitable for formulating practical control problems since the perturbation structures permitted in \mathcal{H}_∞ is much too restricted to deal with many practical specifications. A much more general but less well known design framework is based on the *structured singular value* or μ theory. μ theory allows the inclusion of much more natural and specialized perturbation models and it furthermore nicely separates stability and performance issues, a result which can not be obtained in the \mathcal{H}_∞ framework. Interestingly, the computational engine in μ control synthesis is still the \mathcal{H}_∞ optimization algorithm.

Unfortunately, even though μ theory is comprehensible straightforward with simple and insightful results, it has not been as widely recognized as \mathcal{H}_∞ theory. There are several reasons for this. First of all, the practical computation of the structured singular value μ is a very difficult and in fact, yet unsolved, mathematical problem. Fortunately, tight upper and lower bounds on μ may be effectively computed. Furthermore, algorithms for computing these bounds have become commercially available with the release of the MATLAB *μ -Analysis and Synthesis Toolbox* [BDG⁺93]. Thus for practical controller design, the mathematical complexity of μ is no longer such a critical issue. Another reason for μ -theory not being more widespread is the limited amount of literature on μ . Usually the

simplicity of the theory is hidden in messy mathematical expressions connected with the computation of μ .

Since μ cannot be directly computed unless in some special cases, it is clear that controller synthesis using μ must be problematic as well. The approach usually taken is to pose an upper bound problem, which is solved iteratively through a series of \mathcal{H}_∞ optimizations and μ upper bound computations. This scheme is usually denoted *D-K iteration*. However, *D-K iteration* is only well developed for purely complex perturbations. Many practical control problems unfortunately call for the use of both real and complex perturbations. Thus a method for μ synthesis for mixed real and complex perturbation sets is needed.

One objective of this thesis is to provide a thorough introduction to robust control design with special attention to μ methods. The treatment will not focus excessively on finer mathematical points but rather it will address practical design issues. A main result is a new algorithm, denoted *μ -K iteration*, which solves the mixed μ problem.

Modern robust control synthesis techniques aim at providing robustness with respect to both plant perturbations (robust stability) and additive disturbances (robust performance). It is assumed that information of noise and perturbations is available. One way of acquiring such information is by physical modeling. However, this is usually a quite complex task unless extremely simple systems are considered. A different approach could be by system identification. Unfortunately, classical identification methods assume that all uncertainty is in the form of additive noise. There is thus a gap between robust control and system identification. This gap has hampered the application of robust control methods to practical problems.

The gap between robust control methods and system identification results was realized by a number of researchers around 1990, see e.g. [GS89a, WL90b, Gev91]. The development of formal techniques for estimation of model uncertainty has since been the focus of active research and numerous results have been published, see [Bai92] and references therein.

In this thesis a discussion of these recent results will be provided. Unfortunately the estimation of model error bounds from finite noisy data becomes a very difficult problem when the true system cannot be represented within the model set. In fact, it is well-known that a priori knowledge of the noise and unmodeled dynamics is necessary to compute such bounds. Most of the attempts on estimation of model error bounds have relied upon hard bound prior knowledge of the noise and unmodeled dynamics to compute hard uncertainty bounds on the nominal model. However, the necessary a priori knowledge of the unmodeled dynamics seems very difficult to obtain in practice. Here, we will consider some recent results on estimation of frequency domain model error bounds where the model bias is embedded in a stochastic framework. This approach is thus denoted the

stochastic embedding approach. A central feature of the stochastic embedding approach is that the necessary a priori knowledge can be estimated from the model residuals.

The main point of this work is then that the results on the stochastic embedding approach for uncertainty estimation can be combined with the derived method for mixed real and complex μ synthesis to constitute a coherent design approach for linear systems control design. A step-by-step design method is proposed. Currently only scalar control problems can be considered, since the stochastic embedding approach has been developed for scalar systems only. Future research will have to reveal whether an extension to multivariable systems is possible.

1.1 The Organization of the Thesis

The thesis is split into 4 parts. Part I considers robust control, Part II system identification and estimation of model uncertainty and Part III the combination of the results given in the previous parts into a coherent design philosophy. Finally in Part IV the major results are reviewed and discussed.

1.1.1 Part I, Robust Control – Theory and Design

The purpose of this part is to formulate the necessary framework for the control analysis and synthesis part of the proposed synergistic control design methodology. First in Chapter 3 an introduction to norms and spaces used in robust control design is given. Then in Chapter 4 we will review “classical” singular value \mathcal{H}_∞ control design. In \mathcal{H}_∞ control it is assumed that the model uncertainty can be described by a single complex perturbation block. However, usually much finer perturbation structures are available including both real and complex blocks. Such uncertainty structures can only be handled conservatively in an \mathcal{H}_∞ framework. Furthermore we will show how the *robust performance* problem, that is guaranteed performance in presence of uncertainty, also cannot be non-conservatively addressed using an \mathcal{H}_∞ approach *even if the perturbation is a single complex block*.

This motivates us then in Chapter 5 to consider the structured singular value μ . Using μ , we may develop a robust control framework where real and complex perturbation blocks which enter the nominal system in a linear fractional manner can be addressed without conservatism. A very large class of perturbation models may be cast into this structure. Furthermore the robust performance problem can be handled non-conservatively. We will start by presenting the “classical” results on μ . As discussed earlier, only upper and lower bounds on μ can be computed unless for some special very simple cases. Even though these bounds are usually

quite tight, at least for purely complex perturbation sets, the control synthesis problem becomes very difficult. The usual approach for complex perturbation sets is the iterative scheme *D-K iteration* which generally seems to work well in practice although convergence cannot be guaranteed.

Unfortunately, in order to develop our central result, we will need a control synthesis procedure which can be applied for mixed real and complex perturbation sets. Some of the first results on mixed μ synthesis was given in the thesis by Peter Young [You93]. Young proposes an iterative scheme denoted *D,G-K iteration* which solves the mixed μ problem. Unfortunately the approach is much more involved than the corresponding *D-K iteration* for purely complex blocks. We will present a different approach, denoted *μ -K iteration* which sacrifices some of the convergence properties that can be obtained with *D,G-K iteration*. In return, *μ -K iteration* can be performed more easily. Furthermore, the iteration seems to work quite well in practice.

The *μ -K iteration* procedure is the central result of Part I.

Finally, we will present two design examples. In Chapter 6 mixed μ control of a CD servo drive is considered. The second design in Chapter 7 is concerned with control of an advanced short take off and vertical landing aircraft.

1.1.2 Part II, System Identification and Estimation of Model Error Bounds

The main purpose of this part is to investigate methods for quantification of frequency domain model uncertainty. First in Chapter 9 we will review the “classical” results. In Chapter 10 we will consider some special cases, in particular fixed denominator models with basis functions which are orthonormal in the space of strictly proper stable transfer functions. The classical results can be applied in the case where the true system can be represented within the model set. This is however often an inadequate assumption in connection with robust control. Thus we will next consider methodologies where this is not a requirement. Specifically, in Chapter 11 we will consider the stochastic embedding approach where the undermodeling is embedded in a stochastic framework. It is then possible to extend the classical results to the case where undermodeling is present. In order to evaluate the frequency domain uncertainty estimates, the covariance matrices for the noise and the undermodeling must be known. It can be shown that if it is assumed that both the noise and the undermodeling impulse response are Gaussian and the covariance matrices are parameterized, the parameters themselves can be estimated through maximum likelihood techniques. The main result of Part II is new parameterizations for these covariance matrices.

Finally, in Chapter 12 we will present an example where different parameteriza-

tions of the undermodeling have been compared.

1.1.3 Part III, A Synergistic Control Systems Design Philosophy

In this part a coherent identification based robust control design philosophy is developed for scalar systems. In Chapter 13 it is shown how estimated frequency domain uncertainty ellipses may be represented with a mixed real and complex perturbation set. Then the proposed μ - K iteration procedure can be applied to solve the corresponding robust control problem. A step-by-step design procedure for scalar systems is outlined.

To illustrate the design methodology, an example is given in Chapter 14. This example considers control of a small domestic water supply system where the control problem is to maintain water pressure for flow disturbances.

1.1.4 Part VI, Conclusions

In Chapter 15 the main results of the thesis are summarized and directions for further research are given.

Part I

Robust Control – Theory and Design

Chapter 2

Introduction to Robust Control

Contents

2.1	μ Theory	12
2.1.1	μ Synthesis	12
2.2	An Overview	13

Design of controllers with guaranteed closed loop stability and performance for uncertain plants has been the focus of active research for almost 2 decades now. Most of the research on robust control has focused on \mathcal{H}_∞ like problems. However it turns out that many practical problems do not readily fit the standard \mathcal{H}_∞ problem setup since the involved model uncertainty is structured rather than unstructured. An \mathcal{H}_∞ control design will then be potentially conservative and thus will limit the obtainable performance of the closed loop system.

2.1 μ Theory

Fortunately theory exists that non-conservatively handles these problems, namely the *structured singular value* (SSV) or μ theory. In many practical applications μ theory is more appropriate for system analysis and controller synthesis. μ theory has not been as widely recognized as \mathcal{H}_∞ theory, probably due to the small amount of literature on μ and to the computational difficulties associated with μ . Recently however algorithms for computing μ^1 have become commercially available through the MATLAB *μ -Analysis and Synthesis Toolbox* [BDG⁺93]. Also the literature on μ is improving, see e.g. the excellent introduction to μ -analysis by Holohan [Hol94].

2.1.1 μ Synthesis

An approach to controller synthesis using μ for complex perturbations, frequently denoted *D-K iteration*, has been known for some time now [DC85] and controller synthesis for structured complex perturbation sets can be accomplished with the aid of the MATLAB μ toolbox.

Unfortunately many practical application problem calls for the use of mixed real and complex perturbation sets. For example, analysis of plant parameter variations which is an often encountered problem rely on the use of mixed or even purely real perturbation sets. Until recently controller synthesis under mixed perturbation sets was an unsolved problem. A solution to this problem was probably first given by Young [You93, You94]. Unfortunately the synthesis procedure proposed by Young is quite involved. Even though it relies on the same principles it is certainly more mathematically complex than *D-K* iteration used for purely complex perturbation sets.

The main emphasis in this part of the thesis will be on μ -analysis and synthesis. However, in order to put things into perspective, a survey of robust control design methods using the \mathcal{H}_∞ approach will be given initially. The role of singular values will be discussed as will some of the commonly used singular value bounded unstructured uncertainty descriptions. The potential conservatism inherent in an unstructured uncertainty assumption will be emphasized. It will be shown how the nominal performance problem and the robust stability problem can be addressed with \mathcal{H}_∞ methods. However, it turns out that the robust performance problem cannot be non-conservatively formulated in an \mathcal{H}_∞ framework. Then it will be shown how the structured singular value may be used to overcome the shortcomings of the \mathcal{H}_∞ approach. Controller design using μ will then be presented both for purely complex and for mixed real and complex perturbation structures. A novel approach to mixed μ synthesis, denoted *μ -K iteration*, will

¹More accurately: upper and lower bounds on μ .

be presented. The μ - K iteration procedure is computationally simpler than the procedure proposed by Young. Furthermore, as we shall show, μ - K iteration seems to work quite well in practice.

2.2 An Overview

The remainder of this part of the thesis is organized as follows. In Chapter 3 an introduction to spaces and norms frequently used in modern robust control is given. In Chapter 4 an introduction to “classical” singular value based \mathcal{H}_∞ robust control analysis and synthesis is given. In Chapter 5 robust stability and performance will be addressed using the structured singular value μ . Various μ synthesis techniques will be presented and discussed. In Chapter 6 a mixed μ optimal controller will be designed for a simple model of a CD player servo using μ - K iteration. Finally in Chapter 7 a major flight control case study will be given. The control of an Advanced Short Take-Off and Vertical Landing (ASTOVL) aircraft will be considered at low speeds in the transition zone between jet-borne and fully wing-borne flight. In this flight condition the aircraft is unstable in the longitudinal axis and the nominal model is very ill-conditioned especially at low frequencies.

Chapter 3

Spaces and Norms in Robust Control Theory

Contents

3.1	Normed Spaces	16
3.1.1	Vector and Matrix Norms	16
3.1.2	Singular Values	18
3.2	Banach and Hilbert Spaces	23
3.2.1	Convergence and Completeness	23
3.3	Lebesgue and Hardy Spaces	24
3.3.1	Time Domain Spaces	24
3.3.2	Frequency Domain Spaces	27
3.3.3	Transfer Function Norms	29
3.4	Summary	31

In order to fully comprehend and appreciate modern robust control theory some mathematical prerequisites from functional analysis are necessary. In many fine textbooks on robust control this prior knowledge is either assumed or discussed only very briefly. However, we believe that an introduction to the relevant spaces

and norms used in modern control theory is mandatory. Conversely, if the reader is completely familiar with functional analysis he may skip this chapter. As it turns out, the necessary mathematical tools are conceptually quite straightforward even though some are computationally involved. The results presented here are taken mainly from [Dai90] and [Fra87] and are all given without proof.

3.1 Normed Spaces

Let H be a *linear space* over the *field* \mathbf{K} , where \mathbf{K} is either the field \mathbf{C} of complex numbers or the field \mathbf{R} of real numbers. A *norm* on H is a function denoted $\|\cdot\|$ from H to \mathbf{R} having the following properties

$$\|f\| \geq 0 \quad (3.1)$$

$$\|f\| = 0 \quad \text{iff } f = 0 \quad (3.2)$$

$$\|\alpha f\| = |\alpha| \|f\| \quad (3.3)$$

$$\|f + g\| \leq \|f\| + \|g\| \quad (\text{triangle inequality}) \quad (3.4)$$

where $f, g \in H$ and $\alpha \in \mathbf{K}$. Thus a norm is a single real number measuring the “size” of an element of H . Given a linear space H there may be many possible norms on H . Given a linear space H and a norm $\|\cdot\|$ on H , the pair $(H, \|\cdot\|)$ is denoted a *normed space*.

3.1.1 Vector and Matrix Norms

Let H be the space \mathbf{C}^n which is a linear space. Then $x \in \mathbf{C}^n$ means that $x = (x_1, x_2, \dots, x_n)$ with $x_i \in \mathbf{C}, \forall i$. Clearly, \mathbf{C}^n is the space of complex n -vectors. For $x \in \mathbf{C}^n$ the Hölder or p -norms are defined by:

$$\|x\|_p = \left(\sum_{i=1}^n |x_i|^p \right)^{1/p} \quad (3.5)$$

In control theory, the 1-, 2- and ∞ -norm are most important since they have obvious physical interpretations:

$$\|x\|_1 = \sum_{i=1}^n |x_i| \quad (3.6)$$

$$\|x\|_2 = \sqrt{\sum_{i=1}^n |x_i|^2} = \sqrt{x^* x} \quad (3.7)$$

$$\|x\|_\infty = \max_i |x_i| \quad (3.8)$$

In (3.7) on the facing page, x^* denotes the complex conjugate transpose of x . Notice that the 2-norm $\|x\|_2$ is the usual Euclidean length of the complex vector x . All norms on \mathbf{C}^n are *equivalent norms* which means that if $\|\cdot\|_\alpha$ and $\|\cdot\|_\beta$ are norms on \mathbf{C}^n , then there exists a pair $c_1, c_2 > 0$ so that

$$c_1\|x\|_\alpha \leq \|x\|_\beta \leq c_2\|x\|_\alpha, \quad \forall x \in \mathbf{C}^n \quad (3.9)$$

In particular, $\forall x \in \mathbf{C}^n$:

$$\|x\|_2 \leq \|x\|_1 \leq \sqrt{n}\|x\|_2 \quad (3.10)$$

$$\|x\|_\infty \leq \|x\|_2 \leq \sqrt{n}\|x\|_\infty \quad (3.11)$$

$$\|x\|_\infty \leq \|x\|_1 \leq n\|x\|_\infty \quad (3.12)$$

Now let us consider the space $H = \mathbf{C}^{m \times n}$, namely the space of $m \times n$ complex matrices. $\mathbf{C}^{m \times n}$ is also a linear space. Matrix p -norms on $\mathbf{C}^{m \times n}$ are defined in terms of the p -norms for vectors on \mathbf{C}^n :

$$\|A\|_p = \sup_{x \in \mathbf{C}^n, x \neq 0} \frac{\|Ax\|_p}{\|x\|_p}, \quad \forall A \in \mathbf{C}^{m \times n} \quad (3.13)$$

Notice that the matrix p -norms are *induced norms*. They are induced by the corresponding p -norms on vectors. One can think of $\|A\|_p$ as the maximum *gain* of the matrix A measured by the p -norm ratio of vectors before and after multiplication by A . In general matrix p -norms are difficult to compute. However, for $p = 1, 2$, or ∞ there exist simple algorithms to compute $\|A\|_p$ exactly. If $A = [a_{ij}] \in \mathbf{C}^{m \times n}$ we have

$$\|A\|_1 = \max_j \sum_{i=1}^m |a_{ij}| \quad \text{maximum column sum} \quad (3.14)$$

$$\|A\|_2 = \bar{\sigma}(A) \quad \text{maximum singular value} \quad (3.15)$$

$$\|A\|_\infty = \max_i \sum_{j=1}^n |a_{ij}| \quad \text{maximum row sum} \quad (3.16)$$

A fourth norm which is important in modern control theory is the F -norm or *Frobenius norm*. It is given simply as the root sum of squares of the magnitude of all the matrix elements:

$$\|A\|_F = \sqrt{\sum_{i=1}^m \sum_{j=1}^n |a_{ij}|^2}, \quad \forall A \in \mathbf{C}^{m \times n} \quad (3.17)$$

Notice that the F -norm is not an induced norm.

The F - and p -norms on $\mathbf{C}^{m \times n}$ are also equivalent norms. Thus there are upper and lower bounds on the ratio between any two different norms applied to the same matrix. If one type of norm for a given matrix tends towards zero or infinity, so do all other norms. Let $A = [a_{ij}] \in \mathbf{C}^{m \times n}$. Then

$$\|A\|_2 \leq \|A\|_F \leq \sqrt{n} \|A\|_2 \quad (3.18)$$

$$\max_{i,j} |a_{ij}| \leq \|A\|_2 \leq \sqrt{mn} \max_{i,j} |a_{ij}| \quad (3.19)$$

$$\|A\|_2 \leq \sqrt{\|A\|_1 \|A\|_\infty} \quad (3.20)$$

$$\frac{1}{\sqrt{n}} \|A\|_\infty \leq \|A\|_2 \leq \sqrt{m} \|A\|_\infty \quad (3.21)$$

$$\frac{1}{\sqrt{m}} \|A\|_1 \leq \|A\|_2 \leq \sqrt{n} \|A\|_1 \quad (3.22)$$

The matrix 2-norm and F -norm are invariant under multiplication by unitary or orthogonal matrices. Assume that $Q^*Q = I$ and $Z^*Z = I$ for $Q \in \mathbf{C}^{m \times m}$ and $Z \in \mathbf{C}^{n \times n}$. Then

$$\|QAZ\|_F = \|A\|_F \quad (3.23)$$

$$\|QAZ\|_2 = \|A\|_2 \quad (3.24)$$

This property is crucial to many proofs in robust control theory.

3.1.2 Singular Values

In modern control theory singular values have been used to extend the classical frequency response Bode plot to multivariable systems. Consider the input-output relation

$$y(s) = G(s)u(s) \quad (3.25)$$

where $G(s)$ is a transfer function matrix. How do we then evaluate the frequency response $G(j\omega)$? An obvious choice would be to pick one of the induced matrix norms introduced previously. The 1-, 2- and ∞ -norm all have potential engineering applications. However, the control theory for using them in design or analysis is only well-developed for the 2-norm. Thus let us evaluate the frequency response of $G(s)$ at the frequency ω by

$$\|G(j\omega)\|_2 = \sup_{u \in \mathbf{C}^n, u \neq 0} \frac{\|G(j\omega)u(j\omega)\|_2}{\|u(j\omega)\|_2} = \bar{\sigma}(G(j\omega)) \quad (3.26)$$

Letting $0 \leq \omega \leq \infty$ we may compute the matrix 2-norm for every ω to obtain an upper bound for the “gain” of the transfer matrix $G(s)$. However, we would like

to have a lower bound on $G(j\omega)$ as well. This lower bound can be obtained with the *minimum singular value* given by

$$\underline{\sigma}(G(j\omega)) = \inf_{u \in \mathbf{C}^n, u \neq 0} \frac{\|G(j\omega)u(j\omega)\|_2}{\|u(j\omega)\|_2} \quad (3.27)$$

Thus if we measure the “gain” of the system $G(s)$ as the 2-norm ratio of the input and output, then the maximum and minimum singular values of $G(j\omega)$ will constitute upper and lower bounds on this gain. In fact, we may assess the system “gain” even more detailed using the *singular value decomposition* given below. Let us, however, first introduce the following important lemma which establishes the relation between the singular values and the eigenvalues of a complex matrix.

Lemma 3.1 (Singular values and Eigenvalues) *The singular values of a complex matrix $A \in \mathbf{C}^{m \times n}$, denoted $\sigma_i(A)$, are the k largest nonnegative square roots of the eigenvalues of A^*A where $k = \min\{n, m\}$. Thus*

$$\sigma_i(A) = \sqrt{\lambda_i(A^*A)} \quad i = 1, 2, \dots, k \quad (3.28)$$

It is usually assumed that the singular values are ordered such that $\sigma_i \geq \sigma_{i+1}$.

Thus

$$\bar{\sigma}(A) = \sigma_1(A) = \sup_{u \in \mathbf{C}^n, u \neq 0} \frac{\|Au\|_2}{\|u\|_2} = \|A\|_2 \quad (3.29)$$

$$\underline{\sigma}(A) = \sigma_k(A) = \inf_{u \in \mathbf{C}^n, u \neq 0} \frac{\|Au\|_2}{\|u\|_2} = \|A^{-1}\|_2^{-1} \quad \text{if } A^{-1} \text{ exists} \quad (3.30)$$

The ratio between the maximum and minimum singular value is denoted the condition number κ :

$$\kappa(A) = \frac{\bar{\sigma}(A)}{\underline{\sigma}(A)} \quad (3.31)$$

Let us then introduce the singular value decomposition.

Lemma 3.2 (Singular Value Decomposition) *Let $G \in \mathbf{C}^{m \times n}$ be a complex matrix. Then there exist two unitary¹ matrices $Y \in \mathbf{C}^{m \times m}$, $U \in \mathbf{C}^{n \times n}$ and a*

¹A unitary matrix U satisfies the equation $U^*U = I$.

diagonal matrix $\Sigma \in \mathbf{R}^{m \times n}$ such that

$$G = Y\Sigma U^* \quad (3.32)$$

$$= \begin{bmatrix} y_1 & y_2 & \cdots & y_m \end{bmatrix} \begin{bmatrix} \Sigma_k & 0 \\ 0 & 0 \end{bmatrix} \begin{bmatrix} u_1^* \\ u_2^* \\ \vdots \\ u_n^* \end{bmatrix} \quad (3.33)$$

$$= \sum_{i=1}^k y_i \sigma_i u_i^* \quad (3.34)$$

where

$$\begin{aligned} \Sigma_k &: \text{diag}(\sigma_1, \sigma_2, \dots, \sigma_k). \\ y_1 \rightarrow y_m &: \text{The } m \text{ columns of } Y. \\ u_1^* \rightarrow u_n^* &: \text{The } n \text{ rows of } U^* \end{aligned}$$

This is known as the singular-value decomposition (SVD) of the matrix G .

An interpretation for the SVD of *real* matrix A is as follows. Any real matrix A , looked at geometrically, maps a unit radius hyper-sphere into a hyper-ellipsoid. The singular values $\sigma_i(A)$ give the lengths of the principal axis of the ellipsoid. The *singular vectors* y_i give the mutually orthogonal directions of these major axes and the singular vectors u_i are mapped into the y_i vectors with gain σ_i , that is, $Au_i = \sigma_i y_i$.

Example 3.1 (SVD of a Real Matrix) This example is taken from [MZ89]. Let A be given by

$$A = \begin{bmatrix} 0.8712 & -1.3195 \\ 1.5783 & -0.0947 \end{bmatrix} \quad (3.35)$$

The SVD of A is given by $A = Y\Sigma U^*$ with

$$Y = \frac{1}{\sqrt{2}} \begin{bmatrix} 1 & 1 \\ 1 & -1 \end{bmatrix}, \Sigma = \begin{bmatrix} 2 & 0 \\ 0 & 1 \end{bmatrix}, U = \frac{1}{2} \begin{bmatrix} \sqrt{3} & -1 \\ -1 & -\sqrt{3} \end{bmatrix} \quad (3.36)$$

A geometrical interpretation is given in Figure 3.1 on the facing page with $U = [u_1, u_2]$ and $Y = [y_1, y_2]$.

In the following some of the important properties of singular values are stated:

$$\bar{\sigma}(G) = \sup_{u \in \mathbf{C}^n, u \neq 0} \frac{\|Gu\|_2}{\|u\|_2} \quad (3.37)$$

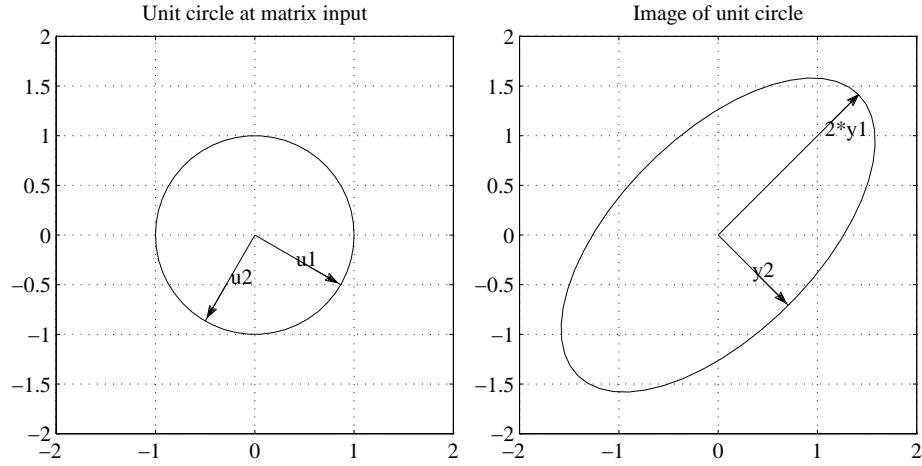


Figure 3.1: Singular value decomposition of a real matrix.

$$\underline{\sigma}(G) = \inf_{u \in \mathbf{C}^n, u \neq 0} \frac{\|Gu\|_2}{\|u\|_2} \quad (3.38)$$

$$\underline{\sigma}(G) \leq |\lambda_i(G)| \leq \bar{\sigma}(G) \quad (3.39)$$

$$\bar{\sigma}(G) = \frac{1}{\underline{\sigma}(G^{-1})} \quad (3.40)$$

$$\underline{\sigma}(G) = \frac{1}{\bar{\sigma}(G^{-1})} \quad (3.41)$$

$$\bar{\sigma}(\alpha G) = |\alpha| \bar{\sigma}(G) \quad (3.42)$$

$$\bar{\sigma}(G + H) \leq \bar{\sigma}(G) + \bar{\sigma}(H) \quad (3.43)$$

$$\bar{\sigma}(GH) \leq \bar{\sigma}(G) \bar{\sigma}(H) \quad (3.44)$$

$$\max\{\bar{\sigma}(G), \bar{\sigma}(H)\} \leq \bar{\sigma}([G \ H]) \leq \sqrt{2} \max\{\bar{\sigma}(G), \bar{\sigma}(H)\} \quad (3.45)$$

$$\sum_{i=1}^n \sigma_i^2 = \text{tr} \{G^*G\} \quad (3.46)$$

where

- $\lambda_i(G)$: The i -th eigenvalue of G .
- Property (3.40) and (3.41) : Prerequisites the existence of G^{-1} .
- α : A constant (complex) scalar.
- $\text{tr} \{G^*G\}$: The trace of G^*G .

Consider the input-output matrix equation:

$$y(j\omega) = G(j\omega)u(j\omega) \quad (3.47)$$

Using Equation (3.34) on page 20 we may formulate this as:

$$y(j\omega) = \sum_{i=1}^k y_i \sigma_i u_i^* u(j\omega) \quad (3.48)$$

Since U is unitary $u_i^* u_j$ will be orthogonal to each other so that $u_i^* u_j = 0$, for $i \neq j$ and $u_i^* u_i = 1$. Now assume that $u(j\omega) = \alpha u_j$. The input-output equation then becomes:

$$y(j\omega) = \sum_{i=1}^k y_i \sigma_i u_i^* u_j \alpha \quad (3.49)$$

$$= \sigma_j \alpha y_j \quad (3.50)$$

This illustrates that if the input vector $u(j\omega)$ is in the direction of u_j then the gain of the system is precisely σ_j and the output vector $y(j\omega)$ is then precisely in the direction of y_j . The sets $\{u_1, u_2, \dots, u_n\}$ and $\{y_1, y_2, \dots, y_m\}$ are not surprisingly known as the *input* respectively *output principal directions*. The singular values σ_i are also known as the principal or directional gains of the system matrix G .

Thus when $G(s)$ is a transfer function matrix we can plot the singular values $\sigma_i(G(j\omega))$ for $i = 1, \dots, k$ as functions of frequency ω . These curves are the multivariable generalization of the SISO amplitude-ratio Bode plot. For multivariable systems the amplification of the input vector sinusoid $ue^{j\omega t}$ depends on the direction of the complex vector u as illustrated above. The amplification is at least $\underline{\sigma}(G(j\omega))$ and at most $\bar{\sigma}(G(j\omega))$. The condition number $\kappa(G(j\omega))$, see (3.31) on page 19, plotted versus frequency ω outlines the system gain sensitivity to the direction of the input vector. If $\kappa(G(j\omega)) \gg 1$ the gain of the transfer function matrix will vary considerably with the input direction and $G(s)$ is said to be *ill-conditioned*. Conversely, if $\kappa(G(j\omega)) \approx 1, \forall \omega \geq 0$, the gain of the transfer matrix will be insensitive to the input direction and the system is said to be *well-conditioned*. A well-conditioned multivariable system behaves much like a single-variable system and controller design for well-conditioned system are fairly straightforward. For ill-conditioned systems, however, much more care has to be taken in both design and analysis.

3.2 Banach and Hilbert Spaces

A *scalar product* (or inner product) on H is a function denoted $\langle \cdot, \cdot \rangle$ from $H \times H$ to \mathbf{K} having the following properties

$$\langle f, g + h \rangle = \langle f, g \rangle + \langle f, h \rangle \quad (3.51)$$

$$\langle f, \alpha g \rangle = \alpha \langle f, g \rangle \quad (3.52)$$

$$\langle f, g \rangle = \langle g, f \rangle^* \quad (\text{Hermitian}) \quad (3.53)$$

$$\langle f, f \rangle \geq 0 \quad (3.54)$$

$$\langle f, f \rangle = 0 \quad \text{iff } f = 0 \quad (3.55)$$

where $f, g, h \in H$ and $\alpha \in \mathbf{K}$. A scalar product $\langle \cdot, \cdot \rangle$ induces a norm, namely, $\|f\| = \langle f, f \rangle^{1/2}$. Given the linear space H and a scalar product $\langle \cdot, \cdot \rangle$ on H , the pair $(H, \langle \cdot, \cdot \rangle)$ is denoted a *pre-Hilbert space*.

3.2.1 Convergence and Completeness

Let $(H, \|\cdot\|)$ be a normed space. Having defined a norm $\|\cdot\|$ we can assess convergence in H . A sequence $\{f_n\}$, $n = 1, 2, \dots$ in H converges to $f \in H$, and f is the limit of the sequence, if the sequence of real positive numbers $\|f - f_n\|$ converges to zero. If such f exists, then the sequence is *convergent*.

A sequence $\{f_n\}$, $n = 1, 2, \dots$ in H is called a *Cauchy sequence* if for each $\epsilon > 0$ there exists a natural number $n_0 \in \mathbf{N}$ such that for $n, m \geq n_0$ we have $\|f_n - f_m\| \leq \epsilon$. Intuitively, the elements in a Cauchy sequence eventually cluster around each other. They are “trying to converge”. Clearly every convergent sequence is a Cauchy sequence. However, in an arbitrary normed space not every Cauchy sequence is convergent. A normed space $(H, \|\cdot\|)$ is said to be *complete* if every Cauchy sequence is convergent. A pre-Hilbert space $(H, \langle \cdot, \cdot \rangle)$ is said to be complete if it is complete with respect to the norm induced by the scalar product $\langle \cdot, \cdot \rangle$.

A complete normed space is called a *Banach space* and a complete pre-Hilbert space is denoted a *Hilbert space*.

Example 3.2 \mathbf{C}^n and \mathbf{R}^n are Banach spaces under the norms $\|\cdot\|_1$, $\|\cdot\|_2$ and $\|\cdot\|_\infty$ defined by (3.6)-(3.8) on page 16.

Example 3.3 \mathbf{C}^n and \mathbf{R}^n are Hilbert spaces under the scalar product

$$\langle x, y \rangle = \sum_{i=1}^m x_i^* y_i = x^* y \quad (3.56)$$

The corresponding induced norm is the 2-norm since

$$\|x\| = \langle x, x \rangle^{1/2} = \sqrt{x^* x} = \|x\|_2 \quad (3.57)$$

3.3 Lebesgue and Hardy Spaces

So far we have only considered the space $\mathbf{C}^{m \times n}$, that is, spaces whose elements are constant matrices (or constant vectors as special cases). However, the concepts introduced above apply also to linear spaces whose elements are time domain or frequency domain functions (or operators). Two such spaces are important in robust control theory, namely *Lebesgue* and *Hardy spaces*. In \mathcal{H}_∞ control theory, \mathcal{H} stands for Hardy.

3.3.1 Time Domain Spaces

Let us consider vector-valued functions of a continuous time variable. We may then define norms for such functions (operator norms) which are fully analogous to the corresponding vector norms. Consider e.g. a function $f(t)$ defined for all time $t \in \mathbf{R}$ and taking values in \mathbf{R}^n (or \mathbf{C}^n). Restrict $f(t)$ to be *square-Lebesgue integrable*:

$$\int_{-\infty}^{\infty} \|f(t)\|_2^2 dt < \infty \quad (3.58)$$

where the norm $\|f(t)\|_2$ in (3.58) is the vector 2-norm introduced in Section 3.1.1 on page 16, see Equation (3.7). The set of all such signals is a Banach space under the norm

$$\|f\|_2 = \sqrt{\int_{-\infty}^{\infty} \|f(t)\|_2^2 dt} = \sqrt{\int_{-\infty}^{\infty} f(t)^* f(t) dt} \quad (3.59)$$

This space is called the *Lebesgue space* $\mathcal{L}_2(\mathbf{R}, \mathbf{R}^n)$ ($\mathcal{L}_2(\mathbf{R}, \mathbf{C}^n)$). The first argument gives the *domain* ($\mathcal{D}(f)$), or input space, and the second gives the *range* ($\mathcal{R}(f)$), or output space. Quite often in the literature these arguments are dropped for brevity. Thus, which version of the Lebesgue space is meant must be determined from the context. To avoid any confusing we will keep the arguments here. Notice the difference between the vector 2-norm:

$$\|f(t_0)\|_2 = \sqrt{f(t_0)^* f(t_0)} \quad (3.60)$$

for a given value of t_0 of t and the operator 2-norm:

$$\|f\|_2 = \sqrt{\int_{-\infty}^{\infty} f(t)^* f(t) dt} \quad (3.61)$$

The subspace of $\mathcal{L}_2(\mathbf{R}, \mathbf{R}^n)$ for which $f(t) = 0, \forall t < 0$ (causal time functions) is called a *Hardy space* $\mathcal{H}_2(\mathbf{R}, \mathbf{R}^n)$ under the norm (3.59) on the facing page.

Similarly to the operator 2-norm we may construct operator 1- and ∞ -norms.

- $\mathcal{L}_1(\mathbf{R}, \mathbf{R}^n)$ is the (Banach) space of *absolute-Lebesgue integrable* vector-valued functions of time:

$$\int_{-\infty}^{\infty} \|f(t)\|_1 dt = \int_{-\infty}^{\infty} \sum_{i=1}^n |f_i(t)| dt < \infty \quad (3.62)$$

with norm

$$\|f\|_1 = \int_{-\infty}^{\infty} \sum_{i=1}^n |f_i(t)| dt \quad (3.63)$$

$\mathcal{H}_1(\mathbf{R}, \mathbf{R}^n)$ is the subspace of $\mathcal{L}_1(\mathbf{R}, \mathbf{R}^n)$ for which $f(t) = 0, \forall t < 0$.

- $\mathcal{L}_{\infty}(\mathbf{R}, \mathbf{R}^n)$ is the (Banach) space of bounded real vector-valued functions of time:

$$\sup_{t \in \mathbf{R}} \max_i |f_i(t)| < \infty \quad (3.64)$$

with norm

$$\|f\|_{\infty} = \sup_{t \in \mathbf{R}} \max_i |f_i(t)| \quad (3.65)$$

$\mathcal{H}_{\infty}(\mathbf{R}, \mathbf{R}^n)$ is the subspace of $\mathcal{L}_{\infty}(\mathbf{R}, \mathbf{R}^n)$ for which $f(t) = 0, \forall t < 0$.

A large class of causal time domain signals have finite values for the above 3 norms and thus are members of all three spaces $\mathcal{H}_1(\mathbf{R}, \mathbf{R}^n)$, $\mathcal{H}_2(\mathbf{R}, \mathbf{R}^n)$ and $\mathcal{H}_{\infty}(\mathbf{R}, \mathbf{R}^n)$. The following example, taken from [Dai90], demonstrate some of the distinctions.

Example 3.4 (Hardy Spaces for Scalar Functions) Consider the two functions

$$f_1(t) = \begin{cases} 0 & \forall t < 0 \\ 2e^{-t/2} \sin(3t) & \forall t \geq 0 \end{cases} \quad (3.66)$$

$$f_2(t) = \begin{cases} 0 & \forall t < 0 \\ 1 & \forall t \geq 0 \end{cases} \quad (3.67)$$

Notice that $f_2(t)$ is the ordinary step functions. Now $f_1(t)$ belongs to all three spaces $\mathcal{H}_1(\mathbf{R}, \mathbf{R})$, $\mathcal{H}_2(\mathbf{R}, \mathbf{R})$ and $\mathcal{H}_{\infty}(\mathbf{R}, \mathbf{R})$. Both its absolute and its square are integrable from 0 to ∞ and it has finite peak. In contrast, the step function $f_2(t)$ is a member of $\mathcal{H}_{\infty}(\mathbf{R}, \mathbf{R})$ only, since neither of the 1- or 2-norms have finite values. $f_1(t)$ and $f_2(t)$ is shown in Figure 3.2 on the following page.

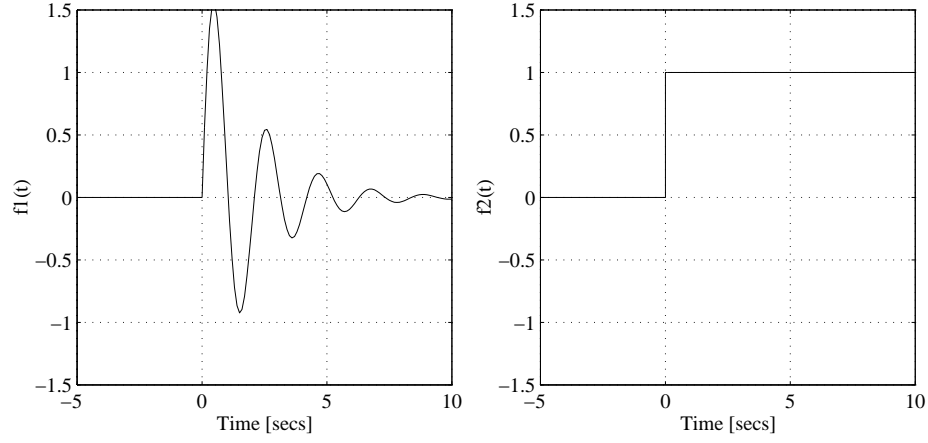


Figure 3.2: The functions $f_1(t)$ (left) and $f_2(t)$ (right).

In both the new robust control theory and the older LQG theory, only $\mathcal{L}_2(\mathbf{R}, \mathbf{R}^n)$ is used for time-domain signals. The operator 2-norm $\|f\|_2$ can be thought of as the (square root of the) energy of a signal and is obviously closely related to the root-mean-square (RMS) level of signals. The time domain spaces $\mathcal{L}_1(\mathbf{R}, \mathbf{R}^n)$ and $\mathcal{L}_\infty(\mathbf{R}, \mathbf{R}^n)$ do have potential engineering applications but the control theory for using them in design or analysis is not yet well-developed even though it is an area of intensive research. Since $\mathcal{L}_1(\mathbf{R}, \mathbf{R}^n)$ can represent fuel usage, and $\mathcal{L}_\infty(\mathbf{R}, \mathbf{R}^n)$ can treat the issue of actuator or sensor saturation, there are strong motivations for developing such theories.

Example 3.5 $\mathcal{L}_2(\mathbf{R}, \mathbf{R}^n)$ and $\mathcal{L}_2(\mathbf{R}, \mathbf{C}^n)$ are Hilbert spaces under the scalar product

$$\langle f, g \rangle = \int_{-\infty}^{\infty} f(t)^* g(t) dt \quad (3.68)$$

The corresponding induced norm is the 2-norm since

$$\|f\| = \langle f, f \rangle^{1/2} = \sqrt{\int_{-\infty}^{\infty} f(t)^* f(t) dt} = \sqrt{\int_{-\infty}^{\infty} \|f(t)\|_2^2 dt} = \|f\|_2 \quad (3.69)$$

3.3.2 Frequency Domain Spaces

Now consider the vector valued function $f(j\omega)$ which is defined for all frequencies $-\infty < \omega < \infty$ (that is, on the imaginary axis), takes values in \mathbf{C}^n and is square-Lebesgue integrable on the imaginary axis. The space of all such functions is a Hilbert space under the scalar product

$$\langle f, g \rangle = \frac{1}{2\pi} \int_{-\infty}^{\infty} f(j\omega)^* g(j\omega) d\omega \quad (3.70)$$

It is denoted the Lebesgue space $\mathcal{L}_2(j\mathbf{R}, \mathbf{C}^n)$. The corresponding induced norm is

$$\|f\| = \langle f, f \rangle^{1/2} = \sqrt{\frac{1}{2\pi} \int_{-\infty}^{\infty} f(j\omega)^* f(j\omega) d\omega} = \|f\|_2 \quad (3.71)$$

Next, $\mathcal{H}_2(\mathbf{C}, \mathbf{C}^n)$ is the (Hardy) space of all functions $f(s)$ which are analytic in $\Re(s) > 0$ (i.e., no right half plane (RHP) poles), take values in \mathbf{C}^n and satisfy the *uniform square-integrability condition*

$$\sup_{\xi} \frac{1}{2\pi} \int_{-\infty}^{\infty} f(\xi + j\omega)^* f(\xi + j\omega) d\omega < \infty \quad (3.72)$$

Functions in $\mathcal{H}_2(\mathbf{C}, \mathbf{C}^n)$ are not defined *a priori* on the imaginary axis. However, we can get there in the limit. If $f(s) \in \mathcal{H}_2(\mathbf{C}, \mathbf{C}^n)$ then the limit

$$\tilde{f}(j\omega) = \lim_{\xi \rightarrow 0} f(\xi + j\omega) \quad (3.73)$$

exists and belong to $\mathcal{L}_2(j\mathbf{R}, \mathbf{C}^n)$. The mapping $f(s) \rightarrow \tilde{f}(j\omega)$ from $\mathcal{H}_2(\mathbf{C}, \mathbf{C}^n)$ to $\mathcal{L}_2(j\mathbf{R}, \mathbf{C}^n)$ is norm-preserving. It is therefore customary to consider $\mathcal{H}_2(\mathbf{C}, \mathbf{C}^n)$ as a Hilbert space under the scalar product (3.70) and with induced norm (3.71).

Notice that we have used the same notation for the time- and frequency domain operator 2-norm $\|f\|_2$. It can be shown that they are closely related. To do so we need the following definition

Definition 3.1 (Isomorphisms) *Let H_1 and H_2 be normed space. An operator U from H_1 into H_2 is called an isometry, if $\mathcal{D}(U) = H_1$ (the domain of U is H_1) and $\|Uf\|_2 = \|f\|_1$ (the norm of f on H_1 equals the norm of Uf on H_2) for all $f \in H_1$. An isometry U from H_1 into H_2 is called an isomorphism of H_1 onto H_2 if $\mathcal{R}(U) = H_2$ (the range of U is H_2). Thus an isomorphism is a one-to-one mapping from one normed space to another which preserves norms.*

We then have the following important lemma, see e.g. [Fra87].

Lemma 3.3 (Fourier Transform) *The Fourier transform is a Hilbert space isomorphism from the time domain Lebesgue space $\mathcal{L}_2(\mathbf{R}, \mathbf{R}^n)$ to the frequency domain Lebesgue space $\mathcal{L}_2(j\mathbf{R}, \mathbf{C}^n)$ and from the time domain Hardy space $\mathcal{H}_2(\mathbf{R}, \mathbf{R}^n)$ to the frequency domain Hardy space $\mathcal{H}_2(\mathbf{C}, \mathbf{C}^n)$.*

Lemma 3.3 says in particular that $\mathcal{H}_2(\mathbf{C}, \mathbf{C}^n)$ is just the set of Laplace transforms of signals in $\mathcal{H}_2(\mathbf{R}, \mathbf{R}^n)$. Furthermore, if $f(t) \in \mathcal{H}_2(\mathbf{R}, \mathbf{R}^n)$, then its Laplace transform $f(s) \in \mathcal{H}_2(\mathbf{C}, \mathbf{C}^n)$ and

$$\sqrt{\int_0^\infty f(t)^* f(t) dt} = \sqrt{\frac{1}{2\pi} \int_{-\infty}^\infty f(j\omega)^* f(j\omega) d\omega} \quad (3.74)$$

since they are related by a norm preserving isomorphism. Equation (3.74) can also be recognized as a result of *Parseval's Theorem*.

Finally we will present 4 frequency domain spaces of matrix-valued functions.

- $\mathcal{L}_2(j\mathbf{R}, \mathbf{C}^{m \times n})$ is the space of all functions $F(j\omega)$, defined on the imaginary axis, which take values in $\mathbf{C}^{m \times n}$ and are square-integrable on the imaginary axis. $\mathcal{L}_2(j\mathbf{R}, \mathbf{C}^{m \times n})$ is a Hilbert space under the scalar product

$$\langle F, G \rangle = \frac{1}{2\pi} \int_{-\infty}^\infty \text{tr} \{F(j\omega)^* G(j\omega)\} d\omega \quad (3.75)$$

The corresponding induced norm is given by

$$\|F\|_2 = \langle F, F \rangle^{1/2} = \sqrt{\frac{1}{2\pi} \int_{-\infty}^\infty \text{tr} \{F(j\omega)^* F(j\omega)\} d\omega} \quad (3.76)$$

- $\mathcal{H}_2(\mathbf{C}, \mathbf{C}^{m \times n})$ is the space of all functions $F(s)$ which are analytical in $\Re(s) > 0$ (no RHP poles), take values in $\mathbf{C}^{m \times n}$ and satisfy the uniform square-integrability condition

$$\sup_{\xi > 0} \frac{1}{2\pi} \int_{-\infty}^\infty \text{tr} \{F(\xi + j\omega)^* F(\xi + j\omega)\} d\omega < \infty \quad (3.77)$$

Using similar arguments as in the $\mathcal{H}_2(\mathbf{C}, \mathbf{C}^n)$ case it is customary to consider $\mathcal{H}_2(\mathbf{C}, \mathbf{C}^{m \times n})$ as a Hilbert space under the scalar product (3.75) and with induced norm (3.76).

- $\mathcal{L}_\infty(j\mathbf{R}, \mathbf{C}^{m \times n})$ is the space of all functions $F(j\omega)$, defined on the imaginary axis, which take values in $\mathbf{C}^{m \times n}$ and are bounded on the imaginary axis:

$$\sup_{\omega \in \mathbf{R}} \|F(j\omega)\|_2 < \infty \quad (3.78)$$

The 2-norm in (3.78) on the facing page is the usual (constant) matrix 2-norm, see (3.15) on page 17, which is equal to the maximum singular value. $\mathcal{L}_\infty(j\mathbf{R}, \mathbf{C}^{m \times n})$ is a Banach space under the norm

$$\|F\|_\infty = \sup_{\omega \in \mathbf{R}} \|F(j\omega)\|_2 = \sup_{\omega \in \mathbf{R}} \bar{\sigma}(F(j\omega)) \quad (3.79)$$

- $\mathcal{H}_\infty(\mathbf{C}, \mathbf{C}^{m \times n})$ is the space of all functions $F(s)$ which are analytic in $\Re(s) > 0$ (no RHP poles), take values in $\mathbf{C}^{m \times n}$ and are bounded in the RHP:

$$\sup_{\Re(s) > 0} \|F(s)\|_2 < \infty \quad (3.80)$$

With similar arguments as in the $\mathcal{H}_2(\mathbf{C}, \mathbf{C}^n)$ case it is customary to consider $\mathcal{H}_\infty(\mathbf{C}, \mathbf{C}^{m \times n})$ as a Banach space under the norm (3.79).

Notice that (frequency domain) functions in $\mathcal{L}_2(j\mathbf{R}, \mathbf{C}^{m \times n})$ and $\mathcal{L}_\infty(j\mathbf{R}, \mathbf{C}^{m \times n})$ are defined only on the imaginary axis, their domain is $j\mathbf{R}$. It is thus not meaningful to talk about their poles and zeros or their stability. They are simply frequency responses, not transfer functions. Conversely, the domain of functions in $\mathcal{H}_2(\mathbf{C}, \mathbf{C}^{m \times n})$ and $\mathcal{H}_\infty(\mathbf{C}, \mathbf{C}^{m \times n})$ is the entire complex plane \mathbf{C} . They are (stable) transfer functions, not just frequency responses.

$\mathcal{H}_2(\mathbf{C}, \mathbf{C}^{m \times n})$ and $\mathcal{H}_\infty(\mathbf{C}, \mathbf{C}^{m \times n})$ are stable spaces since they do not allow poles in the RHP. Transfer functions in $\mathcal{H}_2(\mathbf{C}, \mathbf{C}^{m \times n})$, however, must roll off at high frequencies to fulfill (3.77) on the facing page. In contrast, transfer functions in $\mathcal{H}_\infty(\mathbf{C}, \mathbf{C}^{m \times n})$ may maintain non-zero gain as $\omega \rightarrow \infty$. In terms of state-space realizations (A, B, C, D) , the D matrix must be zero for a transfer function in $\mathcal{H}_2(\mathbf{C}, \mathbf{C}^{m \times n})$.

3.3.3 Transfer Function Norms

Let $G(s) \in \mathcal{H}_2(\mathbf{C}, \mathbf{C}^{m \times n})$ be a stable transfer function matrix. The norm

$$\|G(s)\|_2 = \sqrt{\frac{1}{2\pi} \int_{-\infty}^{\infty} \text{tr} \{G(j\omega)^* G(j\omega)\} d\omega} \quad (3.81)$$

is then called the *transfer function 2-norm*. We will use the notation $\|G(s)\|_2$ to emphasize that we are dealing with a norm of a transfer function matrix. Methods for reliable and efficient computation of (3.81) are commercially available e.g. through the MATLAB *μ -Analysis and Synthesis Toolbox* [BDG⁺93].

An popular interpretation of the transfer function 2-norm goes as follows. Let the input-output relation be

$$y(s) = G(s)u(s) \quad (3.82)$$

and let $u(t)$ be a vector white noise process with covariance matrix $E\{u(t)u^T(t)\} = I$. Then the RMS output power of $y(t)$ is given by

$$E\{y^T(t)y(t)\} = \|G(s)\|_2^2 \quad (3.83)$$

Thus, the 2-norm measures the RMS response to white noise. All quadratic-norm control schemes, like e.g. LQ optimal control and Kalman-Bucy optimal filtering, minimizes the 2-norm of a closed loop transfer function matrix. In classical LQG theory, cost functions are given in the time domain. However, it is now well-known that they have frequency domain interpretations. Minimizing the 2-norm of a transfer function matrix thus controls the output for a specific input signal, namely vector white noise. In contrast, as we shall see shortly, minimizing the ∞ -norm of a transfer function matrix controls the output for a specified set of bounded input signals.

Let $G(s) \in \mathcal{H}_\infty(\mathbf{C}, \mathbf{C}^{m \times n})$ be a stable transfer function matrix. The norm

$$\|G(s)\|_\infty = \sup_{\omega} \bar{\sigma}(G(j\omega)) \quad (3.84)$$

is then called the *transfer function ∞ -norm*. Methods for reliable and efficient computation of (3.84) are commercially available e.g. through the MATLAB *μ -Analysis and Synthesis Toolbox* [BDG⁺93]. We then have the following lemma, see e.g. [Fra87].

Lemma 3.4 *If $G(s) \in \mathcal{H}_\infty(\mathbf{C}, \mathbf{C}^{m \times n})$, $y(s) = G(s)u(s)$ with $u(s) \in \mathcal{H}_2(\mathbf{C}, \mathbf{C}^n)$ then $y(s) \in \mathcal{H}_2(\mathbf{C}, \mathbf{C}^m)$ and*

$$\|G(s)\|_\infty = \sup_{u(s) \neq 0} \frac{\|G(s)u(s)\|_2}{\|u(s)\|_2} \quad (3.85)$$

where $\|\cdot\|_2$ is the frequency domain operator 2-norm (3.71) on page 27. Similarly if $u(t) \in \mathcal{H}_2(\mathbf{R}, \mathbf{R}^n)$, then $y(t) \in \mathcal{H}_2(\mathbf{R}, \mathbf{R}^m)$ and

$$\|G(s)\|_\infty = \sup_{u(t) \neq 0} \frac{\|y\|_2}{\|u\|_2} \quad (3.86)$$

where $\|\cdot\|_2$ is the time domain operator 2-norm (3.59) on page 24.

Thus the transfer function ∞ -norm can be interpreted as induced by the operator 2-norm. $\|G(s)\|_\infty$ is the transfer function analogue to the induced matrix 2-norm for a constant matrix; compare (3.85) with (3.13) on page 17. In contrast, $\|G(s)\|_2$ is the transfer function analogue to the Frobenius norm $\|A\|_F$ for a constant matrix. Like the Frobenius norm, the norm $\|G(s)\|_2$ is not an induced norm. Thus it is not equal to the maximum possible gain for any of the three operator norms $\|\cdot\|_1$, $\|\cdot\|_2$ or $\|\cdot\|_\infty$. Conversely, the transfer function ∞ -norm equals the maximum possible gain in signal energy measured by the operator 2-norm for a set of bounded input signals, namely $u(t) \in \mathcal{H}_2(\mathbf{R}, \mathbf{R}^n)$.

3.4 Summary

Sets, norms and spaces frequently used in robust control theory were discussed. It was illustrated how the familiar vector p -norms induce corresponding matrix norms. Of particular interest are the matrix 1, 2 and ∞ norms partly because they have obvious physical interpretations and partly because they can be effectively computed. In “classical” robust control theory the main emphasis has been put on the matrix 2-norm. However, recently also the 1- and ∞ -norm have attracted considerable attention. It is well known that the matrix 2-norm equals the maximum singular value. In Section 3.1.2 on page 18 a thorough introduction to singular values and the singular value decomposition were given. The singular value concept has played a key role in modern control theory for a number of reasons, in particular because it enables us to extend the classical Bode plot to multivariable systems. A well known problem with multivariable systems is that the “gain” of a transfer function matrix is not unique: it depends on the direction of the input vector. The maximum (minimum) singular value measures the maximum (minimum) possible gain of a transfer matrix frequency response $G(j\omega)$ in terms of the 2-norm of the input vector before and after multiplication by $G(j\omega)$. Thus the gain of $G(j\omega)$ is bounded by its maximum and minimum singular value as the input vector varies over all possible directions. By plotting the singular values $\bar{\sigma}(G(j\omega))$ and $\underline{\sigma}(G(j\omega))$ for each frequency ω we obtain a *singular value Bode plot*; the multivariable generalization of the classical magnitude Bode plot.

Next, Banach and Hilbert spaces were introduced. In particular, Lebesgue and Hardy were considered. These spaces are standard in robust control theory. We then illustrated how the concepts introduced for constant vectors and matrices can be extended to linear spaces whose elements are time domain or frequency domain functions. In particular, the transfer function 2-norm and the transfer function ∞ -norm were considered. An important interpretation of the transfer function ∞ -norm is that it is induced by the frequency domain 2-norm and thus represents the transfer function analogue to the induced matrix 2-norm for a constant matrix. The transfer function ∞ -norm equals the supremum over frequency of the maximum singular value. Thus it measures the maximum gain of $G(j\omega)$ for all input directions and all frequencies. Furthermore, it was shown that the transfer function ∞ -norm also equals the maximum possible gain in signal energy measured by the time domain 2-norm for a signals in $\mathcal{H}_2(\mathbf{R}, \mathbf{R}^n)$.

Chapter 4

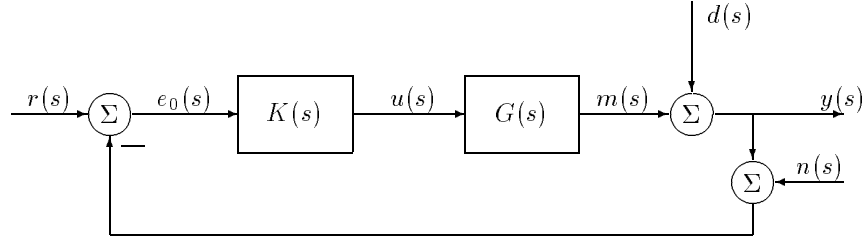
Robust Control Design using Singular Values

Contents

4.1	Nominal Stability	35
4.2	Nominal performance	36
4.3	Robust Stability	42
4.3.1	The Small Gain Theorem	43
4.4	Robust Performance	49
4.5	Computing the \mathcal{H}_∞ Optimal Controller	55
4.5.1	Remarks on the \mathcal{H}_∞ Solution	58
4.6	Discrete-Time Results	61
4.7	Summary	61

Consider the general multivariable feedback scheme shown in Figure 4.1 on the following page. The plant and controller transfer function matrix are denoted $G(s)$ and $K(s)$ respectively.

Notice that the control configuration in Figure 4.1 on the next page is a *one-degree-of-freedom* control configuration. Disturbances $d(s)$ and reference sig-

Figure 4.1: *General feedback control configuration.*

nals $r(s)$ have apart from the sign the same effect on the control error $e(s) = r(s) - y(s)$. If r and d vary in a similar manner then one only a single controller is needed to compensate for r and d in e . However, if d and r behave differently then using a one-degree-of-freedom control scheme some compromise has to be found. If there are strict requirements on both set-point tracking and disturbance attenuation, an acceptable compromise might not exist. Then additional controller blocks have to be included into the control configuration. For example, a pre-compensator on $r(s)$ is often included to improve the transient response of the closed loop system. Using *two-degree-of-freedom* control configurations design of the feedback controller $K(s)$ and the pre-compensator can be handled sequentially and independently. First the feedback compensator $K(s)$ is designed to fulfill the following goals:

- Nominal closed loop stability.
- Rejection of disturbances and measurement noise for the nominal closed loop system (nominal performance).
- Robust closed loop stability.
- Robust performance.

Robust stability means that the closed loop system is stable under all possible perturbations to the plant $G(s)$. Robust performance will be used to indicate that the closed loop system is stable and that the performance requirements are met under all possible perturbations to the plant $G(s)$.

Having determined the feedback controller $K(s)$ it can secondly be judged whether a pre-compensator is needed to improve the transient response properties of the controlled system. The determination of such a compensator is then reduced to an open loop problem which can usually be solved through simple pole-zero cancellations.

In this work we will deal exclusively with the feedback problem.

4.1 Nominal Stability

The stability of a multivariable feedback control system is determined by the extended or generalized Nyquist stability criterion [MZ89].

Theorem 4.1 (Generalized Nyquist Stability Criterion I) *If the open loop transfer function matrix $G(s)K(s)$ has p poles in the right-half s -plane, then the closed loop system is stable if and only if the map of $\det(I + G(s)K(s))$, as s traverses the Nyquist \mathcal{D} contour once, encircles the origin p times anticlockwise assuming no right-half s -plane zero-pole cancellations have occurred forming the product $G(s)K(s)$.*

Remember that the Nyquist \mathcal{D} contour goes up the imaginary axis from the origin to infinity, then along a semicircular arc in the right half plane until it meets the negative imaginary axis and finally up to the origin. If any poles of $G(s)K(s)$ are encountered on the imaginary axis the contour is indented so as to exclude these poles.

An equivalent criterion can be established using *characteristic loci*. If $\lambda_i(\omega)$ denotes an eigenvalue of $G(j\omega)K(j\omega)$ the *characteristic loci* is defined as the graphs of $\lambda_i(\omega)$ for $1 \leq i \leq n$ where n is the size of the product $G(s)K(s)$ as $j\omega$ encircles the Nyquist \mathcal{D} contour. Now let $\Delta \arg$ [rad] denote the change in the argument as s traverses the \mathcal{D} contour so that $\Delta \arg / (2\pi)$ equals the number of origo encirclements. Since the determinant equals the product of the eigenvalues we then have that

$$\Delta \arg \{ \det(I + G(s)K(s)) \} = \Delta \arg \left\{ \prod_i \lambda_i(I + G(s)K(s)) \right\} \quad (4.1)$$

$$= \Delta \arg \left\{ \prod_i (1 + \lambda_i(G(s)K(s))) \right\} \quad (4.2)$$

$$= \sum_i \Delta \arg (1 + \lambda_i(G(s)K(s))) \quad (4.3)$$

Since the number of encirclements of $1 + \lambda_i(G(j\omega)K(j\omega))$ around origo equals the number of encirclements of $\lambda_i(G(j\omega)K(j\omega))$ around the Nyquist point -1 we thus have the equivalent generalized Nyquist criterion in Theorem 4.2 on the following page.

Theorem 4.2 (Generalized Nyquist Stability Criterion II) *If the open loop transfer function matrix $G(s)K(s)$ has p poles in the right-half s -plane, then the closed loop system is stable if and only if the characteristic loci of $G(s)K(s)$ encircle the point $(-1 + 0j)$ p times anticlockwise assuming no right-half s -plane zero-pole cancellations have occurred.*

The Generalized Nyquist Stability Criterion will be used in assessing not only nominal stability but also robust stability of an uncertain closed loop system, see Section 4.3 on page 42.

4.2 Nominal performance

From Figure 4.1 on page 34 it is easily seen that

$$y(s) = T_o(s) (r(s) - n(s)) + S_o(s)d(s) \quad (4.4)$$

$$e_o(s) = S_o(s) (r(s) - d(s) - n(s)) \quad (4.5)$$

$$e(s) = r(s) - y(s) = S_o(s) (r(s) - d(s)) + T_o(s)n(s) \quad (4.6)$$

$$u(s) = M_o(s) (r(s) - n(s) - d(s)) \quad (4.7)$$

where

$$T_o(s) = (I + G(s)K(s))^{-1} G(s)K(s) = G(s)K(s) (I + G(s)K(s))^{-1} \quad (4.8)$$

$$S_o(s) = (I + G(s)K(s))^{-1} \quad (4.9)$$

$$M_o(s) = K(s) (I + G(s)K(s))^{-1} = (I + K(s)G(s))^{-1} K(s) \quad (4.10)$$

are the complementary sensitivity, sensitivity and control sensitivity functions respectively. The subscript $(\cdot)_o$ emphasizes that the sensitivity functions are all evaluated at the plant output. Since matrix multiplication is not commutative $G(s)K(s) \neq K(s)G(s)$ in general. It is thus necessary to distinguish between the sensitivity functions evaluated at the plant input and at the plant output, i.e. at the actuators and the sensors respectively. The sensitivity functions at the plant input are given by:

$$T_i(s) = K(s)G(s) (I + K(s)G(s))^{-1} = (I + K(s)G(s))^{-1} K(s)G(s) \quad (4.11)$$

$$S_i(s) = (I + K(s)G(s))^{-1} \quad (4.12)$$

$$M_i(s) = (I + K(s)G(s))^{-1} K(s) = M_o(s) \quad (4.13)$$

It is seen that $M_i(s) = M_o(s) = M(s)$, so the control sensitivity is independent of the chosen loop breaking point. The relevance of the input sensitivities will become clear shortly.

Now let $\delta(s) = r(s) - d(s)$ denote the “generic” external disturbance. Then from Equation (4.4)-(4.7) on the facing page the following observations can be made

- For good disturbance error reduction, that is for $\delta(s)$ to affect $e(s)$ to the least extent, (4.6) on the facing page shows that the sensitivity $S_o(s)$ should be small.
- For good sensor noise error reduction, that is for $n(s)$ to affect $e(s)$ to the least extent, (4.6) on the facing page shows that the complementary sensitivity $T_o(s)$ should be small.
- For disturbances $\delta(s)$ and noise $n(s)$ to affect the control input $u(s)$ to the least extent Equation (4.7) on the facing page shows that the control sensitivity $M(s)$ should be small.

For scalar systems the size of the (scalar) transfer functions $S_o(s)$, $T_o(s)$ and $M(s)$ are naturally measured by the absolute value of the complex valued frequency responses $|S_o(j\omega)|$, $|T_o(j\omega)|$ and $|M(j\omega)|$. However, for multivariable systems the frequency responses $S_o(j\omega)$, $T_o(j\omega)$ and $M(j\omega)$ will be complex valued matrices. Thus some scalar measure of the size of a complex valued matrix is needed. Since eigenvalues are used in Theorem 4.2 on the facing page it is tempting to use the *spectral radius* ρ

$$\rho(A) = \max_i |\lambda_i(A)| \quad (4.14)$$

as measure. However, it is a well known fact that eigenvalues may give poor indication of the “gain” of a transfer function matrix $G(j\omega)$ if the gain is measured as the 2-norm ratio of the output $y(j\omega)$ to the input $u(j\omega)$, see Example 4.1. As discussed in Chapter 3 there is a sound physical motivation for using the *2-norm gain* as measure for the size of $G(j\omega)$. Other equally well motivated measures (norms) exists, but the control theory is not yet fully developed for these measures.

In Chapter 3 it was shown that the *singular values* of $G(j\omega)$ for all $\omega \geq 0$ is the multivariable generalizations of the SISO amplitude Bode plot if we use the 2-norm as measure.

Example 4.1 (Eigenvalues and Singular Values) Consider the plant $G(s)$ is given by:

$$G(s) = \begin{bmatrix} 7 & -8 \\ -6 & 7 \end{bmatrix} \begin{bmatrix} \frac{1}{s+1} & 0 \\ 0 & \frac{2}{s+2} \end{bmatrix} \begin{bmatrix} 7 & -8 \\ -6 & 7 \end{bmatrix} \quad (4.15)$$

$$= \frac{1}{(s+1)(s+2)} \begin{bmatrix} 2-47s & -56s \\ 42s & 2+50s \end{bmatrix} \quad (4.16)$$

In Figure 4.2 the size of the eigenvalues $|\lambda_i(G(j\omega))|$ are compared with the singular values $\sigma_i(G(j\omega))$. Notice that the eigenvalues do not show that the 2-norm gain of the system is very dependent on the direction of the input vector. The current example is a slightly modified version of Example 1 in [Ber94].

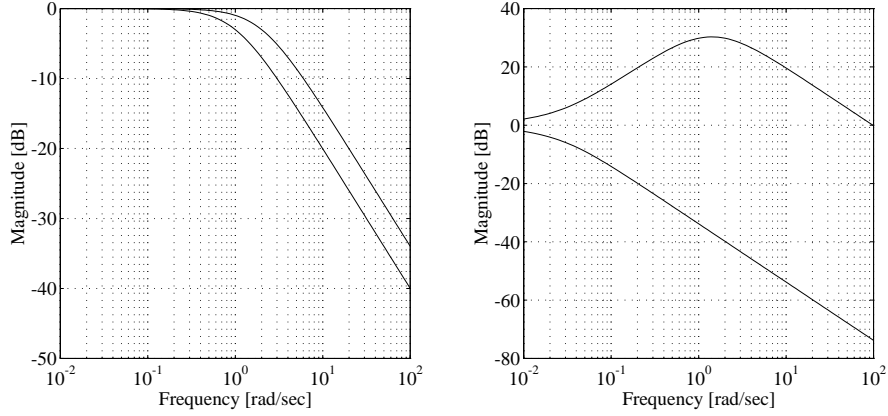


Figure 4.2: The eigenvalues (left) and singular values (right) of $G(j\omega)$.

Let us then return to the sensitivity functions $S_o(s)$, $T_o(s)$ and $M(s)$. Using largest singular value as measure, we may now specify standard performance requirements in terms of the maximum singular value. For good rejection of generic disturbances $\delta(s)$ we will e.g. require that:

$$\bar{\sigma}(S_o(j\omega)) = \|S_o(j\omega)\|_2 \ll 1 \quad (4.17)$$

Similarly, for good sensor noise rejection we will require:

$$\bar{\sigma}(T_o(j\omega)) = \|T_o(j\omega)\|_2 \ll 1 \quad (4.18)$$

and for low sensitivity of the input to noise and disturbances

$$\bar{\sigma}(M(j\omega)) = \|M(j\omega)\|_2 \ll 1 \quad (4.19)$$

However, because $T_o(j\omega) + S_o(j\omega) = I$ the sensitivity $S_o(j\omega)$ and the complementary sensitivity $T_o(j\omega)$ cannot both be small in the same frequency range. Consequently it is demonstrated by (4.17) and (4.18) that optimal tracking or disturbance rejection and optimal sensor noise rejection cannot be obtained *in*

the same frequency range! This is a well-known result from classical control. Fortunately the spectra of disturbances $\delta(s)$ are usually concentrated at low frequencies whereas the spectra of measurement noise $n(s)$ is concentrated at higher frequencies. Thus one may shape the complementary sensitivity $T_o(j\omega)$ and the sensitivity $S_o(j\omega)$ such that $\bar{\sigma}(S_o(j\omega))$ is small at low frequencies and $\bar{\sigma}(T_o(j\omega))$ is small at high frequencies. In modern process control systems, sensor noise will frequently not be of primary concern. However, as we shall see in the next section, robustness to unstructured uncertainty places bounds on the sensitivity functions as well.

Applying weighting functions on the sensitivity functions we may select the frequency area of interest. A typical performance specification for robust control is given as a weighted sensitivity specification:

$$\sup_{\omega} \bar{\sigma}(W_{p2}(j\omega)S_o(j\omega)W_{p1}(j\omega)) = \|W_{p2}(s)S_o(s)W_{p1}(s)\|_{\infty} \leq 1 \quad (4.20)$$

where $W_{p1}(s)$ and $W_{p2}(s)$ denotes the input and output weight respectively, see Figure 4.3. It is assumed that the weights have been scaled such that a unity bound on the RHS makes sense. The norm $\|\cdot\|_{\infty}$ in (4.20) is the transfer function ∞ norm introduced in Section 3.3.3 on page 29.

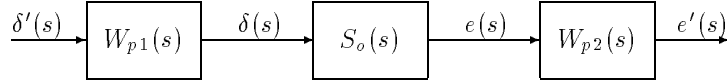


Figure 4.3: *Output sensitivity $S_o(s)$ with input weight $W_{p1}(s)$ and output weight $W_{p2}(s)$.*

The *normalized input vector* $\delta'(s)$ is assumed to belong to the Hardy space $\mathcal{H}_2(\mathbf{C}, \mathbf{C}^n)$ with norm bounded by 1.

$$\mathcal{D}' = \left\{ \delta'(s) \left| \|\delta'\|_2 = \frac{1}{2\pi} \sqrt{\int_{-\infty}^{\infty} \delta(j\omega)^* \delta(j\omega) d\omega} \leq 1 \right. \right\} \quad (4.21)$$

The input weight $W_{p1}(s)$ is used to transform the normalized inputs $\delta'(s)$ to the physical inputs $\delta(s) = W_{p1}(s)\delta'(s)$. For example, disturbances δ are usually expected to have small amplitude at high frequencies. Thus, if disturbance rejection is of primary interest a low pass filter would be a possible choice for $W_{p1}(s)$. If step set-point changes are most important we should choose an input weight such that the physical input $\delta(s) = s^{-1}$, see Example 4.2 on the following page.

Also if the physical inputs are measured in different units, $W_{p1}(s)$ can be used to normalize $\delta(s)$ such that $\delta'(s)$ have equal relative magnitude.

Example 4.2 (Performance Input Weights) *The following example is from [MZ89]. Assume that we expect steps on $\delta(s)$. Thus we must choose an input weight $W_{p1}(s)$ such that $\delta(s) = s^{-1}$ and $\delta'(s) \in \mathcal{D}'$. For scalar systems a seemingly obvious choice would be $W_{p1}(s) = s^{-1}$ corresponding to an impulse on the normalized input $\delta'(s)$. However, $\delta'(s) = 1$ is **not** a member of the set \mathcal{D}' since the integral becomes unbounded. Thus this will not work. The weight*

$$W_{p1}(s) = \frac{s + \beta}{s\sqrt{2\beta}} \quad \beta > 0 \quad (4.22)$$

has the desired characteristics since the normalized input

$$\delta'(s) = \frac{\sqrt{2\beta}}{s + \beta} \quad (4.23)$$

satisfies

$$\|\delta'\|_2 = \sqrt{\frac{1}{2\pi} \int_{-\infty}^{\infty} \delta(j\omega)^* \delta(j\omega) d\omega} = \sqrt{\frac{1}{2\pi} \int_{-\infty}^{\infty} \frac{2\beta}{\omega^2 + \beta^2} d\omega} = 1 \quad (4.24)$$

so that $\delta'(s) \in \mathcal{D}'$ and $\delta(s)$ will be given by

$$\delta(s) = W_{p1}(s)\delta'(s) = \frac{s + \beta}{s\sqrt{2\beta}} \frac{\sqrt{2\beta}}{s + \beta} = \frac{1}{s} \quad (4.25)$$

The physical inputs $\delta(s)$ are consequently assumed to belong to the set

$$\mathcal{D} = \left\{ \delta(s) \mid \|W_{p1}^{-1}\delta\|_2 \leq 1 \right\} \quad (4.26)$$

Treating sets of generic disturbances $\delta(s)$ is attractive because at the design stage it is rarely possible to predict exactly what type of set-point changes $r(s)$ or disturbances $d(s)$ are going to occur during actual operation. Of course, in principle, the control performance could deteriorate significantly if the assumed disturbances for the design is not exactly equal to the input encountered in practice.

The output weight $W_{p2}(s)$ is used to trade off the relative importance of the individual errors in $e(s)$ and to weigh the frequency range of primary interest.

Using Lemma 3.4 on page 30 we may give the following interpretation of the performance specification (4.20) on the preceding page. Let \mathcal{D}'_t denote the set of

normalized causal inputs in the time domain

$$\mathcal{D}'_t = \left\{ \delta'(t) \left| \|\delta'\|_2 = \sqrt{\int_0^\infty \delta'(t)^T \delta'(t) dt} \leq 1 \right. \right\} \quad (4.27)$$

Clearly $\delta'(t)$ belongs to the Hardy space $\mathcal{H}_2(\mathbf{R}, \mathbf{R}^n)$. If $\delta'(t) \in \mathcal{D}'_t$ then $\delta'(s) \in \mathcal{D}'$. Then if $W_{p2}(s)S_o(s)W_{p1}(s) \in \mathcal{H}_\infty(\mathbf{C}, \mathbf{C}^{m \times n})$ (a stable proper transfer function matrix with no poles on the imaginary axis) the normalized output $e'(t)$ will belong to $\mathcal{H}_2(\mathbf{R}, \mathbf{R}^n)$ and the 2-norm of $e'(t)$ will be bounded by

$$\sup_{\delta'(t) \in \mathcal{D}'_t} \|e'\|_2 = \sup_{\delta'(t) \in \mathcal{D}'_t} \sqrt{\int_0^\infty e'(t)^T e'(t) dt} = \|W_{p2}(s)S_o(s)W_{p1}(s)\|_\infty \quad (4.28)$$

The nominal performance objective is then defined as follows.

Definition 4.1 (Nominal Performance Problem) *The nominal performance problem is, given weighting functions $W_{p1}(s)$ and $W_{p2}(s)$, to design a stabilizing controller $K(s)$ such that the cost function*

$$\mathcal{J}_{np} = \|W_{p2}(s)S_o(s)W_{p1}(s)\|_\infty \quad (4.29)$$

is minimized. Thus

$$K(s) = \arg \min_{K(s) \in \mathcal{K}_S} \|W_{p2}(s)S_o(s)W_{p1}(s)\|_\infty \quad (4.30)$$

*where \mathcal{K}_S denotes the set of all stabilizing controllers and $\inf(\cdot)$ denotes the infimum. If a controller can achieve $\|W_{p2}(s)S_o(s)W_{p1}(s)\|_\infty < 1$, we say that the closed loop system has **nominal performance**.*

A very convenient way of formulating the nominal performance problem is by use of the *2x2 Block Problem Formulation*. In Figure 4.4 on the next page it is shown how the weights $W_{p1}(s)$ and $W_{p2}(s)$ may be include into the closed loop system in Figure 4.1 on page 34 if disturbance attenuation is considered. The augmented closed loop system may then be represented as a 2×2 block problem. The *generalized plant* $N(s)$ contains the nominal plant $G(s)$ as well as weighting functions to reflect nominal performance objectives. If set-point changes are of primary importance $d'(s)$ may be replaced by a normalized reference $r'(s)$.

The transfer function from $d'(s)$ to $e'(s)$ is given by the *linear fractional transformation* (LFT):

$$e'(s) = F_l(N(s), K(s))d'(s) \quad (4.31)$$

$$= (N_{11}(s) + N_{12}(s)K(s)(I - N_{22}(s)K(s))^{-1}N_{21}(s)) d'(s) \quad (4.32)$$

$$= W_{p2}(s)S_o(s)W_{p1}(s)d'(s) \quad (4.33)$$

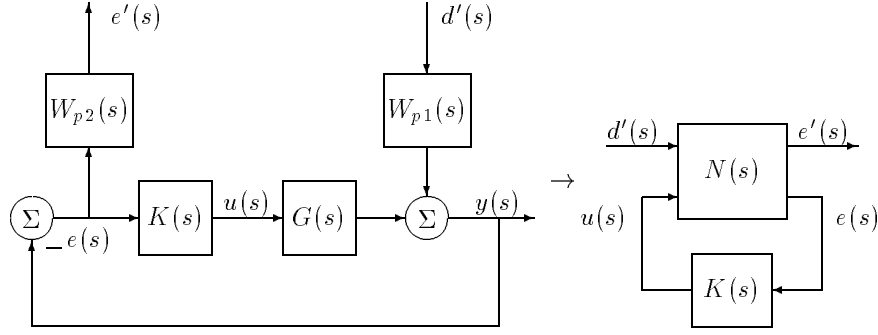


Figure 4.4: *Nominal performance problem. Augmented closed loop system and corresponding 2×2 block problem.*

Now the optimal nominal performance problem is one of finding a controller such that:

$$K(s) = \arg \min_{K(s) \in \mathcal{K}_S} \|F_l(N(s), K(s))\|_\infty \quad (4.34)$$

The problem (4.34) is a standard \mathcal{H}_∞ problem which can be solved with well-known techniques, see Section 4.5 on page 55.

The above formulation of performance objectives are not restricted to “ordinary” sensitivity problems. If e.g. disturbances enter the loop not only on the output $y(s)$ but also on the input or even as an additional input to $G(s)$ this will merely change the transfer matrix expression in (4.20) on page 39. Similar rejection of generic disturbances on both error $e(s)$ and control signal $u(s)$ may also easily be incorporated. However, we will then consider the complete transfer matrix from all disturbance inputs $d'(s)$ to all error signals $e'(s)$, thus including all cross-terms. True multi-objective performance measures cannot be considered in the standard \mathcal{H}_∞ framework.

4.3 Robust Stability

In the early 1980’s it was realized by a number of researchers, see e.g [DS81], that robustness to unmodeled dynamics place upper bounds on the sensitivity functions introduced in Section 4.2 on page 36.

Let $G(s)$ and $G_T(s)$ denote the nominal model and true system respectively. Then introduce the following perturbation models:

- Additive uncertainty: $G_T(s) = G(s) + \tilde{\Delta}(s)$.
- Input multiplicative uncertainty: $G_T(s) = G(s)(I + \tilde{\Delta}(s))$.
- Output multiplicative uncertainty: $G_T(s) = (I + \tilde{\Delta}(s))G(s)$.
- Inverse input multiplicative uncertainty: $G_T(s) = G(s)(I + \tilde{\Delta}(s))^{-1}$.
- Inverse output multiplicative uncertainty: $G_T(s) = (I + \tilde{\Delta}(s))^{-1}G(s)$.

The perturbation block $\tilde{\Delta}(s)$ is now assumed to be an unstructured full complex block bounded using the matrix 2-norm:

$$\|\tilde{\Delta}(j\omega)\|_2 = \bar{\sigma}(\tilde{\Delta}(j\omega)) \leq \ell(\omega), \quad \forall \omega \geq 0 \quad (4.35)$$

The perturbation $\tilde{\Delta}(j\omega)$ is thus a full complex matrix bounded in magnitude by a frequency dependent scalar. As before, the choice of the bounding norm is a compromise between those that best describe the plant perturbation and those that lead to tractable mathematical problems. Using the 2-norm the perturbation models above describes well the effects of high frequency unmodeled dynamics, infinite-dimensional electro-mechanical resonances and time delays. The perturbation structure (4.35) will, however, lead to conservative descriptions of structured uncertainty like parameter variations. An important reason for using the 2-norm to bound $\tilde{\Delta}(j\omega)$ is that it leads to simple expressions for robust stability.

Usually two diagonal weighting matrices $W_{u1}(s)$ and $W_{u2}(s)$ are introduced such that

$$\tilde{\Delta}(s) = W_{u2}(s)\Delta(s)W_{u1}(s) \quad (4.36)$$

and $\bar{\sigma}(\Delta)(j\omega) \leq 1, \forall \omega$. Usually the input weight $W_{u1}(s)$ is used to perform any necessary scaling and $W_{u2}(s)$ is used as a frequency weight to approximate $\ell(\omega)$. There is seldom any reason not to choose $W_{u1}(s)$ and $W_{u2}(s)$ as diagonal matrices.

4.3.1 The Small Gain Theorem

Now the celebrated *Small Gain Theorem*, see e.g. [DV75], will be introduced and applied in connection with the above uncertainty structures. Consider the closed loop system in Figure 4.1 on page 34 and let $P(s) = G(s)K(s)$ be a square transfer function matrix.

Theorem 4.3 (Small Gain Theorem) *Assume that $P(s)$ is stable. Then the closed loop system is stable if the spectral radius $\rho(P(j\omega)) < 1, \forall \omega$.*

Proof of Theorem 4.3 (By contradiction) Assume that the spectral radius $\rho(P(j\omega)) < 1, \forall \omega$ and that the closed loop system is unstable. Applying Theorem 4.1 on page 35 instability implies that the map of $\det(I + P(s))$ encircles the origin as s traverses the Nyquist \mathcal{D} contour. Because the Nyquist contour is closed so is the map of $\det(I + P(s))$. Then there exists an $\epsilon \in [0, 1]$ and a frequency ω^* such that

$$\det(I + \epsilon P(j\omega^*)) = 0 \quad \text{i.e. the map goes through the origin} \quad (4.37)$$

$$\Leftrightarrow \prod_i \lambda_i(I + \epsilon P(j\omega^*)) = 0 \quad (4.38)$$

$$\Leftrightarrow 1 + \epsilon \lambda_i(P(j\omega^*)) = 0 \quad \text{for some } i \quad (4.39)$$

$$\Leftrightarrow \lambda_i(P(j\omega^*)) = -\frac{1}{\epsilon} \quad \text{for some } i \quad (4.40)$$

$$\Rightarrow |\lambda_i(P(j\omega^*))| \geq 1 \quad \text{for some } i \quad (4.41)$$

which is a contradiction since we assumed that $\rho(P(j\omega)) < 1, \forall \omega$. \square

Theorem 4.3 states that for an open-loop stable system, a sufficient condition for closed loop stability is to keep the loop “gain” measured by $\rho(P(j\omega))$ less than unity. Fortunately this is only a sufficient condition for stability. Otherwise the usual performance requirement of high controller gain for low frequencies could not be achieved. Theorem 4.3 thus provides only a sufficient, that is, a potentially (very) conservative condition for stability.

The Small Gain Theorem will now be used to assess the closed loop stability under unstructured norm bounded perturbations of the form (4.35) on the preceding page. This application is classic in \mathcal{H}_∞ control theory. A famous and often quoted paper on this is [DS81]. Let us e.g. assume an additive perturbation:

$$G_T(s) = G(s) + W_{u2}(s)\Delta(s)W_{u1}(s) \quad (4.42)$$

where $\bar{\sigma}(\Delta(j\omega)) \leq 1$. This can be represented in block-diagram form as in Figure 4.5 on the facing page. Let $P(s)$ denote the transfer matrix “seen” by Δ , see also Figure 4.5 on the facing page. It is easily seen that

$$P(s) = W_{u1}(s)K(s)(I + G(s)K(s))^{-1}W_{u2}(s) \quad (4.43)$$

$$= W_{u1}(s)M(s)W_{u2}(s) \quad (4.44)$$

We then have the following theorem.

Theorem 4.4 (Robust Stability) *Assume that the interconnection $P(s)$ is stable and that the perturbation $\Delta(s)$ is of such a form that the perturbed closed*

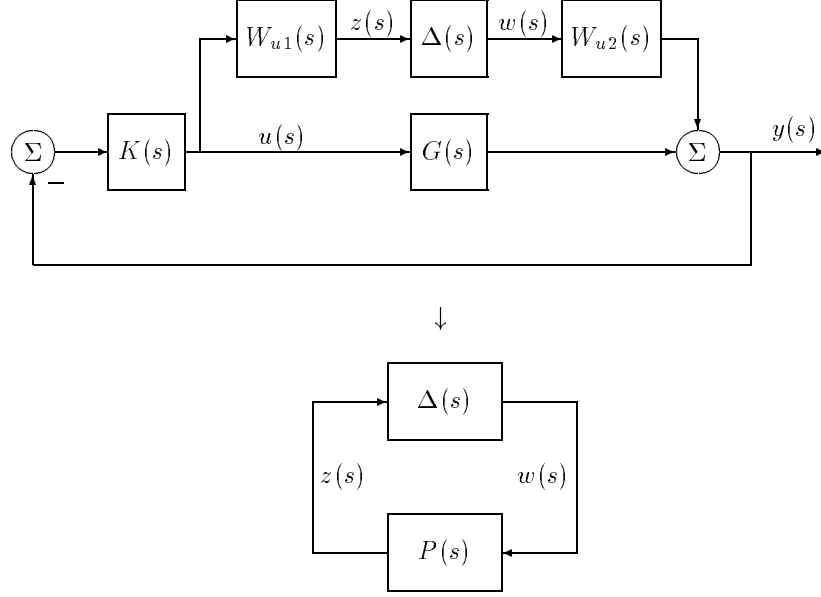


Figure 4.5: Closed loop system with additive perturbation. $P(s)$ denotes the transfer function “seen” by the perturbation Δ .

loop system is stable if and only if the map of $\det(I - P(s)\Delta(s))$ as s traverses the \mathcal{D} contour does not encircle the origin. Then the closed loop system in Figure 4.5 is stable for all perturbations $\Delta(s)$ with $\bar{\sigma}(\Delta(j\omega)) \leq 1$ if and only if one of the following four equivalent conditions are satisfied:

$$\det(I - P(j\omega)\Delta(j\omega)) \neq 0 \quad \forall \omega, \forall \Delta(j\omega) \ni \bar{\sigma}(\Delta(j\omega)) \leq 1 \quad (4.45)$$

$$\Leftrightarrow \rho(P(j\omega)\Delta(j\omega)) < 1 \quad \forall \omega, \forall \Delta(j\omega) \ni \bar{\sigma}(\Delta(j\omega)) \leq 1 \quad (4.46)$$

$$\Leftrightarrow \bar{\sigma}(P(j\omega)) < 1 \quad \forall \omega \quad (4.47)$$

$$\Leftrightarrow \|P(s)\|_{\infty} < 1 \quad (4.48)$$

Proof of Theorem 4.4 Assume that there exist a perturbation $\Delta^*(s)$ such that $\bar{\sigma}(\Delta^*(j\omega)) \leq 1$ and that the closed loop system is unstable. Then the map of $\det(I - P(s)\Delta(s))$ encircles the origin as s traverses the Nyquist \mathcal{D} contour. Because the Nyquist contour is closed so is the map of $\det(I - P(s)\Delta(s))$. Consequently there exists an $\epsilon \in [0, 1]$ and a frequency ω^* such that

$$\det(I - P(j\omega^*)\epsilon\Delta^*(j\omega^*)) = 0. \quad (4.49)$$

Since

$$\bar{\sigma}(\epsilon\Delta^*(j\omega^*)) = \epsilon\bar{\sigma}(\Delta^*(j\omega^*)) \leq 1 \quad (4.50)$$

$\epsilon\Delta^*(s)$ is just another perturbation from the set of possible perturbations. Thus the closed loop system is stable if and only if (4.45) on the preceding page is satisfied. The sufficiency of (4.46) on the page before follows directly from Theorem 4.3 on page 44. Since

$$\begin{aligned} \rho(P(j\omega)\Delta(j\omega)) &\leq \bar{\sigma}(P(j\omega)\Delta(j\omega)) \leq \bar{\sigma}(P(j\omega))\bar{\sigma}(\Delta(j\omega)) \\ &\leq \bar{\sigma}(P(j\omega)) \leq \|P(s)\|_\infty \end{aligned} \quad (4.51)$$

both (4.47) on the page before and (4.48) on the preceding page are sufficient conditions for closed loop stability.

To prove necessity of (4.46) on the page before assume that there exists a $\Delta^*(s)$ for which $\bar{\sigma}(\Delta^*(j\omega)) \leq 1$ and a frequency ω^* such that $\rho(P(j\omega^*)\Delta^*(j\omega^*)) = 1$. Then

$$|\lambda_i(P(j\omega^*)\Delta^*(j\omega^*))| = 1 \quad \text{for some } i \quad (4.52)$$

$$\Leftrightarrow \lambda_i(P(j\omega^*)\Delta^*(j\omega^*)) = e^{j\theta} \quad \text{for some } i \quad (4.53)$$

$$\Leftrightarrow \lambda_i(P(j\omega^*)e^{-j\theta}\Delta^*(j\omega^*)) = +1 \quad \text{for some } i \quad (4.54)$$

$$\Leftrightarrow \lambda_i(P(j\omega^*)\tilde{\Delta}^*(j\omega^*)) = +1 \quad \text{for some } i \quad (4.55)$$

where $\tilde{\Delta}^*(s)$ is just another perturbation from the set and $\rho(P(j\omega^*)\tilde{\Delta}^*(j\omega^*)) = 1$. Therefore

$$\det(I - P(j\omega^*)\tilde{\Delta}^*(j\omega^*)) = 0 \quad (4.56)$$

and the necessity of (4.46) on the preceding page) has been shown.

To prove necessity of (4.47) on the page before we will show that there exists a perturbation $\Delta^*(s)$ for which $\bar{\sigma}(\Delta^*(j\omega)) \leq 1$ such that $\det(I - P(j\omega^*)\Delta^*(j\omega^*)) = 0$ if $\bar{\sigma}(P(j\omega^*)) = 1$. To do so, let $D = \text{diag}\{1, 0, \dots, 0\}$ and perform a singular value decomposition of $P(j\omega^*)$:

$$P(j\omega^*) = U\Sigma V^H \quad (4.57)$$

where U and V are unitary matrices. Let $\Delta^*(j\omega^*) = VDU^H$. Since U and V are unitary $\bar{\sigma}(\Delta^*) = 1$. We then have that

$$\begin{aligned} \det(I - P(j\omega^*)\Delta^*(j\omega^*)) &= \det(I - U\Sigma V^H VDU^H) = \det(I - U\Sigma DU^H) = \\ &= \det(U(I - \Sigma D)U^H) = \det(U)\det(I - \Sigma D)\det(U^H) = \det(I - \Sigma D) = 0 \end{aligned} \quad (4.58)$$

since the first row and column in $I - \Sigma D$ are zero. In fact, there exists an infinite number of perturbations for which (4.58) is fulfilled since we may choose $D = \text{diag}\{1, \sigma_2, \dots, \sigma_k\}$ where $\sigma_i \leq 1$ for $i = 2, \dots, k$. \square

The above proof is due to Lethomaki [Let81]. Theorem 4.4 on page 44 states that if $\|P(s)\|_\infty < 1$, there is no perturbation $\Delta(s)$ ($\bar{\sigma}(\Delta(j\omega)) \leq 1$) which makes $\det(I - P(s)\Delta(s))$ encircle the origin as s traverses the Nyquist \mathcal{D} contour. Notice that we *assumed* that the absence of encirclements is necessary and sufficient to maintain stability. This is the case, for example, when all perturbations $\Delta(s)$ are stable or when $G_T(s)$ and $G(s)$ has the same number of unstable (right half plane) poles. Any one of these assumptions are standard in robust control.

Notice that the ∞ -norm constraint (4.48) on page 45 in Theorem 4.4 is *not* conservative since we have bounded the uncertainty in terms of the spectral norm (maximum singular value). Thus if $\|P(s)\|_\infty \geq 1$ there exists a perturbation $\Delta^*(s)$ for which $\bar{\sigma}(\Delta^*(j\omega)) \leq 1$ that will destabilize the closed loop system. If the uncertainty is tightly represented by $\Delta(s)$, then the singular value bound on $P(j\omega)$ is thus a tight robustness bound.

Now let us return to the additively perturbed closed loop system in Figure 4.5 on page 45. From Theorem 4.4 on page 44, robust stability of the closed loop system is thus obtained if and only if

$$\bar{\sigma}(P(j\omega)) < 1 \quad \forall \omega \quad (4.59)$$

$$\Leftrightarrow \bar{\sigma} \left(W_{u1}(j\omega)K(j\omega) (I + G(j\omega)K(j\omega))^{-1} W_{u2}(j\omega) \right) < 1 \quad \forall \omega \quad (4.60)$$

$$\Leftrightarrow \bar{\sigma} (W_{u1}(j\omega)M(j\omega)W_{u2}(j\omega)) < 1 \quad \forall \omega \quad (4.61)$$

As for additive uncertainty, we may compute singular value bounds that ensure robust stability under other perturbation models. In Table 4.1 results are given for the uncertainty structures introduced previously.

Perturbation	Stability Norm Bound
Additive uncertainty	$\ W_{u1}(s)M(s)W_{u2}(s)\ _\infty < 1$
Input multiplicative uncertainty	$\ W_{u1}(s)T_i(s)W_{u2}(s)\ _\infty < 1$
Output multiplicative uncertainty	$\ W_{u1}(s)T_o(s)W_{u2}(s)\ _\infty < 1$
Inverse input mult. uncertainty	$\ W_{u1}(s)S_i(s)W_{u2}(s)\ _\infty < 1$
Inverse output mult. uncertainty	$\ W_{u1}(s)S_o(s)W_{u2}(s)\ _\infty < 1$

Table 4.1: *Different uncertainty descriptions and their influence on the sensitivity functions.*

The robust stability objective is thus, given e.g. an additive uncertainty specification $W_{u2}(s)\Delta(s)W_{u1}(s)$, to design a nominally stabilizing controller $K(s)$ such

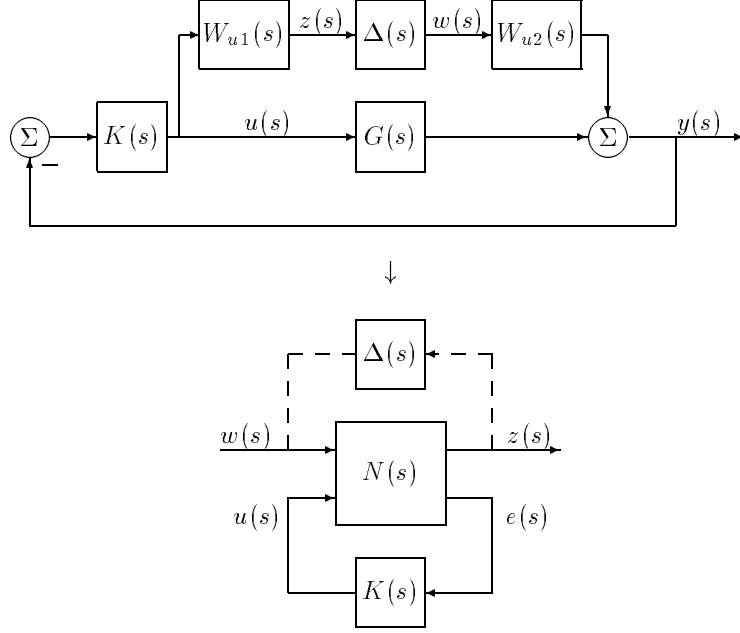


Figure 4.6: Uncertain closed loop system and corresponding 2×2 block problem.

that the cost function

$$\mathcal{J}_u = \|W_{u1}(s)M(s)W_{u2}(s)\|_\infty \quad (4.62)$$

is minimized. Thus

$$K(s) = \arg \min_{K(s) \in \mathcal{K}_S} \|W_{u1}(s)M(s)W_{u2}(s)\|_\infty \quad (4.63)$$

where \mathcal{K}_S denotes the set of all nominally stabilizing controllers. If a controller can achieve $\mathcal{J}_u < 1$, we say that the closed loop system is *robustly stable*. Notice then how the structure of the robust stability problem (4.63) equals the structure of the nominal performance problem (4.30) on page 41. Consequently the robust stability problem may be formulated as a 2×2 block problem as well. Given an additive uncertainty specification, a 2×2 block problem formulation may be derived, see Figure 4.6. Compare also with Figure 4.5 on page 45.

The transfer function from $w(s)$ to $z(s)$ is given by the LFT

$$z(s) = F_l(N(s), K(s))w(s) \quad (4.64)$$

$$= W_{u1}(s)K(s) (I + G(s)K(s))^{-1} W_{u2}(s)w(s) \quad (4.65)$$

$$= W_{u1}(s)M(s)W_{u2}(s)w(s) \quad (4.66)$$

The optimal robust stability problem is thus one of finding the controller given by

$$K(s) = \arg \min_{K(s) \in \mathcal{K}_s} \|F_l(N(s), K(s))\|_\infty \quad (4.67)$$

Like the nominal performance problem, the robust stability problem (4.67) is a standard \mathcal{H}_∞ problem with a known solution.

4.4 Robust Performance

The robust performance objective is derived from (4.29) on page 41 with nominal sensitivity $S_o(s)$ replaced by perturbed sensitivity $\tilde{S}_o(s)$:

$$\mathcal{J}_{rp} = \left\| W_{p2}(s)\tilde{S}_o(s)W_{p1}(s) \right\|_\infty \quad (4.68)$$

Let us once more illustrate with an additive uncertainty model. The robust performance problem can then be formulated as in Figure 4.7 on the following page.

Let $P(s) = F_l(N(s), K(s))$. Then the transfer function from $d'(s)$ to $e'(s)$ is given by the LFT

$$e'(s) = F_u(P(s), \Delta(s))d'(s) \quad (4.69)$$

$$= \left[P_{22}(s) + P_{21}(s)\Delta(s) (I - P_{11}(s)\Delta(s))^{-1} P_{12}(s) \right] d'(s) \quad (4.70)$$

$$= W_{p2}(s) (I + G(s)K(s) + G(s)W_{u2}(s)\Delta(s)W_{u1}(s))^{-1} W_{p1}(s) \quad (4.71)$$

$$= W_{p2}(s)\tilde{S}_o(j\omega)W_{p1}(s) \quad (4.72)$$

The optimal robust performance problem can then be formulated

$$K(s) = \arg \min_{K(s) \in \mathcal{K}_s} \sup_{\Delta(s) \ni \|\Delta(s)\|_\infty \leq 1} \|F_u(F_l(N(s), K(s)), \Delta(s))\|_\infty \quad (4.73)$$

If

$$\|F_u(F_l(N(s), K(s)), \Delta(s))\|_\infty = \|F_u(P(s), \Delta(s))\|_\infty < 1 \quad (4.74)$$

for all $\Delta(s)$ with $\|\Delta(s)\|_\infty \leq 1$, we say that the closed loop system has *robust performance*. Notice that the robust performance condition (4.74) is similar to the

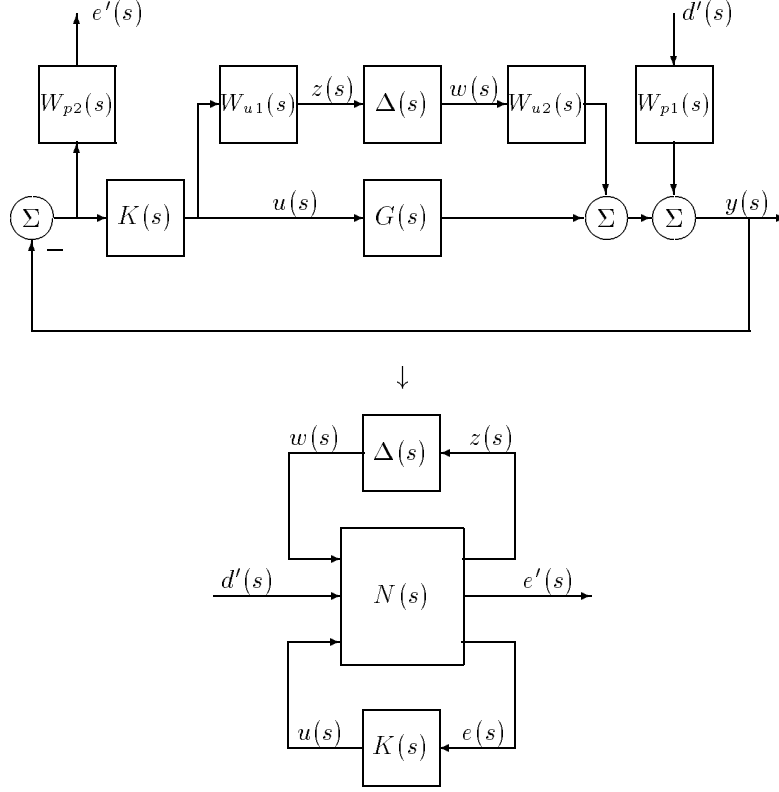


Figure 4.7: Robust performance problem with additive uncertainty.

robust stability condition (4.48) in Theorem 4.4 on page 44. Hence we conclude: *the system $F_u(P(s), \Delta(s))$ satisfies the robust performance condition (4.74) on the page before if and only if it is robustly stable for a norm bounded matrix perturbation $\Delta_p(s)$ with $\bar{\sigma}(\Delta_p(j\omega)) \leq 1$.* Thus by augmenting the perturbation structure with a full complex performance block $\Delta_p(s)$ the robust performance condition can be equivalenced with a robust stability condition, see also Figure 4.8 on the facing page.

Let $\tilde{\Delta}(s) = \text{diag}\{\Delta(s), \Delta_p(s)\}$ denote the augmented perturbation matrix. We then have the following theorem.

Theorem 4.5 (Robust Performance) *Assume that the interconnection $P(s) = F_l(N(s), K(s))$ is stable and that the perturbation $\tilde{\Delta}(s)$ is of such a form that the perturbed closed loop system in Figure 4.8 on the facing page is stable*

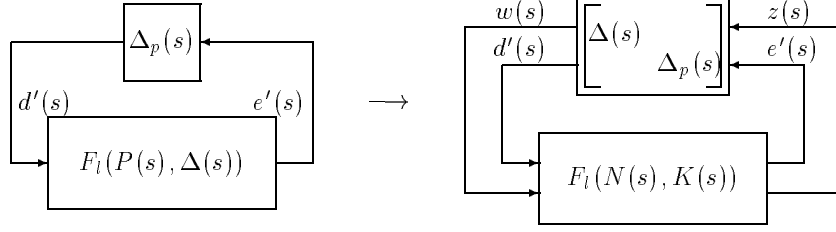


Figure 4.8: Block diagram structure for robust performance check. The perturbation structure is augmented with a full complex performance block $\Delta_p(s)$.

if and only if the map of $\det(I - P(s)\tilde{\Delta}(s))$ as s traverses the \mathcal{D} contour does not encircle the origin. Then the system $F_u(P(s), \Delta(s))$ will satisfy the robust performance criterion (4.74) on page 49 if and only if $P(s)$ is stable for all perturbations $\tilde{\Delta}(s)$ with $\bar{\sigma}(\tilde{\Delta}(j\omega)) \leq 1$:

$$\det(I - P(j\omega)\tilde{\Delta}(j\omega)) \neq 0 \quad \forall \omega, \forall \tilde{\Delta}(j\omega) \ni \bar{\sigma}(\tilde{\Delta}(j\omega)) \leq 1 \quad (4.75)$$

$$\Leftrightarrow \rho(P(j\omega)\tilde{\Delta}(j\omega)) < 1 \quad \forall \omega, \forall \tilde{\Delta}(j\omega) \ni \bar{\sigma}(\tilde{\Delta}(j\omega)) \leq 1 \quad (4.76)$$

$$\Leftrightarrow \|P(s)\|_\infty < 1 \quad (4.77)$$

Proof of Theorem 4.5 Follows from Theorem 4.4 on page 44. Since the structure on $\tilde{\Delta}(s)$ is restricted, (4.77) is a sufficient condition only. \square

Clearly robust performance implies both nominal performance and robust stability. Thus a necessary condition for robust performance in connection with additive uncertainty is:

$$\mathcal{J}_{np} = \|W_{p2}(s)S_o(s)W_{p1}(s)\|_\infty < 1 \quad (4.78)$$

$$\mathcal{J}_u = \|W_{u1}(s)M(s)W_{u2}(s)\|_\infty < 1 \quad (4.79)$$

The sufficient condition for robust performance (4.77) implies that the transfer function $P(s) = F_l(N(s), K(s))$ from $[w(s); d'(s)]$ to $[z(s); e'(s)]$ has ∞ -norm less than one. We may thus formulated an \mathcal{H}_∞ problem:

$$K(s) = \arg \min_{K(s) \in \mathcal{K}_S} \|F_l(N(s), K(s))\|_\infty \quad (4.80)$$

with a known solution. If

$$\|F_l(N(s), K(s))\|_\infty < 1 \quad (4.81)$$

the closed loop system will have robust performance. However, since (4.77) on the preceding page is a sufficient condition only it may be arbitrarily conservative. The next two examples will shed some light on this issue.

Example 4.3 (Robust Performance Problem I) *Assume that a performance specification on the output sensitivity function $S_o(s)$ of the form (4.20) on page 39 is given. Also an additive robust stability specification on the control sensitivity function $M(s)$ of the form (4.61) on page 47 is assumed. The problem considered is thus the one illustrated in Figure 4.7 on page 50. The closed loop system $F_l(N(s), K(s))$ is then given by*

$$F_l(N(s), K(s)) = - \begin{bmatrix} W_{u1}(s)M(s)W_{u2}(s) & W_{u1}(s)M(s)W_{p1}(s) \\ W_{p2}(s)S_o(s)W_{u2}(s) & W_{p2}(s)S_o(s)W_{p1}(s) \end{bmatrix} \quad (4.82)$$

A sufficient conditions for robust performance is thus $\|F_l(N(s), K(s))\|_\infty < 1$. Furthermore since

$$\|F_l(N(s), K(s))\|_\infty < 1 \quad (4.83)$$

$$\Leftrightarrow \bar{\sigma} \left(\begin{bmatrix} W_{u1}(j\omega)M(j\omega)W_{u2}(j\omega) & W_{u1}(j\omega)M(j\omega)W_{p1}(j\omega) \\ W_{p2}(j\omega)S_o(j\omega)W_{u2}(j\omega) & W_{p2}(j\omega)S_o(j\omega)W_{p1}(j\omega) \end{bmatrix} \right) < 1 \quad \forall \omega \quad (4.84)$$

$$\Rightarrow \max(\bar{\sigma}(W_{u1}(j\omega)M(j\omega)W_{u2}(j\omega)), \bar{\sigma}(W_{u1}(j\omega)M(j\omega)W_{p1}(j\omega)), \bar{\sigma}(W_{p2}(j\omega)S_o(j\omega)W_{u2}(j\omega)), \bar{\sigma}(W_{p2}(j\omega)S_o(j\omega)W_{p1}(j\omega))) < 1 \quad \forall \omega \quad (4.85)$$

$$\Rightarrow \bar{\sigma}(W_{u1}(j\omega)M(j\omega)W_{u2}(j\omega)) < 1, \bar{\sigma}(W_{p2}(j\omega)S_o(j\omega)W_{p1}(j\omega)) < 1 \quad \forall \omega \quad (4.86)$$

the robust performance condition will imply both robust stability and nominal performance. However, due to the off-diagonal elements in $F_l(N(s), K(s))$, the robust performance criterion may be conservative in the general case. If the weighting functions $W_{p1}(s)$ and $W_{u2}(s)$ are restricted to scalar transfer functions multiplied with a unity matrix of appropriate dimension, that is if

$$W_{p1}(s) = w_{p1}(s) \cdot I, \quad W_{u2}(s) = w_{u2}(s) \cdot I \quad (4.87)$$

where $w_{p1}(s)$ and $w_{u2}(s)$ are scalar systems, it will now be shown that the sufficient robust performance conditions (4.77) on the preceding page is only slightly conservative. Because of (4.87) the uncertainty weights may be gathered in $\tilde{W}_{u1}(s) = W_{u1}(s)w_{u2}(s)$ and the performance weights in $\tilde{W}_{p2}(s) = W_{p2}(s)w_{p1}(s)$. The robust performance requirement can then be written

$$\bar{\sigma}(F_l(N(j\omega), K(j\omega))) < 1 \quad \forall \omega \quad (4.88)$$

$$\Leftrightarrow \bar{\sigma} \left(\begin{bmatrix} \tilde{W}_{u1}(j\omega)M(j\omega) & \tilde{W}_{u1}(j\omega)M(j\omega) \\ \tilde{W}_{p2}(j\omega)S_o(j\omega) & \tilde{W}_{p2}(j\omega)S_o(j\omega) \end{bmatrix} \right) < 1 \quad \forall \omega \quad (4.89)$$

$$\Leftrightarrow \quad \bar{\sigma} \left(\begin{bmatrix} \tilde{W}_{u1}(j\omega)M(j\omega) \\ \tilde{W}_{p2}(j\omega)S_o(j\omega) \end{bmatrix} \right) < \frac{1}{\sqrt{2}} \quad \forall \omega \quad (4.90)$$

$$\Leftarrow \quad \max\{\bar{\sigma}(\tilde{W}_{u1}(j\omega)M(j\omega)), \bar{\sigma}(\tilde{W}_{p2}(j\omega)S_o(j\omega))\} < \frac{1}{2} \quad \forall \omega \quad (4.91)$$

The inequality (4.90) follows since

$$\bar{\sigma} \left(\begin{bmatrix} \tilde{W}_{u1}(j\omega)M(j\omega) & \tilde{W}_{u1}(j\omega)M(j\omega) \\ \tilde{W}_{p2}(j\omega)S_o(j\omega) & \tilde{W}_{p2}(j\omega)S_o(j\omega) \end{bmatrix} \right) = \sqrt{2}\bar{\sigma} \left(\begin{bmatrix} \tilde{W}_{u1}(j\omega)M(j\omega) \\ \tilde{W}_{p2}(j\omega)S_o(j\omega) \end{bmatrix} \right) \quad (4.92)$$

Thus (4.91) becomes a sufficient condition for robust performance. Consequently if the nominal performance and robust stability criterions are satisfied with some margin – namely a factor 2 – robust performance will be guaranteed. Conversely, for a nominal performance and additive uncertainty specification restricted as in (4.87) on the facing page, robust performance can **not** be arbitrarily poor if nominal performance and robust stability is obtained since $\|F_l(N(s), K(s))\|_\infty$ then will be bounded by two (implied by (4.91) \rightarrow (4.88)). Fully equivalent results can be found for output multiplicative uncertainty.

Example 4.4 (Robust Performance Problem II) Now let us assume a standard performance specification as in Example 4.3 but an input multiplicative robust stability specification on the input complementary sensitivity $T_i(s)$, see Table 4.1 on page 47. We may rewrite this as an additive perturbation simply by multiplying $W_{u2}(s)$ in Example 4.3 with the plant transfer function $G(s)$. The (sufficient) robust performance condition then becomes

$$\bar{\sigma}(F_l(N(j\omega), K(j\omega))) < 1 \quad \Leftrightarrow \quad (4.93)$$

$$\bar{\sigma} \left(\begin{bmatrix} W_{u1}(j\omega)M(j\omega)G(j\omega)W_{u2}(j\omega) & W_{u1}(j\omega)M(j\omega)W_{p1}(j\omega) \\ W_{p2}(j\omega)S_o(j\omega)G(j\omega)W_{u2}(j\omega) & W_{p2}(j\omega)S_o(j\omega)W_{p1}(j\omega) \end{bmatrix} \right) < 1 \quad (4.94)$$

for all $\omega \geq 0$. Note that $M(s)G(s) = T_i(s)$. Again, due to the off-diagonal elements in $F_l(N(s), K(s))$, the condition (4.94) may be conservative. In fact, even if the weightings are restricted as in (4.87) on the facing page it will be shown that (4.94) may be arbitrarily conservative. With weightings restricted as in (4.87) on the facing page note that the robust stability criterion becomes

$$\bar{\sigma} \left(\tilde{W}_{u1}(j\omega)M(j\omega)G(j\omega) \right) < 1 \quad \forall \omega \quad (4.95)$$

$$\Leftarrow \quad \bar{\sigma} \left(\tilde{W}_{u1}(j\omega)M(j\omega)\bar{\sigma}(G(j\omega)) \right) < 1 \quad \forall \omega \quad (4.96)$$

$$\Leftrightarrow \quad \bar{\sigma} \left(\bar{\sigma}(G(j\omega))\tilde{W}_{u1}(j\omega)M(j\omega) \right) < 1 \quad \forall \omega \quad (4.97)$$

which corresponds to robust stability for an additive perturbation $\Delta(s)\bar{\sigma}(G(s))\tilde{W}_{u1}(s)$. Thus if the system is stable for the additive perturbation $\Delta(s)\bar{\sigma}(G(s))\tilde{W}_{u1}(s)$ it will also be stable for the input multiplicative

perturbation $\Delta(s)\tilde{W}_{u1}(s)$. Notice that this corresponds to approximating $G(s)$ with its largest singular value and moving it to the uncertainty input weight $\tilde{W}_{u1}(s)$, see Figure 4.9.

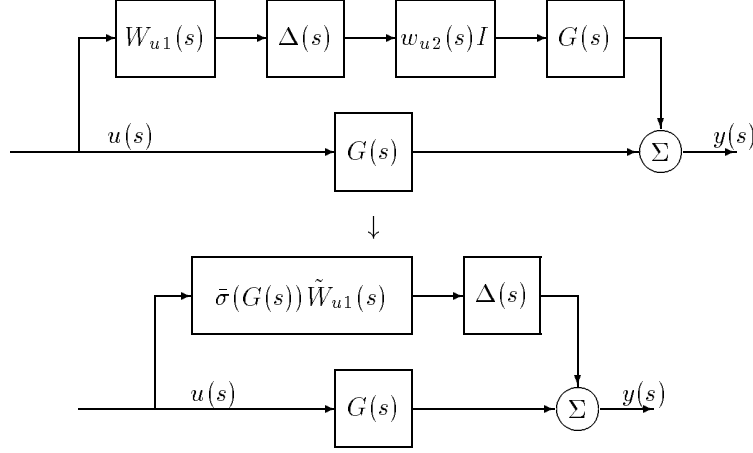


Figure 4.9: Approximating $G(s)$ with its largest singular value in the uncertainty specification.

A sufficient condition for robust performance is then that for all $\omega \geq 0$:

$$\bar{\sigma}(F_l(N(j\omega), K(j\omega))) < 1 \quad (4.98)$$

$$\Leftrightarrow \bar{\sigma} \left(\begin{bmatrix} \bar{\sigma}(G(j\omega))\tilde{W}_{u1}(j\omega)M(j\omega) & \bar{\sigma}(G(j\omega))\tilde{W}_{u1}(j\omega)M(j\omega) \\ \tilde{W}_{p2}(j\omega)S_o(j\omega) & \tilde{W}_{p2}(j\omega)S_o(j\omega) \end{bmatrix} \right) < 1 \quad (4.99)$$

$$\Leftrightarrow \bar{\sigma} \left(\begin{bmatrix} \bar{\sigma}(G(j\omega))\tilde{W}_{u1}(j\omega)M(j\omega) \\ \tilde{W}_{p2}(j\omega)S_o(j\omega) \end{bmatrix} \right) < \frac{1}{\sqrt{2}} \quad (4.100)$$

$$\Leftrightarrow \begin{cases} \bar{\sigma}(G(j\omega))\bar{\sigma}(\tilde{W}_{u1}(j\omega)T_i(j\omega)G^{-1}(j\omega)) < \frac{1}{2} \\ \bar{\sigma}(\tilde{W}_{p2}(j\omega)S_o(j\omega)) < \frac{1}{2} \end{cases} \quad (4.101)$$

$$\Leftrightarrow \begin{cases} \frac{\bar{\sigma}(G(j\omega))}{\underline{\sigma}(G(j\omega))}\bar{\sigma}(\tilde{W}_{u1}(j\omega)T_i(j\omega)) < \frac{1}{2} \\ \bar{\sigma}(\tilde{W}_{p2}(j\omega)S_o(j\omega)) < \frac{1}{2} \end{cases} \quad (4.102)$$

$$\Leftrightarrow \begin{cases} \bar{\sigma}(\tilde{W}_{u1}(j\omega)T_i(j\omega)) < \frac{1}{2\kappa(G(j\omega))} \\ \bar{\sigma}(\tilde{W}_{p2}(j\omega)S_o(j\omega)) < \frac{1}{2} \end{cases} \quad (4.103)$$

Thus (4.103) becomes a sufficient condition for robust performance. Inequality (4.103) shows that even when nominal performance and robust stability are satisfied with reasonable margin, the (sufficient) robust performance criterion can be violated by an arbitrarily large amount if the plant is ill-conditioned. Conversely, if $\kappa(G(j\omega)) \approx 1, \forall \omega$, then robust performance can not be arbitrarily poor if nominal performance and robust stability are obtained.

4.5 Computing the \mathcal{H}_∞ Optimal Controller

Let us finally briefly present a solution to the \mathcal{H}_∞ optimal control problem. The problem of solving minimizations of the form

$$K(s) = \arg \min_{K(s) \in \mathcal{K}_s} \|F_l(N(s), K(s))\|_\infty \quad (4.104)$$

was probably the single most important research area within the automatic control community in the 1980's. At first, only algorithms that produced ∞ optimal controllers of very high order were available, see e.g. [Fra87]. For polynomial systems numerical algorithms were available which provided \mathcal{H}_∞ optimal controllers of the same order as the augmented plant $N(s)$, see e.g. [Gri86, Gri88, Kwa85]. However, the numerics were only efficient for scalar systems. Then in early 1988, Doyle, Glover, Khargonekar and Francis announced an state-space \mathcal{H}_∞ solution which, like the LQG solution, involved only two Ricatti equations and yielded a controller with the same order as the generalized plant. The results were presented at the 1988 American Control Conference and in the 1989 IEEE paper [DGKF89]. This was a major breakthrough for \mathcal{H}_∞ control theory. The parallels now apparent between \mathcal{H}_∞ and LQG theory are pervasive. Both controllers have a state estimator-state feedback structure, two Ricatti equations provides the full state feedback matrix K_c and the output injection matrix K_f in the estimator, respectively. The paper [DGKF89] is now known simply as the DGKF paper.

Given a block 2×2 system $N(s)$ like in Figure 4.4 on page 42 and a required upper bound γ on the closed loop infinity norm $\|F_l(N(s), K(s))\|_\infty$ the solution returns a parameterization, which we will denote the DGKF Parameterization, $K(s) = F_l(J(s), Q(s))$ of all stabilizing controllers such that $\|F_l(N(s), K(s))\|_\infty < \gamma$, see Figure 4.10 on the following page. Any stable transfer function matrix $Q(s)$ satisfying $\|Q(s)\|_\infty < \gamma$ will stabilize the closed loop system and cause

$\|F_l(N(s), K(s))\|_\infty < \gamma$. Any $Q(s)$ which is unstable or has $\|Q(s)\|_\infty > \gamma$ will destabilize the closed loop system, or cause $\|F_l(N(s), K(s))\|_\infty > \gamma$ or both. The solution is provided by Theorem 4.6.

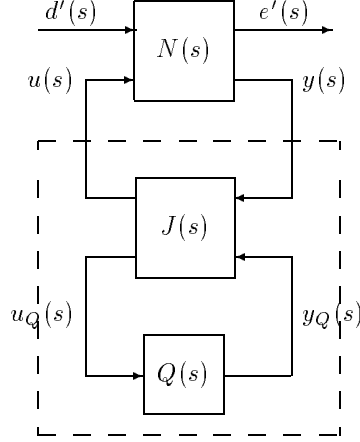


Figure 4.10: The DGKF parameterization of all stabilizing controllers.

Definition 4.2 (Ricatti Solution) Denote the solution X to the Ricatti equation

$$A^T X + XA - XRX + Q = 0 \quad (4.105)$$

by $X = \mathbf{Ric}(H)$ where H is the associated Hamiltonian matrix

$$H = \begin{bmatrix} A & -R \\ -Q & -A^T \end{bmatrix} \quad (4.106)$$

Theorem 4.6 (\mathcal{H}_∞ -Suboptimal Control Problem) The following solution is taken from [Dai90]. Let $N(s)$ be given by its state-space matrices A , B , C and D and introduce the notation:

$$N(s) = \left[\begin{array}{c|cc} A & B_1 & B_2 \\ \hline C_1 & D_{11} & D_{12} \\ C_2 & D_{21} & D_{22} \end{array} \right] \quad (4.107)$$

Make the following assumptions:

1. (A, B_1) and (A, B_2) are stabilizable.

2. (C_1, A) and (C_2, A) are detectable.
3. $D_{12}^T D_{12} = I$ and $D_{21} D_{21}^T = I$.
4. $D_{11} = D_{22} = 0$.

Let

$$\tilde{D}_{12} = I - D_{12} D_{12}^T, \quad \tilde{D}_{21} = I - D_{21}^T D_{21} \quad (4.108)$$

and solve the two Ricatti equations:

$$X_\infty = \mathbf{Ric} \begin{bmatrix} A - B_2 D_{12}^T C_1 & \gamma^{-2} B_1 B_1^T - B_2 B_2^T \\ -C_1^T \tilde{D}_{12}^T \tilde{D}_{12} C_1 & -(A - B_2 D_{12}^T C_1)^T \end{bmatrix} \quad (4.109)$$

$$Y_\infty = \mathbf{Ric} \begin{bmatrix} (A - B_1 D_{21}^T C_2)^T & \gamma^{-2} C_1^T C_1 - C_2^T C_2 \\ -B_1 \tilde{D}_{21} \tilde{D}_{21}^T B_1^T & -(A - B_1 D_{21}^T C_2) \end{bmatrix} \quad (4.110)$$

Form the state feedback matrix K_c , the output injection matrix K_f and the matrix Z_∞ :

$$K_c = (D_{12}^T C_1 + B_2^T X_\infty) \quad (4.111)$$

$$K_f = (B_1 D_{21}^T + Y_\infty C_2^T) \quad (4.112)$$

$$Z_\infty = (I - \gamma^{-2} Y_\infty X_\infty)^{-1} \quad (4.113)$$

If $X_\infty \geq 0$ and $Y_\infty \geq 0$ exist and if the spectral radius $\rho(X_\infty Y_\infty) < \gamma^2$, then the \mathcal{H}_∞ DGKF Parameterization is given by:

$$J(s) = \left[\begin{array}{c|cc} A_\infty & Z_\infty K_f & Z_\infty (B_2 + \gamma^{-2} Y_\infty C_1^T D_{12}) \\ \hline -K_c & 0 & I \\ - (C_2 + \gamma^{-2} D_{21} B_1^T X_\infty) & I & 0 \end{array} \right] \quad (4.114)$$

$$= \begin{bmatrix} J_{11}(s) & J_{12}(s) \\ J_{21}(s) & J_{22}(s) \end{bmatrix} \quad (4.115)$$

where A_∞ is given by

$$A_\infty = A - B_2 K_c + \gamma^{-2} B_1 B_1^T X_\infty - Z_\infty K_f (C_2 + \gamma^{-2} D_{21} B_1^T X_\infty) \quad (4.116)$$

Stabilizing controllers $K(s)$ may now be constructed by connecting $J(s)$ to any stable transfer function matrix $Q(s)$ with $\|Q(s)\|_\infty < \gamma$:

$$K(s) = F_l(J(s), Q(s)) = J_{11}(s) + J_{12}(s)Q(s) (I - J_{22}(s)Q(s))^{-1} J_{21}(s) \quad (4.117)$$

The ∞ -norm of the closed loop system $F_l(N(s), F_l(J(s), Q(s)))$ satisfy:

$$\|F_l(N(s), F_l(J(s), Q(s)))\|_\infty < \gamma \quad (4.118)$$

The controller obtained for $Q(s) = 0$ is known as the central \mathcal{H}_∞ controller.

4.5.1 Remarks on the \mathcal{H}_∞ Solution

Notice that Theorem 4.6 on page 56 does not provide the optimal \mathcal{H}_∞ control law. Rather it provides a control law satisfying $\|F_l(N(s), K(s))\|_\infty < \gamma$ after γ has been specified, provided that a control law exists which can do this. Consequently the designer must iterate on γ to approach the optimal ∞ -norm γ_0 . This is different to the LQG-optimal control problem where the optimal solution is found without iteration. The central controller obtained for $Q(s) = 0$ is not generally the controller achieving the smallest ∞ -norm of the closed loop system. However, since it is a valid controller, given the desired bound γ , it is customary to choose this particular controller for implementation. Specifically, in the commercially available software [CS92, BDG⁺93], this is the controller returned by the \mathcal{H}_∞ control synthesis algorithms.

Furthermore note that even though the \mathcal{H}_∞ problem is stated in the frequency domain, the solution is presented in state space form. This combination of frequency domain specifications and state space computation has become symptomatic in modern control theory with polynomial systems being an exception.

Consider the necessary assumptions 1-4. Assumption 1 and 2 are clearly reasonable. They simply state that the generalized plant shall be stabilizable and detectable. Assumption 3 can only be met, if D_{12} has no more columns than rows (is “tall”) and if D_{21} has no more rows than columns (is “fat”). This implies that:

$$\dim e'(s) \geq \dim u(s), \quad \dim d'(s) \geq \dim y(s) \quad (4.119)$$

where $\dim x$ denotes the dimension of x . Consequently the number of external outputs (error signals) must be equal to or exceed the number of controlled inputs (actuators) and equivalently, the number of external inputs must be equal to or exceed the number of measured outputs (sensors). For SISO systems, since $\dim u = \dim y = 1$, it simply means that both d' and e' should be present. Clearly a fair assumption. For MIMO systems, however, we may form sensible problems where (4.119) is not fulfilled. By adding fictitious inputs or outputs with small weights this may be avoided.

Given a general D matrix where D_{12} and D_{21}^T has full column rank and the desired upper bound γ , a series of scalings and loop shifting operations can be carried out to put D into the form:

$$D_{11} = 0 \quad (4.120)$$

$$D_{12} = \begin{bmatrix} 0 \\ I \end{bmatrix} \quad (4.121)$$

$$D_{21} = \begin{bmatrix} 0 & I \end{bmatrix} \quad (4.122)$$

$$D_{22} = 0 \quad (4.123)$$

so that assumptions 3 and 4 are fulfilled. A suitable loop shifting and scaling algorithm is described in Appendix A on page 287. The necessary rank conditions on D_{12} and D_{21} imply that:

$$\text{rank } D_{12} = \dim u, \quad \text{rank } D_{21} = \dim y \quad (4.124)$$

These two conditions are very common in the literature on robust control. In the MATLAB software [CS92, BDG⁺93] they must be fulfilled both for the \mathcal{H}_2 and the \mathcal{H}_∞ problem. The rank condition on D_{12} states that there must be a direct path from the control input $u(s)$ to the error output $e'(s)$. In other words, the open loop transfer function from $u(s)$ to $e'(s)$ must have equal number of poles and zeros. Equivalently for the rank condition on D_{21} to be fulfilled there must be a direct path from the external input $d'(s)$ to the measured output $y(s)$. However it is easy to formulate sensible control problems within the 2×2 block structure that do not fulfill the rank conditions (4.124). These problems may usually be reformulated so as to fulfill (4.124), but it does mean that care has to be taken when formulating the 2×2 problem.

The structure of the \mathcal{H}_∞ controller is shown in Figure 4.11 on the following page. Like the LQG solution it involves a feedback estimator for the estimated state vector $\hat{x}(s)$ and a full state feedback matrix K_c . In contrast to the LQG solution, a scaling matrix Z_∞ appears in series with the output injection matrix K_f and a few extra terms appear for $B_Y = \gamma^{-2} D_{21} B_1^T X_\infty$, $B_X = \gamma^{-2} B_1 B_1^T X_\infty$ and $B_Q = Z_\infty (B_2 + \gamma^{-2} Y_\infty C_1^T D_{12})$.

It can be shown, see e.g. [TCB95], that for $\gamma \rightarrow \infty$ the corresponding *Youla parameterization* for the \mathcal{H}_2 (or LQG) problem is recovered from the DGKF Parameterization. Consequently the \mathcal{H}_2 problem is simply a special case of the \mathcal{H}_∞ problem. Comparing the Hamiltonians for the \mathcal{H}_∞ and \mathcal{H}_2 Riccati equations reveal that the only difference is the extra terms $\gamma^{-2} B_1 B_1^T$ and $\gamma^{-2} C_1 C_1^T$ in the upper right corners. The \mathcal{H}_2 full state feedback matrix K_c does not depend on B_1 ; that is, the way in which the external signal $d'(s)$ enter the system does not affect the \mathcal{H}_2 state feedback solution. However it does affect the \mathcal{H}_∞ state feedback solution. Similarly, the \mathcal{H}_2 optimal state estimator (the Kalman filter) does not depend on C_1 ; that is, equal weight is put on all states. In contrast, the \mathcal{H}_∞ state estimator is influenced by C_1 ; that is, by which linear combination of states appears at the external output $e'(s)$.

Most of the robustness problems of LQG optimal control stem from the degradation of the closed loop response when Kalman filter state estimates are substituted for measured states in the state feedback control law. Some states usually contribute more to the loop gain than others, but LQG or \mathcal{H}_2 state estimation cannot compensate for this, since all states are weighted equally. In the \mathcal{H}_∞ state estimator, the designer can tradeoff the contribution of the different states through the C_1 matrix and thus make the closed loop response more insensitive

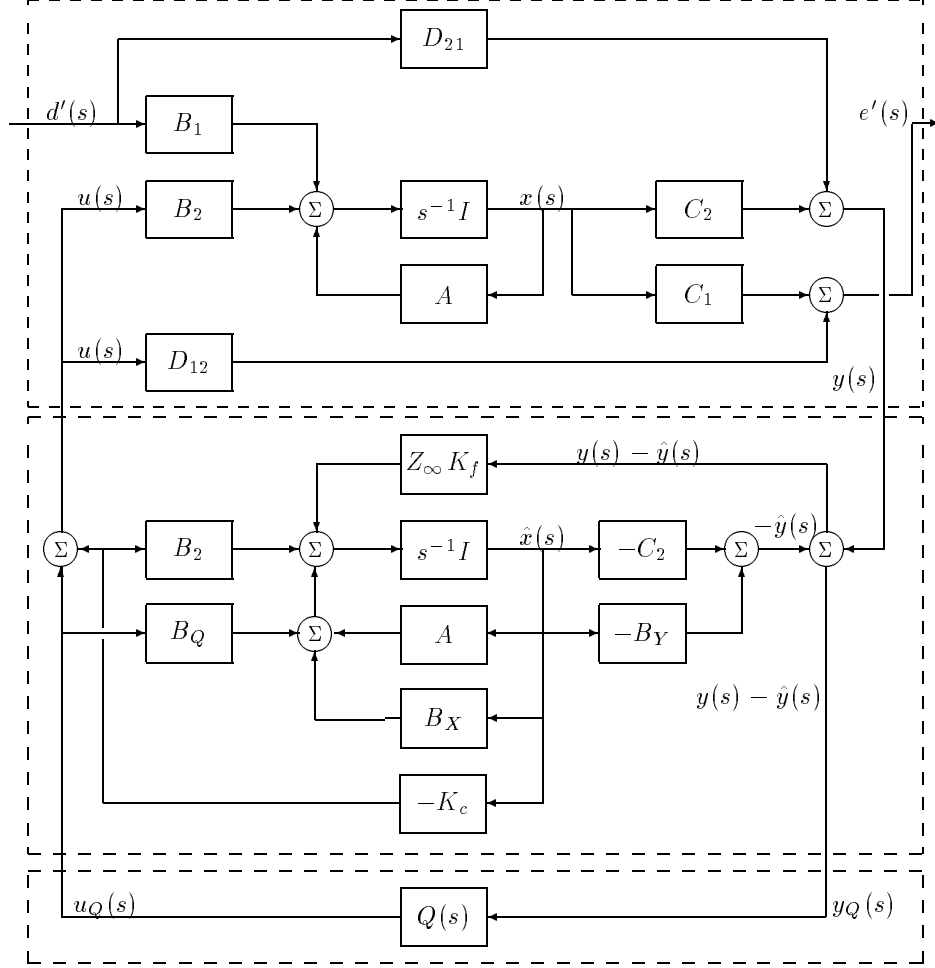


Figure 4.11: \mathcal{H}_∞ suboptimal control configuration. $N(s)$ is within the top dashed box, $J(s)$ within the middle dashed box and $Q(s)$ in the lower dashed box. $B_Q = Z_\infty(B_2 + \gamma^{-2}Y_\infty C_1^T D_{12})$, $B_Y = \gamma^{-2}D_{21}B_1^T X_\infty$ and $B_X = \gamma^{-2}B_1B_1^T X_\infty$.

to modeling errors. Similarly a tradeoff of the external inputs can be made when computing the full state feedback matrix K_c , thus enhancing the closed loop performance. \mathcal{H}_∞ synthesis simply chooses from a wider set of possible stabilizing control laws than \mathcal{H}_2 , so naturally one would expect to be able to obtain higher performance and robustness levels using \mathcal{H}_∞ , given a fixed set of sensors and bandwidth constraints.

There exists commercially available software, e.g. [CS92, BDG⁺93] for solving the \mathcal{H}_∞ control problem. The software performs an iteration on γ to find the optimal controller.

4.6 Discrete-Time Results

In the current chapter we have only presented continuous-time results. However, it is well-known, see e.g. [KD88], that for sufficiently small sampling time the bilinear transformation:

$$z = e^{sT_s} \approx \frac{1 + s\frac{T_s}{2}}{1 - s\frac{T_s}{2}} \quad (4.125)$$

$$\Leftrightarrow s \approx \frac{2}{T_s} \frac{z - 1}{z + 1} \quad (4.126)$$

links the continuous-time and discrete-time results. Here T_s denotes the sampling time. Thus if the robust design problem is posed in discrete-time, we may transform $N(z)$ to continuous-time via (4.125), compute the \mathcal{H}_∞ optimal continuous-time control law and back-transform the controller to discrete-time via (4.126). In particular, this is the approach taken in the MATLAB toolboxes [CS92, BDG⁺93].

Discrete-time algorithms which solves the Z -domain 2×2 problem directly have been developed. For a detailed treatment see [Sto92]. However, the discrete-time results are rather messy and the commercially available software which supports it are yet limited.

4.7 Summary

The classical \mathcal{H}_∞ results in robust control were presented. It was shown how both nominal performance and robust stability can be addressed using a 2×2 block problem formulation. Given any of the unstructured complex perturbations introduced in Section 4.3 on page 42 the closed loop system may be rewritten in $P\Delta$ form as in Figure 4.5 on page 45. Then, assuming that every plant in the set described by $\Delta(s)$ with $\bar{\sigma}(\Delta) \leq 1$ can occur in practice, $\|P(s)\|_\infty < 1$

is a non-conservative condition for robust stability. It was then shown how the robust performance problem can be addressed by augmenting the robust stability problem with a full complex performance block. The robust performance problem then can be formulated as a 2×2 block problem.

However, even though the robust stability criterion (4.48) on page 45 is non-conservative, in formulating the controller synthesis as a 2×2 block problem some conservatism will always be introduced when robust performance is considered. This is so because the perturbation structure of the robust performance problem is diagonal ($\tilde{\Delta} = \text{diag}\{\Delta, \Delta_p\}$). Unfortunately, with \mathcal{H}_∞ we can only consider full blocks. Thus the off-diagonal elements in this full block will introduce conservatism in the \mathcal{H}_∞ solution. For standard additive and output multiplicative uncertainty, the robust performance condition will be reasonably tight, namely up to a factor 2. This applies also for standard input multiplicative uncertainty *provided the plant is well-conditioned*. For ill-conditioned plants, robust performance may be arbitrarily poor even though nominal performance and robust stability are obtained. In other words, for ill-conditioned plants the closed loop properties at the plant input may be very different from those at the plant output. For example, the robustness to output multiplicative uncertainty may be satisfactory even though the robustness to input multiplicative uncertainty is very poor.

Generally it can be concluded, that if an unstructured complex perturbation model is tight, that is if all plants included by the perturbation structure can occur in practice, and if the plant is reasonably well-conditioned, the optimal \mathcal{H}_∞ controller will not be very conservative in the sense that robust performance will not be arbitrarily poor given nominal performance and robust stability.

On the other hand, if an unstructured complex perturbation model is conservative or if the plant is ill-conditioned, an 2×2 block problem \mathcal{H}_∞ optimal controller may be very conservative. In such cases much is to be gained using the structured singular value μ . In the next section robust control design with structured singular values will be considered.

Chapter 5

Robust Control Design using Structured Singular Values

Contents

5.1	μ Analysis	64
5.1.1	Robust Stability	64
5.1.2	Robust Performance	71
5.1.3	Computation of μ	74
5.2	μ Synthesis	78
5.2.1	Complex μ Synthesis – D - K Iteration	78
5.2.2	Mixed μ Synthesis – D, G - K Iteration	80
5.2.3	Mixed μ Synthesis – μ - K Iteration	85
5.3	Summary	90

As we showed in the previous chapter there are two main limitations in connection with \mathcal{H}_∞ control theory. Probably the most important is that we can only handle full complex perturbation structures $\Delta(s) \in \mathbf{C}^{n \times m}$ non-conservatively in

an \mathcal{H}_∞ robustness test. The other main limitation is that the robust performance problem can only be considered conservatively *even for a full complex perturbation set* because performance and robustness cannot be separated in the \mathcal{H}_∞ framework. The conservatism introduced depends on the applied perturbation model and the condition number of the plant. In this chapter we shall show that both these limitations may be overcome using the *structured singular value* μ .

Firstly we will consider the analysis problem, that is, given a controller $K(s)$ how do we test for robust stability and robust performance using μ ? Secondly the synthesis problem of finding $K(s)$ will be investigated.

5.1 μ Analysis

5.1.1 Robust Stability

We will consider control problems which can be represented in a $N\Delta K$ -framework as illustrated in Figure 5.1.

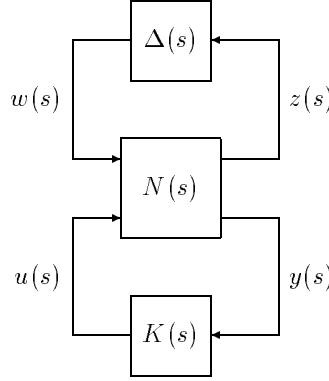


Figure 5.1: The $N\Delta K$ formulation of robust stability problem.

Comparing with Figure 4.6 on page 48 the similarities with the 2×2 block problem are obvious. However, now $\Delta(s)$ will not be restricted to only a full complex block. Rather it is assumed that $\Delta(s)$ has a block diagonal structure as follows. Assume that $\Delta(s)$ is a member of the bounded subset:

$$\mathbf{B}\Delta = \{\Delta(s) \in \Delta \mid \bar{\sigma}(\Delta(j\omega)) < 1\} \quad (5.1)$$

where Δ is defined by:

$$\Delta = \left\{ \text{diag} \left(\delta_1^r I_{r_1}, \dots, \delta_{m_r}^r I_{r_{m_r}}, \delta_1^c I_{r_{m_r+1}}, \dots, \delta_{m_c}^c I_{r_{m_r+m_c}}, \Delta_1, \dots, \Delta_{m_c} \right) \mid \right. \\ \left. \delta_i^r \in \mathbf{R}, \delta_i^c \in \mathbf{C}, \Delta_i \in \mathbf{C}^{r_{m_r+m_c+i} \times r_{m_r+m_c+i}} \right\} \quad (5.2)$$

Thus we are considering real and complex uncertainty which enters the nominal model in a *linear fractional manner*. Very general classes of robustness problems can be cast into this formulation including for example parametric uncertainty, see Example 5.1. Clearly, the block diagonal structure on Δ allows much more detailed uncertainty models compared with the \mathcal{H}_∞ approach where $\Delta(s)$ is simply a full complex block. Notice that a full complex block is of course just a special element of the above set Δ .

Let us also define also the *corresponding complex perturbation set* Δ_c :

$$\Delta_c = \left\{ \text{diag} \left(\delta_1^c I_{r_1}, \dots, \delta_{m_r+m_c}^c I_{r_{m_r+m_c}}, \Delta_1, \dots, \Delta_{m_c} \right) \mid \right. \\ \left. \delta_i^c \in \mathbf{C}, \Delta_i \in \mathbf{C}^{r_{m_r+m_c+i} \times r_{m_r+m_c+i}} \right\} \quad (5.3)$$

where the real perturbations δ^r have been replaced by complex perturbations δ^c . This uncertainty set will be use in connection with mixed μ synthesis.

Example 5.1 (Diagonal Perturbation Formulation I) *This example is a slightly modified version of that given in [Hol94]. Suppose the plant is given by:*

$$G(s) = \frac{\alpha}{\beta s + 1} \quad (5.4)$$

where the DC gain α and the time constant β is only known within $\pm 10\%$, say

$$\alpha = [27.0, 33.0], \quad \beta = [0.9, 1.1] \quad (5.5)$$

We now want to express α and β by their nominal values 30 and 1 and some perturbations Δ_α and Δ_β where $|\Delta_{\alpha,\beta}| \leq 1$. This can for example be accomplished as follows:

$$\alpha = 30 \left(1 + \frac{1}{10} \Delta_\alpha \right) \quad (5.6)$$

$$\beta = 1.0 \left(1 + \frac{1}{10} \Delta_\beta \right) \quad (5.7)$$

with the constraints:

$$\Delta_\alpha \in [-1, +1], \quad \Delta_\beta \in [-1, +1] \quad (5.8)$$

Let us by $\mathbf{B}\Delta$ denote the set $[-1, +1]$. Then the transfer function $G(s)$ may be written:

$$G(s) = \frac{30(1 + 0.1\Delta_\alpha)}{(1 + 0.1\Delta_\beta)s + 1} \quad (5.9)$$

with

$$\Delta_\alpha, \Delta_\beta \in \mathbf{B}\Delta \quad (5.10)$$

In block diagram form $G(s)$ may be given as in Figure 5.2.

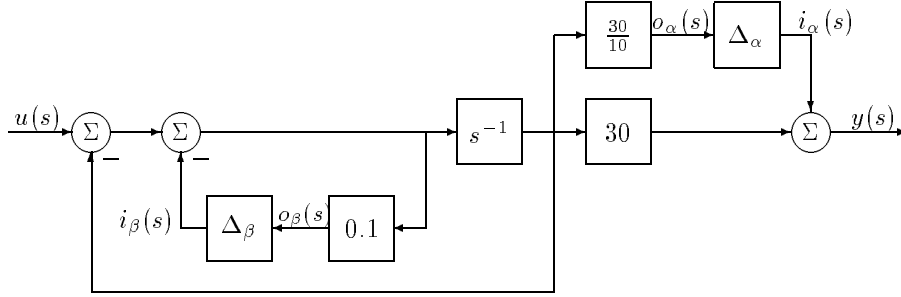


Figure 5.2: Example 5.1 on the page before: Block diagram of $G(s)$.

Now in order to find the corresponding $N\Delta K$ form we need to remove the Δ -blocks in Figure 5.2 and find the transfer functions from the three inputs $i_\alpha(s)$, $i_\beta(s)$ and $u(s)$ to the three outputs $o_\alpha(s)$, $o_\beta(s)$ and $y(s)$. In matrix form one may find that

$$\begin{bmatrix} o_\alpha(s) \\ o_\beta(s) \\ y(s) \end{bmatrix} = \begin{bmatrix} 0 & -\frac{30}{10(s+1)} & \frac{30}{10(s+1)} \\ 0 & -\frac{s}{10(s+1)} & \frac{s}{10(s+1)} \\ 1 & -\frac{30}{s+1} & \frac{30}{s+1} \end{bmatrix} \begin{bmatrix} i_\alpha(s) \\ i_\beta(s) \\ u(s) \end{bmatrix} \quad (5.11)$$

The uncertainty blocks are described by:

$$\begin{bmatrix} i_\alpha(s) \\ i_\beta(s) \end{bmatrix} = \begin{bmatrix} \Delta_\alpha o_\alpha(s) \\ \Delta_\beta o_\beta(s) \end{bmatrix} = \begin{bmatrix} \Delta_\alpha & 0 \\ 0 & \Delta_\beta \end{bmatrix} \begin{bmatrix} o_\alpha(s) \\ o_\beta(s) \end{bmatrix} \quad (5.12)$$

Now let:

$$w(s) \triangleq \begin{bmatrix} i_\alpha(s) \\ i_\beta(s) \end{bmatrix} \quad (5.13)$$

$$z(s) \triangleq \begin{bmatrix} o_\alpha(s) \\ o_\beta(s) \end{bmatrix} \quad (5.14)$$

$$N(s) \triangleq \begin{bmatrix} 0 & -\frac{30}{10(s+1)} & \frac{30}{10(s+1)} \\ 0 & -\frac{s}{10(s+1)} & \frac{s}{10(s+1)} \\ 1 & -\frac{30}{s+1} & \frac{30}{s+1} \end{bmatrix} \quad (5.15)$$

$$\Delta(s) \triangleq \text{diag}\{\Delta_\alpha, \Delta_\beta\} = \begin{bmatrix} \Delta_\alpha & 0 \\ 0 & \Delta_\beta \end{bmatrix} \quad (5.16)$$

Then the uncertain system is described by the equations:

$$\begin{bmatrix} z(s) \\ y(s) \end{bmatrix} = N(s) \begin{bmatrix} w(s) \\ u(s) \end{bmatrix} \quad (5.17)$$

$$w(s) = \Delta(s)z(s) \quad (5.18)$$

and can readily be put into the $N\Delta K$ structure.

Example 5.2 (Diagonal Perturbation Formulation II) Let us next consider a standard second order lag:

$$G(s) = \frac{\alpha\omega_n^2}{s^2 + 2\zeta\omega_n + \omega_n^2} \quad (5.19)$$

Assume that the gain α , damping coefficient ζ and natural frequency ω_n is known only to belong to the following sets

$$\alpha = \alpha_o(1 + \delta_\alpha\Delta_\alpha) \quad (5.20)$$

$$\zeta = \zeta_o(1 + \delta_\zeta\Delta_\zeta) \quad (5.21)$$

$$\omega_n = \omega_{n_o}(1 + \delta_\omega\Delta_\omega) \quad (5.22)$$

with

$$\Delta_\alpha, \Delta_\zeta, \Delta_\omega \in \mathbf{B}\mathbf{\Delta} \quad \mathbf{B}\mathbf{\Delta} = [-1; +1] \quad (5.23)$$

A state-space representation of $G(s)$ is given in Figure 5.3 on the next page. Due to the increased complexity of this system compared with the first order system in Example 5.1 on page 65 we will work with state space representations. Define the states as:

$$x_1 = \dot{y}, \quad x_2 = y \quad (5.24)$$

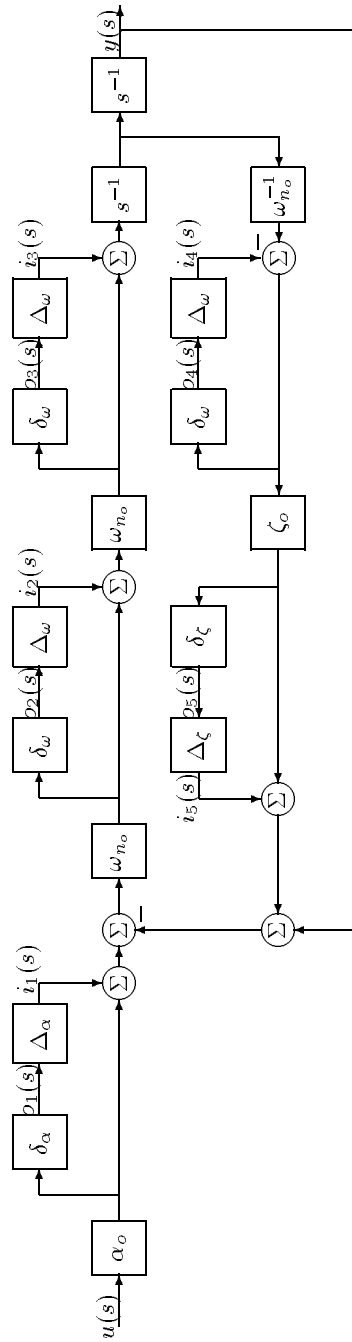


Figure 5.3: Transfer function representation of uncertain second order lag.

A few manipulations reveal that the augmented system $N(s)$ can be written

$$N(s) = \left[\begin{array}{c|c} A & B \\ \hline C & D \end{array} \right] = \left[\begin{array}{cc|cc} -2\zeta_o\omega_{n_o} & -\omega_{n_o}^2 & \omega_{n_o}^2 & \omega_{n_o} & 1 \\ 1 & 0 & 0 & 0 & 0 \\ \hline 0 & 0 & 0 & 0 & 0 \\ -2\delta_\omega\zeta_o & -\delta_\omega\omega_{n_o} & \delta_\omega\omega_{n_o} & 0 & 0 \\ -2\delta_\omega\zeta_o\omega_{n_o} & -\delta_\omega\omega_{n_o}^2 & \delta_\omega\omega_{n_o}^2 & \delta_\omega\omega_{n_o} & 0 \\ \delta_\omega\omega_{n_o}^{-1} & 0 & 0 & 0 & 0 \\ 2\delta_\zeta\zeta_o\omega_{n_o}^{-1} & 0 & 0 & 0 & 0 \\ 0 & 1 & 0 & 0 & 0 \\ \hline & 2\zeta_o\omega_{n_o}^2 & -\omega_{n_o}^2 & \alpha\omega_{n_o}^2 & \\ & 0 & 0 & 0 & \\ \hline & 0 & 0 & \alpha\delta_\alpha & \\ 2\delta_\omega\zeta_o\omega_{n_o} & -\delta_\omega\omega_{n_o} & \delta_\omega\alpha\omega_{n_o} & & \\ 2\delta_\omega\zeta_o\omega_{n_o}^2 & -\delta_\omega\omega_{n_o}^2 & \delta_\omega\alpha\omega_{n_o}^2 & & \\ \delta_\omega & 0 & 0 & & \\ -2\delta_\zeta\zeta_o & 0 & 0 & & \\ 0 & 0 & 0 & & \end{array} \right] \quad (5.25)$$

where we have used the notation introduced in Theorem 4.6 on page 56.

Proceeding as in Example 5.1 on page 65, define

$$w(s) = [i_1(s) \ i_2(s) \ i_3(s) \ i_4(s) \ i_5(s)]^T \quad (5.26)$$

$$z(s) = [o_1(s) \ o_2(s) \ o_3(s) \ o_4(s) \ o_5(s)]^T \quad (5.27)$$

$$\Delta(s) = \text{diag} \{ \Delta_\alpha, \Delta_\omega, \Delta_\omega, \Delta_\omega, \Delta_\zeta \} \quad (5.28)$$

Then the uncertain second order lag is described by the equations

$$\begin{bmatrix} z(s) \\ y(s) \end{bmatrix} = N(s) \begin{bmatrix} w(s) \\ u(s) \end{bmatrix} \quad (5.29)$$

$$w(s) = \Delta(s)z(s) \quad (5.30)$$

and can readily be put into the $N\Delta K$ structure. Notice that in this example the perturbation block structure includes repeated scalar blocks:

$$\Delta = \begin{bmatrix} \delta_1 & 0 & 0 \\ 0 & \delta_2 I_{3 \times 3} & 0 \\ 0 & 0 & \delta_3 \end{bmatrix} \quad (5.31)$$

As illustrated by the 2 above examples, highly structured uncertainty descriptions can be represented in the $N\Delta K$ framework in a straightforward manner. However, the extraction of the uncertainty blocks may involve a lot of tedious

algebra. Fortunately, in the MATLAB *μ -Analysis and Synthesis Toolbox* a very handy `m`-function (`sysic.m`) is available which automizes the necessary system interconnections.

Dynamic uncertainty as introduced in Section 4.3 on page 42 may be included through complex blocks of appropriate size.

As before, denote by $F_l(N(s), K(s)) = P(s)$ the transfer function obtained by closing the lower loop in Figure 5.1 on page 64. $P(s)$ is the *generalized closed loop transfer function*. $P(s)$ is given by the LFT

$$P(s) = F_l(N(s), K(s)) \quad (5.32)$$

$$= N_{11}(s) + N_{12}(s)K(s) (I - N_{22}(s)K(s))^{-1} N_{21}(s) \quad (5.33)$$

Robust stability under structured perturbations $\Delta(s) \in \mathbf{B}\Delta$ is then determined by the following theorem which is an extension of Theorem 4.4 on page 44.

Theorem 5.1 *Assume that the interconnection $P(s)$ is stable and that the perturbation $\Delta(s)$ is of such a form that the perturbed closed loop system is stable if and only if the map of $\det(I - P(s)\Delta(s))$ as s traverses the Nyquist \mathcal{D} contour does not encircle the origin. Then the closed loop system in Figure 5.1 on page 64 is stable for all perturbations $\Delta(s) \in \mathbf{B}\Delta$ if and only if*

$$\det(I - P(j\omega)\Delta(j\omega)) \neq 0 \quad \forall \omega, \forall \Delta(j\omega) \in \mathbf{B}\Delta \quad (5.34)$$

$$\Leftrightarrow \rho(P(j\omega)\Delta(j\omega)) < 1 \quad \forall \omega, \forall \Delta(j\omega) \in \mathbf{B}\Delta \quad (5.35)$$

$$\Leftarrow \bar{\sigma}(P(j\omega)) < 1 \quad \forall \omega \quad (5.36)$$

Proof of Theorem 5.1 The proof follows easily from Theorem 4.4 on page 44 with $\Delta(s) \in \mathbf{B}\Delta$. \square

Note that (5.36) is only a sufficient condition for robust stability. The necessity of the similar condition (4.47) on page 45 for unstructured perturbations follows from the fact that the unstructured perturbation set include *all* $\Delta(s)$ with $\bar{\sigma}(\Delta(j\omega)) \leq 1$. Here, however, we restrict the set of perturbations to $\Delta(s) \in \mathbf{B}\Delta$ and therefore, in general, condition (5.36) can be arbitrarily conservative. Rather than a singular value constraint we need some measure which takes into account the structure of the perturbations $\Delta(s)$. This is precisely the structured singular value μ .

Given a matrix $P \in \mathbf{C}^{n \times m}$, the positive real-valued function μ is then defined by:

$$\mu_{\Delta}(P) \triangleq \frac{1}{\min \{ \bar{\sigma}(\Delta) : \Delta \in \mathbf{B}\Delta, \det(I - P\Delta) = 0 \}} \quad (5.37)$$

unless no $\Delta \in \mathbf{\Delta}$ makes $I - P\Delta$ singular, in which case $\mu_{\mathbf{\Delta}}(P) = 0$. Thus $1/\mu_{\mathbf{\Delta}}(P)$ is the “size” of the smallest perturbation Δ , measured by its maximum singular value, which makes $I - P\Delta$ singular ($\det(I - P\Delta) = 0$). If $P(s)$ is a transfer function we can interpret $1/\mu_{\mathbf{\Delta}}(P(j\omega))$ as the size of the smallest perturbation $\Delta(j\omega)$ which shifts the characteristic loci of the transfer matrix $P(s)$ to the Nyquist point -1 at the frequency ω .

From the definition of μ and Theorem 5.1 on the facing page we now have the following theorem for assessing robust stability, see also [DP87, PD93]:

Theorem 5.2 (Robust Stability with μ) *Assume that the interconnection $P(s)$ is stable and that the perturbation $\Delta(s)$ is of such a form that the perturbed closed loop system is stable if and only if the map of $\det(I - P(s)\Delta(s))$ as s traverses the Nyquist \mathcal{D} contour does not encircle the origin. Then the closed loop system in Figure 5.1 on page 64 is stable for all perturbations $\Delta(s) \in \mathbf{B\Delta}$ if and only if :*

$$\|\mu_{\mathbf{\Delta}}(P(s))\|_{\infty} \leq 1 \quad (5.38)$$

where:

$$\|\mu_{\mathbf{\Delta}}(P(s))\|_{\infty} \triangleq \sup_{\omega} \mu_{\mathbf{\Delta}}(P(j\omega)) \quad (5.39)$$

5.1.2 Robust Performance

For robust performance we will include the normalized exogenous disturbances $d'(s)$ and the normalized error signals (controlled outputs) $e'(s)$ into the $N\Delta K$ formulation. Then we may obtain the general framework for robustness analysis and synthesis of linear systems illustrated as in Figure 5.4 on the next page. Any linear interconnection of control inputs u , measured outputs y , disturbances d' , controlled outputs (error signals) e' , perturbations w and a controller K can be expressed within this framework.

Within the general framework analysis and synthesis constitutes two special cases as illustrated in Figure 5.4 on the following page. Like the 2×2 block problem, scalings and weights are conventionally absorbed into the transfer function N in order to normalize d' , e' and $\Delta(s)$ to norm 1. Notice that if we partition $P(s)$ into four blocks consistent with the dimensions of the two input (w , d') and two output (z , e') vectors we can identify $P_{11}(s)$ as the transfer matrix $P(s)$ introduced in the previous section, see e.g. Theorem 5.2. Context will determine which $P(s)$ we refer to.

For robust performance the transfer function F_u from d' to e' may be partitioned

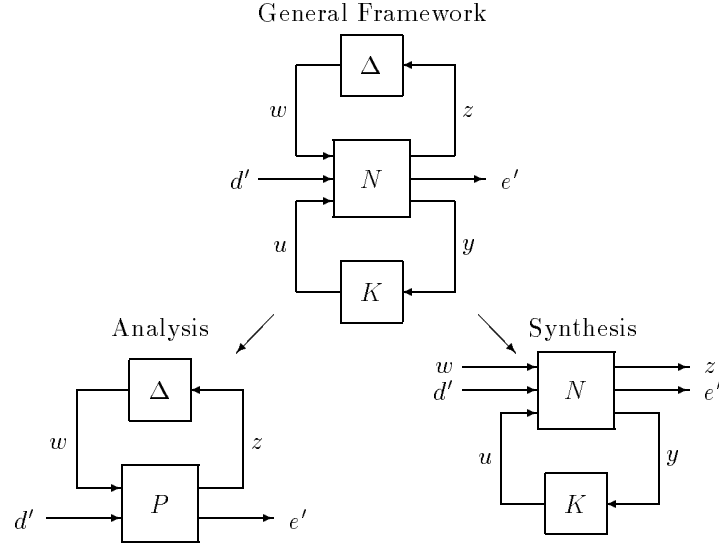


Figure 5.4: A general framework for analysis and synthesis of linear control systems.

as a linear fractional transformation:

$$e'(s) = F_u(P(s), \Delta(s))d'(s) \quad (5.40)$$

$$= \left[P_{22}(s) + P_{21}(s)\Delta(s) (I - P_{11}(s)\Delta(s))^{-1} P_{12}(s) \right] d'(s) \quad (5.41)$$

Here $P_{22}(s)$ is the weighted nominal performance function and $F_u(P(s), \Delta(s))$ is thus the weighted perturbed performance function. Now from (5.41) the robust performance objective becomes

$$\|F_u(P(s), \Delta(s))\|_\infty = \sup_{\omega} \bar{\sigma}(F_u(P(j\omega), \Delta(j\omega))) < 1 \quad \forall \Delta(j\omega) \in \mathbf{B}\mathbf{\Delta} \quad (5.42)$$

As in Section 4.4 on page 49 we notice that the condition for robust performance is a singular value constraint similar to the robust stability condition (4.47) on page 45 and conclude: *the robust performance objective (5.42) is satisfied if and only if the interconnection $F_u(P(s), \Delta(s))$ is robustly stable for a norm bounded matrix perturbation $\Delta_p(s)$ with $\bar{\sigma}(\Delta_p(j\omega)) \leq 1$.* Hence by augmenting the perturbation structure with a full complex performance block $\Delta_p(s)$ the robust performance condition can be equivalenced with an unstructured robust stability condition, see Figure 4.8 on page 51. However, in the μ -framework we can perform

this augmentation naturally since the allowed perturbation structure is block diagonal.

We thus have the following theorem for assessing robust performance, see [DP87, PD93]:

Theorem 5.3 (Robust Performance with μ) *Let an \mathcal{H}_∞ performance specification be given on the transfer function from d' to e' – typically a weighted sensitivity specification – of the form:*

$$\|F_u(P(s), \Delta(s))\|_\infty = \sup_\omega \bar{\sigma}(F_u(P(j\omega), \Delta(j\omega))) < 1 \quad (5.43)$$

Then $F_u(P(s), \Delta(s))$ is stable and $\|F_u(P(s), \Delta(s))\|_\infty < 1$, $\forall \Delta(s) \in \mathbf{B}\mathbf{\Delta}$ if and only if

$$\|\mu_{\tilde{\Delta}}(P(s))\|_\infty \leq 1 \quad (5.44)$$

where the perturbation set is augmented with a full complex performance block:

$$\tilde{\Delta} = \{ \text{diag}(\Delta, \Delta_p) \mid \Delta \in \mathbf{\Delta}, \Delta_p \in \mathbf{C}^{k \times k} \} \quad (5.45)$$

Theorem 5.3 is the real payoff for measuring performance in terms of the ∞ -norm and bounding model uncertainty in the same manner. Using μ it is then possible to test for both robust stability and robust performance in a non-conservative manner. Indeed, if the uncertainty is modeled exactly by $\Delta(s)$, i.e. if all plants in the norm-bounded set can really occur in practice, then the μ condition for robust performance is necessary and sufficient. Notice how the μ theorems provides much tighter conditions for robust performance compared with the \mathcal{H}_∞ results in Section 4.4 on page 49. Performance and stability conditions are now separated, much tighter uncertainty descriptions may be given due to the diagonal structure on $\mathbf{\Delta}$ and non-conservative results are provided for all perturbation models and even for ill-conditioned systems.

Equation (5.44) provides a very simple test for checking robust performance. Plotting $\mu_{\tilde{\Delta}}(P(j\omega))$ versus frequency ω will reveal whether the conditions of Theorem 5.3 are met.

Since $\Delta_1 = \text{diag}\{\Delta, 0\}$ and $\Delta_2 = \text{diag}\{0, \Delta_p\}$ are special cases of $\Delta \in \tilde{\Delta}$ it is clear that

$$\mu_{\tilde{\Delta}}(P(j\omega)) \geq \max\{\mu_{\Delta}(P_{11}(j\omega)), \mu_{\Delta_p}(P_{22}(j\omega)) = \bar{\sigma}(P_{22}(j\omega))\} \quad (5.46)$$

which implies that for robust performance it is necessary that the closed loop system is robustly stable and satisfies the nominal performance objective.

5.1.3 Computation of μ

As we have shown above μ is a powerful tool for assessing robust stability and robust performance under structured and/or unstructured perturbations. Unfortunately the computation of μ is a very difficult and yet unsolved mathematical problem. Equation (5.37) on page 70 is not suitable for computing μ since the implied optimization problem may have multiple local maxima [DP87, FTD91]. However tight upper and lower bounds for μ may be effectively computed for both complex and mixed perturbations sets. Algorithms for computing these bounds have been documented in several papers, see e.g. [DP87, YND91]. For simplicity assume in the following that $P \in \mathbf{C}^{n \times n}$ is square.

5.1.3.1 μ with Complex Perturbations

Let us first consider computation of μ when the perturbation structure consists of complex elements only; thus $m_r = 0$ in (5.2) on page 65. Then we can relate $\mu_{\Delta}(P)$ to familiar linear algebra quantities when Δ is one of two extreme sets [DPZ91]:

- If $\Delta = \{\delta^c I_n \mid \delta^c \in \mathbf{C}\}$ ($m_r = 0, m_c = 1, m_C = 0$ in (5.2)), then $\mu_{\Delta}(P) = \rho(P)$, the spectral radius.
- If $\Delta = \{\Delta \mid \Delta \in \mathbf{C}^{n \times n}\}$ ($m_r = 0, m_c = 0, m_C = 1$ in (5.2)), then $\mu_{\Delta}(P) = \bar{\sigma}(P)$, the maximum singular value.

For a general complex perturbation Δ we have that

$$\{\delta^c I_n \mid \delta^c \in \mathbf{C}\} \subset \Delta \subset \{\Delta \mid \Delta \in \mathbf{C}^{n \times n}\} \quad (5.47)$$

Thus, directly from the definition of μ (5.37) on page 70 we conclude that

$$\rho(P) \leq \mu_{\Delta}(P) \leq \bar{\sigma}(P) \quad (5.48)$$

However, these bounds are insufficient since the gap between $\rho(P)$ and $\bar{\sigma}(P)$ can be arbitrarily large. Thus the bounds (5.48) must be tightened. This is done through transformations on P that *do not affect* $\mu_{\Delta}(P)$ but *do affect* $\rho(P)$ and $\bar{\sigma}(P)$. Define the following two subsets of $\mathbf{C}^{n \times n}$:

$$\mathbf{Q} = \left\{ Q \in \Delta \mid m_r = 0, \delta_i^{c*} \delta_i^c = 1, \Delta_i^* \Delta_i = I_{r_{m_c+i}} \right\} \quad (5.49)$$

$$\mathbf{D} = \left\{ \text{diag} \left(D_1, \dots, D_{m_c}, d_1 I_{r_{m_c+1}}, \dots, d_{m_C} I_{r_{m_c+m_C}} \right) \mid D_i \in \mathbf{C}^{r_i \times r_i}, D_i^* = D_i > 0, d_i \in \mathbf{R}, d_i > 0 \right\} \quad (5.50)$$

It can then be shown, see e.g. the original paper on μ by Doyle [Doy82], that for any $\Delta \in \mathbf{\Delta}$ (with $m_r = 0$), $Q \in \mathbf{Q}$ and $D \in \mathbf{D}$,

$$Q^* \in \mathbf{Q}, \quad Q\Delta \in \mathbf{\Delta}, \quad \Delta Q \in \mathbf{\Delta}, \quad \bar{\sigma}(Q\Delta) = \bar{\sigma}(\Delta Q) = \bar{\sigma}(\Delta), \quad (5.51)$$

$$D\Delta = \Delta D \quad (5.52)$$

From (5.51) and (5.52) follows the next theorem.

Theorem 5.4 (Upper and Lower Bounds on Complex μ) *For all $Q \in \mathbf{Q}$ and $D \in \mathbf{D}$*

$$\mu_{\Delta}(PQ) = \mu_{\Delta}(QP) = \mu_{\Delta}(P) = \mu_{\Delta}(DPD^{-1}) \quad (5.53)$$

Thus the bounds in Equation (5.48) may be tightened to

$$\max_{Q \in \mathbf{Q}} \rho(QP) \leq \mu_{\Delta}(P) \leq \inf_{D \in \mathbf{D}} \bar{\sigma}(DPD^{-1}) \quad (5.54)$$

The lower bound $\max_{Q \in \mathbf{Q}} \rho(QP)$ is in fact an equality [Doy82] but $\rho(QP)$ is unfortunately non-convex with multiple local maxima which are not global. Hence local search cannot be guaranteed to obtain μ but can only yield a lower bound. Computation of the upper bound is a convex problem, so the global minimum $\inf_{D \in \mathbf{D}} \bar{\sigma}(DPD^{-1})$ can, in principle at least, be found. Unfortunately, the upper bound is not always equal to μ . It can be shown that for block structures $\mathbf{\Delta}$ with $m_r = 0$ and $2m_c + m_C \leq 3$, the upper bound is always equal to $\mu_{\Delta}(P)$. However for block structures with $2m_c + m_C > 3$, there exists matrices for which μ is less than the infimum. Nevertheless even in the case where the upper bound do not equal μ exactly numerical experience suggests that the upper bound in general is reasonably tight.

With the release of the MATLAB *μ -Analysis and Synthesis Toolbox* [BDG⁺93] in 1993 commercially available routines exists for computing the bounds in Theorem 5.4. In practical control design (with purely complex perturbations), the mathematical problems with computation of μ may thus be considered rather theoretical.

5.1.3.2 μ with Mixed Real and Complex Perturbations

Computation of the mixed real and complex μ problem has been the focus of intensive research over the last decade, see e.g. [FTD91, YND91, YND92, You93]. It is beyond the scope of this work to treat the bounds on mixed μ ¹ in any great detail. A complete treatment may be found in the thesis by Young [You93]. Here

¹We will often refer to the mixed real and complex μ problem simply as the mixed μ problem.

we will merely state some of the important results on the subject. Let us start by defining the following sets:

$$\mathbf{Q} = \left\{ Q \in \Delta \mid \delta_i^r \in [-1; 1], \delta_i^c \delta_i^c = 1, \Delta_i^* \Delta_i = I_{r_{m_r+m_c+i}} \right\} \quad (5.55)$$

$$\mathbf{D} = \left\{ \text{diag} (D_1, \dots, D_{m_r+m_c}, d_1 I_{r_{m_r+m_c+1}}, \dots, d_{m_c} I_{r_m}) \mid D_i \in \mathbf{C}^{r_i \times r_i}, D_i^* = D_i > 0, d_i \in \mathbf{R}, d_i > 0 \right\} \quad (5.56)$$

$$\mathbf{G} = \left\{ \text{diag} (G_1, \dots, G_{m_r}, O_{r_{m_r+1}}, \dots, O_{r_m}) \mid G_i \in \mathbf{C}^{r_i \times r_i}, G_i = G_i^* \right\} \quad (5.57)$$

$$\hat{\mathbf{D}} = \left\{ \text{diag} (D_1, \dots, D_{m_r+m_c}, d_1 I_{r_{m_r+m_c+1}}, \dots, d_{m_c} I_{r_m}) \mid D_i \in \mathbf{C}^{r_i \times r_i}, \det(D_i) \neq 0, d_i \in \mathbf{C}, d_i \neq 0 \right\} \quad (5.58)$$

$$\hat{\mathbf{G}} = \left\{ \text{diag} (g_1, \dots, g_{n_r}, O_{n_c}) \mid g_i \in \mathbf{R} \right\} \quad (5.59)$$

where $r_m = r_{m_r+m_c+m_c}$, $n_r = \sum_{i=1}^{m_r} r_i$ and $n_c = n - n_r$. Notice that for compatibility with $P(s)$ we must have that $\sum_{i=1}^m r_i = n$.

We then have the upper and lower bounds as in Theorem 5.5 [FTD91].

Theorem 5.5 (Upper and Lower Bounds on Mixed μ [FTD91]) *Let $\bar{\lambda}_R$ denote the largest real eigenvalue and let $\rho_R(P)$ denote the real spectral radius of P :*

$$\rho_R(P) \triangleq \max \{ |\lambda_R(P)| : \lambda_R(P) \text{ is a real eigenvalue of } P \} \quad (5.60)$$

If P has no real eigenvalues then $\rho_R(P) = 0$. Furthermore suppose that α_ is the result of the minimization problem*

$$\alpha_* = \inf_{D \in \mathbf{D}, G \in \mathbf{G}} \min_{\alpha \in \mathbf{R}} \{ \alpha \mid \bar{\lambda}_R (P^* D P + j (G P - P^* G) - \alpha D) \leq 0 \} \quad (5.61)$$

then

$$\rho_R(P) \leq \mu_\Delta(P) \leq \sqrt{\max(0, \alpha_*)} \quad (5.62)$$

Notice that computation of the upper bound involves a Linear Matrix Inequality (LMI). A variety of numerical techniques exist to tackle such minimizations. Furthermore, numerical recipes for solving LMIs is an area of intensive research.

However, even for comparatively medium size problems ($n \leq 100$), the optimization over the D and G scaling matrices could involve thousands of parameters. Thus, in order to tackle such problems with reasonably computation times, straightforward application of brute force optimization techniques will not suffice. Therefore the above bounds have been reformulated exploiting the specific structure of the mixed μ upper bound problem, see e.g. [YND92]. Several forms of the upper bound can be found as stated in Theorem 5.6.

Theorem 5.6 (Reformulation of Mixed μ Upper Bound) *Suppose we have a matrix $P \in \mathbf{C}^{n \times n}$ and a real scalar $\beta > 0$. Furthermore for any $D \in \mathbf{C}^{n \times n}$ denote $P_D = D P D^{-1}$. Then the following statements are equivalent:*

1. *There exists matrices $D_1 \in \mathbf{D}$, $G_1 \in \mathbf{G}$ such that:*

$$\bar{\lambda}_R(P^* D_1 P + j(G_1 P - P^* G_1) - \beta^2 D_1) \leq 0 \quad (5.63)$$

2. *There exists matrices $D_2 \in \mathbf{D}$, $G_2 \in \mathbf{G}$ (or $D_2 \in \hat{\mathbf{D}}$, $G_2 \in \hat{\mathbf{G}}$) such that:*

$$\bar{\lambda}_R(P_{D_2}^* P_{D_2} + j(G_2 P_{D_2} - P_{D_2}^* G_2)) \leq \beta^2 \quad (5.64)$$

3. *There exists matrices $D_3 \in \mathbf{D}$, $G_3 \in \mathbf{G}$ (or $D_3 \in \hat{\mathbf{D}}$, $G_3 \in \hat{\mathbf{G}}$) such that:*

$$\bar{\sigma} \left[\left(\frac{P_{D_3}}{\beta} - jG_3 \right) (I + G_3^2)^{-\frac{1}{2}} \right] \leq 1 \quad (5.65)$$

4. *There exists matrices $D_4 \in \mathbf{D}$, $G_4 \in \mathbf{G}$ (or $D_4 \in \hat{\mathbf{D}}$, $G_4 \in \hat{\mathbf{G}}$) such that:*

$$\bar{\sigma} \left[(I + G_4^2)^{-\frac{1}{4}} \left(\frac{P_{D_4}}{\beta} - jG_4 \right) (I + G_4^2)^{-\frac{1}{4}} \right] \leq 1 \quad (5.66)$$

Proofs may be found in [You93]. Using the equivalence relations from the above Theorem we may easily form alternative upper bounds on μ . In particular, the bound implemented in the MATLAB μ toolbox is derived from (5.66). Define β^* as:

$$\beta^* = \inf_{\beta \in \mathbf{R}_+, G \in \hat{\mathbf{G}}, D \in \hat{\mathbf{D}}} \{ \beta \mid \bar{\sigma}(P_{DG}) \leq 1 \} \quad (5.67)$$

with P_{DG} given by

$$P_{DG} = (I + G^2)^{-\frac{1}{4}} \left(\frac{D P D^{-1}}{\beta} - jG \right) (I + G^2)^{-\frac{1}{4}} \quad (5.68)$$

then

$$\max_{Q \in \mathbf{Q}} \rho(QP) \leq \mu_{\Delta}(P) \leq \beta^* \quad (5.69)$$

5.2 μ Synthesis

For robust synthesis the transfer function F_l from $[w \ d']^T$ to $[z \ e']^T$ may be partitioned as the linear fractional transformation:

$$\begin{bmatrix} z(s) \\ e'(s) \end{bmatrix} = F_l(N(s), K(s)) \begin{bmatrix} w(s) \\ d'(s) \end{bmatrix} = \begin{bmatrix} N_{11}(s) + N_{12}(s)K(s) & (I - N_{22}(s)K(s))^{-1} N_{21}(s) \end{bmatrix} \begin{bmatrix} w(s) \\ d'(s) \end{bmatrix} \quad (5.70)$$

Noticing that $F_l(N(s), K(s)) = P(s)$ and using Theorem 5.3 on page 73 a stabilizing controller $K(s)$ achieves robust performance if and only if for each frequency $\omega \in [0, \infty]$, the structured singular value satisfies:

$$\mu_{\tilde{\Delta}}(F_l(N(j\omega), K(j\omega))) < 1 \quad (5.71)$$

Consequently the robust performance problem becomes one of synthesizing a nominally stabilizing controller $K(s)$ that minimizes $\mu_{\tilde{\Delta}}(F_l(N, K))$ across frequency:

$$K(s) = \arg \min_{K(s) \in \mathcal{K}_S} \left\| \mu_{\tilde{\Delta}}(F_l(N(s), K(s))) \right\|_{\infty} \quad (5.72)$$

where \mathcal{K}_S denotes the set of all nominally stabilizing controllers.

5.2.1 Complex μ Synthesis – D - K Iteration

Unfortunately (5.72) is not tractable since μ cannot be directly computed. Rather the upper bound on μ is used to formulate the control problem. For purely complex perturbations, $m_r = 0$ in (5.2) on page 65, the upper bound problem becomes

$$K(s) = \arg \min_{K(j\omega) \in \mathcal{K}_S} \sup_{\omega} \inf_{D(\omega) \in \mathbf{D}} \left\{ \bar{\sigma}(D(\omega) F_l(N(j\omega), K(j\omega)) D^{-1}(\omega)) \right\} \quad (5.73)$$

Unfortunately, it is also not known how to solve (5.73). However an approximation to complex μ synthesis can be made by the following iterative scheme. For a fixed controller $K(s)$, the problem of finding $D(\omega)$ at a set of chosen frequency points ω is just the complex μ upper bound problem which is a convex problem with known solution. Having found these scalings we may fit a real rational stable minimum phase transfer function matrix $D(s)$ to $D(\omega)$ by fitting each element of $D(\omega)$ with a real rational stable minimum phase SISO transfer function. We may impose the extra constraint that the approximations $D(s)$ should be minimum phase (so that $D^{-1}(s)$ is stable too) since any phase in $D(s)$ is absorbed into

the complex perturbations. For a given magnitude of $D(\omega)$, the phase corresponding to a minimum phase transfer function system may be computed using complex cepstrum techniques. Accurate transfer function estimates may then be generated using standard frequency domain least squares techniques.

For given scalings $D(s)$ the problem of finding a controller $K(s)$ which minimizes the norm $\|F_l(D(s)N(s)D^{-1}(s), K(s))\|_\infty$ will be reduced to a standard \mathcal{H}_∞ problem. Repeating this procedure, denoted D - K iteration, several times will yield the complex μ optimal controller provided the algorithm converges. Even though the computation of the D scalings and the optimal \mathcal{H}_∞ controller are both convex problems, the D - K iteration procedure is *not jointly convex* in $D(s)$ and $K(s)$ and counter examples of convergence has been given [Doy85]. However, D - K iteration seems to work quite well in practice and has been successfully applied to a large number of applications. The D - K iteration procedure may be outlined as below.

Procedure 5.1 (D - K Iteration)

1. Given an augmented system $N(s)$, let $i = 1$ and $D_i^*(\omega) = I, \forall \omega$.
2. Fit a stable minimum phase transfer function matrix $D_i(s)$ to the pointwise scalings $D_i^*(\omega)$. Augment $D_i(s)$ with a unity matrix of appropriate size such that $D_i(s)$ is compatible with $N(s)$. Construct the interconnection $N_{D_i}(s) = D_i(s)N(s)D_i^{-1}(s)$.
3. Find the \mathcal{H}_∞ optimal controller $K_i(s)$:

$$K_i(s) = \arg \min_{K(s) \in \mathcal{K}_s} \|F_l(N_{D_i}(s), K(s))\|_\infty \quad (5.74)$$

4. Compute the new scalings $D_{i+1}^*(\omega)$ solving the complex μ upper bound problem

$$D_{i+1}^*(\omega) = \arg \min_{D(\omega) \in \mathbf{D}} \{ \bar{\sigma} (D(\omega)F_l(N(j\omega), K_i(j\omega))D^{-1}(\omega)) \} \quad (5.75)$$

pointwise across frequency ω .

5. Compare $D_{i+1}^*(\omega)$ and $D_i^*(\omega)$. Stop if they are close. Otherwise let $i = i+1$ and repeat from 2.

Notice that we use the \mathcal{H}_∞ optimal control solution to synthesize the controller in step 3. The K -step of the procedure may be illustrated as in Figure 5.5 on the following page.

With the release of the MATLAB *μ -Analysis and Synthesis Toolbox* commercially available software now exists to support complex μ synthesis using D - K iteration. The procedure 5.1 may be implemented quite easily with the aid of the toolbox.

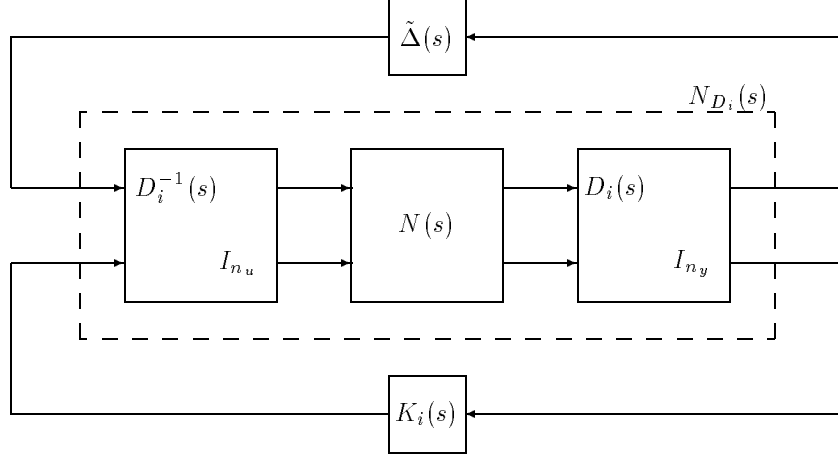


Figure 5.5: K -step of D - K iteration. n_u and n_y are the number of manipulated and controlled variables respectively.

In the current release of the μ toolbox (Version 2.0), repeated scalar complex blocks are not supported in connection with D - K iteration. For repeated scalar blocks, notice that the corresponding D scaling is a full matrix. Thus the number of SISO transfer function approximations needed in connection with D - K iteration grows quadratically with the number of repeated scalar perturbations. An approximation to D - K iteration with repeated scalar blocks can of course be made simply by considering them as uncorrelated. However, the design will then not be optimal but by analyzing the final design with the true perturbation structure the amount of conservatisms introduced can be assessed.

Notice furthermore that an approximation to mixed real and complex μ synthesis can be achieved with D - K iteration by approximating the mixed perturbation set Δ with the corresponding complex set Δ_c , see (5.3) on page 65. Thus all real perturbations are approximated with complex ones. Again, the design will not be optimal but through μ analysis the design may be tested against the true perturbation structure.

5.2.2 Mixed μ Synthesis – D , G - K Iteration

The general mixed real and complex μ problem is unfortunately much more difficult than the purely complex μ problem. In fact, until recently it was an

unsolved problem. In his thesis [You93] and the papers [YÅ94, You94] Young has presented a solution, denoted *D, G-K iteration*, to the mixed μ synthesis problem. This approach is strongly motivated by the *D-K* procedure for purely complex perturbations. Young chooses the formulation 3 from Theorem 5.6 on page 77 to pose the mixed μ upper bound problem

$$K(s) = \arg \min_{K(j\omega) \in \mathcal{K}_S} \sup_{\omega} \inf_{D(\omega) \in \mathbf{D}, G(\omega) \in \mathbf{G}} \inf_{\beta(\omega) \in \mathbf{R}_+} \{ \beta(\omega) \mid \bar{\sigma}(\Gamma(\omega)) \leq 1 \} \quad (5.76)$$

where

$$\Gamma(\omega) = \left(\frac{D(\omega) F_l(N(j\omega), K(j\omega)) D^{-1}(\omega)}{\beta(\omega)} - jG(\omega) \right) (I + G^2(\omega))^{-\frac{1}{2}} \quad (5.77)$$

We will denote this a *direct* upper bound problem emphasizing that the problem is posed directly in line with the way the upper bound is computed. Again no known solution to (5.77) exists. Rather it must be solved iteratively similarly to *D-K* iteration. For fixed $K(s)$ the problem of finding $D(\omega)$, $G(\omega)$ and $\beta(\omega)$ is just the mixed μ upper bound problem. Having found these scalings we may fit real rational transfer function matrices to them such that the interconnection is stable. For given β , $D(s)$ and $G(s)$ transfer matrices the problem of finding the controller $K(s)$ will be reduced to a standard \mathcal{H}_∞ problem.

However, the upper bound problem in (5.76)-(5.77) is not in the form of a singular value minimization such as (5.73), but rather a minimization subject to a singular value constraint. Thus we cannot proceed as before for purely complex perturbations. Instead we need the following 2 theorems which tell us how the mixed μ upper bound scales. Easy proofs may be found in [You93].

Theorem 5.7 (Scaling of Mixed μ Upper Bound I) *Suppose we have matrices $P \in \mathbf{C}^{n \times n}$, $D \in \mathbf{D}$, $G \in \mathbf{G}$ and a real scalar $\beta > 0$ such that*

$$\bar{\sigma} \left(\left(\frac{DPD^{-1}}{\beta} - jG \right) (I + G^2)^{-\frac{1}{2}} \right) \leq 1 \quad (5.78)$$

Thus β is an upper bound on $\mu_\Delta(P)$. Then for any real $\hat{\beta} > \beta$ there exists matrices $\hat{D} \in \mathbf{D}$, $\hat{G} \in \mathbf{G}$ such that

$$\bar{\sigma} \left(\left(\frac{\hat{D}P\hat{D}^{-1}}{\hat{\beta}} - j\hat{G} \right) (I + \hat{G}^2)^{-\frac{1}{2}} \right) < 1 \quad (5.79)$$

Theorem 5.8 (Scaling of Mixed μ Upper Bound II) *Suppose we have matrices $P \in \mathbf{C}^{n \times n}$, $D \in \mathbf{D}$, $G \in \mathbf{G}$ and real scalars $\beta > 0$ and $0 < r \leq 1$ such that*

$$\bar{\sigma} \left(\left(\frac{DPD^{-1}}{\beta} - jG \right) (I + G^2)^{-\frac{1}{2}} \right) \leq r \quad (5.80)$$

Then there exists matrices $\hat{D} \in \mathbf{D}$, $\hat{G} \in \mathbf{G}$ such that

$$\bar{\sigma} \left(\left(\frac{\hat{D}P\hat{D}^{-1}}{r\beta} - j\hat{G} \right) (I + \hat{G}^2)^{-\frac{1}{2}} \right) \leq 1 \quad (5.81)$$

such that $r\beta$ is an upper bound on $\mu_{\Delta}(P)$.

Both these results are obviously true in the complex case for $G = O_n$ since

$$\bar{\sigma} \left(\frac{DPD^{-1}}{\beta} \right) \leq 1 \Leftrightarrow \frac{\beta}{\bar{\beta}} \bar{\sigma} \left(\frac{DPD^{-1}}{\beta} \right) \leq \frac{\beta}{\bar{\beta}} \Leftrightarrow \bar{\sigma} \left(\frac{DPD^{-1}}{\bar{\beta}} \right) < 1 \quad (5.82)$$

$$\bar{\sigma} \left(\frac{DPD^{-1}}{\beta} \right) \leq r \Leftrightarrow \bar{\sigma} \left(\frac{DPD^{-1}}{r\beta} \right) \leq 1 \quad (5.83)$$

However, the results are not so obvious in the mixed case. In particular, note that Theorem 5.8 on the page before applies *only* for $r \leq 1$.

Young then proposes the following iterative scheme for mixed μ synthesis.

Procedure 5.2 (\mathbf{D}, \mathbf{G} -K Iteration [You93])

1. Given an augmented system $N(s)$, let $i = 1$, $D_i^*(w) = I_n, \forall w$, $G_i^*(\omega) = O_n, \forall \omega$ and $\beta_i^* = 1$.
2. Fit transfer function matrices $D_i(s)$ and $G_i(s)$ to the pointwise scalings $D_i^*(\omega)$ and $jG_i^*(\omega)$ so that $D_i(j\omega)$ approximates $D_i^*(\omega)$ and $G_i(j\omega)$ approximates $jG_i^*(\omega)$. Replace $D_i(s)$ and $G_i(s)$ with appropriate factors so that $D_i(s)$, $D_i^{-1}(s)$, $G_{h,i}(s)$ and $G_i(s)G_{h,i}(s)$ are all stable, where $G_{h,i}(s)$ is a spectral factor satisfying $(I + G_i(s)G_i(-s)^T)^{-1} = G_{h,i}(s)G_{h,i}(-s)^T$. Augment $D_i(s)$ and $G_{h,i}(s)$ with identity matrices, and $G_i(s)$ with a zero matrix of appropriate dimensions so that $D_i(s)$, $G_i(s)$ and $G_{h,i}(s)$ are all compatible with $N(s)$. Construct the interconnection

$$N_{DG_i}(s) = (D_i(s)N(s)D_i^{-1}(s) - \beta_i^*G_i(s))G_{h,i}(s) \quad (5.84)$$

3. Find the \mathcal{H}_∞ optimal controller $K_i(s)$:

$$K_i(s) = \arg \min_{K(s) \in \mathcal{K}_S} \|F_l(N_{DG_i}(s), K(s))\|_\infty \quad (5.85)$$

4. Compute the maximum upper bound $\beta_{i+1}^* = \|\mu_{\hat{\Delta}}(F_l(N(s), K(s)))\|_\infty$:

$$\beta_{i+1}^* = \sup_{\omega \in \mathbf{R}} \inf_{D(\omega) \in \mathbf{D}, G(\omega) \in \mathbf{G}} \inf_{\beta(\omega) \in \mathbf{R}_+} \{\beta(\omega) \mid \bar{\sigma}(\Gamma) \leq 1\} \quad (5.86)$$

where Γ is given by

$$\Gamma = \left(\frac{D(\omega)F_l(N(j\omega), K_i(j\omega))D^{-1}(\omega)}{\beta(\omega)} - jG(\omega) \right) (I + G^2(\omega))^{-\frac{1}{2}} \quad (5.87)$$

5. Calculate the new scalings $D_{i+1}^*(\omega)$ and $G_{i+1}^*(\omega)$ solving the minimization problem

$$\inf_{D_{i+1}^*(\omega) \in \mathbf{D}, G_{i+1}^*(\omega) \in \mathbf{G}} \bar{\sigma} \left(\left(\frac{D_{i+1}^*(\omega) F_l(N(j\omega), K_i(j\omega)) D_{i+1}^{*-1}(\omega)}{\beta_{i+1}^*} - jG_{i+1}^*(\omega) \right) \left(I + G_{i+1}^{*2}(\omega) \right)^{-\frac{1}{2}} \right) \quad (5.88)$$

pointwise across frequency.

6. Compare the new scalings $D_{i+1}^*(\omega)$ and $G_{i+1}^*(\omega)$ with the previous ones. Stop if they are close. Otherwise let $i = i + 1$ and repeat from 2.

The similarities between the D - K iteration, see Procedure 5.1 on page 79, and the above D, G - K iteration are obvious. However, there is one notable difference, namely the determination of the scaling matrices in step 5 of the D, G - K iteration. Notice that $D_{i+1}^*(\omega)$ and $G_{i+1}^*(\omega)$ are *not* the scalings from the μ upper bound computation in step 4. Rather it is a similar minimization with *constant* $\beta = \beta_{i+1}^*$. As we shall soon see, this “twist” is necessary to avoid “pop-up” type phenomena where for some frequencies a small increase in the maximum singular value creates a very large increase in μ .

D, G - K iteration, as the corresponding D - K iteration for complex perturbations, cannot be guaranteed to converge to the global minimum of (5.76) on page 81 since the procedure is not jointly convex in the scalings and the controller. However, we can show that it is monotonically non-increasing in $\mu_{\hat{\Delta}}(F_l(N(s), K(s)))$ given perfect realizations of the scaling matrices. Then under weak conditions the procedure will converge to a local minimum of μ . Having converged to such a point, the controller $K_i(s)$ from step 3 in Procedure 5.2 on the facing page is the final mixed μ controller which satisfies

$$\sup_{\omega \in \mathbf{R}} \mu_{\hat{\Delta}}(F_l(N(j\omega), K(j\omega))) \leq \beta_{i+1}^* \quad (5.89)$$

Again we have used the \mathcal{H}_∞ optimal control solution to synthesize the controller in step 3. The K -step of D, G - K iteration can be illustrated as in Figure 5.6 on the next page

In order to show that Procedure 5.2 on the facing page is non-increasing in μ we will need the results from Theorem 5.7 and 5.8 on page 81. Note that β_{i+1}^* was defined in step 4 as the maximum of the μ upper bound across frequency. Thus if $\beta_{i+1}(\omega)$ denotes the μ upper bound across frequency ω , then $\beta_{i+1}^* \geq \beta_{i+1}(\omega)$ for all frequencies, with $\beta_{i+1}^* = \beta_{i+1}(\omega)$ only for those frequency points where the maximum is achieved. Then Theorem 5.7 on page 81 guarantees that in step 5

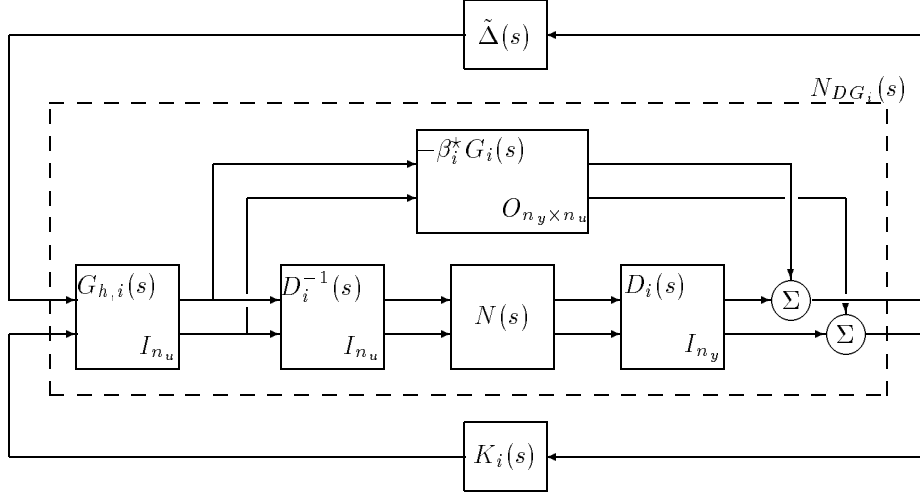


Figure 5.6: K -step of D, G - K iteration. n_u and n_y are the number of manipulated and controlled variables respectively.

we can achieve:

$$\bar{\sigma} \left(\left(\frac{D_{i+1}^*(\omega) F_l(N(j\omega), K_i(j\omega)) D_{i+1}^{*-1}(\omega)}{\beta_{i+1}^*} - jG_{i+1}^*(\omega) \right) \left(I + G_{i+1}^{*2}(\omega) \right)^{-\frac{1}{2}} \right) < 1 \quad (5.90)$$

for all frequency points where $\beta_{i+1}^* > \beta_{i+1}(\omega)$ and

$$\bar{\sigma} \left(\left(\frac{D_{i+1}^*(\omega) F_l(N(j\omega), K_i(j\omega)) D_{i+1}^{*-1}(\omega)}{\beta_{i+1}^*} - jG_{i+1}^*(\omega) \right) \left(I + G_{i+1}^{*2}(\omega) \right)^{-\frac{1}{2}} \right) = 1 \quad (5.91)$$

for points where $\beta_{i+1}^* = \beta_{i+1}$. Then note that for perfect realizations of the (new) scalings $D_{i+1}(s)$ and $G_{i+1}(s)$ in step 2 of the next iteration we will have that

$$\|F_l(N_{DG_{i+1}}(s), K_i(s))\|_\infty = \beta_{i+1}^* \quad (5.92)$$

Thus if we close the new augmented system $N_{DG_{i+1}}(s)$ with the previous controller, the maximum singular value of the interconnection equals β_{i+1}^* . Thus we

are guaranteed the existence of a stabilizing controller in step 3 achieving at least this level since we may simply choose the previous controller. Thus the new \mathcal{H}_∞ optimal controller $K_{i+1}(s)$ will satisfy

$$\|F_l(N_{DG_{i+1}}(s), K_{i+1}(s))\|_\infty = r\beta_{i+1}^* \quad (5.93)$$

for some $r \in [0, 1]$. Then Theorem 5.8 on page 81 implies that $r\beta_{i+1}^*$ is now an upper bound for mixed μ across frequency. Thus the new $\beta = \beta_{i+2}^*$ in step 4 will yield $\beta_{i+2}^* \leq r\beta_{i+1}^* \leq \beta_{i+1}^*$. Consequently the iteration is monotonically non-increasing in the upper bound. Furthermore if the new \mathcal{H}_∞ optimal controller $K_{i+1}(s)$ achieves any improvement over the old one $K_i(s)$ so that $r < 1$ then the peak value of the mixed μ upper bound across frequency ω will be strictly decreased.

Thus the way the interconnection $N_{DG_{i+1}}(s)$ is constructed guarantees that if the new controller $K_{i+1}(s)$ reduces the \mathcal{H}_∞ norm of $F_l(N_{DG_{i+1}}(s), K_{i+1}(s))$, then the peak value of the mixed μ upper bound across frequency is reduced. It is important to have this guarantee because it ensures that we do not suffer from any “pop-up” type phenomena as discussed above. The possibility of this type of behavior is a direct consequence of the fact that Theorem 5.8 on page 81 does not hold for $r > 1$. The D, G - K iteration procedure explicitly inhibits such “pop-up” type of behavior.

The necessary factorizations required to carry out step 2 in the D, G - K iteration above are described in [You93]. Note however that for the general upper bound problem the scalings cannot in general be restricted to be minimum phase since the phase is not absorbed into the (real) perturbations. Thus the scalings must be fitted both in magnitude and phase. One exception is the diagonal elements of the D -scalings. For the G scalings we must require that the phase of the diagonal elements of $G_i(j\omega)$ is 90° for all frequencies ω . The fitting of these purely imaginary diagonal elements can only be obtained using high order all pass structures. Since the order of $G_i^*(s)$ adds to the order of the controller $K(s)$, the final controller will usually be of very high order.

Successful results on D, G - K iteration has been reported for simple mixed μ problems, see e.g. [You94]. However, the need for fitting purely complex scalings with high order all-pass transfer functions as well as the general need for fitting both in phase and magnitude severely hampers the practical use of D, G - K iteration for mixed μ synthesis. In many applications the G scalings seem to change quite suddenly. Thus it may be very difficult to obtain any reasonable fit for G .

5.2.3 Mixed μ Synthesis – μ - K Iteration

As discussed above the general D, G - K approach for controller synthesis with mixed perturbation sets Δ provides a procedure which is monotonically non-

increasing in the mixed μ upper bound. Unfortunately, the D, G - K -iteration is much more complicated than the corresponding D - K iteration for purely complex perturbations. In particular the fitting of scaling matrices is much more complex in the mixed case since we are forced to fit both in phase and magnitude. Especially fitting the purely imaginary diagonal elements of $jG^*(\omega)$ with high order all-pass structures will be difficult and furthermore result in augmented systems $N_{DG_i}(s)$ of very high orders. Even though the commercially available software tools for \mathcal{H}_∞ optimal controller synthesis works quite well also for high order systems, when the order exceeds 100, the algorithms slow down rather dramatically, even on high-performance UNIX installations.

In the following we will propose a new approach to mixed μ synthesis, denoted μ - K iteration, which sacrifices some of the guaranteed convergence properties of D, G - K iteration, but which on the other hand only requires that scalings are fitted in magnitude.

Whereas the D, G - K approach is a *direct* upper bound minimization, μ - K iteration is an *indirect* upper bound minimization in the sense that the augmented system matrix corresponding to $N_{DG}(s)$ above does not directly reflect the structure of the μ upper bound as in (5.77) on page 81.

The main idea of the proposed μ - K iteration scheme is to perform a scaled D - K iteration where the ratio between mixed and complex μ is taken into account through an additional scaling matrix $\Gamma(s)$. Given the augmented system $N(s)$ and any stabilizing controller $K(s)$ we may compute upper bounds for μ across frequency given both the “true” mixed perturbation set $\tilde{\Delta}$ and a fully complex approximation $\tilde{\Delta}_c$, see Equation (5.3) on page 65. In order to “trick” the \mathcal{H}_∞ optimal controller in the next iteration to concentrate more on mixed μ , we will construct a system $N_{D\Gamma}(s)$ such that $\bar{\sigma}(F_l(N_{D\Gamma}(j\omega), K(j\omega)))$ approximates the mixed μ upper bound just computed. This is fully equivalent to D, G - K iteration. In μ - K iteration, however, the structure of the approximation is different. $N_{D\Gamma}(s)$ is constructed by applying two scalings to the original system $N(s)$. A D scaling such that $\bar{\sigma}(F_l(N_{D\Gamma}(j\omega), K(j\omega)))$ approximates the complex μ upper bound and a Γ scaling to shift from complex to mixed μ . In order to avoid the “pop-up” type phenomena discussed in connection with D, G - K iteration, the Γ scalings are filtered through a first order filter with filter constant α .

The iteration is performed as follows:

Procedure 5.3 (μ - K Iteration)

1. Given the augmented system $N(s)$, let $\gamma_0(s) = 1$, $D_0(s) = I$ and $N_{D\Gamma_0}(s)$ be given by

$$N_{D\Gamma_0}(s) = \begin{bmatrix} \gamma_0(s)I_{n_{ze}} & 0 \\ 0 & I_{n_y} \end{bmatrix} D_0(s)N(s)D_0^{-1}(s) \quad (5.94)$$

$$= \Gamma_0(s)D_0(s)N(s)D_0^{-1}(s) = N(s). \quad (5.95)$$

n_y denotes the number of controlled outputs $y(s)$ and n_{ze} denotes the number of external outputs $z(s) + e'(s)$. Let $K_0(s) = K_1(s)$ be a stabilizing controller and $i = 1$.

2. Compute the mixed and corresponding complex μ upper bounds $\bar{\mu}_{\bar{\Delta}}(F_l(N(j\omega), K_i(j\omega)))$ and $\bar{\mu}_{\bar{\Delta}_e}(F_l(N(j\omega), K_i(j\omega)))$ at each frequency ω . Note that the complex μ upper bound equals $\bar{\sigma}(D_i^*(\omega)F_l(N(j\omega), K_i(j\omega))D_i^{*-1}(\omega))$ where the scalings $D_i^*(\omega)$ are found solving the minimizations

$$D_i^*(\omega) = \arg \min_{D \in \mathbf{D}} \bar{\sigma}(DF_l(N(j\omega), K_i(j\omega))D^{-1}) \quad \forall \omega \geq 0. \quad (5.96)$$

3. Compute $\beta_i(\omega)$ given by:

$$\beta_i(\omega) = \frac{\bar{\mu}_{\bar{\Delta}}(F_l(N(j\omega), K_i(j\omega)))}{\bar{\mu}_{\bar{\Delta}_e}(F_l(N(j\omega), K_i(j\omega)))} \frac{1}{|\gamma_{i-1}(j\omega)|} - 1 \quad (5.97)$$

4. Fit, in magnitude, a stable minimum phase transfer function matrix $D_i(s)$ to $D_i^*(\omega)$ so that $D_i(j\omega)$ approximates $D_i^*(\omega)$ across frequency ω . Augment $D_i(s)$ with a unity matrix of appropriate size such that $D_i(s)$ is compatible with $N(s)$.

5. Determine an upper bound for the constant $\alpha_i \in [0; 1]$ according to

$$\bar{\alpha}_i(\omega) = \begin{cases} \min\{1, \xi_i(\omega)\} & \text{if } \beta_i(\omega) > 0 \\ 1 & \text{if } \beta_i(\omega) \leq 0 \end{cases} \quad (5.98)$$

where $\xi_i(\omega)$ is given by

$$\xi_i(\omega) = \left(\frac{\|F_l(N_{D\Gamma_{i-1}}(s), K_{i-1}(s))\|_\infty}{\bar{\sigma}(F_l(D_i(j\omega)N(j\omega)D_i^{-1}(j\omega), K_i(j\omega)))} \frac{1}{|\gamma_{i-1}(j\omega)|} - 1 \right) \frac{1}{\beta_i(\omega)} \quad (5.99)$$

6. Choose a constant $\alpha_i = \kappa \inf_\omega \bar{\alpha}_i(\omega)$ where $\kappa \in [0; 1]$ and compute for all ω :

$$\gamma_i^*(\omega) = (1 - \alpha_i)|\gamma_{i-1}(j\omega)| + \alpha_i \frac{\bar{\mu}_{\bar{\Delta}}(F_l(N(j\omega), K_i(j\omega)))}{\bar{\mu}_{\bar{\Delta}_e}(F_l(N(j\omega), K_i(j\omega)))} \quad (5.100)$$

Fit, in magnitude, a stable minimum phase scalar transfer function $\gamma_i(s)$ to $\gamma_i^*(\omega)$ such that $\gamma_i(j\omega)$ approximates $\gamma_i^*(\omega)$ across frequency ω .

7. Construct

$$N_{D\Gamma_i}(s) = \begin{bmatrix} \gamma_i(s)I_{n_{ze}} & 0 \\ 0 & I_{n_y} \end{bmatrix} D_i(s)N(s)D_i^{-1}(s) \quad (5.101)$$

$$= \Gamma_i(s)D_i(s)N(s)D_i^{-1}(s) \quad (5.102)$$

and compute the optimal \mathcal{H}_∞ controller:

$$K_{i+1}(s) = \arg \min_{K(s) \in \mathcal{K}_S} \|F_l(N_{D\Gamma_i}(s), K(s))\|_\infty \quad (5.103)$$

8. Compute the mixed and corresponding complex μ upper bounds $\bar{\mu}_{\tilde{\Delta}}(F_l(N(j\omega), K_{i+1}(j\omega)))$ and $\bar{\mu}_{\tilde{\Delta}_e}(F_l(N(j\omega), K_{i+1}(j\omega)))$ at each frequency ω . Computation of $\bar{\mu}_{\tilde{\Delta}_e}(F_l(N(j\omega), K_{i+1}(j\omega)))$ provides the scalings $D_{i+1}^*(\omega)$ for the next iteration.

9. Compute $\beta_{i+1}(\omega)$ given by:

$$\beta_{i+1}(\omega) = \frac{\bar{\mu}_{\tilde{\Delta}}(F_l(N(j\omega), K_{i+1}(j\omega)))}{\bar{\mu}_{\tilde{\Delta}_e}(F_l(N(j\omega), K_{i+1}(j\omega)))} \frac{1}{|\gamma_i(j\omega)|} - 1 \quad (5.104)$$

10. If $\sup_\omega |\beta_{i+1}(\omega)| > \sup_\omega |\beta_i(\omega)|$ return to 6 and reduce κ . Otherwise let $i = i + 1$.

11. Compare $D_{i+1}(s)$ and $\gamma_i(s)$ with the previous scalings $D_i(s)$ and $\gamma_{i-1}(s)$. Stop if they are close and $\sup_\omega |\beta_{i+1}(\omega)| \approx 0$. Otherwise repeat from step 4.

Clearly, μ - K iteration is not so conceptually straight forward as D - K iteration for purely complex perturbation nor D, G - K iteration for mixed perturbation sets. The main obstacle is to avoid the “pop-up” phenomena.

In order to clarify matters a bit, let us assume perfect realizations of the D and Γ scalings and that we may choose $\alpha_1 = 1$. Then

$$\bar{\sigma}(F_l(N_{D\Gamma_1}(j\omega), K_1(j\omega))) = F_l(\Gamma_1(j\omega)D_1(j\omega)N(j\omega)D_1^{-1}(j\omega), K_1(j\omega)) \quad (5.105)$$

$$= |\gamma_1(j\omega)| \bar{\sigma}(F_l(D_1(j\omega)N(j\omega)D_1^{-1}(j\omega), K_1(j\omega))) \quad (5.106)$$

$$= |\gamma_1(j\omega)| \bar{\mu}_{\tilde{\Delta}_e}(F_l(N(j\omega), K_1(j\omega))) \quad (5.107)$$

$$= \bar{\mu}_{\tilde{\Delta}}(F_l(N(j\omega), K_1(j\omega))) \quad \text{for } \alpha_1 = 1 \quad (5.108)$$

and the controller $K_2(s)$ will minimize the ∞ -norm of an augmented system which closed with the previous controller $K_1(s)$ has maximum singular value approximating mixed μ . New mixed and complex μ bounds may then be computed and the procedure may be repeated. Unfortunately it is not possible to choose

$\alpha_i = 1$ in general since we may then suffer from “pop-up” type phenomena, where for some frequencies a small increase in the maximum singular value of $N_{D\Gamma_i}(s)$ creates a very large increase in μ . However by reducing α , that is by filtering γ through a stable first order filter, the “pop-up” type phenomena may be avoided with proper choice of α . Thus filtering $\gamma(s)$ in μ - K iteration is the equivalent of step 5 in D, G - K iteration. Filtering $\gamma(s)$ does *not* provide the same guarantee for a monotonically non-increasing μ upper bound as we can achieve in D, G - K iteration. However, numerical experience suggests that it works well in practice.

As before we use the \mathcal{H}_∞ optimal control solution to synthesize the controller in step 7. The K -step of μ - K iteration can be illustrated as in Figure 5.7.

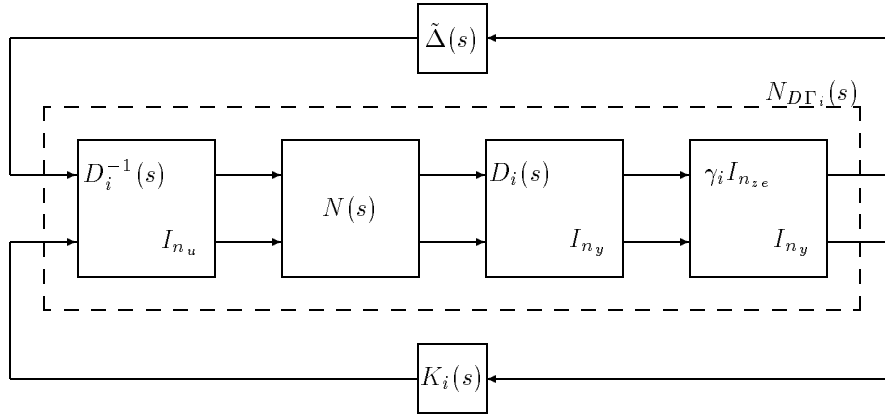


Figure 5.7: K -step of μ - K iteration. n_u , n_y and n_{ze} are the number of manipulated inputs $u(s)$, measured outputs $y(s)$ and exogenous outputs $z(s)$ and $e'(s)$ respectively.

As shown in Equation (5.108) on the facing page, $\bar{\sigma}(F_l(N_{D\Gamma_i}(j\omega), K_i(j\omega)))$ equals the upper bound $\bar{\mu}_{\tilde{\Delta}}(F_l(N(j\omega), K_i(j\omega)))$ for perfect realizations of the scalings $\gamma_i(s)$ and $D_i(s)$ and for $\alpha_i = 1$. For $\alpha_i \neq 1$ this is not true. However if

$$|\gamma_{i-1}(j\omega)| \rightarrow \frac{\bar{\mu}_{\tilde{\Delta}}(F_l(N(j\omega), K_i(j\omega)))}{\bar{\mu}_{\tilde{\Delta}_e}(F_l(N(j\omega), K_i(j\omega)))} \quad \text{for } i \rightarrow \infty \quad (5.109)$$

then from (5.100) on page 87 and perfect realization of $\gamma_i(j\omega)$:

$$|\gamma_{i-1}(j\omega)| \rightarrow |\gamma_i(j\omega)| \quad \text{for } i \rightarrow \infty \quad (5.110)$$

and

$$\bar{\sigma}(F_l(\Gamma_i(j\omega)D_i(j\omega)N(j\omega)D_i^{-1}(j\omega), K_i(j\omega))) \rightarrow \bar{\mu}_{\tilde{\Delta}}(F_l(N(j\omega), K_i(j\omega))) \quad (5.111)$$

for $i \rightarrow \infty$. Notice that Equation (5.109) on the preceding page implies that $\beta_i(\omega) \rightarrow 0$. Thus in order to reach a local minimum for $\|\bar{\mu}_{\bar{\Delta}}(F_l(N(s), K(s)))\|_\infty$ the necessary conditions are:

1. The iteration must be monotonically non-increasing in $\|F_l(N_{D\Gamma_i}(s), K_i(s))\|_\infty$, that is

$$\|F_l(N_{D\Gamma_i}(s), K_i(s))\|_\infty \leq \|F_l(N_{D\Gamma_{i-1}}(s), K_{i-1}(s))\|_\infty \quad \forall i \quad (5.112)$$

2. Furthermore the iteration must be monotonically non-increasing in $\|\beta_i(\omega)\|_\infty$, that is

$$\|\beta_i(\omega)\|_\infty \leq \|\beta_{i-1}(\omega)\|_\infty \quad \forall i \quad (5.113)$$

In Appendix B on page 293 it is shown that the criteria (5.112) can be met by choosing $\bar{\alpha}_i(\omega)$ as in (5.98). If κ then can be chosen to fulfill the criteria (5.113) the iteration will converge to a local minimum for $\|\bar{\mu}_{\bar{\Delta}}(F_l(N(s), K(s)))\|_\infty$.

We then have the following lemma:

Lemma 5.1 *The μ -K iteration procedure described above is monotonically non-increasing in $\|F_l(N_{D\Gamma_i}(s), K_i(s))\|_\infty$ given perfect realizations of the $D(s)$ and $\gamma(s)$ scalings. Provided $\|\beta(\omega)\|_\infty$ converges to zero the procedure will converge to a local minimum for $\|\bar{\mu}_{\bar{\Delta}}(F_l(N(j\omega), K_i(j\omega)))\|_\infty$.*

Numerical evidence suggests that κ can indeed be chosen to fulfill (5.113). For $\alpha_i = 0$, $\gamma_i(s) = \gamma_{i-1}(s)$ and we will only concentrate on reducing the \mathcal{H}_∞ bound in (5.112). Conversely, if $\beta_i(\omega) > 0$, for some ω , then for $\kappa = 1$ it can be shown, see Appendix B, that

$$\|F_l(N_{D\Gamma_i}(s), K_i(s))\|_\infty = \|N_{D\Gamma_{i-1}}(s), K_{i-1}(s)\|_\infty \quad (5.114)$$

Thus in this situation, we will only concentrate on the criteria (5.113) during the i 'th step of the iteration. By choosing α (or κ) in between these two extremes, we may attempt to fulfill both criteria (5.112) and (5.113). However, it is likely that examples may be constructed where no κ fulfilling (5.113) can be found.

Notice that for a purely complex perturbation set, if we choose $\kappa = 1$ then $\beta_i(\omega) = 0$, $\forall \omega, \forall i$ and $\gamma_i(s) = 1$, $\forall i$. Then μ -K iteration will reduce to standard D -K iteration.

5.3 Summary

An introduction to the structured singular value μ has been given. Using a $N\Delta K$ framework we addressed the robust stability problem for possibly repeated real

and complex uncertainties which enter the nominal model in a linear fractional manner. This uncertainty description is superior to the assumption in connection with \mathcal{H}_∞ control where only full complex blocks can be considered. Using μ we then derived simple expressions for both robust stability and robust performance with an ∞ norm bounded performance cost function. Thus we can consider robust performance non-conservatively for a very large class of perturbation structures, including parametric uncertainty and mixed dynamic and parametric uncertainty.

Unfortunately, μ cannot be directly computed since the implied optimization problem is non-convex and may have multiple local minima. This fact has naturally hampered the application of μ theory to real control systems design. Rather than trying to compute μ itself, it is then customary to look for upper and lower bounds on μ . From the definition of μ it is easy to see that μ is bounded from below by the spectral radius and from above by the singular value. The idea is to utilize transformations which are μ -invariant to refine these bounds. In the original paper on μ [Doy82], Doyle derived such bounds for purely complex perturbation sets. The complex μ upper bound is generally very close to the true μ value.

However, one of the powerful features of μ is that it can handle real perturbations (parametric uncertainty) as well. Unfortunately, the purely real (for robust stability analysis with parametric uncertainty only) or the mixed real and complex (for robust stability analysis for mixed uncertainty or for robust performance analysis in general) upper bound is more complicated. During the past 5 years, formulation of mixed μ upper and lower bounds have received considerable attention within the automatic control community. Today, some of these bounds are commercially available through the MATLAB μ toolbox. However, in general the bounds on mixed μ seem to be much more conservative than the purely complex μ bounds. In particular, for a large number of real perturbations, the gap between the upper and lower bound may be quite large.

Nevertheless, for a limited number (less than 10-15) of non-repeated real uncertainties, the bounds on μ seem in general to be quite tight. Thus from a control engineer's point of view, the mathematical subtleties in μ is of minor importance in connection with μ analysis.

This is unfortunately not true when it comes to μ synthesis. Since we cannot compute μ (unless in some very simple cases, where the upper bound is equal to μ) it is clear that controller design with μ will be difficult. The approach usually taken is to consider an upper bound problem instead. However, even for purely complex perturbations this is still an unsolved mathematical problem despite the fact that it has received much attention. For complex perturbation sets an iterative scheme, known as *D-K iteration*, has been known for some time. This approach possesses no guaranteed convergence properties. Nevertheless it

seems to work quite successfully in practice and has been applied to a large number of applications. Furthermore, with the release of the MATLAB μ -Analysis and Synthesis Toolbox commercially available software exists to support D - K iteration.

On the other hand, for mixed real and complex perturbations until recently no known methodology was available for solving the synthesis problem. Then in 1993, Young [You93] presented a iterative solution procedure, denoted D, G - K iteration, to the mixed μ problem. The D, G - K iteration is a more or less straightforward generalization of D - K iteration. Unfortunately, since the problem is posed directly in line with the way μ is computed we now need to fit scalings both in magnitude and phase. In complex μ synthesis, we need only to fit in magnitude since any phase is absorbed into the complex perturbations. In mixed real and complex μ synthesis, the phase is not absorbed since the perturbations are real; thus the need for fitting both in phase and magnitude. This considerably complicates matters, in particular since one of the scaling matrices are purely imaginary for all frequencies.

A novel approach for mixed μ synthesis is then proposed. Here we consider a corresponding complex problem, where we approximate all real perturbations with complex ones. Then we only need to fit scalings in magnitude. We then introduce an additional scaling matrix to shift from complex to mixed μ . With this new approach, denoted μ - K iteration, we cannot obtain the same guarantee for monotonically non-increasing behavior as for D, G - K iteration. However, as we shall show in the next Chapter, μ - K iteration seems to work quite well in practice.

Chapter 6

Mixed μ Control of a Compact Disc Servo Drive

Contents

6.1	Complex μ Design	95
6.2	Mixed μ Design	96
6.3	Summary	102

The main purpose of this chapter is to illustrate how the proposed μ - K iteration performs on a practical design example. A compact disc (CD) servo drive has been chosen as application partly because it is a simple and illustrative example and partly because it enables us to compare the results with reported results from D , G - K iteration by Young [You93, YÅ94].

The servo arm for a computer disc drive or a compact disc player is essentially a small flexible structure, whose dynamics will depend on various physical quantities. Provided the product is to be mass produced, the control design for the servo should work for any product from the assembly line and thus the design should be insensitive to variations in the parameters of the servo model.

Here a very simple idealized model of the servo is considered. The control problem

formulation is identical to that in [YÅ94]. It is assumed that the low frequency plant dynamics can be approximated by a double integrator with an uncertain gain:

$$G_T(s) = \frac{k_p}{s^2}, \quad 0.1 \leq k_p \leq 10. \quad (6.1)$$

Notice that the ratio of $k_{p,max}$ to $k_{p,min}$ is as large as 100. The model is assumed valid up to the frequency $\omega_o = 100$ rad/s. The parameters k_p and ω_o do not necessarily reflect physical meaningful numbers. This is, however, of minor importance here, since the main objective is to illustrate different design techniques. The robust performance control problem is thus to design a fixed dynamic controller which stabilizes the plant and complies with performance demands for all possible plants. To ensure that the controller rolls off at frequencies above ω_o a complementary sensitivity specification is included into the design. Performance requirements are given as a standard sensitivity specification. The control problem can then be specified as in Figure 6.1.

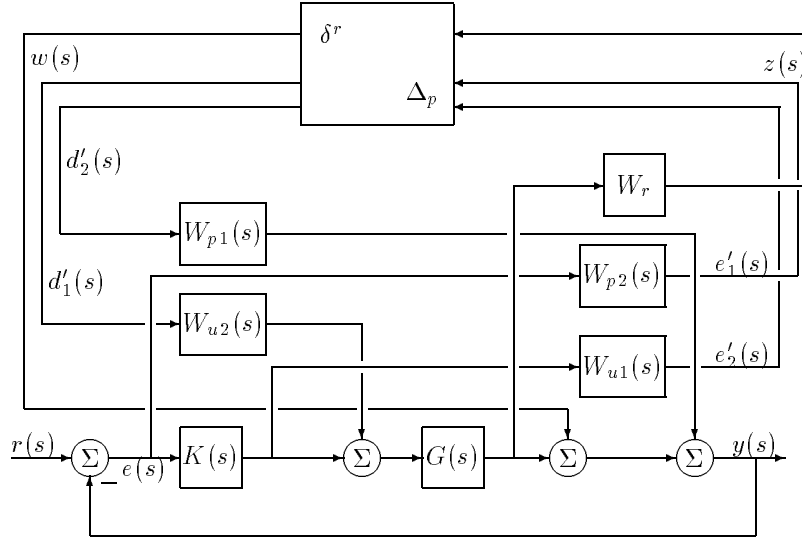


Figure 6.1: Control problem set-up for the compact disc servo drive.

Notice that the perturbed low frequency plant (6.1) can be written

$$G_T(s) = \frac{1}{s^2} (5.05 + 4.95\delta^r) = \frac{5.05}{s^2} \left(1 + \frac{4.95}{5.05}\delta^r \right) = G(s) (1 + W_r\delta^r) \quad (6.2)$$

where $\delta^r \in \mathbf{R}$ is a real scalar perturbation $\delta^r \in [-1, 1]$. The sensitivity weights on $S(s)$ and $T(s)$ are standard weights taken from [YÅ94]:

$$W_{u1}(s) = W_{u2}(s) = \frac{5(s + 0.001)}{s + 5} \quad (6.3)$$

$$W_{p1}(s) = W_{p2}(s) = \frac{0.03}{s + 0.05} \quad (6.4)$$

Notice that we have gathered the weighted sensitivity functions $W_{p2}SW_{p1}$ and $W_{u1}TW_{u2}$ into a single performance specification. We in fact believe that this is a somewhat awkward way of specifying the control problem, since the complementary sensitivity weights $W_{u1}(s)$ and $W_{u2}(s)$ introduced to make the controller roll off at high frequencies reflect an uncertainty specification rather than a performance specification. Thus it could have been introduced via a separate scalar uncertainty block δ^c . In this way we would decouple the specifications on the sensitivity and complementary sensitivity. However, in order to compare our results with those reported in [You93, YÅ94] we will keep the formulation in Figure 6.1 on the facing page.

6.1 Complex μ Design

Our first approach will be to design a complex μ optimal controller:

$$K_{\mu_c}(s) = \arg \min_{K(j\omega) \in \mathcal{K}_S} \sup_{\omega} \mu_{\tilde{\Delta}^c}(F_l(N(j\omega), K(j\omega))) \quad (6.5)$$

Hence, at first we approximate the real perturbation δ^r with a complex one δ^c . The complex μ problem was solved using D - K iteration as outlined in Procedure 5.1 on page 79. The results from the iteration is shown in Figure 6.2 on the next page and tabulated in Table 6.1 on page 97.

In Figure 6.2 on the next page $\mu_{\tilde{\Delta}^c}(F_l(N(j\omega), K(j\omega)))$ for each iteration is shown across frequency. As seen the iteration converges rapidly with a final complex μ peak at 1.40. Using a third order approximation for $D(s)$, the final complex μ controller had 12 states. Using the standard model reduction facilities in the MATLAB μ toolbox it was possible to reduce the order to 7 with very little increase in $\mu_{\tilde{\Delta}^c}(F_l(N(j\omega), K(j\omega)))$.

In Figure 6.2 on the following page also the mixed μ result for the final controller $K_{\mu_c}(s)$ is shown. Notice how there is a noticeable dive in mixed μ around 0.5 rad/s. It thus seem possible that a significant improvement in control performance can be obtained by applying mixed μ synthesis.

Finally in Figure 6.2 on the next page the step responses for $k_p = 1$ (nominal), $k_p = 0.1$ and $k_p = 10$ are shown. Even though the controller performs quite well,

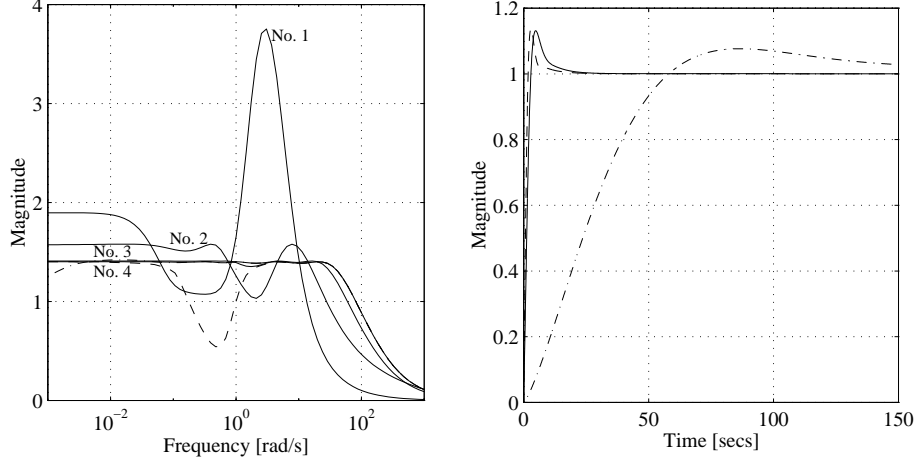


Figure 6.2: Results from D - K iteration on the CD player servo. Shown are on the left $\mu_{\hat{\Delta}_e}(F_l(N(j\omega), K(j\omega)))$ for each iteration 1-4 and for the 7th order reduced controller (dash-dotted). Also on the left are $\mu_{\hat{\Delta}}(F_l(N(j\omega), K_{\mu_c}(j\omega)))$ (dashed). On the right are the step responses for $k_p = 1$ (solid), $k_p = 0.1$ (dash-dotted) and $k_p = 10$ (dashed).

see also Table 6.1 on the facing page, the responses for different values of the gain k_p are very different, with the high gain response being much faster than the low gain response as expected. If it is desired that the closed loop response is invariant to variations in k_p a prefilter may be included in the design as it is done in [YÅ94]. Our objective here will however be the feedback design.

The results in Figure 6.2 are similar to the results presented in [YÅ94].

6.2 Mixed μ Design

In order to improve the results from the D - K iteration, μ - K iteration as outlined in Procedure 5.3 on page 86 was applied to the servo problem. The complex μ optimal controller $K_{\mu_c}(s)$ is then an obvious choice for the initial controller $K_0(s)$. Let us illustrate the first run through of the μ - K iteration. Thus let $N(s)$ be the augmented open loop plant derived from Figure 6.1 on page 94. Then $N_{D\Gamma_0}(s) = D_0(s)N(s)D_0^{-1}(s)$ where $D_0(s)$ is the scaling matrix from step 2 in the final D - K iteration. Furthermore $K_0(s) = K_1(s) = K_{\mu_c}(s)$. The complex

	Iteration No.				
	1	2	3	4	7th order K
$\ \mu_{\tilde{\Delta}_e} F_l(N(s), K_i(s))\ _\infty$	3.75	1.60	1.41	1.40	1.42
$\ \mu_{\tilde{\Delta}} F_l(N(s), K_i(s))\ _\infty$	–	–	–	1.40	1.42

	Overshoot	Settling time
$k_p = 0.1$	1.14	6.4 secs
$k_p = 1$	1.13	13.6 secs
$k_p = 10$	1.08	∞

Table 6.1: Results from D - K iteration on the CD player servo.

and mixed μ upper bounds in step 2 of Procedure 5.3 on page 86 are the bounds illustrated in Figure 6.2 on the facing page. The scalings $D_1^*(\omega)$ are returned by the MATLAB μ -Analysis and Synthesis Toolbox `mu.m` command. We may then compute $\beta_1(\omega)$ as

$$\beta_1(\omega) = \frac{\bar{\mu}_{\tilde{\Delta}}(F_l(N(j\omega), K_1(j\omega)))}{\bar{\mu}_{\tilde{\Delta}_e}(F_l(N(j\omega), K_1(j\omega)))} \frac{1}{|\gamma_0(j\omega)|} - 1 \quad (6.6)$$

$$= \frac{\bar{\mu}_{\tilde{\Delta}}(F_l(N(j\omega), K_1(j\omega)))}{\bar{\mu}_{\tilde{\Delta}_e}(F_l(N(j\omega), K_1(j\omega)))} - 1 \quad (6.7)$$

since $\gamma_0(\omega) = 1, \forall \omega$. $\beta_1(\omega)$ is shown in Figure 6.3 on the following page. Note that $\beta_1(\omega)$ is simply the ratio between mixed and complex μ minus 1. Using the μ toolbox command `musynfit.m` we may next fit the scalings $D_1^*(\omega)$ with a real rational stable minimum phase transfer function matrix as required in step 4 of μ - K iteration. `musynfit.m` furthermore automatically augment with an appropriate unity matrix. Since mixed μ is always smaller than the corresponding complex μ :

$$\bar{\mu}_{\tilde{\Delta}}(F_l(N(j\omega), K_1(j\omega))) \leq \bar{\mu}_{\tilde{\Delta}_e}(F_l(N(j\omega), K_1(j\omega))) \quad \forall \omega \quad (6.8)$$

we will always have that $\beta_1(\omega) \leq 0, \forall \omega$ in the first run through of μ - K iteration. Thus in step 5 of Procedure 5.3 on page 86 we will have that $\bar{\alpha}_i(\omega) = 1, \forall \omega$. Thus there is no need for calculating $\xi_1(\omega)$, see Equation (5.99) on page 87.

Then in step 6 let us choose $\kappa = 1$. Then $\gamma_1^*(\omega)$ will be equal to the mixed to complex μ ratio:

$$\gamma_1^*(\omega) = \frac{\bar{\mu}_{\tilde{\Delta}}(F_l(N(j\omega), K_1(j\omega)))}{\bar{\mu}_{\tilde{\Delta}_e}(F_l(N(j\omega), K_1(j\omega)))} \frac{1}{|\gamma_0(j\omega)|} = \beta_1(\omega) + 1 \quad (6.9)$$

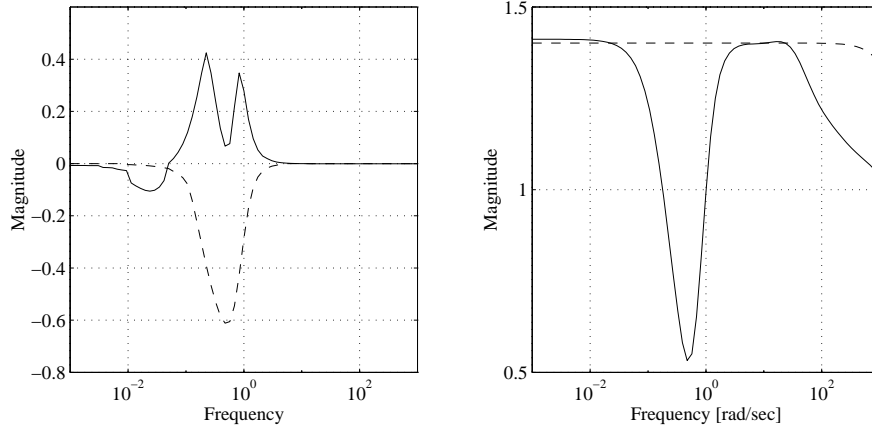


Figure 6.3: Results from first iteration on the CD player servo. On the left is shown $\beta_2(\omega)$ and $\beta_1(\omega)$ (dashed) and on the right is shown $\bar{\sigma}(F_l(N_{D\Gamma_0}(j\omega), K_0(j\omega)))$ (dashed) and $\bar{\sigma}(F_l(N_{D\Gamma_1}(j\omega), K_1(j\omega)))$.

A scalar transfer function $\gamma_1(s)$ is then fitted, in magnitude, to $\gamma_1^*(\omega)$. Here we may use the fitting routine `fitmag.m` from the μ toolbox. Next the augmented system $N_{D\Gamma_1}(s)$ is formed:

$$N_{D\Gamma_1}(s) = \begin{bmatrix} \gamma_1(s)I_3 & 0 \\ 0 & 1 \end{bmatrix} D_1(s)N(s)D_1^{-1}(s) \quad (6.10)$$

and the \mathcal{H}_∞ optimal controller $K_2(s)$:

$$K_2(s) = \arg \min_{K(s) \in \mathcal{K}_S} \|F_l(N_{D\Gamma_1}(s), K(s))\|_\infty \quad (6.11)$$

is computed, e.g. using the `hinfsyn.m` function from the μ toolbox.

Then in step 8 of the μ - K iteration we compute upper bounds for mixed and complex μ , the latter providing the D -scalings $D_2^*(\omega)$ for the next iteration. In step 9 we finally find $\beta_2(\omega)$ given by:

$$\beta_2(\omega) = \frac{\bar{\mu}_{\tilde{\Delta}}(F_l(N(j\omega), K_2(j\omega)))}{\bar{\mu}_{\tilde{\Delta}_e}(F_l(N(j\omega), K_2(j\omega)))} \frac{1}{|\gamma_1(j\omega)|} - 1 \quad (6.12)$$

$\beta_2(\omega)$ is also shown in Figure 6.3. Since

$$\sup_{\omega} |\beta_2(\omega)| < \sup_{\omega} |\beta_1(\omega)| \quad (6.13)$$

the condition in step 10 for terminating the first run through is fulfilled. Since $\sup_{\omega} |\beta_2(\omega)|$ is not close to zero we will repeat the iteration from step 4.

The second parameter besides β which we use to judge the convergence properties of the μ - K iteration is the ∞ -norm $\|F_l(N_{D\Gamma_i}(s), K_i(s))\|_{\infty}$. Note that we need this norm to compute $\xi_i(\omega)$ in step 5. In Figure 6.3 on the facing page we have plotted $\bar{\sigma}(F_l(N_{D\Gamma_0}(j\omega), K_0(j\omega)))$ and $\bar{\sigma}(F_l(N_{D\Gamma_1}(j\omega), K_1(j\omega)))$ across frequency ω . Note that Appendix B guarantees that

$$\|F_l(N_{D\Gamma_i}(s), K_i(s))\|_{\infty} \leq \|F_l(N_{D\Gamma_{i-1}}(s), K_{i-1}(s))\|_{\infty} \quad (6.14)$$

for perfect realizations of the D and γ scalings. The results in Figure 6.3 on the facing page confirms this except for a little overshoot at low frequencies due to imperfect scalings. This is in fact trivial for the first iteration since $K_0(s) = K_1(s)$ and $|\gamma_1(j\omega)| \leq 1 = |\gamma_0(j\omega)|$ for all frequencies ω . However, for the next iterations this result is not so trivial, see Appendix B on page 293.

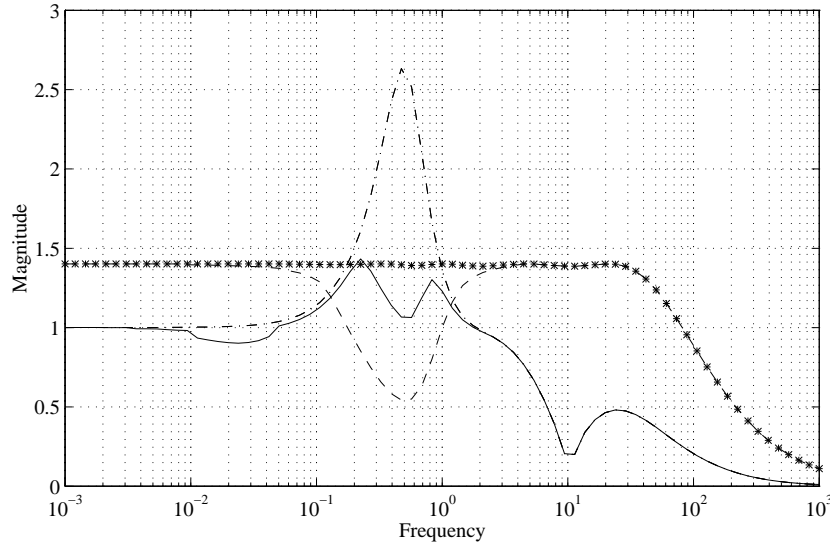


Figure 6.4: μ results from first μ - K iteration on the CD servo. New (solid) and previous (dashed) mixed μ upper bound and new (dash-dotted) and previous (*) complex μ upper bound.

Finally let us have a look at μ . In Figure 6.4 $\mu_{\bar{\Delta}}(F_l(N(j\omega), K_1(j\omega)))$ (initial mixed μ), $\mu_{\bar{\Delta}}(F_l(N(j\omega), K_2(j\omega)))$ (new mixed μ), $\mu_{\bar{\Delta}_c}(F_l(N(j\omega), K_1(j\omega)))$ (ini-

tial complex μ) and $\mu_{\tilde{\Delta}_c}(F_l(N(j\omega), K_1(j\omega)))$ (new complex μ) are shown versus frequency.

Note that with the γ scaling we have put less emphasis on the mid-frequency range thus providing the opportunity for reducing μ outside this frequency range. Then, of course, the new mixed μ value will increase in the mid frequency range. Here we have not obtained any decrease in the maximum μ upper bound across frequency, since $\|\mu_{\tilde{\Delta}}(F_l(N(s), K_1(s)))\|_\infty \approx \|\mu_{\tilde{\Delta}}(F_l(N(s), K_2(s)))\|_\infty$. Note that we have not postulated that this would be the case in every iteration. However, we have shifted the emphasis of mixed μ and as we shall see, during the next iterations $\sup_\omega \beta_i(\omega) \rightarrow 0$ and mixed μ will decrease down to approximately one.

In Table 6.2, the results of the μ - K iteration is given. Notice how $\sup_\omega \beta(\omega)$ converges to zero indicating that the γ scalings approximates the mixed to complex μ ratio. The ∞ -norm $\|F_l(P_i(s), K_i(s))\|_\infty$ is monotonically decreasing as shown in Appendix B. κ had to be reduced from iteration 3+ in order to reduce the β peaks (mixed μ pop-up phenomena).

Iteration No.	μ - K Iteration						
	1	2	3	4	5	6	7
$\ \mu_{\tilde{\Delta}_c}(F_l(N(s), K_i(s)))\ _\infty$	1.40	—	—	—	—	—	2.46
$\ \mu_{\tilde{\Delta}}(F_l(N(s), K_i(s)))\ _\infty$	1.40	1.43	1.15	1.06	1.08	1.06	1.02
$\sup_\omega \beta_i(\omega)$	0.61	0.42	0.30	0.13	0.07	0.06	0.04
$\ F_l(P_i(s), K_i(s))\ _\infty$	1.40	1.41	1.32	1.12	1.05	1.024	1.019
$\inf_1 \omega \bar{\alpha}_i(\omega)$	—	1	0.95	1	1	0.62	0.32
κ	—	1	1	0.5	0.5	0.5	1

	Overshoot	Settling time
$k_p = 0.1$	1.32	13.9 secs
$k_p = 1$	1.36	20.6 secs
$k_p = 10$	1.10	102 secs

Table 6.2: Results from μ - K iteration on the C.D. player servo.

In Figure 6.5 on the facing page, mixed and complex μ is shown for the initial (complex μ optimal) and final mixed μ optimal controller. Mixed μ peaks at approximately 1.02 and a 25% improvement has thus been obtained through μ - K iteration. Notice how this is achieved at the expense of complex μ , which peaks at almost 2.5 for the mixed μ optimal controller $K_\mu(s)$.

In Figure 6.5 on the facing page, also the step responses are shown for different values of the uncertain gain k_p . Comparing with the results for the the complex

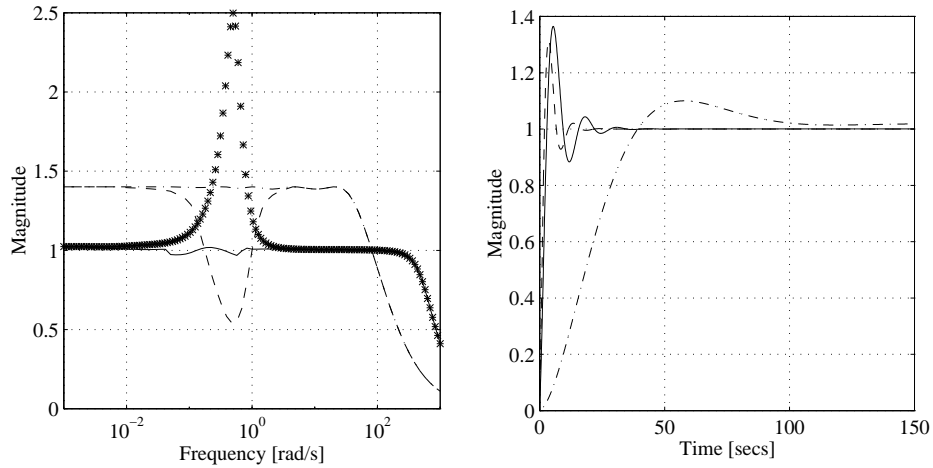


Figure 6.5: Results from μ - K iteration on the C.D. player servo. Shown are on the left $\mu_{\tilde{\Delta}}(F_l(N(j\omega), K(j\omega)))$ (dashed and solid) and $\mu_{\tilde{\Delta}_c}(F_l(N(j\omega), K(j\omega)))$ (dash-dotted and dotted) for the initial (complex μ optimal) and final mixed μ optimal controller respectively. On the right are the step responses for $k_p = 1$ (solid), $k_p = 0.1$ (dash-dotted) and $k_p = 10$ (dashed).

μ optimal controller $K_{\mu_c}(s)$, see Figure 6.2 on page 96, we note that the mixed μ controller is more invariant to changes in k_p . The worst-case rise- and settling time (for $k_p = 0.1$) has been much improved. The expense has been an increase in overshoot. Using a prefilter, these overshoots may be removed.

In [YÅ94], D, G - K iteration is used to find a mixed μ controller for the C.D. player servo. Here mixed μ was reported to peak at 1.25 for a ninth order realization of the final mixed μ controller. In order to compare this result with the μ - K iteration result, the final controller $K_{\mu}(s)$, which had 26 states, must be reduced using model reduction. Using the routines provided in the MATLAB μ toolbox, $K_{\mu}(s)$ was reduced to ninth order with virtually no increase in μ . With the reduced order controller $K_{\mu,r}(s)$ $\mu_{\tilde{\Delta}}(F_l(N(j\omega), K_{\mu,r}(j\omega)))$ also peaked at 1.02. For lower order realizations there were, however, a significant increase in mixed μ .

In this case, it thus seems that μ - K iteration performs better than D, G - K iteration. We believe that the reason for this is problems in fitting the G scalings. In Figure 6.6 on the following page, $G(\omega)$ is shown for the final mixed μ controller $K_{\mu}(s)$. Notice that $G(\omega)$ is identically zero for a large part of the frequency range (namely at those frequency points where mixed and complex μ are identical) but

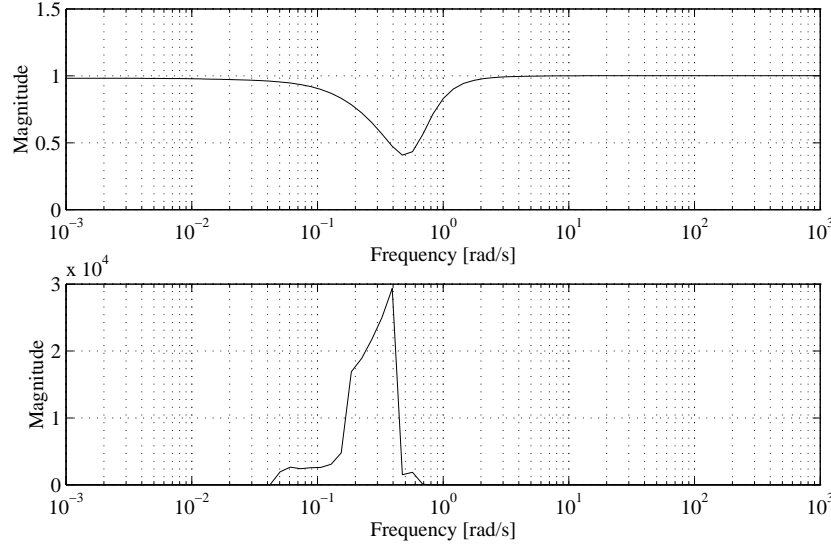


Figure 6.6: γ scalings to be fitted in μ - K iteration (top) and G scalings to be fitted in D, G - K iteration (bottom).

rapidly rise to approximately $2 \cdot 10^4$ at those frequencies where mixed and complex μ differs. Fitting an all-pass transfer function to this kind of data will be very difficult. The corresponding γ scaling in μ - K iteration behaves much better as can be seen in Figure 6.6.

6.3 Summary

The control of compact disc servo drive was considered. A very simple model of a CD drive is a double integrator with uncertain gain. Here the ratio of the maximum to minimum gain was 100. Using weighting functions from [YÅ94] the control design was formulated as a $N\Delta K$ problem. Initially a complex μ design was performed, thus treating the real perturbation as a complex one. The result (after model reduction) was a 7th order controller which achieved a real μ peaking at 1.42. The complex μ value $\mu_{\tilde{\Delta}_c}(F_l(N(j\omega), K(j\omega)))$ peaked also at 1.42¹. However, whereas complex μ was flat across frequency ω there was a

¹Note that $\mu_{\tilde{\Delta}}(F_l(N(j\omega), K(j\omega)))$ and $\mu_{\tilde{\Delta}_c}(F_l(N(j\omega), K(j\omega)))$ are equal for $\omega = 0$ and ∞ because then $F_l(N(j\omega), K(j\omega))$ is real.

noticeable dive in the mixed μ response. Thus significant improvement should be possible with a mixed μ design. This was confirmed using μ - K iteration. The final controller had 9 states (after model reduction) and the corresponding mixed μ response peaked at 1.02. Thus the complex μ result was improved by 25%. This was achieved at the expense of complex μ which peaked at 2.5 for the mixed μ controller. Compared with the results reported by Young & Åström on D, G - K iteration for the same system (mixed μ peaked at 1.25) we obtained much better results using μ - K iteration.

Chapter 7

μ Control of an Ill-Conditioned ASTOVL Aircraft

Contents

7.1	The Aircraft Model	106
7.1.1	Plant Scaling	107
7.1.2	Dynamics of the Scaled Aircraft Model	108
7.2	Control Objectives	110
7.2.1	Robustness	111
7.2.2	Performance	115
7.3	Formulation of Control Problem	117
7.4	Evaluation of Classical Control Design	119
7.5	Controller Design using μ	123
7.6	Summary	129

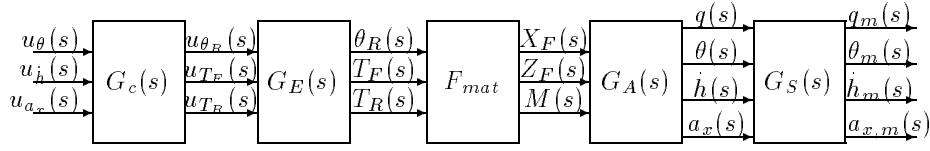
In this chapter the methods introduced in Chapter 5 will be applied in control of an advanced short take-off and vertical landing (ASTOVL) aircraft. The model

applied for the vehicle is valid at low speeds in the transition zone from jet-borne to fully wing-borne flight. In this flight condition the aircraft is unstable in the longitudinal axis and there is very poor decoupling between pilot commands and aircraft response. Furthermore the aircraft is extremely ill-conditioned as the gain of the system decays to zero at steady-state for one particular input direction. The limits this assign on the closed loop system will be thoroughly investigated. The control objectives for the aircraft will be discussed and a performance specification will be derived with due attention to the special gain characteristics of the system. For robustness to dynamic uncertainty, a diagonal dynamic multiplicative perturbation models will be applied at both input and output. A classical control configuration will then be investigated. For a modern design approach the general $N\Delta K$ framework becomes a very natural way of formulating the control problem. This furthermore possesses the advantage that the uncertainty specification may easily be augmented with a parametric uncertainty description as well. This has been investigated in [TCABG95]. Here we will however confine ourselves to considering dynamic uncertainty. A complex μ optimal controller will be designed for the aircraft using D - K iteration.

7.1 The Aircraft Model

The aircraft model describes a complete pitch axis system for a generic canard-delta configuration with flap and foreplane angles fixed, see [Irv91]. The aircraft is controlled using vectored thrust produced from engine nozzles at the front and the rear of the aircraft. The thrust is split with one part being directed through the rear nozzle at a variable angle, θ_R to the horizontal, producing a thrust, T_R , and the remainder through the front nozzle inclined at a fixed angle, θ_F to the horizontal, producing a thrust, T_F . The forward thrust can be augmented with plenum chamber burning when required. The aircraft is controlled by varying the rear nozzle angle, θ_R , and the magnitude of the thrusts, T_R and T_F . The pilot commands for pitch attitude θ , height rate \dot{h} and longitudinal acceleration a_x are processed by the flight control computer hardware $G_c(s)$ which also converts pilot commands into demands on the controlled variables θ_R , T_F and T_R through a 3×3 axis transformation matrix. The thrusts produced by the engine, $G_E(s)$, are then resolved via a force transformation matrix, F_{mat} , into an axial force, X_F , a normal force, Z_F , and a pitching moment, M , which are the inputs to the rigid aircraft model, denoted $G_A(s)$.

The model for the rigid aircraft, $G_A(s)$, represents the linearized, rigid-body dynamics of a canard-delta configured aircraft. The model is linearized for straight and level flight at 100 ft, Mach no. 0.151 and 6° angle of attack. The dynamics at this particular operating point are unstable.

Figure 7.1: The rigid-body model of the aircraft $G(s)$.

The pitch rate q [deg/s], pitch attitude θ [deg], height rate \dot{h} [ft/s] and longitudinal acceleration a_x [g] are measured and available for feedback. The diagonal transfer function matrix modeling the sensors is denoted $G_S(s)$.

The complete model of the aircraft is thus given as in Figure 7.1. A detailed description of the rigid body aircraft model is given in Appendix C. The open loop transfer function $G(s) = G_S(s)G_A(s)F_{mat}G_{Eng}(s)G_c(s)$ has 26 states, 4 outputs and 3 inputs. The aircraft model is thus a high order non-square system.

7.1.1 Plant Scaling

Notice that the input/outputs of the aircraft model are measured in different units. If norm-based control design methods like \mathcal{H}_∞ or μ are applied, the control problem will be skewed if not due attention is taken to scale the plant so that the relative magnitude (or importance) of the different input/outputs will be approximately equal. This is done by multiplication on the left and right with 2 diagonal matrices $N_u(s)$ and $N_y(s)$:

$$G_s(s) = N_y(s)G(s)N_u^{-1}(s) \quad (7.1)$$

$N_u(s)$ and $N_y(s)$ should be chosen so that the relative magnitude of the inputs/outputs equal unity and so that the input and output are scaled to norm 1. A popular method for choosing the scaling matrices is the use of expected maximum magnitude. In Table 7.1 the expected maximum magnitude for each input/output are given.

Signal	u_θ	$u_{\dot{h}}$	u_{a_x}	q	θ	\dot{h}	a_x
Units	°	ft/s	g	°/s	°	ft/s	g
Expected max. value	± 30	± 100	± 2	± 30	± 30	± 100	± 2

Table 7.1: Expected maximum magnitude for each input/output component.

From Table 7.1 on the preceding page the scalings are then chosen as

$$N_u = \text{diag} \left\{ \frac{1}{30}, \frac{1}{100}, \frac{1}{2} \right\}, \quad N_y = \text{diag} \left\{ \frac{1}{30}, \frac{1}{30}, \frac{1}{100}, \frac{1}{2} \right\} \quad (7.2)$$

Now the system “seen” by the controller will have input and output with maximum magnitude scaled to norm one. If the controller for the scaled system is denoted $K_s(s)$, the controller for the true system $K(s)$ will be given by:

$$K(s) = N_u^{-1}(s)K_s(s)N_y(s) \quad (7.3)$$

Throughout the remainder of this chapter we will almost exclusively deal with the scaled plant $G_s(s)$ and controller $K_s(s)$. In order not to lengthen the notation excessively, unless any confusion may occur, we will from now on use $G(s)$ and $K(s)$ to denote the scaled plant and controller respectively.

7.1.2 Dynamics of the Scaled Aircraft Model

The dynamics of the scaled aircraft model will now be investigated using singular values. In Figure 7.2 on the facing page the singular value Bode plot of the (scaled) plant $G(s)$ is shown. The plant is seen to be very ill-conditioned. Notice how one of the singular values decays to zero at steady-state ($\omega = 0$), thus making the condition number of the plant infinity at steady-state. In other words, the plant model $G(j\omega)$ loses rank at steady-state. This of course imposes some unusual limitations on the achievable performance of the closed loop system.

Let the singular value decomposition of $G(j\omega)$ be

$$G(j\omega) = Y(\omega)\Sigma(\omega)U^*(\omega) \quad (7.4)$$

$$= \begin{bmatrix} y_1 & y_2 & y_3 & y_4 \end{bmatrix} \begin{bmatrix} \sigma_1 & 0 & 0 \\ 0 & \sigma_2 & 0 \\ 0 & 0 & \sigma_3 \\ 0 & 0 & 0 \end{bmatrix} \begin{bmatrix} u_1^* \\ u_2^* \\ u_3^* \end{bmatrix} \quad (7.5)$$

Here y_i and u_i are the output and input principal directions respectively, see Section 3.1.2 on page 18. Since U is unitary u_1 , u_2 and u_3 will be mutually orthogonal and we may partition the input $u(j\omega)$ after the input principal directions:

$$u(j\omega) = \alpha_1(\omega)u_1(\omega) + \alpha_2(\omega)u_2(\omega) + \alpha_3(\omega)u_3(\omega) \quad (7.6)$$

In other words we express $u(j\omega)$ in the coordinate system defined by U . The output is then given by:

$$y(j\omega) = Y(\omega)\Sigma(\omega)U^*(\omega) (\alpha_1(\omega)u_1(\omega) + \alpha_2(\omega)u_2(\omega) + \alpha_3(\omega)u_3(\omega)) \quad (7.7)$$

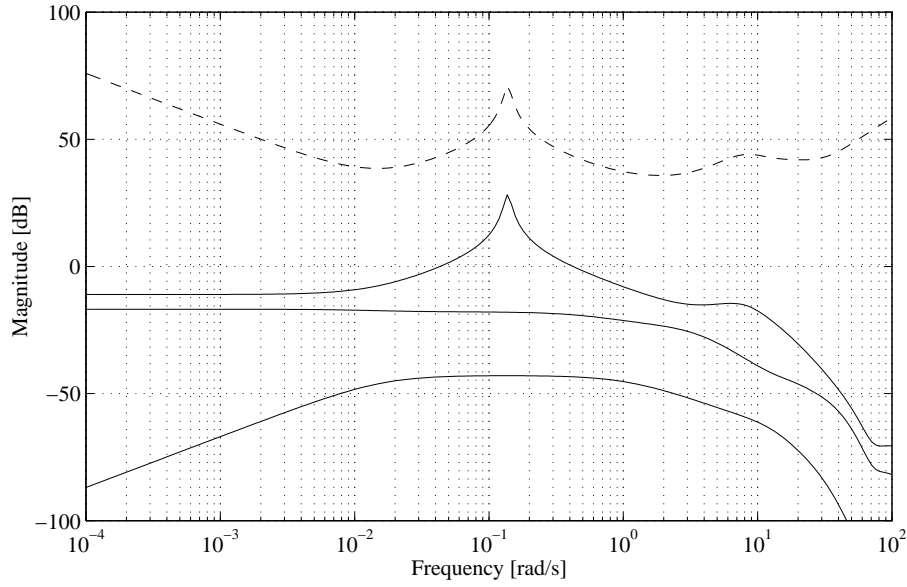


Figure 7.2: *Singular value Bode plot of the plant $G(s)$ (solid) and plant condition number (dashed).*

$$= \sum_{i=1}^3 y_i(\omega) \sigma_i(\omega) \alpha_i(\omega) \quad (7.8)$$

$$= \sigma_1(\omega) \alpha_1(\omega) y_1(\omega) + \sigma_2(\omega) \alpha_2(\omega) y_2(\omega) + \sigma_3(\omega) \alpha_3(\omega) y_3(\omega) \quad (7.9)$$

Thus the output $y(j\omega)$ will be confined to the region spanned by $y_1(\omega)$, $y_2(\omega)$ and $y_3(\omega)$. We cannot require outputs in direction of $y_4(\omega)$ since we can only control as many output directions as we have inputs.

Furthermore, at steady-state, σ_3 tends to zero as well and the output $y(j0)$ becomes confined to the region spanned by $y_1(0)$ and $y_2(0)$. It turns out that for frequencies below 10^{-4} rad/s, $Y(\omega)$ remains fairly constant. A good constant approximation is

$$Y(\omega) \approx \tilde{Y} = \begin{bmatrix} \tilde{y}_1 & \tilde{y}_2 & \tilde{y}_3 & \tilde{y}_4 \end{bmatrix} \quad \text{for } \omega < 10^{-4} \quad (7.10)$$

$$= \begin{bmatrix} 0 & 0 & 0 & -1j \\ 0.923 & -0.291 & 0.252j & 0 \\ 0.300 & -0.954 & 0 & 0 \\ -0.240 & -0.076 & -0.968j & 0 \end{bmatrix} \quad \text{for } \omega < 10^{-4} \quad (7.11)$$

where the imaginary parts are due to plant transmission zeros at $s = 0$. Since $\tilde{y}_{11} = 0$ and $\tilde{y}_{21} = 0$ the pitch rate q cannot be controlled in the low frequency area. However, we have no intentions of trying to do so. In fact, in the existing classical PI design, the pitch rate is used to stabilize the plant, but is not controlled itself.

Now \tilde{y}_3 is mainly in the direction of the longitudinal acceleration $a_x(s)$ and therefore *independent* low frequency control of the longitudinal acceleration becomes difficult. That is, we cannot achieve acceleration in the low frequency range without changing either the height rate $\dot{h}(s)$ or the pitch attitude $\theta(s)$. This is not surprising, since our model is valid in the transition zone between jet-borne and wing-borne flight where any change in longitudinal velocity strongly affects the aircraft lift.

The above singular value analysis has revealed that care must be taken when formulating the control objectives for the system. In the next section it will be shown how the singular value decomposition of $G(s)$ may be utilized to choose adequate weighting functions for robust control design.

7.2 Control Objectives

The singular value analysis made above illustrated that independent control of the pitch rate $q(s)$ will be difficult in the low frequency area. It is furthermore obvious that control of pitch attitude and pitch rate cannot be accomplished independently. It thus seems reasonable to omit direct control of the pitch rate and just use $q(s)$ as feedback (without reference).

A control configuration for the aircraft can thus be formulated as illustrated in Figure 7.3 on the facing page. The pilot commands for pitch attitude, $r_\theta(s)$, height rate, $r_{\dot{h}}(s)$, and longitudinal acceleration, $r_{a_x}(s)$ are compared with the measured values and the corresponding error signals, $e_\theta(s)$, $e_{\dot{h}}(s)$ and $e_{a_x}(s)$ are fed into the controller $K(s)$ together with the measured pitch rate $q_m(s)$.

There are four main control objectives that will be considered when designing a controller for the ASTOVL vehicle.

1. **Stability.** The controller must stabilize the aircraft. The closed loop poles must thus all be located in the left half s -plane.
2. **Robust stability.** The controller must be robustly stable in the face of unmodeled dynamics and parametric uncertainty.
3. **Nominal performance.** There are two main performance demands to the controlled aircraft. It must have adequate response to pilot commands for pitch attitude, height rate and longitudinal acceleration. Furthermore,

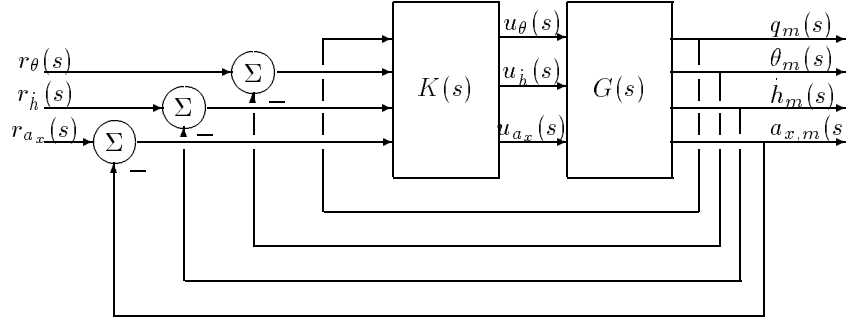


Figure 7.3: Block diagram of controlled aircraft.

rejection of gust disturbances on the airframe must be satisfactory. Here we will consider pilot command response only.

4. Robust performance. Nominal performance specifications must be met by uncertain closed loop system as well.

7.2.1 Robustness

It is critical that the controller stabilizes not only the nominal plant, but also a family of plants covering the inevitable parametric and dynamic uncertainty in the model. Here we will lump all the effects of uncertainty into a dynamic uncertainty description.

The robustness towards unmodeled dynamics can be investigated using the singular value methods in Section 4.3 on page 42. If, e.g. an unstructured input multiplicative uncertainty model is used, the true system is assumed to be given by:

$$G_T(s) = G(s) \left(I + \tilde{\Delta}(s) \right) \quad (7.12)$$

where $\tilde{\Delta}(s)$ is bounded in magnitude by:

$$\bar{\sigma}(\tilde{\Delta}(j\omega)) < \ell(\omega), \quad \forall \omega \geq 0 \quad (7.13)$$

From Theorem 4.4 on page 44, the perturbed system will remain stable if and only if:

$$\bar{\sigma}(T_i(j\omega)) < \ell^{-1}(\omega), \quad \forall \omega \geq 0 \quad (7.14)$$

Usually a diagonal weighting function $W_u(s)$ is introduced so that:

$$\tilde{\Delta}(s) = W_u(s)\Delta \quad (7.15)$$

where $\bar{\sigma}(\Delta) < 1$ and $\bar{\sigma}(W_u(j\omega)) = \ell(\omega)$, $\forall \omega \geq 0$. $W_u(s)$ is often given as:

$$W_u(s) = w(s) \cdot I \quad (7.16)$$

where $w(s)$ is a SISO transfer function satisfying $|w(j\omega)| = \ell(\omega)$ and I is the identity matrix of appropriate dimension.

Unfortunately completely unstructured uncertainty descriptions as above may be very conservative for ill-conditioned or poorly scaled systems. To see this assume an unstructured input multiplicative uncertainty description like (7.12) with $\tilde{\Delta}(s)$ given by (7.15). It is then easy to show that the perturbed plant $G_T(s)$ is given by:

$$G_T(s) = G(s) + G(s)\Delta W_u(s) = G(s) + G_\Delta(s) \quad (7.17)$$

where $G_\Delta(s)$ is given by

$$G_\Delta(s) = G(s)\Delta W_u(s) = w(s) \cdot \begin{bmatrix} G_{11}\Delta_{11} + G_{12}\Delta_{21} + G_{13}\Delta_{31} \\ G_{21}\Delta_{11} + G_{22}\Delta_{21} + G_{23}\Delta_{31} \\ G_{31}\Delta_{11} + G_{32}\Delta_{21} + G_{33}\Delta_{31} \\ G_{41}\Delta_{11} + G_{42}\Delta_{21} + G_{43}\Delta_{31} \\ G_{11}\Delta_{12} + G_{12}\Delta_{22} + G_{13}\Delta_{32} & G_{11}\Delta_{13} + G_{12}\Delta_{23} + G_{13}\Delta_{33} \\ G_{21}\Delta_{12} + G_{22}\Delta_{22} + G_{23}\Delta_{32} & G_{21}\Delta_{13} + G_{22}\Delta_{23} + G_{23}\Delta_{33} \\ G_{31}\Delta_{12} + G_{32}\Delta_{22} + G_{33}\Delta_{32} & G_{31}\Delta_{13} + G_{32}\Delta_{23} + G_{33}\Delta_{33} \\ G_{41}\Delta_{12} + G_{42}\Delta_{22} + G_{43}\Delta_{32} & G_{41}\Delta_{13} + G_{42}\Delta_{23} + G_{43}\Delta_{33} \end{bmatrix} \quad (7.18)$$

Here Δ_{ij} denotes the i, j 'th entry of Δ . The dependency on s has been omitted for clarity. Now if there is large differences in the gains of $G_{ij}(s)$ *row-wise* that is, if for example

$$|G_{11}(j\omega)| \ll |G_{12}(j\omega)|, |G_{13}(j\omega)|, \quad \text{for some frequency range} \quad (7.19)$$

we will have that for those frequencies

$$|G_{\Delta_{11}}(j\omega)| = |w(j\omega)| |G_{11}(j\omega)\Delta_{11} + G_{12}(j\omega)\Delta_{21} + G_{13}(j\omega)\Delta_{31}| \quad (7.20)$$

$$\gg |G_{11}(j\omega)| \quad (7.21)$$

unless $|w(j\omega)|$ is very small. Consequently the uncertainty assumption on $G_{11}(s)$ can be very conservative. Generally, if we have large row-wise gain variations in $G(s)$ an unstructured input multiplicative uncertainty description will be potentially very conservative. Equivalently it can be shown that if significantly

column-wise gain variations exist in $G(s)$ an unstructured output multiplicative uncertainty description will be potentially very conservative.

Such gain variations occur typically for poorly scaled or ill-conditioned systems. For the aircraft model it can be checked that there are considerable row-wise gain variations across the entire frequency range and column-wise gain variations in the low frequency area. Thus unstructured perturbation models will surely result in very conservative control designs.

How can we now avoid this conservatism? One remedy is to diagonalize Δ :

$$\Delta = \text{diag} \{ \Delta_{11}, \Delta_{22}, \dots, \Delta_{nn} \}, \quad |\Delta_{ii}(j\omega)| < 1, \forall \omega \geq 0 \quad (7.22)$$

Then for the case of input multiplicative uncertainty the plant uncertainty $G_\Delta(s)$ becomes

$$G_\Delta(s) = G(s)\Delta_1 W_u(s) = w(s)I \begin{bmatrix} G_{11}\Delta_{11} & G_{12}\Delta_{22} & G_{13}\Delta_{33} \\ G_{21}\Delta_{11} & G_{22}\Delta_{22} & G_{23}\Delta_{33} \\ G_{31}\Delta_{11} & G_{32}\Delta_{22} & G_{33}\Delta_{33} \\ G_{41}\Delta_{11} & G_{42}\Delta_{22} & G_{43}\Delta_{33} \end{bmatrix} \quad (7.23)$$

which is less potentially conservative. The diagonalization of Δ corresponds to assuming that the uncertainty acts individually on each input (or output for output multiplicative uncertainty). We will assume this diagonal uncertainty structure for the aircraft control design. Notice that the control design will now be a μ -problem, since we have enforced a structure on $\Delta(s)$. We can thus *not* use the singular value tests from Table 4.1 on page 47¹. Rather we must use the results from Chapter 5 to assess whether the closed loop system is robustly stable. From Theorem 5.2 on page 71 the closed loop system will remain stable under perturbations Δ if and only if

$$\sup_{\omega} \mu_\Delta(P(j\omega)) \leq 1 \quad (7.24)$$

where $P(s)$ is the transfer function matrix “seen” by the perturbation.

Another well-known design problem in connection with ill-conditioned systems is that the closed loop properties can be very different when evaluated at different loop breaking points. In [TCB95] it is shown that for the current aircraft the robustness to diagonal multiplicative uncertainty like (7.22) may be adequate when the uncertainty acts at the plant output, but very poor if the uncertainty acts at the plant input. Thus the robustness properties may be very different at the plant input and output. In order to avoid this situation we will assume a diagonal multiplicative perturbation at *both* plant input and output. It is thus assumed that the true plant belongs to the set given by

$$G_T(s) = (I + \tilde{\Delta}_o(s))G(s)(I + \tilde{\Delta}_i(s)) \quad (7.25)$$

¹They will at least be potentially conservative.

where $\tilde{\Delta}_{o/i}(s)$ is a diagonal perturbation:

$$\tilde{\Delta}_{i/o}(s) = W_{i/o}(s)\Delta(s) = w_{i/o}(s)I\Delta(s) \quad (7.26)$$

where $w_{i/o}(s)$ is a scalar transfer function specifying the expected maximum magnitude of $\tilde{\sigma}(\tilde{\Delta}_{i/o}(j\omega))$ and $\Delta(s)$ is given by (7.22) on the page before. Since the plant has been scaled, it is assumed that $w_i(s) = w_o(s) = w_u(s)$. Since the nominal model is believed to be structurally correct in the low frequency range, the dynamic uncertainty at low frequencies will be quite small – say 5%. However, at higher frequencies the nominal model becomes more and more uncertain and in the neighborhood of the natural frequency of the airframe the dynamic uncertainty will be large, probably more than 100%. $w_u(s)$ was chosen as:

$$w_u(s) = \frac{10^{15/20}(s+1)}{s+112} \quad (7.27)$$

In Figure 7.4 the singular value Bode plot of $w_u(s)$ is shown. Notice that the steady-state gain is $0.05 \approx -26$ dB, corresponding to 5% uncertainty. The uncertainty then rises to 100% around 20 rad/sec and continues to increase above that frequency in order to illustrate the large uncertainty of the rigid-body airframe model around the natural frequency of the airframe.

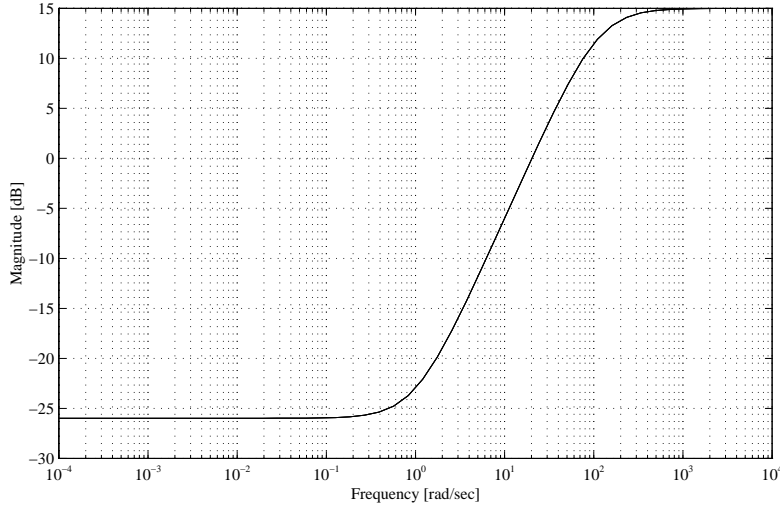


Figure 7.4: *Singular value Bode plot of the uncertainty specification $W_u(s) = w_u(s)I$.*

7.2.2 Performance

The major performance demand on the controlled aircraft is probably that the pilot command response should be satisfactory. Thus the transfer function from references $r(s)$ to the control error $e(s)$ should be small across the controlled frequency range (up to the closed loop bandwidth ω_b). Since we have not included the pitch rate $q(s)$ into the control error $e(s)$ this transfer matrix will *not* be equal to the standard output sensitivity $S_o(s)$. Nevertheless we will use the term output sensitivity since the implied transfer matrix measures the sensitivity to disturbances (references) at the plant output. However, as was shown in Section 7.1.2 on page 108, independent control of the longitudinal acceleration $a_x(s)$ in the low frequency range is not feasible. If we attempt to obtain this by specifying standard performance weightings with uniform high gain for low frequencies, the controller will use a lot of effort to try to accomplish an impossible task. This will surely deteriorate the overall control performance.

To avoid this we must specify a control error weight $W_e(s)$ which does *not* penalize error signals in the direction of \tilde{y}_3 in the low frequency range. Fortunately such a weighting matrix can be easily constructed from \tilde{Y} . Let $W_e(s)$ be given by:

$$W_e(s) = \begin{bmatrix} w_1(s) & 0 & 0 \\ 0 & w_2(s) & 0 \\ 0 & 0 & w_3(s) \end{bmatrix} Y_W^T \quad (7.28)$$

where Y_W is given by:

$$Y_W = \Re e (\tilde{Y}_{2:4,1:3}) = \begin{bmatrix} y_{w1} & y_{w2} & y_{w3} \end{bmatrix} \quad (7.29)$$

$$= \begin{bmatrix} -0.923 & -0.291 & 0.252 \\ 0.300 & -0.954 & 0 \\ -0.240 & -0.076 & -0.968 \end{bmatrix} \quad (7.30)$$

$w_1(s)$ and $w_2(s)$ are standard error weights with high gain at low frequencies. $w_3(s)$ has low gain at low frequencies, but should be equal to $w_{(1,2)}(s)$ for frequencies above, say 0.1 rad/sec. Notice that Y_W is equal to \tilde{Y} , see Equation (7.11) on page 109, except that the subsystem corresponding to the controlled variables has been selected and that the imaginary parts have been changed into real parts. For a norm based design method like μ the latter changes nothing and real weighting matrices seem more natural. Now if the error $e(j\omega)$ is in the direction of \tilde{y}_3 ($e(j\omega) = \beta \tilde{y}_3$), the weighted signal will be given by:

$$e'(j\omega) = W_e(j\omega)e(j\omega) \quad (7.31)$$

$$= W_e(j\omega)\beta \tilde{y}_3 \quad (7.32)$$

$$= \begin{bmatrix} 0 & 0 & j\beta w_3(j\omega) \end{bmatrix}^T \quad (7.33)$$

Consequently, if the gain of $w_3(s)$ is small in the low frequency range, less weight will be put on the unreachable output direction. The following performance weightings were chosen for the aircraft design:

$$w_1(s) = \frac{0.5(s + 1.25)}{s + 6.25 \cdot 10^{-3}} \quad (7.34)$$

$$w_2(s) = \frac{0.5(s + 1.25)}{s + 6.25 \cdot 10^{-3}} \quad (7.35)$$

$$w_3(s) = \frac{0.5(s + 1.25)(s + 1.25 \cdot 10^{-4})}{(s + 0.03125)(s + 0.0125)} \quad (7.36)$$

In Figure 7.5, the singular value Bode plot of $W_e(s)$ is shown. Notice that because Y_W is unitary, the singular values are simply the gain characteristics of the individual weightings $w_1(s) \rightarrow w_3(s)$. Notice also how $w_3(s)$ reflects the small weight we impose on the unreachable output at low frequencies.

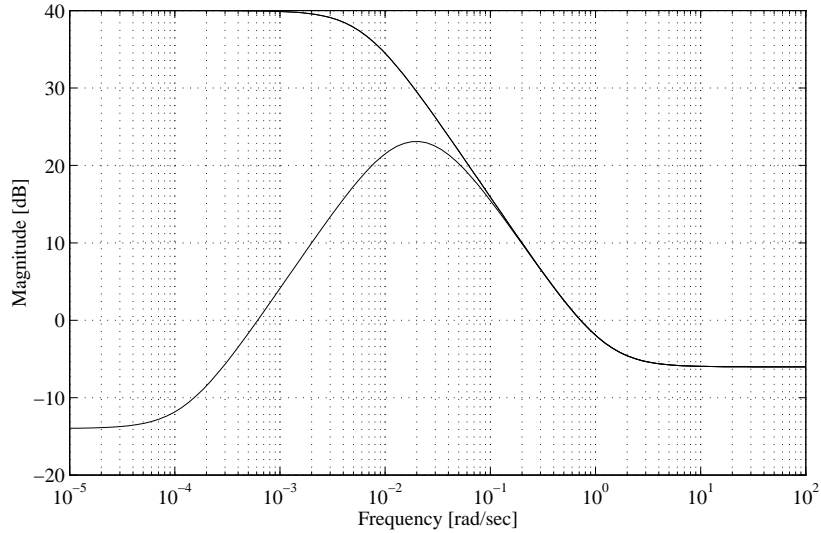
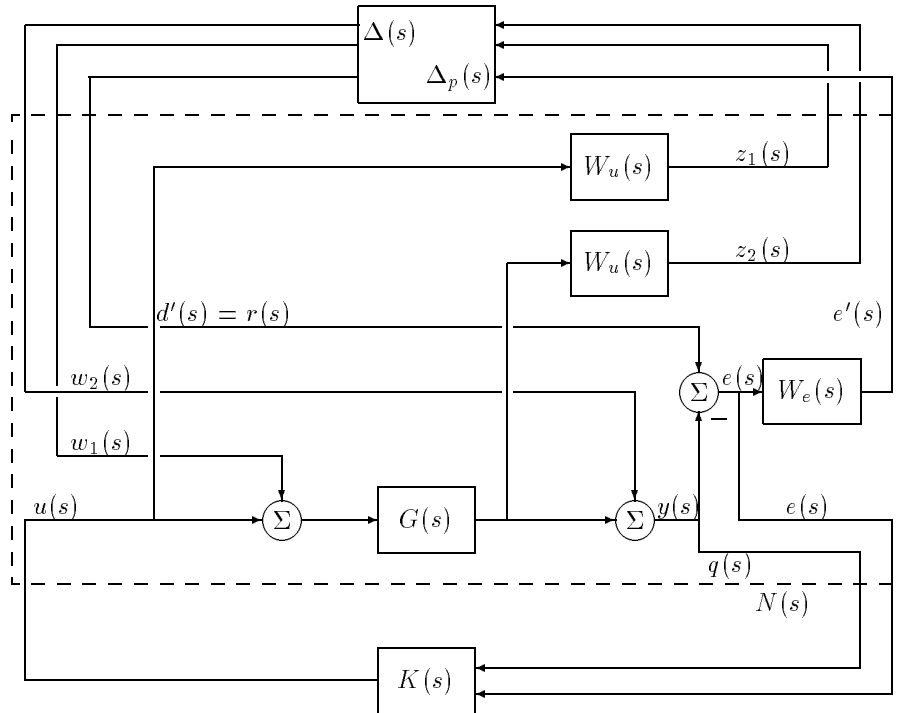


Figure 7.5: Singular value Bode plot of the performance weight $W_e(s)$.

Now the aircraft robust performance control problem will be formulated using the $N\Delta K$ framework introduced in Section 5.1.2 on page 71. With simultaneous input and output multiplicative diagonal uncertainty and a command response performance specification as above, the control problem set-up then becomes as illustrated in Figure 7.6.



The results from Section 5.1 on page 64 may then be utilized to assess the performance and robustness of the controlled system as follows. The perturbation $\Delta(s)$ belongs to the bounded subset

$$\mathbf{B}\Delta = \{\Delta(s) \in \Delta \mid \bar{\sigma}(\Delta(j\omega)) < 1\} \quad (7.37)$$

where Δ is given by

$$\Delta = \{\text{diag}\{\delta_1, \delta_2, \delta_3, \delta_4, \delta_5, \delta_6, \delta_7\} \mid \delta_i \in \mathbf{C}\} \quad (7.38)$$

We then have:

- The closed loop system will be robustly stable iff:

$$\sup_{\omega} \mu_{\Delta}(P_{11}(j\omega)) \leq 1 \quad (7.39)$$

where $P(s) = F_l(N(s), K(s))$. $P_{11}(s)$ is thus the transfer matrix from the perturbations $w(s) = [w_1(s), w_2(s)]^T$ to $z(s) = [z_1(s), z_2(s)]^T$.

- The system will have nominal performance if:

$$\sup_{\omega} \bar{\sigma}(P_{22}(j\omega)) \leq 1 \quad (7.40)$$

$P_{22}(s)$ is the transfer matrix from the disturbances $d'(s)$ to the control errors $e'(s)$.

- The system will have robust performance, that is, it will be robustly stable and:

$$\sup_{\omega} \bar{\sigma}(F_u(P(j\omega), \Delta(j\omega))) \leq 1 \quad (7.41)$$

iff

$$\sup_{\omega} \mu_{\tilde{\Delta}}(P(j\omega)) \leq 1 \quad (7.42)$$

The augmented uncertainty block $\tilde{\Delta}$ is given by:

$$\tilde{\Delta} = \{\text{diag}(\Delta, \Delta_p) \mid \Delta \in \Delta, \Delta_p \in \mathbf{C}^{3 \times 3}\} \quad (7.43)$$

Since $\tilde{\Delta}$ consists of purely complex non-repeated blocks we may apply standard D - K iteration to find the optimal μ controller for the system. We will thus iteratively solve the minimization problem:

$$\inf_{K(s) \in \mathcal{K}_S} \sup_{\omega} \inf_{D(\omega) \in \mathbf{D}} \{\bar{\sigma}(D(\omega)F_l(N(j\omega), K(j\omega))D^{-1}(\omega))\} \quad (7.44)$$

The algorithms provided in the MATLAB *μ -Analysis and Synthesis Toolbox* may be readily applied to do so.

7.4 Evaluation of Classical Control Design

Before we proceed with the μ design let us evaluate the existing classical controller design for the aircraft. The existing classical PI controller configuration is displayed in Figure 7.7. The aircraft dynamics were first stabilized using pitch rate feedback through a PI controller $K_q(s)$ with lead filter $L_f(s)$:

$$K_q(s) = \frac{13(s + 0.5)}{s} \quad (7.45)$$

$$L_f(s) = \frac{1 + 0.125s}{1 + 0.0208s} \quad (7.46)$$

The remaining loops were closed in the order pitch attitude $K_\theta(s)$, height rate $K_{\dot{h}}(s)$ and longitudinal acceleration $K_{a_x}(s)$:

$$K_\theta(s) = 0.95 \quad (7.47)$$

$$K_{\dot{h}}(s) = \frac{-15(s + 0.175)}{s} \quad (7.48)$$

$$K_{a_x}(s) = \frac{20(s + 10.0)}{s} \quad (7.49)$$

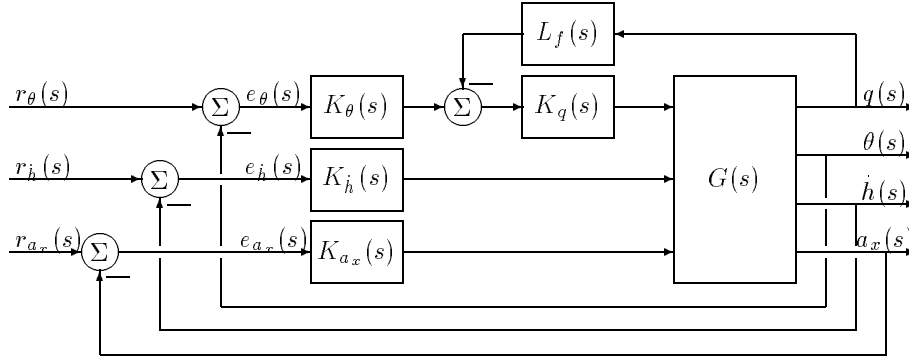


Figure 7.7: Classical controller configuration.

The individual controllers may be gathered in one transfer function matrix $K(s)$, like in Figure 7.3 on page 111. It is easy to see that

$$K(s) = \begin{bmatrix} K_q(s)L_f(s) & K_q(s)K_\theta(s) & 0 & 0 \\ 0 & 0 & K_{\dot{h}}(s) & 0 \\ 0 & 0 & 0 & K_{a_x}(s) \end{bmatrix} \quad (7.50)$$

The above controllers are for the true unscaled plant. In order to evaluate the closed loop system against the robustness and performance demand introduced previously, we will use the scaled plant and scale the classical controller:

$$K_s(s) = N_u K(s) N_y^{-1} \quad (7.51)$$

where $K_s(s)$ denotes the scaled version of the classical controller $K(s)$.

In order to check whether the classical controller comply with the stated demands we check the performance and robustness conditions given in Section 7.3 on page 117. It can easily be verified that the closed loop system is nominally stable, since all poles of $F_l(N(s), K_s(s))$ are situated in the left-half s -plane. Robust stability, nominal performance and robust performance will then be checked.

In Figure 7.8 on the facing page $\mu_{\Delta}(P_{11}(j\omega))$, the singular values of $P_{22}(j\omega)$ and $\mu_{\tilde{\Delta}}(P(j\omega))$ are shown across frequency ω . Notice from Figure 7.8 on the facing page that the closed loop system is *not* robustly stable since $\mu_{\Delta}(P_{11}(j\omega))$ peaks at approximately 1.4. Thus, with the applied perturbation model there exists a perturbation with

$$\bar{\sigma}(\Delta(j\omega)) = \frac{1}{1.4} = 0.71 \quad (7.52)$$

for which the closed loop system will become unstable. Furthermore since $\sup_{\omega} \bar{\sigma}(P_{22}(j\omega)) > 10$ the nominal performance specification is far from being met and as a consequence we of course cannot obtain robust performance. $\mu_{\tilde{\Delta}}(P(j\omega))$ peaks at approximately 11.8. This means that there exists a perturbation $\Delta(s)$ with

$$\bar{\sigma}(\Delta(j\omega)) = \frac{1}{11.8} = 0.085 \quad (7.53)$$

for which the perturbed weighted sensitivity specification $F_u(\Delta(s), P(s))$ gets large

$$\bar{\sigma}(F_u(\Delta(j\omega), P(j\omega))) = 11.8 \quad (7.54)$$

Whether or not the performance specification is met for the perturbed closed loop system is of course of minor importance when closed loop stability cannot be guaranteed.

Notice how the robustness problems are concentrated at high frequencies whereas the performance problems occur at low frequencies. This should indicate that it will be possible to improve the design.

In Figure 7.9 on page 122 the (nominal) step responses of the system are shown for maximum size steps applied on pitch attitude θ , height rate \dot{h} and longitudinal acceleration a_x . The results are further investigated in Table 7.2 on page 123,

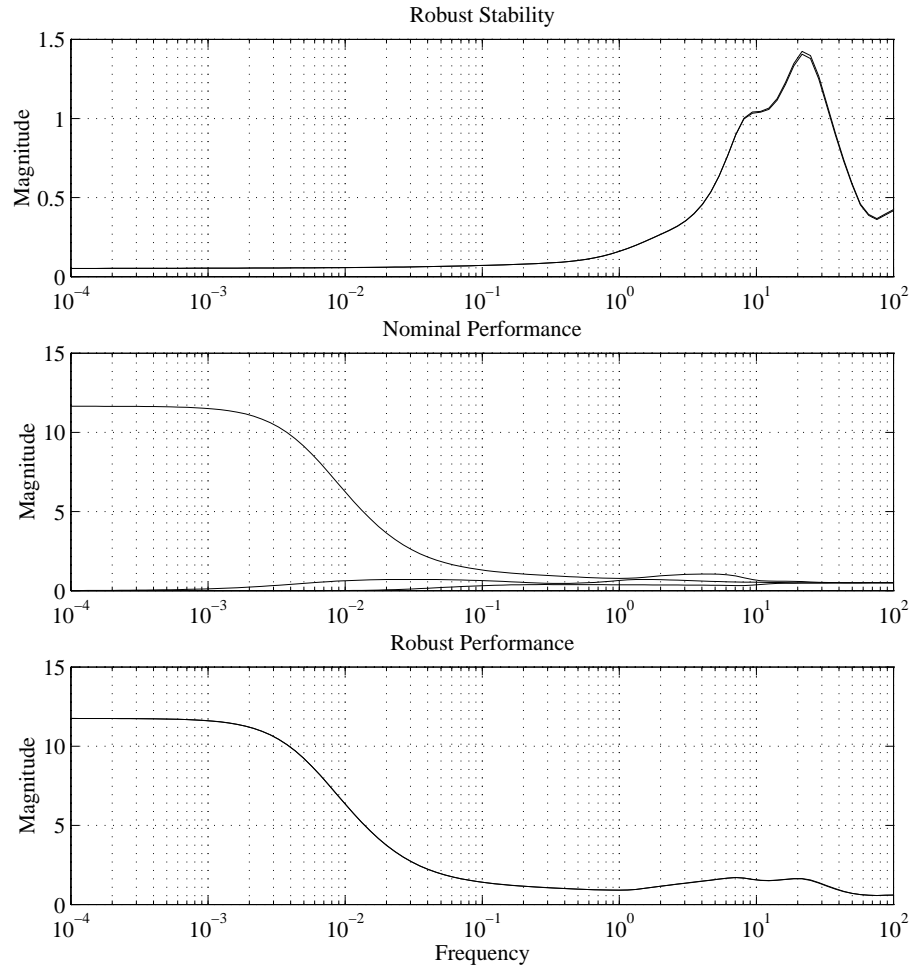


Figure 7.8: Results from applying the classical controller on the aircraft. Shown are $\mu_{\Delta}(P_{11}(j\omega))$ (top), $\sigma(P_{22}(j\omega))$ (center) and $\mu_{\hat{\Delta}}(P(j\omega))$ (bottom).

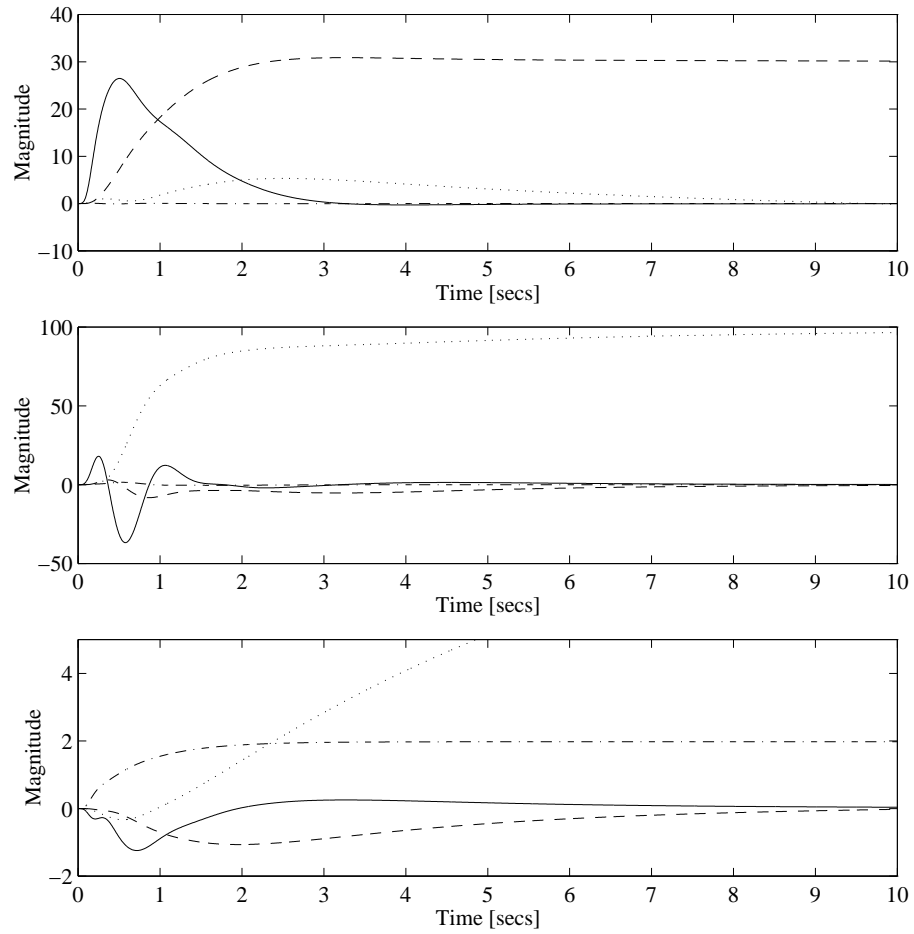


Figure 7.9: *Transient responses for classical control configuration. Shown are step responses from step on pitch (top), height rate (center) and acceleration (bottom). Shown signals are pitch rate (solid), pitch (dashed), height rate (dotted) and longitudinal acceleration (dash-dotted).*

		Maximum absolute deviation on			
Step on	step size	pitch rate $\dot{\theta}$ [°/sec]	pitch θ [°]	height rate \dot{h} [ft/sec]	acc. a_x [g]
pitch θ	30 °	26.5	–	5.3	0.08
height rate \dot{h}	100 ft/sec	36.7	8.2	–	1.54
long. acc. a_x	2 g	1.24	1.07	11.3	–
		Maximum relative deviation on			
Step on	step size	$\dot{\theta}$ [%]	θ [%]	\dot{h} [%]	a_x [%]
pitch θ	30 °	–	–	5.3 %	4 %
height rate \dot{h}	100 ft/sec	–	27.3 %	–	77 %
long. acc. a_x	2 g	–	3.6 %	11.3 %	–

Table 7.2: *Maximum absolute and relative-to-maximum step-size deviation on pitch rate $q(t)$, pitch attitude $\theta(t)$, height rate $\dot{h}(t)$ and longitudinal acceleration $a_x(t)$ for each reference step.*

where the maximum cross coupling effects are given. Both absolute and relative-to-maximum-step-size values are given.

The cross coupling from height rate to pitch (27.3%) and longitudinal acceleration (77%), see Table 7.2, are unacceptable.

7.5 Controller Design using μ

Now we will apply μ -synthesis in order to improve the classical design. The control problem is thus formulated as in Figure 7.6 on page 117 and we will apply D - K iteration to solve it. In Figure 7.10 on the following page, the result of the D - K iteration is shown. The maximum upper bound for $\mu_{\bar{\Delta}}(P(j\omega))$ for selected iterations are also given in Table 7.3 on the next page.

Note that compared with the CD servo example presented in Chapter 6, the D - K iteration procedure here converges very slowly. However, after 25 iterations we obtain closed loop robust performance. After 28 iterations the decrease in μ per iteration became negligible. The final controller was of very high order (92 states). However, using model reduction methods it was possible to reduce the order to 30 with very little degradation in control performance, see Table 7.3 on the following page. However, using controller approximations with fewer states implied a significant increase in μ . Since the nominal model (without weighting

Iteration No.	$\sup_{\omega} \mu_{\Delta} (P_{11}(j\omega))$	$\sup_{\omega} \bar{\sigma} (P_{22}(j\omega))$	$\sup_{\omega} \mu_{\bar{\Delta}} (P(j\omega))$
1 (\mathcal{H}_{∞} controller)	0.722	8.40	8.48
2	0.737	2.67	2.81
3	0.436	1.91	2.01
4	0.575	1.58	1.68
5	0.840	1.45	1.54
10	0.462	1.17	1.27
15	0.467	1.04	1.14
20	0.443	0.956	1.06
25	0.467	0.897	0.999
28	0.595	0.869	0.969
Reduced order K_{μ}	0.589	0.869	1.00

Table 7.3: Maximum upper bound for $\mu_{\Delta}(P_{11}(j\omega))$, $\bar{\sigma}(P_{22}(j\omega))$ and $\mu_{\bar{\Delta}}(P(s))$ in each step of D-K iteration.

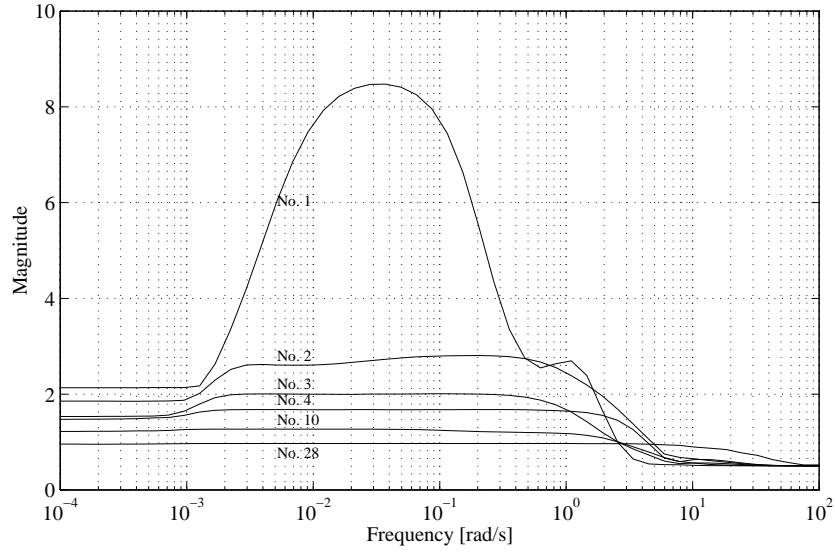


Figure 7.10: Upper bound on the structured singular value $\mu_{\bar{\Delta}}(F_l(N(j\omega), K(j\omega)))$ in D-K iteration.

matrices) has 26 states, a 30th order controller does maybe not seem unreasonable. However, this is still a very high order controller and there will certainly be open questions with regards to numerics in connection with actual implementation. It is, however, beyond the scope of this work to treat this in any detail. Fixed order \mathcal{H}_∞ algorithms may be a solution to the very high order controllers produced by D - K , D , G - K and μ - K iteration.

In Figure 7.11 on the next page the closed loop system obtained with the reduced order controller is analyzed using μ . From Figure 7.11 on the following page notice that robust stability and nominal performance are obtained with some margin to allow for robust performance.

In Figure 7.12 on page 127 the transient response of the closed loop system is evaluated. Here maximum size steps has been applied on pitch attitude θ , height rate \dot{h} and longitudinal acceleration a_x . The results are further investigated in Table 7.4, where the maximum cross coupling effects are given.

		Maximum absolute deviation on			
Step on	step size	pitch rate $\dot{\theta}$ [°/sec]	pitch θ [°]	height rate \dot{h} [ft/sec]	acc. a_x [g]
pitch θ	30 °	25.3	–	1.82	0.073
height rate \dot{h}	100 ft/sec	5.14	1.24	–	0.20
long. acc. a_x	2 g	1.81	1.42	3.25	–
		Maximum relative deviation on			
Step on	step size	pitch rate $\dot{\theta}$ [%]	pitch θ [%]	height rate \dot{h} [%]	acc. a_x [%]
pitch θ	30 °	–	–	1.8 %	3.67 %
height rate \dot{h}	100 ft/sec	–	4.1 %	–	10.2 %
long. acc. a_x	2 g	–	4.7 %	3.3 %	–

Table 7.4: *Maximum absolute and relative-to-maximum-step-size deviation on pitch rate $\dot{q}(t)$, pitch attitude $\theta(t)$, height rate $\dot{h}(t)$ and longitudinal acceleration $a_x(t)$ for each reference step.*

As can be seen from Table 7.4, the transient response has been dramatically improved in comparison with the classical controller. The cross couplings between pitch attitude, height rate and longitudinal acceleration are now acceptable. Furthermore, the μ analysis guarantee that these properties are more or less maintained under the uncertainty allowed by the applied perturbation model. The steady-state errors for pitch attitude, height rate and longitudinal acceleration are 0.75%, 0.63% and 6.3%. The steady-state error for the acceleration may seen

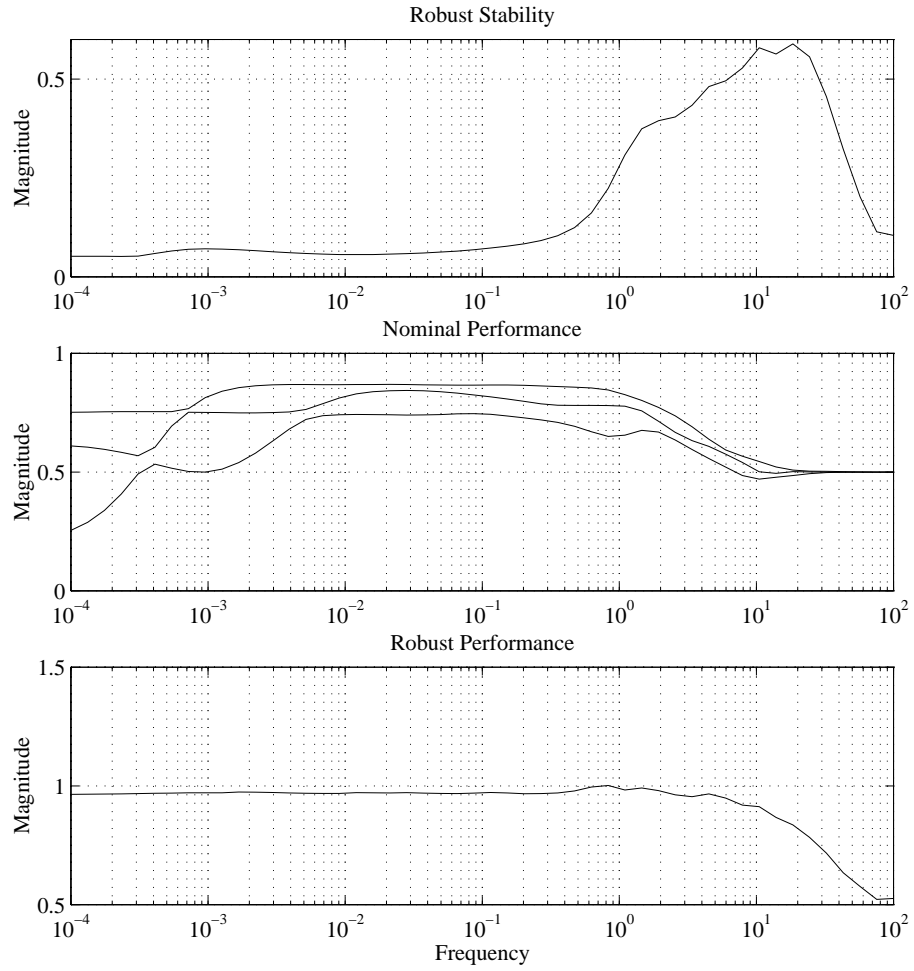


Figure 7.11: Results from applying the μ controller on the aircraft. Shown are $\mu_{\Delta}(P_{11}(j\omega))$ (top), $\sigma(P_{22}(j\omega))$ (center) and $\mu_{\tilde{\Delta}}(P(j\omega))$ (bottom).

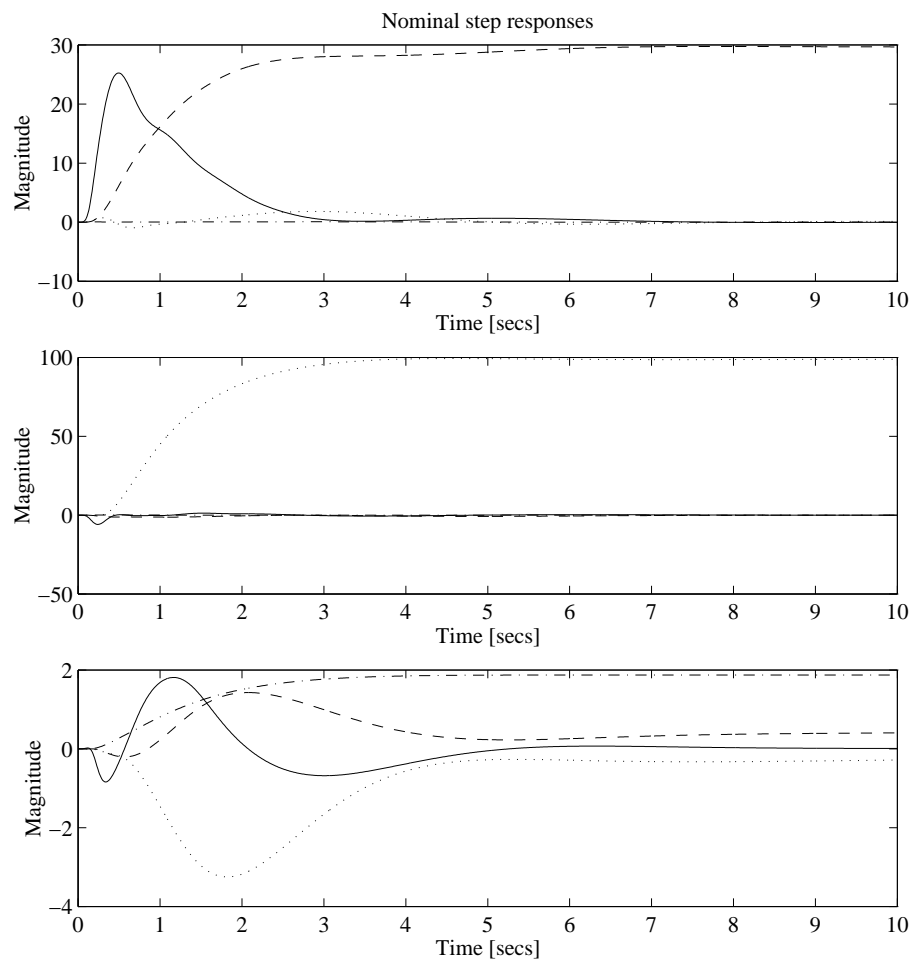


Figure 7.12: Transient responses for μ control system. Shown are step responses from step on pitch (top), height rate (center) and acceleration (bottom). Shown signals are pitch rate (solid), pitch (dashed), height rate (dotted) and longitudinal acceleration (dash-dotted).

quite high. Remember, however, that the singular value analysis in Section 7.1.2 on page 108 revealed that low frequency control of the acceleration a_x is infeasible. In fact, if the simulation in Figure 7.12 on the page before is continued for $t \rightarrow \infty$ it can be seen that $a_x(t)$ slowly rolls off towards zero. Thus the term steady-state above for the acceleration is somewhat misused. However, these phenomena occur far below the frequency range of interest.

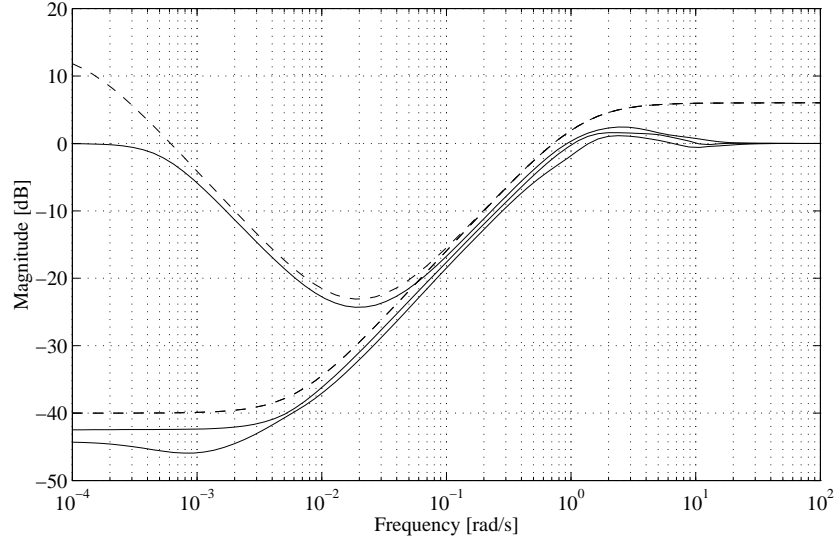


Figure 7.13: *Nominal sensitivity and performance bounds for the aircraft design. Shown are $\bar{\sigma}(F_l(N(j\omega), K(j\omega)))$ (solid) for the reduced order controller and $\bar{\sigma}(W_e(j\omega))$ (dashed).*

Finally, let us investigate the nominal output sensitivity function. As discussed previously in Section 7.2.2 on page 115 the sensitivity function for the aircraft design does not equal the standard output sensitivity $S_o(s)$ because the pitch rate feedback signal is not included in the control error $e(s)$. Let $\tilde{S}(s)$ denote the transfer function from the reference $r(s)$ to the control error $e(s)$. In Figure 7.13, the singular values of $\tilde{S}(j\omega)$ are shown together with the singular values of the performance specification $W_e(s)$. Note how smoothly the μ controller has shaped $\tilde{S}(s)$ to comply with the specifications.

7.6 Summary

The rigid body dynamics of the aircraft was investigated using singular values. It was demonstrated that the system is very ill-conditioned. In fact, the condition number increases to infinity at steady-state. It then becomes impossible to use uniform weightings for controller design. One possible method of choosing performance weights in this case was suggested. A diagonal multiplicative perturbation structure was applied at both plant input and output. A classical control configuration was investigated and it was demonstrated that the cross coupling attenuation of this controller was poor. An optimal μ controller was designed using D - K iteration. μ analysis of the closed loop system revealed that the controller gave significant improvement in both robust stability and performance compared with the classical controller. The transient response for the controller was investigated using step responses. These proved quite satisfactory for the μ design with very good decoupling of pitch, height rate and longitudinal acceleration.

Part II

System Identification and Estimation of Model Error Bounds

Chapter 8

Introduction to Estimation Theory

Contents

8.1	Soft versus Hard Uncertainty Bounds	135
8.2	An Overview	137
8.3	Remarks	137

The use of system identification in control engineering has been a popular alternative to physical modeling for obtaining model descriptions of a given physical system. Application of the fundamental laws from mechanics, thermodynamics, chemistry etc. are often quite complex and time consuming tasks especially if large scale engineering systems are considered. In such cases, when plant input/output measurements are available, system identification provides an alternative for generating a model for use in control design. Usually, system identification involves linear discrete-time models. However, the general ideas are not restricted to such systems, but apply for non-linear continuous-time models as well. In this work, however, we will consider linear discrete-time models exclusively. Considering linear systems the obtained models will be readily applicable in connection with linear control systems design.

The construction of a parametric model from input/output measurements involves four basic entities:

- The data set.
- The model set (candidate models).
- The objective function for the estimation (performance function).
- Model validation.

The data-set used for the identification procedure must be “informative” of the actual physical plant during normal operation. If the system is not excited properly, we will not obtain a reasonable accurate model of the system. In more precise terms, we must require the input(s) to be *persistently exciting*, see [Lju87, Sec. 14.2]. Sometimes, the input/output data are recorded during a specifically designed identification experiment where the user may choose the input signals. *Experiment design* then is concerned with choosing the input signals such that the data set becomes maximally informative subject to possible constraints at hand. Unfortunately, in other cases the user may not have the possibility to affect the experiment but must use data sets from normal operation of the system. Generally we will only obtain knowledge of the system in the particular point of operation from which the data set was obtained. If the plant model is to be used outside this operation point considerations must be made to capture any deviations from the nominal model.

A set of candidate models is obtained by specifying within which collection of models we will look for a suitable one. This is the most important and, unfortunately, the most difficult choice of the system identification procedure. Much engineering intuition and insight is needed to choose the appropriate set of models. Usually we refer to two types of model sets, *black box* and *gray box* models. If the candidate model set is a set of standard linear models employed with no reference to the physical background it is a black box model set. Then the model parameters have no physical interpretation but are merely knobs for adjusting the fit to the data. If, on the other hand, the candidate model is obtained by physical modeling with some unknown physical parameters, it is a grey box model set. Then the model parameters are physical quantities, e.g. masses or moments of inertia. In this work, we will deal with black box modeling only.

Having determined our candidate model set we need to determine the “best” model within this set guided by the available measurements. This is the *identification method*. Typically the assessment of model quality is based on how the models perform when they attempt to reproduce the measured data. Three parameter estimation methods have gained particular interest; *prediction error methods* (PEM), *maximum likelihood methods* and *instrument variable methods*.

Here we will consider mainly the PEM approach. However in connection with estimation of uncertainty bounds we will use maximum likelihood methods as well.

Finally, having determined the best model in our candidate model set we need to assess the quality of this model. This is especially important in connection with robust control, since this is precisely the information needed for constructing an appropriate perturbation structure. In classical identification theory, model quality has been assessed under the assumption that the only source of uncertainty is noisy measurements. It is thus assumed that within our candidate model set there exists a unique model which is a perfect description of the true plant. Of course such a strict condition is never met in practice. However, if the prediction errors, that is, the deviation between the measured and predicted outputs, are almost white noise, the classical results holds with reasonable accuracy.

Unfortunately, in connection with control systems design, it is often desired to have a low order approximation of the plant together with a simple quantification of the implied model imperfections in order to avoid very high order controllers. For restricted complexity models, the classical approach is inadequate since then, very often, the main source of uncertainty is due to the effect of incomplete model structures. Thus the results from classical system identification theory cannot be readily applied in estimation of model uncertainty for modern robust control design.

This gap between control theory and identification theory was recently realized by a number of researchers, see e.g. [GS89b, WL90a, Gev91]. The development of formal techniques for estimation of model uncertainty has since been the focus of active research and numerous results have been published, see e.g. [Bai92] and references therein.

8.1 Soft versus Hard Uncertainty Bounds

Considering finite dimensional linear time invariant (FDLTI) systems, estimation of model uncertainty in the case of restricted complexity model structures and a finite set of noisy data becomes a very difficult problem. On one hand, the structural model error (bias) should be considered a deterministic quantity, since the true system is hopefully deterministic. Consequently the part of the model residuals associated with the undermodeling is deterministic. On the other hand, the model error due to noise (variance) will be a stochastic quantity, since it is caused by the noise in the data. The part of the model residuals associated with the noise is thus stochastic. Consequently the two components of the total model error are fundamentally different quantities and require in principle fundamentally different treatment. However in order to make coherent estima-

tion procedures of the total model error most of the reported results in this field have relied upon treating the undermodeling and the noise as similar quantities. Generally speaking two main paths have been taken:

- The deterministic approach. The model residuals are assumed to be deterministic and bounded in magnitude. These methods will be referred to as *hard bound methods*.
- The stochastic approach. The model residuals are assumed to be stochastic, but non-stationary and correlated with the input. These methods will be referred to as *soft bound methods*.

The research on the deterministic approach has evolved along two different paths. The residuals may be assumed to be deterministic and bounded either in the frequency domain or in the time domain. The frequency domain approach is usually known as \mathcal{H}_∞ *identification*. Here noisy frequency response measurements¹ are used to obtain models with $\|\cdot\|_\infty$ norm error bounds that apply with probability one. In order to compute the bounds prior knowledge of the relative stability of the plant and of the noise bound on the frequency domain measurements is required. This approach is originally due to Parker & Bitmead [PB87] but has been further developed by Helmicki & co-workers [HJN91] and Gu & Khar-gonekar [GK92]. However as pointed out in [NG94] the error bounds obtained through \mathcal{H}_∞ identification can be very conservative. Furthermore, assessing the prior information needed to compute the bounds is a non-trivial task.

The time domain deterministic approach usually relies on *set-membership* identification assuming unknown but bounded noise on the time domain data points. In the fine paper by Wahlberg & Ljung [WL92] a thorough discussion of hard bound estimation from a least-squares perspective is presented. Hard total model error bounds are derived using prior information of the smoothness of the undermodeling impulse response, the shape of the undermodeling frequency response and a hard bound on the measurement noise. Again, the uncertainty estimates tend to be rather conservative and the necessary prior information may be difficult to obtain.

The research on the stochastic approach is mainly due to Goodwin & co-workers. In a series of papers, see e.g. [GS89b, GSM89, GGN91, GGN92] a methodology for estimation of total model error for restricted complexity models has been developed through stochastic embedding of the model bias. As were the case for the hard bound approaches some prior knowledge regarding the true plant and the noise is needed in order to compute the error bounds. Specifically the probability distributions for both the noise and the bias must be known. Also the second order properties – the covariances – of the noise and bias distributions must be

¹Usually obtained through sine-sweep tests.

known. However in the crucial paper [GGN92] it is demonstrated that if the covariances for the noise and the bias are parameterized the parameters themselves may be estimated from the available data set through maximum likelihood methods. Thus the characterization of the necessary prior knowledge becomes qualitatively rather than quantitatively.

For a thorough discussion of the different methods for assessing the model uncertainty refer to the excellent survey paper by Ninness & Goodwin [NG94].

We feel that the possibility of estimating the necessary prior knowledge from the available measurements makes the stochastic embedding approach advantageous to the hard bound approaches. Whereas the necessary prior knowledge of the true system is qualitatively similar for both the soft and the hard bound approaches, the stochastic embedding approach provides the possibility of estimating from data the quantitative part of the otherwise necessary prior knowledge. Furthermore the measurement noise may then be treated as a stochastic process which is most appropriate.

8.2 An Overview

The remainder of this part of the thesis is organized as follows. In Chapter 9, classical prediction error methods are reviewed for a general set of discrete-time linear models. This includes e.g. the classical approach to estimation of frequency domain model uncertainty. Next in Chapter 10, some special cases are considered, in particular fixed denominator models with basis functions which are orthogonal in \mathcal{H}_2 . Then in Chapter 11, following the path outlined by Goodwin and co-workers in [GGN92], we will show how the stochastic embedding approach may result in non-conservative transfer function error bounds.

8.3 Remarks

Our treatment will be limited to scalar systems. The classical estimation methods can be extended to multivariable systems without great difficulty, whereas the extension is not so straightforward for the stochastic embedding approach.

This year, De Vries and Van Den Hof [VH95] have published results on a *mixed soft and hard bound* approach to the estimation of model error bounds. Here periodic input signals are used to distinguish bias and variance contributions to the total model error. Their results show promise but time has not allowed any treatment of this new approach here.

Chapter 9

Classical System Identification

Contents

9.1	The Cramér-Rao Inequality for any Unbiased Estimator	141
9.2	Time Domain Asymptotic Variance Expressions . .	142
9.3	Frequency Domain Asymptotic Variance Expressions	146
9.4	Confidence Intervals for $\hat{\theta}_N$	148
9.5	Frequency Domain Uncertainty Bounds	149
9.6	A Numerical Example	150
9.6.1	Choosing the Model Structure	152
9.6.2	Estimation and Model Validation	155
9.6.3	Results	157
9.7	Summary	163

The purpose of this chapter is to provide an introduction to system identification using prediction error methods (PEM). For a general treatment of system identification refer to any good textbook on the subject, e.g. the two classic

books [Lju87, SS89]. Here we will treat only the PEM approach. Furthermore we shall concentrate on results which are relevant for our purpose, namely estimation of model uncertainty. Specifically, the asymptotic distribution of the parameter estimates will be investigated under different assumptions. The representation and notation generally follows [Lju87, Chap. 9].

The general black-box model structure

$$A(q)y(k) = \frac{B(q)}{F(q)}u(k) + \frac{C(q)}{D(q)}e(k) \quad (9.1)$$

will be assumed with

$$A(q) = 1 + a_1q^{-1} + a_2q^{-2} + \cdots + a_{n_a}q^{-n_a} \quad (9.2)$$

$$B(q) = b_1q^{-1} + b_2q^{-2} + \cdots + b_{n_b}q^{-n_b} \quad (9.3)$$

$$F(q) = 1 + f_1q^{-1} + f_2q^{-2} + \cdots + f_{n_f}q^{-n_f} \quad (9.4)$$

$$C(q) = 1 + c_1q^{-1} + c_2q^{-2} + \cdots + c_{n_c}q^{-n_c} \quad (9.5)$$

$$D(q) = 1 + d_1q^{-1} + d_2q^{-2} + \cdots + d_{n_d}q^{-n_d} \quad (9.6)$$

$e(k) \in \mathcal{N}(0, \lambda)$ denotes normal distributed zero mean noise with variance λ (white noise). q is the shift operator ($qu(k) = u(k+1)$). By $u(k)$ we mean the k 'th element of the sequence $\{u(k)\}$. Let e.g. $\{u(k)\}$ be a sequence obtained by sampling the continuous-time signal $u_c(t)$ with sampling time T_s . Then $\{u(k)\}$ is given by

$$\{u(k)\} = u_c(kT_s) \quad k = 1, 2, \dots, N \quad (9.7)$$

Frequently, we will not distinguish between the sequence $\{u(k)\}$ and the value $u(k)$ if the meaning is clear from the context. The optimal one-step-ahead predictor for (9.1) is given by

$$\hat{y}(k|\theta) = \frac{D(q)B(q)}{C(q)F(q)}u(k) + \frac{C(q) - D(q)A(q)}{C(q)}y(k) \quad (9.8)$$

where θ is the parameter vector:

$$\theta = [a_1, \dots, a_{n_a}, b_1, \dots, b_{n_b}, f_1, \dots, f_{n_f}, c_1, \dots, c_{n_c}, d_1, \dots, d_{n_d}]^T \quad (9.9)$$

A quadratic performance measure:

$$V_N(\theta, Z^N) = \frac{1}{N} \sum_{k=1}^N \frac{1}{2} \epsilon^2(k, \theta) \quad (9.10)$$

will be used for the PEM approach. Here $\epsilon(k, \theta) = y(k) - \hat{y}(k|\theta)$ denote the prediction errors and Z^N emphasize the measurement dependency. The parameter vector estimate $\hat{\theta}_N$ given N measurements is found as

$$\hat{\theta}_N = \arg \min_{\theta} V_N(\theta, Z^N) \quad (9.11)$$

In Appendix D on page 303 an easy implementable (in e.g. MATLAB) search algorithm for computing $\hat{\theta}_N$ is given. We then have

$$V'_N(\hat{\theta}_N, Z^N) = 0 \quad (9.12)$$

with prime denoting differentiation with respect to θ . Furthermore we have:

$$V'_N(\theta, Z^N) = -\frac{1}{N} \sum_{k=1}^N \frac{\partial \hat{y}(k|\theta)}{\partial \theta} (y(k) - \hat{y}(k|\theta)) \quad (9.13)$$

$$= -\frac{1}{N} \sum_{k=1}^N \psi(k, \theta) \epsilon(k, \theta) \quad (9.14)$$

$$V''_N(\theta, Z^N) = \frac{-1}{N} \sum_{k=1}^N \left\{ \frac{\partial^2 \hat{y}(k|\theta)}{\partial \theta^2} y(k) - \frac{\partial \hat{y}(k|\theta)}{\partial \theta} \frac{\partial \hat{y}(k|\theta)}{\partial \theta} - \frac{\partial^2 \hat{y}(k|\theta)}{\partial \theta^2} \hat{y}(k|\theta) \right\} \quad (9.15)$$

$$= \frac{1}{N} \sum_{k=1}^N \psi(k, \theta) \psi^T(k, \theta) - \frac{1}{N} \sum_{k=1}^N \frac{\partial \psi(k, \theta)}{\partial \theta} \epsilon(k, \theta) \quad (9.16)$$

Here $\psi(k, \theta) = \partial \hat{y}(k|\theta) / \partial \theta$ is denoted the *model gradient*.

9.1 The Cramér-Rao Inequality for any Unbiased Estimator

Suppose that the true system is given by:

$$y(k) = G_0(q, \theta_0)u(k) + H_0(q, \theta_0)e_0(k) \quad (9.17)$$

where $e_0(k) \in \mathcal{N}(0, \lambda_0)$. Then it is a well-known result that for *any unbiased estimate* $\hat{\theta}_N$ of θ_0 (i.e., estimators such that $E\{\hat{\theta}_N\} = \theta_0$ regardless of the true

value θ_0) the parameter covariance will obey the *Cramér-Rao Inequality*:

$$\text{Cov}(\sqrt{N}\hat{\theta}_N) = NE \left\{ \left(\hat{\theta}_N - E \left\{ \hat{\theta}_N \right\} \right) \left(\hat{\theta}_N - E \left\{ \hat{\theta}_N \right\} \right)^T \right\} \quad (9.18)$$

$$= NE \left\{ \left(\hat{\theta}_N - \theta_0 \right) \left(\hat{\theta}_N - \theta_0 \right)^T \right\} \quad (9.19)$$

$$\geq \lambda_0 \left[\frac{1}{N} \sum_{k=1}^N E \left\{ \psi(k, \theta_0) \psi^T(k, \theta_0) \right\} \right]^{-1} \quad (9.20)$$

Notice that this bound applies for any N and all parameter estimation methods! Unfortunately, (9.20) is not suitable for computation of $\text{Cov}(\hat{\theta}_N)$ since the true parameter θ_0 is unknown. In the next section we shall develop asymptotic expression for the parameter variance.

9.2 Time Domain Asymptotic Variance Expressions

Given the problem set-up described above it can be shown, see [Lju87, Lemma 8.2], that under weak conditions:

$$\sup_{\theta} |V_N(\theta, Z^N) - \bar{V}(\theta)| \rightarrow 0, \quad \text{for } N \rightarrow \infty \quad (9.21)$$

where

$$\bar{V}(\theta) = \bar{E} \left\{ \frac{1}{2} \epsilon^2(k, \theta) \right\} \quad (9.22)$$

and \bar{E} denotes “statistical expectation”:

$$\bar{E} \left\{ \frac{1}{2} \epsilon^2(k, \theta) \right\} = \lim_{N \rightarrow \infty} \frac{1}{N} \sum_{k=1}^N E \left\{ \frac{1}{2} \epsilon^2(k, \theta) \right\} \quad (9.23)$$

Thus the performance function $V_N(\theta, Z^N)$ converge to the limit function $\bar{V}(\theta)$. Furthermore the minimizing argument $\hat{\theta}_N$ of $V_N(\theta, Z^N)$ converges to the minimizing argument θ^* of $\bar{V}(\theta)$:

$$|\hat{\theta}_N - \theta^*| \rightarrow 0, \quad \text{for } N \rightarrow \infty \quad (9.24)$$

If $V'_N(\hat{\theta}_N, Z^N)$ (for given N) is a differentiable function, then the *mean value theorem* guarantees the existence of a value $\tilde{\theta}$ “between” $\hat{\theta}_N$ and θ^* such that

$$V'_N(\hat{\theta}_N, Z^N) = V'_N(\theta^*, Z^N) + V''_N(\tilde{\theta}, Z^N) (\hat{\theta}_N - \theta^*) = 0 \quad (9.25)$$

Under weak assumptions we then have [Lju87, pp 240]:

$$V_N''(\tilde{\theta}, Z^N) \rightarrow \bar{V}''(\theta^*), \quad \text{for } N \rightarrow \infty \quad (9.26)$$

Thus for $N \rightarrow \infty$ we have

$$V_N'(\theta^*, Z^N) + \bar{V}''(\theta^*) (\hat{\theta}_N - \theta^*) = 0 \quad (9.27)$$

$$\Leftrightarrow (\hat{\theta}_N - \theta^*) = -[\bar{V}''(\theta^*)]^{-1} V_N'(\theta^*, Z^N) \quad (9.28)$$

The second factor on the right-hand side is given by:

$$-V_N'(\theta^*, Z^N) = \frac{1}{N} \sum_{k=1}^N \psi(k, \theta^*) \epsilon(k, \theta^*) \quad (9.29)$$

For $N \rightarrow \infty$ this is a sum of random variables $\psi(k, \theta^*) \epsilon(k, \theta^*)$ with zero mean values. Assuming they had been independent we would have:

$$-\sqrt{N} V_N'(\theta^*, Z^N) = \frac{1}{\sqrt{N}} \sum_{k=1}^N \psi(k, \theta^*) \epsilon(k, \theta^*) \in \mathcal{N}(0, Q) \quad \text{for } N \rightarrow \infty \quad (9.30)$$

with:

$$Q = \lim_{N \rightarrow \infty} E \left\{ \left[\sqrt{N} V_N'(\theta^*, Z^N) \right] \left[\sqrt{N} V_N'(\theta^*, Z^N) \right]^T \right\} \quad (9.31)$$

$$= \lim_{N \rightarrow \infty} N \cdot E \left\{ \left[V_N'(\theta^*, Z^N) \right] \left[V_N'(\theta^*, Z^N) \right]^T \right\} \quad (9.32)$$

However, $\psi(k, \theta^*)$ and $\epsilon(k, \theta^*)$ are not independent but under weak assumptions the dependency between distant terms will decrease and (9.30) will hold approximately. If so we have from (9.28):

$$\sqrt{N} (\hat{\theta}_N - \theta^*) \in \mathcal{N}(0, P_\theta) \quad \text{for } N \rightarrow \infty \quad (9.33)$$

with

$$P_\theta = \lim_{N \rightarrow \infty} E \left\{ \sqrt{N} (\hat{\theta}_N - \theta^*) (\hat{\theta}_N - \theta^*)^T \sqrt{N} \right\} \quad (9.34)$$

$$= \lim_{N \rightarrow \infty} N E \left\{ \left[[\bar{V}''(\theta^*)]^{-1} V_N'(\theta^*, Z^N) \right] \left[[\bar{V}''(\theta^*)]^{-1} V_N'(\theta^*, Z^N) \right]^T \right\} \quad (9.35)$$

$$= \lim_{N \rightarrow \infty} N E \left\{ \left[\bar{V}''(\theta^*) \right]^{-1} \left[V_N'(\theta^*, Z^N) \right] \left[V_N'(\theta^*, Z^N) \right]^T \left[\bar{V}''(\theta^*) \right]^{-1} \right\} \quad (9.36)$$

$$= [\bar{V}''(\theta^*)]^{-1} \lim_{N \rightarrow \infty} N E \left\{ \left[V_N'(\theta^*, Z^N) \right] \left[V_N'(\theta^*, Z^N) \right]^T \right\} [\bar{V}''(\theta^*)]^{-1} \quad (9.37)$$

$$= [\bar{V}''(\theta^*)]^{-1} Q [\bar{V}''(\theta^*)]^{-1} \quad (9.38)$$

For a more rigorous justification of (9.33) and (9.38), see [Lju87, Appendix 9A], where it is shown that the above results hold under weak assumptions.

Let us take a closer look at the parameter estimate covariance matrix P_θ . It is easily seen that $\bar{V}''(\theta^*)$ is given by

$$\bar{V}''(\theta^*) = \lim_{N \rightarrow \infty} \frac{1}{N} \sum_{k=1}^N E \{ \psi(k, \theta^*) \psi^T(k, \theta^*) \} - \lim_{N \rightarrow \infty} \frac{1}{N} \sum_{k=1}^N E \left\{ \frac{\partial \psi(k, \theta^*)}{\partial \theta} \epsilon(k, \theta^*) \right\} \quad (9.39)$$

$$= \bar{E} \{ \psi(k, \theta^*) \psi^T(k, \theta^*) \} - \bar{E} \left\{ \frac{\partial \psi(k, \theta^*)}{\partial \theta} \epsilon(k, \theta^*) \right\} \quad (9.40)$$

Furthermore Q can be written as:

$$Q = \lim_{N \rightarrow \infty} N E \left\{ \left(\frac{1}{N} \sum_{k=1}^N \psi(k, \theta^*) \epsilon(k, \theta^*) \right) \left(\frac{1}{N} \sum_{\tau=1}^N \psi(\tau, \theta^*) \epsilon(\tau, \theta^*) \right)^T \right\} \quad (9.41)$$

$$= \lim_{N \rightarrow \infty} \frac{1}{N} E \left\{ \sum_{k=1}^N \psi(k, \theta^*) \epsilon(k, \theta^*) \sum_{\tau=1}^N \epsilon(\tau, \theta^*) \psi^T(\tau, \theta^*) \right\} \quad (9.42)$$

$$= \lim_{N \rightarrow \infty} \frac{1}{N} \sum_{k=1}^N \sum_{\tau=1}^N E \{ \psi(k, \theta^*) \epsilon(k, \theta^*) \epsilon(\tau, \theta^*) \psi^T(\tau, \theta^*) \}. \quad (9.43)$$

It is now tempting to believe that $\bar{V}''(\theta^*)$ and Q may be estimated from data simply by substitution of θ^* with $\hat{\theta}_N$. However, replacing θ^* with $\hat{\theta}_N$ in the expression for Q , see (9.32) on the preceding page, gives, trivially, $Q = 0$, which is a useless estimate. It is consequently difficult to estimate the covariance P_θ under the given weak assumptions.

The expressions for $\bar{V}''(\theta^*)$ and Q may however be significantly reduced in complexity by strengthening the assumptions. Specifically, assume that the model structure admits an exact description of the true system:

$$y(k) = G_0(q, \theta_0) u(k) + H_0(q, \theta_0) e_0(k) \quad (9.44)$$

where θ_0 is the true parameter value and $e_0(k) \in N(0, \lambda_0)$. Then under (otherwise) weak assumptions

$$\left| \hat{\theta}_N - \theta_0 \right| \rightarrow 0, \quad \text{for } N \rightarrow \infty \quad (9.45)$$

Furthermore it is easy to show that:

$$\epsilon(k, \theta_0) = y(k) - \hat{y}(k|\theta_0) \quad (9.46)$$

$$= y(k) - H^{-1}(q, \theta_0)G(q, \theta_0)u(k) - (1 - H^{-1}(q, \theta_0))y(k) \quad (9.47)$$

$$= H^{-1}(q, \theta_0)y(k) - H^{-1}(q, \theta_0)G(q, \theta_0)u(k) \quad (9.48)$$

$$= e_0(k) \quad (9.49)$$

Equation (9.49) may be used to simplify the expression for P_θ considerably. We now have:

$$\bar{V}''(\theta^*) = \bar{V}''(\theta_0) \quad (9.50)$$

$$= \bar{E} \{ \psi(k, \theta_0) \psi^T(k, \theta_0) \} - \bar{E} \left\{ \frac{\partial \psi(k, \theta_0)}{\partial \theta} \epsilon(k, \theta_0) \right\} \quad (9.51)$$

$$= \bar{E} \{ \psi(k, \theta_0) \psi^T(k, \theta_0) \} - \bar{E} \left\{ \frac{\partial \psi(k, \theta_0)}{\partial \theta} e_0(k) \right\} \quad (9.52)$$

$$= \bar{E} \{ \psi(k, \theta_0) \psi^T(k, \theta_0) \} \quad (9.53)$$

The last equality follows because $\partial \psi(k, \theta_0)/\partial \theta$ is formed from Z^{t-1} (past data) only and hence is uncorrelated with $e_0(k)$. Q is now given by:

$$Q = \lim_{N \rightarrow \infty} \frac{1}{N} \sum_{k=1}^N \sum_{\tau=1}^N E \{ \psi(k, \theta_0) \epsilon(k, \theta_0) \epsilon(\tau, \theta_0) \psi^T(\tau, \theta_0) \} \quad (9.54)$$

$$= \lim_{N \rightarrow \infty} \frac{1}{N} \sum_{k=1}^N \sum_{\tau=1}^N E \{ \psi(k, \theta_0) e_0(k) e_0(\tau) \psi^T(\tau, \theta_0) \} \quad (9.55)$$

$$= \lim_{N \rightarrow \infty} \frac{1}{N} \sum_{k=1}^N \lambda_0 E \{ \psi(k, \theta_0) \psi^T(k, \theta_0) \} \quad (9.56)$$

$$= \lambda_0 \bar{E} \{ \psi(k, \theta_0) \psi^T(k, \theta_0) \} \quad (9.57)$$

since $e_0(k)$ is white noise with variance λ_0 . The expression for P_θ then reduces to:

$$P_\theta = \lambda_0 [\bar{E} \{ \psi(k, \theta_0) \psi^T(k, \theta_0) \}]^{-1} \quad (9.58)$$

$$= \lambda_0 \left[\lim_{N \rightarrow \infty} \frac{1}{N} \sum_{k=1}^N E \{ \psi(k, \theta_0) \psi^T(k, \theta_0) \} \right]^{-1} \quad (9.59)$$

Now notice that the asymptotic covariance matrix P_θ equals the limit (as $N \rightarrow \infty$) of the Cramér-Rao bound in (9.20) on page 142. Consequently, in this sense

the prediction-error estimate has the best possible asymptotic properties one can hope for.

Another very important aspect of the expression for P_θ in (9.59) on the preceding page is that it can be estimated from data. Having processed N data points and computed $\hat{\theta}_N$ a consistent¹ estimate of P_θ is given by:

$$\hat{P}_N = \hat{\lambda}_N \left[\frac{1}{N} \sum_{k=1}^N \psi(k, \hat{\theta}_N) \psi^T(k, \hat{\theta}_N) \right]^{-1} \quad (9.60)$$

$$\hat{\lambda}_N = \frac{1}{N} \sum_{k=1}^N \epsilon^2(k, \hat{\theta}_N) \quad (9.61)$$

The estimates (9.60) and (9.61) are the classical result on the covariance of the parameter estimate. Notice that the covariance $\text{Cov}(\hat{\theta}_N)$ is given by:

$$\text{Cov}(\hat{\theta}_N) = \frac{1}{N} P_\theta \quad (9.62)$$

9.3 Frequency Domain Asymptotic Variance Expressions

Frequency domain expression for the covariance matrix P_θ in (9.59) on the preceding page may also be derived. To ease notation introduce the following definitions:

$$T(q, \theta) \triangleq \begin{bmatrix} G(q, \theta) & H(q, \theta) \end{bmatrix} \quad (9.63)$$

$$\chi(k) \triangleq \begin{bmatrix} u(k) & \epsilon(k) \end{bmatrix}^T \quad (9.64)$$

$$W_u(q, \theta) \triangleq H^{-1}(q, \theta) G(q, \theta) \quad (9.65)$$

$$W_y(q, \theta) \triangleq 1 - H^{-1}(q, \theta) \quad (9.66)$$

$$W(q, \theta) \triangleq \begin{bmatrix} W_u(q, \theta) & W_y(q, \theta) \end{bmatrix} \quad (9.67)$$

$$z(k) \triangleq \begin{bmatrix} u(k) & y(k) \end{bmatrix}^T \quad (9.68)$$

$$\Psi(q, \theta) \triangleq \frac{\partial W(q, \theta)}{\partial \theta} \quad (9.69)$$

The above notation corresponds to the one used in [Lju87]. Now the general model structure may be written

$$y(k) = G(q, \theta)u(k) + H(q, \theta)\epsilon(k) \quad (9.70)$$

$$= T(q, \theta)\chi(k) \quad (9.71)$$

¹A consistent estimate is an estimate that converges to the true value for $N \rightarrow \infty$.

Provided $H(q, \theta)$ is minimum phase, the optimal predictor for (9.71) on the facing page is

$$\hat{y}(k|\theta) = H^{-1}(q, \theta)G(q, \theta)u(k) + (1 - H^{-1}(q, \theta))y(k) \quad (9.72)$$

which may be written

$$\hat{y}(k|\theta) = W_u(q, \theta)u(k) + W_y(q, \theta)y(k) = W(q, \theta)z(k) \quad (9.73)$$

Furthermore, the model gradient $\psi(k, \theta)$ becomes

$$\psi(k, \theta) = \frac{\partial \hat{y}(k|\theta)}{\partial \theta} = \frac{\partial W(q, \theta)}{\partial \theta}z(k) = \Psi(q, \theta)z(k) \quad (9.74)$$

We may now derive an expression for $\Psi(q, \theta)$:

$$\Psi(q, \theta) = \frac{\partial}{\partial \theta} \begin{bmatrix} W_u(q, \theta) & W_y(q, \theta) \end{bmatrix} \quad (9.75)$$

$$= \begin{bmatrix} \frac{\partial}{\partial \theta} (H^{-1}(q, \theta)G(q, \theta)) & \frac{\partial}{\partial \theta} (1 - H^{-1}(q, \theta)) \end{bmatrix} \quad (9.76)$$

$$= \begin{bmatrix} \frac{\frac{\partial G(q, \theta)}{\partial \theta}H(q, \theta) - \frac{\partial H(q, \theta)}{\partial \theta}G(q, \theta)}{(H(q, \theta))^2} & \frac{\frac{\partial H(q, \theta)}{\partial \theta}}{(H(q, \theta))^2} \end{bmatrix} \quad (9.77)$$

$$= \frac{1}{(H(q, \theta))^2} \begin{bmatrix} \frac{\partial G(q, \theta)}{\partial \theta} & \frac{\partial H(q, \theta)}{\partial \theta} \end{bmatrix} \begin{bmatrix} H(q, \theta) & 0 \\ -G(q, \theta) & 1 \end{bmatrix} \quad (9.78)$$

$$= \frac{1}{H(q, \theta)} \frac{\partial T(q, \theta)}{\partial \theta} \begin{bmatrix} 1 & 0 \\ -H^{-1}(q, \theta)G(q, \theta) & H^{-1}(q, \theta) \end{bmatrix} \quad (9.79)$$

The model gradient hence becomes:

$$\psi(k, \theta) = \frac{1}{H(q, \theta)} \frac{\partial T(q, \theta)}{\partial \theta} \begin{bmatrix} 1 & 0 \\ -H^{-1}(q, \theta)G(q, \theta) & H^{-1}(q, \theta) \end{bmatrix} \begin{bmatrix} u(k) \\ y(k) \end{bmatrix} \quad (9.80)$$

$$= \frac{1}{H(q, \theta)} \frac{\partial T(q, \theta)}{\partial \theta} \begin{bmatrix} u(k) & -H^{-1}(q, \theta)G(q, \theta)u(k) + H^{-1}(q, \theta)y(k) \end{bmatrix}^T \quad (9.81)$$

$$= \frac{1}{H(q, \theta)} \frac{\partial T(q, \theta)}{\partial \theta} \begin{bmatrix} u(k) \\ \epsilon(k, \theta) \end{bmatrix} \quad (9.82)$$

The last equality follows since

$$\epsilon(k, \theta) = y(k) - \hat{y}(k|\theta) \quad (9.83)$$

$$= y(k) - H^{-1}(q, \theta)G(q, \theta)u(k) - (1 - H^{-1}(q, \theta))y(k) \quad (9.84)$$

$$= -H^{-1}(q, \theta)G(q, \theta)u(k) + H^{-1}(q, \theta)y(k) \quad (9.85)$$

If the true system can be represented within the model set, we have $\epsilon(k, \theta_0) = e_0(k)$ and:

$$\psi(k, \theta_0) = \frac{1}{H(q, \theta_0)} \frac{\partial T(q, \theta_0)}{\partial \theta} \begin{bmatrix} u(k) \\ e_0(k) \end{bmatrix} = \frac{1}{H(q, \theta_0)} \frac{\partial T(q, \theta_0)}{\partial \theta} \chi_0(k) \quad (9.86)$$

where $\chi_0(k) = [u(k) \ e_0(k)]^T$. Using Parseval's relation and Equation (9.59) on page 145 we obtain:

$$P_\theta = \lambda_0 [\bar{E} \{ \psi(k, \theta_0) \psi^T(k, \theta_0) \}]^{-1} \quad (9.87)$$

$$= \lambda_0 \left[\lim_{N \rightarrow \infty} \frac{1}{N} \sum_{k=1}^N E \{ \psi(k, \theta_0) \psi^T(k, \theta_0) \} \right]^{-1} \quad (9.88)$$

$$= \lambda_0 \left[\frac{1}{2\pi} \int_{-\pi}^{\pi} |H(e^{j\omega T_s}, \theta_0)|^{-2} \frac{\partial T(e^{j\omega T_s}, \theta_0)}{\partial \theta} \Phi_{\chi_0} \frac{\partial T^T(e^{j\omega T_s}, \theta_0)}{\partial \theta} d\omega \right]^{-1} \quad (9.89)$$

$$= \left[\frac{1}{2\pi} \int_{-\pi}^{\pi} \frac{1}{\Phi_\nu(\omega)} \frac{\partial T(e^{j\omega T_s}, \theta_0)}{\partial \theta} \Phi_{\chi_0}(\omega) \frac{\partial T^T(e^{j\omega T_s}, \theta_0)}{\partial \theta} d\omega \right]^{-1} \quad (9.90)$$

since

$$\Phi_\nu(\omega) = \lambda_0 |H(e^{j\omega T_s}, \theta_0)|^{-2} \quad (9.91)$$

$\Phi_{\chi_0}(\omega)$ is the spectrum of $\chi_0(k)$:

$$\Phi_{\chi_0}(\omega) = \begin{bmatrix} \Phi_u(\omega) & \Phi_{ue}(\omega) \\ \Phi_{eu}(\omega) & \lambda_0 \end{bmatrix} \quad (9.92)$$

$\Phi_{ue}(\omega) = \Phi_{eu}(\omega)$ is the cross-spectrum between the input $u(k)$ and the innovations $e_0(k)$. When the system operates in open loop the cross-spectrum is zero and $\Phi_{\chi_0}(\omega)$ becomes a 2-by-2 diagonal matrix. Clearly approximate expressions for P_θ may be obtained from data by substituting θ_0 with $\hat{\theta}_N$ in (9.90).

9.4 Confidence Intervals for $\hat{\theta}_N$

If a random vector η has a Gaussian distribution:

$$\eta \in \mathcal{N}(0, P) \quad (9.93)$$

it is well-known that the scalar:

$$z = \eta^T P^{-1} \eta \quad (9.94)$$

has a χ^2 distribution with $\dim(\eta) = d$ degrees of freedom:

$$z \in \chi^2(d) \quad (9.95)$$

Thus from (9.33) on page 143 we draw the conclusion that the scalar

$$\eta_N = N \cdot \left(\hat{\theta}_N - \theta_0 \right)^T P_{\theta}^{-1} \left(\hat{\theta}_N - \theta_0 \right) \quad (9.96)$$

converges to a χ^2 distribution with $\dim \theta = n$ degrees of freedom as $N \rightarrow \infty$. Equation (9.96) may be used to “draw” n -dimensional confidence ellipsoids for $\hat{\theta}_N$.

9.5 Frequency Domain Uncertainty Bounds

Previously we have concentrated on parameter covariance. However in connection with control design frequency domain expression for the uncertainty is usually required. Hence we need to translate the estimated parameter covariance \hat{P}_N into bounds on the frequency response of the estimated model $G(q, \theta_N)$. However we will face the difficulty that the estimated frequency response $G(e^{j\omega T_s}, \hat{\theta}_N)$ generally will be non-linear in $\hat{\theta}_N$. Instead we may approximate $G(e^{j\omega T_s}, \theta^*)$ with a Taylor series expansion around $\theta = \hat{\theta}_N$:

$$G(e^{j\omega T_s}, \theta^*) \approx G(e^{j\omega T_s}, \hat{\theta}_N) + \frac{\partial G(e^{j\omega T_s}, \hat{\theta}_N)}{\partial \theta} (\theta^* - \hat{\theta}_N) \quad (9.97)$$

Now define:

$$\tilde{g}(e^{j\omega T_s}) \triangleq \begin{bmatrix} \Re \left\{ G(e^{j\omega T_s}, \theta^*) - G(e^{j\omega T_s}, \hat{\theta}_N) \right\} \\ \Im \left\{ G(e^{j\omega T_s}, \theta^*) - G(e^{j\omega T_s}, \hat{\theta}_N) \right\} \end{bmatrix} \quad (9.98)$$

$$\Gamma(e^{j\omega T_s}) \triangleq \begin{bmatrix} \Re \left\{ \frac{\partial G(e^{j\omega T_s}, \hat{\theta}_N)}{\partial \theta} \right\} & \Im \left\{ \frac{\partial G(e^{j\omega T_s}, \hat{\theta}_N)}{\partial \theta} \right\} \end{bmatrix}^T \quad (9.99)$$

so that

$$\tilde{g}(e^{j\omega T_s}) \approx \Gamma(e^{j\omega T_s}) (\theta^* - \hat{\theta}_N) \quad (9.100)$$

Now $\sqrt{N}\tilde{g}(e^{j\omega T_s})$ will have asymptotic normal distribution for $N \rightarrow \infty$ with covariance $P_g(\omega)$:

$$\sqrt{N}\tilde{g}(e^{j\omega T_s}) \in \mathcal{N}(0, P_g(\omega)), \quad \text{for } N \rightarrow \infty \quad (9.101)$$

where the covariance matrix $P_g(\omega)$ is given by

$$P_g(\omega) = \lim_{N \rightarrow \infty} E \left\{ \sqrt{N} \tilde{g}(e^{j\omega T_s}) \tilde{g}^T(e^{j\omega T_s}) \sqrt{N} \right\} \quad (9.102)$$

$$= \lim_{N \rightarrow \infty} E \left\{ \Gamma(e^{j\omega T_s}) \sqrt{N} (\theta^* - \hat{\theta}_N) (\theta^* - \hat{\theta}_N)^T \sqrt{N} \Gamma^T(e^{j\omega T_s}) \right\} \quad (9.103)$$

$$= \Gamma(e^{j\omega T_s}) P_\theta \Gamma^T(e^{j\omega T_s}) \quad (9.104)$$

Using arguments similar to Section 9.4 on page 148 the scalar

$$z(\omega) = N \tilde{g}^T(e^{j\omega T_s}) P_g^{-1}(\omega) \tilde{g}(e^{j\omega T_s}) \quad (9.105)$$

$$= \tilde{g}^T(e^{j\omega T_s}) \left[\Gamma(e^{j\omega T_s}) \frac{1}{N} P_\theta \Gamma^T(e^{j\omega T_s}) \right]^{-1} \tilde{g}(e^{j\omega T_s}) \quad (9.106)$$

will have χ^2 distribution with $\dim \tilde{g}(e^{j\omega T_s}) = 2$ degrees of freedom. Equation (9.106) may then be used to draw confidence ellipses in the complex plane for the frequency response estimate $G(e^{j\omega T_s}, \hat{\theta}_N)$.

Completely analogue, confidence ellipses may be computed for the frequency response estimate $H(e^{j\omega T_s}, \hat{\theta}_N)$.

9.6 A Numerical Example

To illustrate the classical approach to system identification and estimation of frequency domain error bounds we will give a practical example. We will consider identification of a discrete-time model for a wind turbine. The model should be suitable for subsequent controller synthesis.

The wind turbine considered is a 400 kW, variable pitch, but constant speed machine. The control system consists of 3 independent controllers:

- A speed controller which during start-up procedure synchronize the angular velocity of the generator shaft with the grid frequency 50 Hz before the generator is connected to the grid. This controller is used only during start-up of the wind turbine.
- A pitch servo loop which controls the hydraulic pitch actuators. The purpose is to make the pitch follow a given pitch reference from either the speed controller above or the power controller below.
- A power controller which becomes active after the generator has been connected to the grid. The operation of the power controller is twofold. If

wind speed is less than rated, the control output (pitch reference) will simply follow some pre-specified “optimal” curve empirically determined from wind-tunnel experiments. If wind speed exceeds rated value, the power controller shall maintain 400 kW output.

Usually the power controller for wind speeds above rated value is the most difficult part of the control system design. It seems reasonable that modern robust control design methods here should be superior to classical designs. We will thus assume that the control problem at hand is one of maintaining rated power output (400 kW) (attenuating wind speed fluctuations) by varying the pitch of the turbine blades. Thus a nominal model and an uncertainty estimate will be required in rated operation mode, that is for average wind speeds above rated value (approximately 10 m/s). For this purpose 14,400 samples were collected with sampling frequency 8 Hz. The input signal was a fundamental square wave with period 40 secs applied as pitch reference. 45 periods were thus collected. As outlined above the control system includes also a pitch servo mechanism. During the experiment it was equipped with a non-linear proportional controller. However, the intention is not to include the pitch servo into the model of the turbine itself. Thus the actual pitch ϑ [deg] was also recorded and used as input for the identification procedure. The first period of the pitch ϑ is shown in Figure 9.1 on the following page together with measured power output P [100kW] and wind speed v [m/sec] measured at the top of the nacelle. Note how the actual pitch is not purely square due to the pitch servo loop. Furthermore it is clear that the wind speed fluctuations introduce considerable noise on the power output. It is tempting, since a wind speed measurement is available, to include this measurement as an additional input to the estimated model. Unfortunately, because the wind speed measurement is taken at the top of the nacelle, it will be affected by changes in the pitch angle. Also, every time a blade passes the tower disturbances in the wind field around the turbine will be introduced. This will further distort the wind measurement. It is therefore most common to treat the wind speed as a non-measurable disturbance when designing controllers for wind turbines. Thus we will consider it in the same manner for our identification experiment.

	Pitch ϑ [deg]	Power P [100kW]	Wind speed v [m/sec]
Working point	11	346	14.2

Table 9.1: *Working point values for the signals displayed in Figure 9.1 on the following page.*

We have subtracted mean values from the signals in Figure 9.1 on the next page. The means are given in Table 9.1. Note that the working point for the power

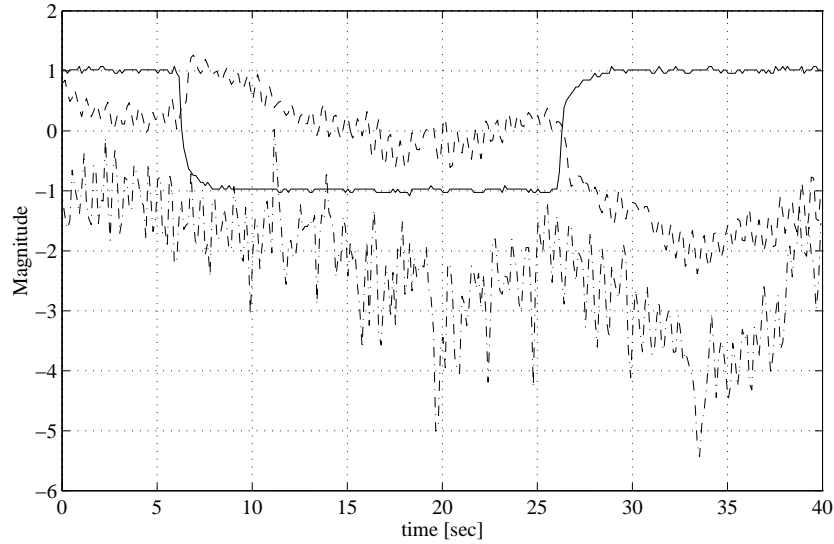


Figure 9.1: *First period of the signals used for identification of the wind turbine. Shown are small signal values for pitch [deg] (solid), power [100kW] (dashed) and wind speed [m/sec] (dash-dotted, off-set 2 m/sec).*

output is slightly below nominal value. However, during an open loop experiment it will be very difficult to maintain an average power output of 400 kW without considerable risk of overloading the generator. Closed loop experiments could have been considered instead. However, this has not been treated in this work.

9.6.1 Choosing the Model Structure

As discussed in Chapter 8 choosing a set of candidate models for the identification procedure is by no means a trivial task. Much engineering ingenuity is often necessary to make this choice and some iterations with different model structures is almost always necessary to obtain useful results. The detailed physics for the wind turbine are very complicated, see e.g. [Lei89]. However, a useful model for control need not be so involved. In Figure 9.2 a block diagram representation of the main components in a dynamic model of the wind turbine is shown.

The wind flow around the turbine blades results in an axial force F_t which bends the tower and a force in the rotational direction which creates the driving torque M on the main shaft. The torque is then transmitted to the generator via

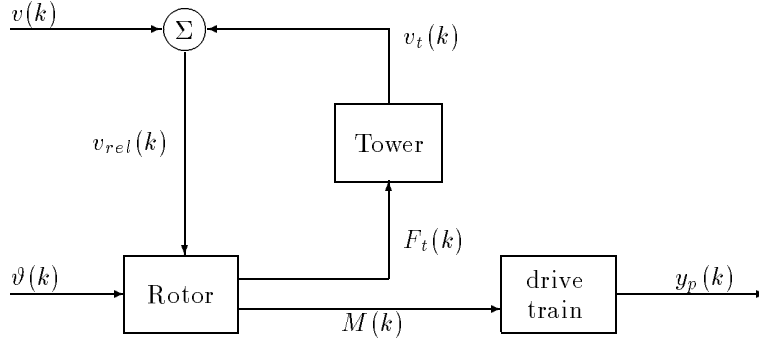


Figure 9.2: *Simple model of a pitch controlled wind turbine.*

the drive train. A reasonable physical model of the drive train (including the generator) is two rotating masses, one on each side of the gearbox, connected with a spring and damped; the generator also acting like a damper. The three necessary states to describe this system is the velocity of the two masses and the difference of their angle.

The tower can also be modeled with a spring and damper. This will require two additional states (position and velocity of the hub). Furthermore, recent results indicate that dynamical effects in the wind flow around the blades also exists. The explanation is that when the pitch changes, the wind distribution around the turbine will also change creating a new wind “tail”. A first order system with time constant from 1–5 secs is a reasonable approximation for single turbines. However, if the turbine is placed in connection with several other turbines, then for certain wind directions the time constant could be much larger.

Furthermore notice how not only the power output but also the tower motion is affected when controlling the pitch. Tower movements then affect the relative wind speed v_{rel} . Thus we have closed loops in the system.

The spectrum for the power output will generally have two high frequency peaks. The first peak is located at the rotational frequency of the rotor. This frequency is usually denoted 1P. A non-symmetric rotor with e.g. one blade having a slightly different pitch than the others cause this peak. The second peak, which is normally more significant, occurs at the 3P frequency and is caused by the three blades passing through the inhomogeneous wind field around the tower. A possible model for the 3P (1P) effect could be white noise filtered through a second order system with a sharp resonance.

Finally the dynamics of the wind speed are also important. These dynamics are very complex. Low-pass filtered white noise can be used to model wind speed variations around the 10 mins average wind speed. However, both dominating frequencies and variance grow with increasing wind speeds. Consequently, if the wind speed is fully described by filtered white noise we will expect the necessary order to be quite large.

Since the wind speed affects the driving torque and thus passes through the same dynamics as the pitch angle a reasonable discrete-time linear model structure for the wind turbine, neglecting the 1P effect, could be

$$y_p(k) = G_t(q) (G_f(q)\vartheta(k) + k_v v(k)) + d(k) \quad (9.107)$$

where y_p , ϑ , v and d denote power output, pitch angle, wind speed and 3P disturbance respectively. $G_t(q)$ is a transfer function describing the drive train and $G_f(q)$ describes the pitch rotor dynamics. A possible model for the wind speed could be filtered white noise

$$v(k) = G_w(q)e_v(k) \quad e_v(k) \in \mathcal{N}(0, \lambda_v) \quad (9.108)$$

Similarly filtered white noise could be used for $d(k)$:

$$d(k) = G_d(q)e_d(k) \quad e_d(k) \in \mathcal{N}(0, \lambda_d) \quad (9.109)$$

Let $G_x(q)$ be given by

$$G_x(q) = \frac{N_x(q)}{D_x(q)} \quad (9.110)$$

with

$$N_x(q) = n_1 q^{-1} + n_2 q^{-2} + \dots + n_{n_x} q^{-n_x} \quad (9.111)$$

$$D_x(q) = 1 + d_1 q^{-1} + d_2 q^{-2} + \dots + d_{d_x} q^{-d_x} \quad (9.112)$$

Then $y_p(k)$ can be written

$$y_p(k) = G_t(q)G_f(q)\vartheta(k) + k_v G_t(q)G_v(q)e_v(k) + G_d(q)e_d(k) \quad (9.113)$$

$$= \frac{N_t(q)N_f(q)}{D_t(q)D_f(q)}\vartheta(k) + k_v \frac{N_t(q)}{D_t(q)} \frac{N_v(q)}{D_v(q)}e_v(k) + \frac{N_d(q)}{D_d(q)}e_d(k) \quad (9.114)$$

$$= \frac{N_t(q)N_f(q)}{D_t(q)D_f(q)}\vartheta(k) + \frac{k_v N_t(q)N_v(q)D_d(q)e_v(k) + N_d(q)D_t(q)D_v(q)e_d(k)}{D_t(q)D_v(q)D_d(q)} \quad (9.115)$$

Note that since we have two white noise sources, the general PEM model (9.1) on page 140 does not include (9.115). However, the nominator in the last term

of (9.115) can be modeled by a moving average (MA) process with a single noise source. Then the wind turbine model fits the PEM structure with

$$A(q) = D_t(q) \quad (9.116)$$

$$B(q) = N_t(q)N_f(q) \quad (9.117)$$

$$F(q) = D_f(q) \quad (9.118)$$

$$D(q) = D_v(q)D_d(q) \quad (9.119)$$

and $C(q)$ some polynomial modeling the single noise source MA process.

Neglecting the tower dynamics, the degrees for each polynomial were chosen as follows

$$\deg(A) = 3 \quad (9.120)$$

$$\deg(B) = 2 \quad (9.121)$$

$$\deg(F) = 1 \quad (9.122)$$

$$\deg(C) = \deg(D) = k \quad (9.123)$$

where k is some positive natural number. The identification procedure was then repeated for increasing values of k until the residuals were close to white noise.

9.6.2 Estimation and Model Validation

A Marquardt's search procedure as outlined in Appendix D on page 303 was implemented in MATLAB in order to find the least squares estimate of the parameter vector θ . 320 samples were used to get rid of initial conditions effects. The data set was split into two parts, each consisting of 7200 samples. The identification procedure was then used on the first data set and the other set was used for model validation. Model validation was performed by analysis of the residuals. The standard two residual tests were performed:

- Are the residuals white noise?
- Are the residuals and past inputs independent?

The typical whiteness test is to determine the covariance estimate

$$\hat{R}_N^\epsilon(\kappa) = \frac{1}{N} \sum_{k=1}^{N-\kappa} \epsilon(k, \hat{\theta}_N) \epsilon(k + \kappa, \hat{\theta}_N) \quad (9.124)$$

If $\{\epsilon(k, \hat{\theta}_N)\}$ indeed is a white noise sequence with variance λ then for $\kappa \ll N$ $\hat{R}_N^\epsilon(\kappa)$ will be approximately normal distributed with zero mean and variance

$\lambda^2 N^{-1}$ (as usual N denotes the number of measurements):

$$E \left\{ \hat{R}_N^\epsilon(\kappa) \right\} = 0 \quad , \kappa \geq 1 \quad (9.125)$$

$$E \left\{ \hat{R}_N^\epsilon(\kappa) \hat{R}_N^\epsilon(\kappa) \right\} = \lambda^2 N^{-1} \quad (9.126)$$

Since $\hat{R}_N^\epsilon(0)$ is an estimate of λ we may reject the hypothesis that the prediction errors are white noise on an α level if

$$\frac{\hat{R}_N^\epsilon(\kappa)}{\hat{R}_N^\epsilon(0)} > \frac{\alpha}{\sqrt{N}} \quad (9.127)$$

For example, if $\alpha = 2.58$ we obtain 99% confidence levels. We may thus plot $\hat{R}_N^\epsilon(\kappa)/\hat{R}_N^\epsilon(0)$ for $0 < \kappa \ll N$ and if the maximum numerical value exceeds $2.58/\sqrt{N}$ for any value of κ the white noise hypothesis must be rejected.

Note that white residuals will require both the deterministic part $G(q, \theta)$ and the stochastic part $H(q, \theta)$ to be an adequate description of the true system. If we are mainly interested in the deterministic system $G_T(q)$ the question is whether the residuals $\epsilon(k, \hat{\theta}_N)$ are independent of the inputs. If not, there is more in the output that originates from the input than explained by the current model $G(q, \hat{\theta}_N)$. Independence between inputs and residuals is usually tested using the cross-covariance estimate:

$$\hat{R}_N^{\epsilon, u}(\kappa) = \frac{1}{N} \sum_{k=\kappa}^N \epsilon(k) u(k - \kappa) \quad (9.128)$$

If $\{\epsilon(k, \hat{\theta}_N)\}$ and $\{u(k)\}$ are independent then $\sqrt{N} \hat{R}_N^{\epsilon, u}(\kappa)$ will be asymptotically normal distributed with zero mean and variance P [Lju87, pp 429]:

$$\sqrt{N} \hat{R}_N^{\epsilon, u}(\kappa) \in \mathcal{N}(0, P) \quad \text{for } N \rightarrow \infty \quad (9.129)$$

with P given by

$$P = \sum_{\kappa=-\infty}^{\infty} R^\epsilon(\kappa) R^u(\kappa) \quad (9.130)$$

and

$$R^\epsilon(\kappa) = \lim_{N \rightarrow \infty} \frac{1}{N} \sum_{k=1}^N \epsilon(\kappa, \hat{\theta}_N) \epsilon(\kappa - k, \hat{\theta}_N) \quad (9.131)$$

$$R^u(\kappa) = \lim_{N \rightarrow \infty} \frac{1}{N} \sum_{k=1}^N u(\kappa) u(\kappa - k) \quad (9.132)$$

Using a data estimate \hat{P}_N for the covariance we may reject the hypothesis that the inputs and prediction errors are independent on an α level if

$$\left| \hat{R}_N^{\epsilon, u}(\kappa) \right| > \alpha \sqrt{\frac{\hat{P}_N}{N}} \quad (9.133)$$

Residual tests should always be performed on a separate test set different from the data set used for the identification procedure.

9.6.3 Results

As described above the degree of the C and D polynomials was increased until the residual tests were both passed. The required number of states for the noise filter was 18. Thus 42 parameters were estimated. Despite the high number of parameters the identification algorithm converged without difficulty. Using numerical search algorithms only convergence to local minima can be obtained. For large number of parameters it can be very difficult to judge whether a given local minima is in fact the global minima. Experiments with different initial values indicated however that the obtained minimum was global.

The corresponding residual tests are shown in Figure 9.3 on the next page. Here 99% confidence levels has been used. The pole-zero configuration for the deterministic and stochastic part of the system is shown in Figure 9.4 on the following page and the Bode plots are given in Figure 9.5 on page 159.

The deterministic part $G(q, \hat{\theta}_N)$ has one pair of complex poles with relative damping 0.3 and natural frequency 1.1 Hz (6.91 rad/s). This corresponds well to values obtained from the turbine manufacturer *Vestas Wind Systems A/S* for a second order approximation to the drive train. We then have an additional pole in -0.15 from $A(q)$ and the pole 0.18 from $F(q)$. The latter corresponds to a time constant of 0.07 secs. This is much faster than reported results on the rotor dynamics. We then have two zeros at $z = 0$ since $n_{n_a} + n_{n_f} - n_{n_b} = 2$ trailing zeros must be added in the nominator of $G(q, \hat{\theta}_N)$ in order to comply with the MATLAB *Control Toolbox* format. Finally we have a zero outside the unit circle at approximately -2. It is then customary to term the system non-minimum phase. However, the interpretation of non-minimum phase zeros for discrete-time systems is not straightforward. The step-response of $G(q, \hat{\theta}_N)$ does not show traditional minimum-phase behavior, see Figure 9.6 on page 159.

Notice how the poles and zeros for the stochastic part $H(q, \hat{\theta}_N)$ mostly comes in pole-zero pairs. Traveling up the unit circle from the point (1,0), the first three pole-zero pairs are very lightly damped. The effects of these pole-zero pairs can be seen in the Bode plot for $H(q, \hat{\theta}_N)$ as sharp resonances; one placed at the 3P frequency and one at the 1P frequency. Furthermore there is a resonance at

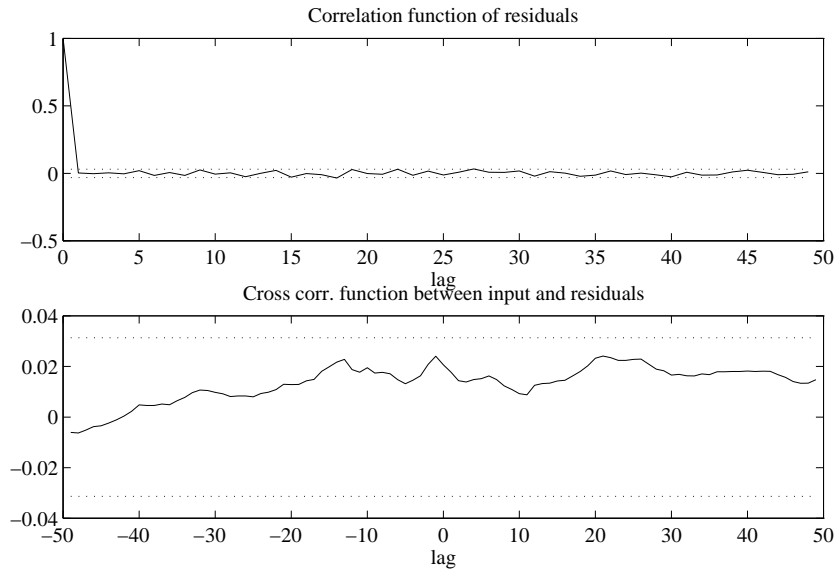


Figure 9.3: *Residual tests for the wind turbine identification. 99% confidence limits are indicated in each plot.*

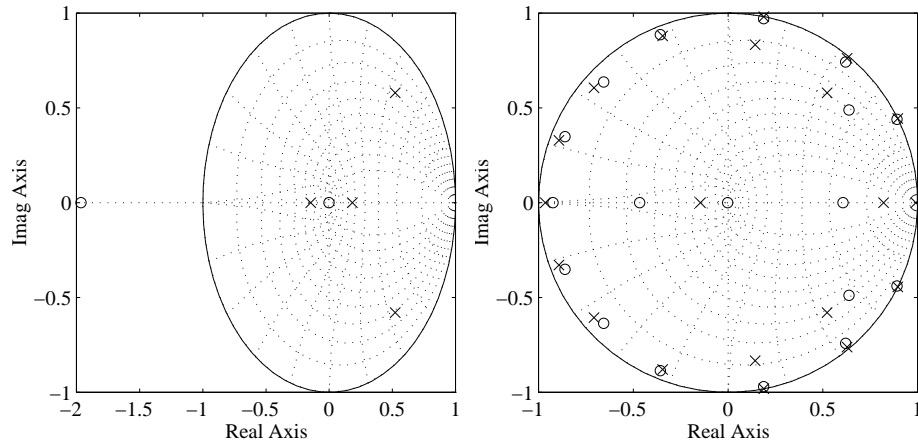


Figure 9.4: *Pole-zero configuration for the deterministic part $G(q, \hat{\theta}_N)$ (left) and stochastic part $H(q, \hat{\theta}_N)$ (right).*

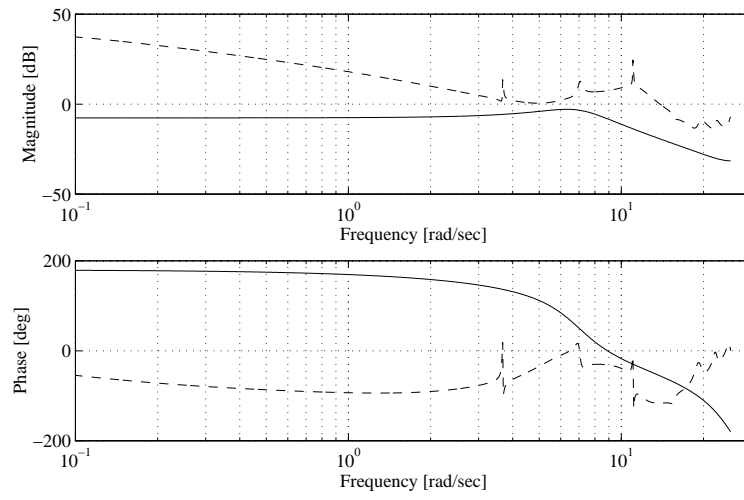


Figure 9.5: *Bode plot for the deterministic (solid) and stochastic (dashed) part of the estimated wind turbine model.*

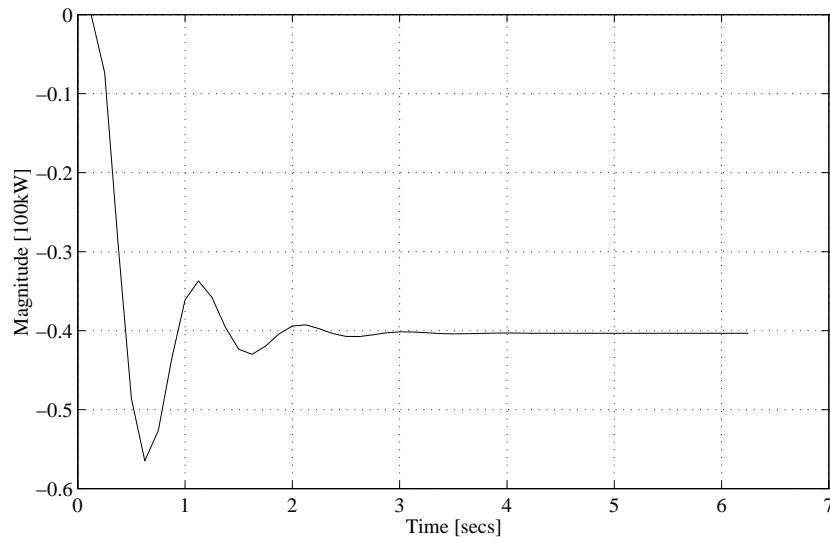


Figure 9.6: *Step response of deterministic part of estimated wind turbine model.*

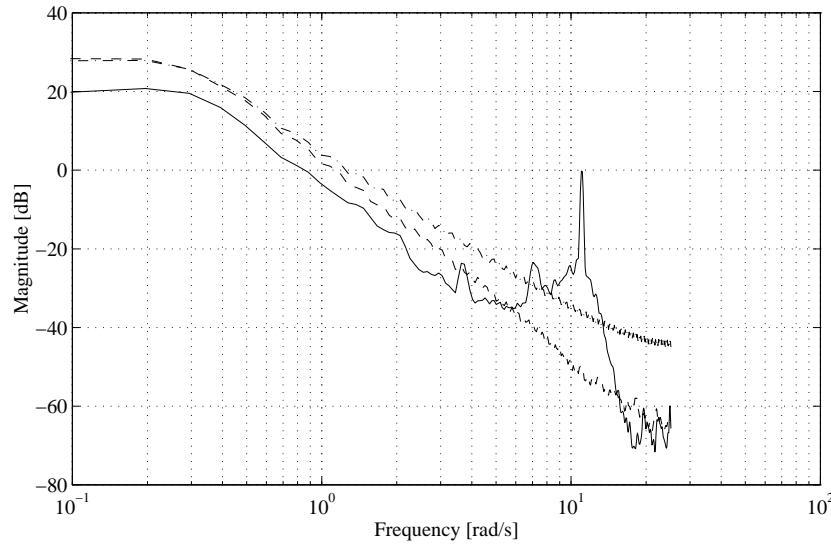


Figure 9.7: *Estimated power spectrum for the pitch input signal (dashed), a pure square wave with the same amplitude and frequency (dash-dotted) and the power output (solid).*

approximately 7 rad/sec corresponding to the second pole-zero pair encountered traveling up the unit circle. This probably stems from the tower resonance which has been included in the noise model. The tower resonance clearly belongs in the $A(q)$ polynomial since it is struck both by the pitch input and the wind speed. Several identification experiments have been conducted with additional parameters in $A(q)$ and $B(q)$. However, it has not been possible to represent the tower resonance in the deterministic part of the model. An explanation of this can be given from the estimated power spectra of both input and output, see Figure 9.7. Note that the spectrum of the pitch input signal in the frequency range where the tower resonance is located has decayed with more than 60 dB compared with the DC value. Thus in our model the output power P in this frequency range must be almost completely characterized by white noise filtered through $C(q)/(D(q)A(q))$. However, then it is not possible to distinguish between high frequency poles in $A(q)$ and $D(q)$. For some reason the resonant poles for the tower is placed in $D(q)$ together with the 1P and 3P dynamics whereas the complex poles for the drive train is placed in $A(q)$.

In other words the frequency content in the input signal (pitch angle) is too small

in the high frequency range. The main problem is that the pitch servo loop is much too slow so that the square wave input in fact is filtered through a low pass filter with small cut-off frequency, see Figure 9.7 on the facing page. However even a pure square wave input with period 40 secs will have little relative energy around 10 rad/sec as shown in Figure 9.7 on the facing page. In order to avoid this problem the pitch servo loop must be retuned and preferably another pitch input signal applied with more energy in the high frequency area.

In Figure 9.7 on the facing page note the resonant peak for the 1P, tower and 3P dynamics can be easily identified in the output power spectrum. Compare with the Bode plot in Figure 9.5 on page 159. Also notice that the drive train complex pole pair are located at almost exactly the same frequency as the tower resonance. If they were included in the same filter it would be very difficult for the identification procedure to distinguish between them. It will furthermore be very difficult for the controller to compensate for both. Finally note that the noise filter also contains a pole at approximately 0.99 corresponding to a time constant of 13.5 secs. This pole is probably due to the rather slow rotor dynamics. The time constant is somewhat larger than usually reported in the literature, but is probably due to neighboring wind turbines. Again the corresponding pole actually belongs in $F(q)$ or $A(q)$ rather than the noise filter denominator $D(q)$. However, the phenomena could be described by filtered white noise which is probably the case here due to the high number of parameters in $D(q)$.

The frequency domain model uncertainty was estimated using the approach outlined in Section 9.5 on page 149. In Figure 9.8 on the next page the nominal Nyquist for the deterministic part $G(q, \theta_N)$ is shown with superimposed 2 standard deviation (95.5%) uncertainty ellipses. These uncertainty ellipses may then be used in a robust control design. In standard \mathcal{H}_∞ control, only frequency domain uncertainty circles can be represented. Thus an \mathcal{H}_∞ design approach could be taken by approximating the ellipses by circumscribed circles. This will provide a set of additive uncertainty circles at each frequency ω . Fitting the radii of these circles with a stable transfer function $G_A(z)$ will provide the uncertain system description

$$\tilde{G}(z) = G(z, \hat{\theta}_N) + G_A(z) = G(z, \hat{\theta}_N) \left(1 + \frac{G_A(z)}{G(z, \hat{\theta}_N)} \right) \quad (9.134)$$

Given the results in Table 4.1 on page 47 a controller will robustly stabilize the plant iff

$$|T(e^{j\omega T_s})| < \left| \frac{G_A(e^{j\omega T_s})}{G(e^{j\omega T_s}, \hat{\theta}_N)} \right| \quad (9.135)$$

where $T(z)$ denotes the closed loop transfer function as usual. Thus by plotting $G_A(e^{j\omega T_s})/G(e^{j\omega T_s}, \hat{\theta}_N)$ against frequency ω we may obtain an upper bound on

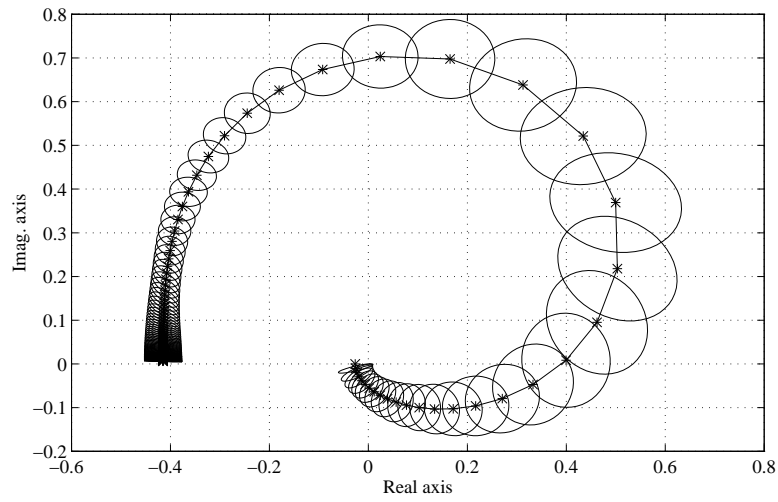


Figure 9.8: *Nominal Nyquist curve with 2 standard deviations uncertainty ellipses.*

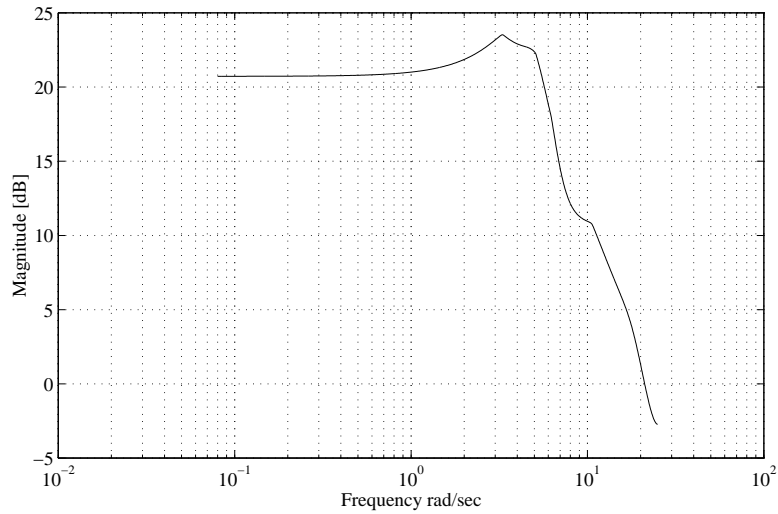


Figure 9.9: *Robustness bound on the complementary sensitivity. (closed loop transfer function).*

the achievable closed loop bandwidth. This is done in Figure 9.9. The maximum bandwidth is approximately 20 rad/sec which is quite close to the Nyquist frequency $\omega_n = \pi/T_s = 25$ rad/sec. Thus a fast control design should be possible with the derived model.

However, because the tower resonance was not included into the deterministic part of the system, the high frequency uncertainty estimates will probably be misleading even though the residual tests were passed. Since the true system will have a resonance in the high frequency area, if the pitch input ϑ has large energy in this area the resonance will be struck from the input. This will surely deteriorate the performance properties in the high frequency area and may even result in instability.

The above example illustrates that care must be taken in connection with high order noise models since some of the deterministic behavior of the true system may in fact be explained by filtered white noise.

9.7 Summary

Classical system identification using the prediction error method (PEM) was reviewed for a general class of black-box models. In particular we considered asymptotic expressions for the parameter variance and showed how these parameter uncertainties can be translated to frequency domain uncertainty ellipses. For the general model structure we must use a first order Taylor approximation since the model is not linear in the parameter vector θ . Unfortunately we may only obtain consistent data estimates of the parameter covariance in the case where the model admits an exact description of the true system. This severely hampers the usefulness of the classical approach in connection with robust control design. Finally a numerical example was presented, namely identification of a model for a 400 kW constant speed, variable pitch wind turbine from a set of input/output measurements. The input applied was a 0.025 Hz fundamental square wave. The model structure was chosen from physical considerations. The order of the deterministic part was fixed and the order of the noise filter was then increased until the prediction errors for a separate test-set became white. The result was a third order model for the deterministic part and a 18th order model for the noise filter. Frequency domain uncertainty ellipses were then estimated for the deterministic part. However, it was argued that some of the truly deterministic dynamics were in fact explained by filtered white noise and thus included in the noise filter. The main reason for this was inadequate excitation in the high frequency area. This caused the frequency domain uncertainty estimate for the deterministic part to be overly optimistic in the high frequency area.

Chapter 10

Orthonormal Filters in System Identification

Contents

10.1 ARX Models	166
10.1.1 Variance of ARX Parameter Estimate	167
10.2 Output Error Models	169
10.2.1 Variance of OE Parameter Estimate	170
10.3 Fixed Denominator Models	171
10.3.1 Variance of Fixed Denominator Parameter Estimate	172
10.3.2 FIR Models	174
10.3.3 Laguerre Models	176
10.3.4 Kautz Models	179
10.4 Combined Laguerre and Kautz Structures	181
10.5 Summary	181

In this chapter we will provide an introduction to the use of orthonormal basis functions in system identification. First let us, however, consider some special cases of the general model structure (9.1) introduced in the previous chapter.

Throughout this chapter we assume that the true system is finite-dimensional, linear and time-invariant (FDLTI) and given by

$$y(k) = G_T(q)u(k) + H_T(q)e_0(k) \quad (10.1)$$

where $e_0(k) \in \mathcal{N}(0, \lambda_0)$ is white noise.

10.1 ARX Models

A very popular set of models is the autoregressive structure with exogenous input, abbreviated ARX models. The ARX model structure can be derived as follows. Assume that our model set is given by

$$y(k) = G(q, \theta)u(k) + H(q, \theta)e(k) \quad (10.2)$$

where $e(k)$ is white noise with variance λ . If the noise filter $H(q, \theta)$ is minimum phase the optimal predictor for $y(k)$ is

$$\hat{y}(k|\theta) = H^{-1}(q, \theta)G(q, \theta)u(k) + (1 - H^{-1}(q, \theta))y(k) \quad (10.3)$$

Then if $H^{-1}(q, \theta)G(q, \theta)$ and $H^{-1}(q, \theta)$ are both stable¹ we may write:

$$H^{-1}(q, \theta)G(q, \theta) = \sum_{k=1}^{\infty} b_k q^{-k} \quad (10.4)$$

$$H^{-1}(q, \theta) - 1 = \sum_{k=1}^{\infty} a_k q^{-k} \quad (10.5)$$

Truncating these expansions at $k = n$ we may rewrite (10.2) as

$$\left(1 + \sum_{k=1}^{n_a} a_k q^{-k}\right) y(k) = \sum_{k=1}^{n_b} b_k q^{-k} u(k) + e(k) \quad (10.6)$$

$$\Leftrightarrow A(q)y(k) = B(q)u(k) + e(k) \quad (10.7)$$

with $A(q)$ and $B(q)$ as in (9.2) and (9.3) on page 140. This is the ARX model structure. For $n_a = 0$ a finite impulse response (FIR) model is derived and for $n_b = 0$ we obtain an autoregressive (AR) model structure. For the ARX model, the optimal predictor (10.3) becomes

$$\hat{y}(k|\theta) = (1 - A(q))y(k) + B(q)u(k) \quad (10.8)$$

¹This is assured, of course, if $H(q, \theta)$ is minimum-phase and if $H(q, \theta)$ and $G(q, \theta)$ have the same unstable poles.

Thus, if we take

$$\theta = [a_1, \dots, a_{n_a}, b_1, \dots, b_{n_b}]^T \quad (10.9)$$

and

$$\phi(k) = [-y(k-1), \dots, -y(k-n_a), u(k-1), \dots, u(k-n_b)]^T \quad (10.10)$$

we may write

$$\hat{y}(k|\theta) = \phi^T(k)\theta. \quad (10.11)$$

The predictor for the ARX model structure is consequently linear in θ . The prediction errors $\epsilon(k, \theta)$ are given by

$$\epsilon(k, \theta) = y(k) - (1 - A(q))y(k) - B(q)u(k) \quad (10.12)$$

$$= [A(q)G_T(q) - B(q)] u(k) + A(q)H_T(q)e(k) \quad (10.13)$$

In Appendix D on page 303 it is shown that the parameter estimate

$$\hat{\theta}_N = \arg \min_{\theta} V_N(\theta, Z^N). \quad (10.14)$$

with $V_N(\theta, Z^N)$ as in (9.10) on page 140 is given by the analytic expression

$$\hat{\theta}_N = \left[\sum_{k=1}^N \phi(k)\phi^T(k) \right]^{-1} \sum_{k=1}^N \phi(k)y(k) \quad (10.15)$$

If we define

$$Y \triangleq [y(1), y(2), \dots, y(N)]^T \quad (10.16)$$

$$\Phi \triangleq [\phi^T(1), \phi^T(2), \dots, \phi^T(N)]^T \quad (10.17)$$

it is easily shown that an equivalent expression for (10.15) is

$$\hat{\theta}_N = (\Phi^T \Phi)^{-1} \Phi^T Y \quad (10.18)$$

10.1.1 Variance of ARX Parameter Estimate

Let us then investigate the quality of the estimate. Under weak assumptions we then have from (9.33) on page 143 that:

$$\sqrt{N}(\hat{\theta}_N - \theta^*) \in \mathcal{N}(0, P_\theta) \quad \text{for } N \rightarrow \infty \quad (10.19)$$

where θ^* is defined by

$$\theta^* \triangleq \arg \min_{\theta} \left\{ \lim_{N \rightarrow \infty} \frac{1}{N} \sum_{k=1}^N E \left\{ \frac{1}{2} \epsilon^2(t, \theta) \right\} \right\} \quad (10.20)$$

The covariance matrix P_{θ} is given by (9.38) on page 143:

$$P_{\theta} = [\bar{V}''(\theta^*)]^{-1} Q [\bar{V}''(\theta^*)]^{-1} \quad (10.21)$$

with $\bar{V}''(\theta^*)$ and Q as in (9.40) and (9.43) respectively. For the ARX structure, the model gradient $\psi(k, \theta)$ is given by

$$\psi(k, \theta) = \frac{\partial \hat{y}(k|\theta)}{\partial \theta} = \phi(k) \quad (10.22)$$

Thus $\partial \psi(k, \theta) / \partial \theta = 0$ and the expressions for $\bar{V}''(\theta^*)$ and Q reduce to

$$\bar{V}''(\theta^*) = \lim_{N \rightarrow \infty} \frac{1}{N} \sum_{k=1}^N E \{ \phi(k) \phi^T(k) \} \quad (10.23)$$

$$Q = \lim_{N \rightarrow \infty} \frac{1}{N} \sum_{k=1}^N \sum_{l=1}^N E \{ \phi(k) \phi^T(l) \epsilon(k, \theta^*) \epsilon(l, \theta^*) \} \quad (10.24)$$

where the prediction errors are given by (10.13) on the preceding page. The expression for the parameter covariance P_{θ} is, however, still quite complicated. The data estimates (9.60) and (9.61) on page 146 will *not* be a consistent estimate, that is converge for $N \rightarrow \infty$, unless in the special case where $G_T(q) = G(q, \theta_0)$ and $H_T(q) = H(q, \theta_0)$ (the true system can be represented within the model set). In this case $\theta^* = \theta_0$, $\epsilon(k, \theta^*) = \epsilon_0(k)$ and the expression for P_{θ} reduce to

$$P_{\theta} = \lambda_0 \left[\lim_{N \rightarrow \infty} \frac{1}{N} \sum_{k=1}^N E \{ \phi(k) \phi^T(k) \} \right] \quad (10.25)$$

Thus we need to require that both the deterministic and stochastic part of the true system can be exactly modeled by the ARX structure in order for the data estimate

$$\hat{P}_N = \hat{\lambda}_N \left[\frac{1}{N} \sum_{k=1}^N \phi(k) \phi^T(k) \right]^{-1} \quad (10.26)$$

$$\hat{\lambda}_N = \frac{1}{N} \sum_{k=1}^N \epsilon^2(k, \hat{\theta}_N) \quad (10.27)$$

to be a consistent estimate of the parameter covariance matrix P_θ . A well-known related problem with ARX models is that even if the true system $G_T(q)$ can be described by $G(q, \theta_0)$ then if the true noise filter $H_T(q)$ cannot be represented by $H(q, \theta) = A(q)$, the parameter estimate $\hat{\theta}_N$ will *not* converge to the true value θ_0 for $N \rightarrow \infty$ because $G(q, \theta)$ and $H(q, \theta)$ are not *independently* parameterized.

10.2 Output Error Models

The output error (OE) model structure is given by

$$y(k) = G(q, \theta)u(k) + e(k) = \frac{B(q)}{F(q)}u(k) + e(k) \quad (10.28)$$

with $B(q)$ and $F(q)$ defined by (9.3) and (9.4) on page 140. The optimal predictor for the OE model structure is given by

$$\hat{y}(k|\theta) = H^{-1}(q, \theta)G(q, \theta)u(k) + (1 - H^{-1}(q, \theta))y(k) \quad (10.29)$$

$$= G(q, \theta)u(k) \quad (10.30)$$

Note that the OE predictor is *not* linear in θ . This means that we have no analytic expression for the parameter estimate $\hat{\theta}_N$ but must resort to numerical methods to determine $\hat{\theta}_N$ as in the general PEM case. The model gradient $\psi(k, \theta)$ for the OE model structure is given by

$$\psi(k, \theta) = \frac{\partial G(q, \theta)}{\partial \theta}u(k) \quad (10.31)$$

Thus $\psi(k, \theta)$ is a deterministic sequence; a crucial property we will utilize in computing the parameter covariance P_θ . The prediction errors $\epsilon(k, \theta)$ are given by

$$\epsilon(k, \theta) = y(k) - \hat{y}(k|\theta) \quad (10.32)$$

$$= (G_T(q) - G(q, \theta))u(k) + H_T(q)e_0(k) \quad (10.33)$$

We will then consider the case where $G_T(q) = G(q, \theta_0)$, that is, $G_T(q)$ is a member of the model set $G(q, \theta)$. We will, however, *not* assume that the true noise filter $H_T(q)$ is given by $H(q, \theta) = 1$. Since $G(q, \theta)$ and $H(q, \theta)$ are independently parameterized, then according to [Lju87, Theorem 8.4]:

$$\theta^* = \arg \min_{\theta} \left\{ \lim_{N \rightarrow \infty} \frac{1}{N} \sum_{k=1}^N E \left\{ \frac{1}{2} \epsilon^2(t, \theta) \right\} \right\} = \theta_0 \quad (10.34)$$

and the prediction errors becomes

$$\epsilon(k, \theta^*) = H_T(q)e_0(k) \quad (10.35)$$

10.2.1 Variance of OE Parameter Estimate

Now the the parameter covariance is given by

$$P_\theta = \lim_{N \rightarrow \infty} \frac{1}{N} E \left\{ \left(\hat{\theta}_N - \theta_0 \right) \left(\hat{\theta}_N - \theta_0 \right)^T \right\} \quad (10.36)$$

$$= [\bar{V}''(\theta_0)]^{-1} Q [\bar{V}''(\theta_0)]^{-1} \quad (10.37)$$

$\bar{V}''(\theta_0)$ is given by

$$\begin{aligned} \bar{V}''(\theta_0) &= \lim_{N \rightarrow \infty} \frac{1}{N} \sum_{k=1}^N E \left\{ \psi(k, \theta_0) \psi^T(k, \theta_0) \right\} - \\ &\quad \lim_{N \rightarrow \infty} \frac{1}{N} \sum_{k=1}^N E \left\{ \frac{\partial \psi(k, \theta_0)}{\partial \theta} H_T(q) e_0(k) \right\} \end{aligned} \quad (10.38)$$

$$= \lim_{N \rightarrow \infty} \frac{1}{N} \sum_{k=1}^N \psi(k, \theta_0) \psi^T(k, \theta_0) - 0 \quad (10.39)$$

$$= \lim_{N \rightarrow \infty} \frac{1}{N} \Psi^T(\theta_0, Z^N) \Psi(\theta_0, Z^N) \quad (10.40)$$

since $\psi(k, \theta)$ is deterministic. $\Psi(\theta, Z^N)$ is given by

$$\Psi(\theta, Z^N) = [\psi(1, \theta), \psi(2, \theta), \dots, \psi(N, \theta)]^T \quad (10.41)$$

Q is given by

$$Q = \lim_{N \rightarrow \infty} \frac{1}{N} \sum_{k=1}^N \sum_{h=1}^N E \left\{ \psi(k, \theta_0) \psi^T(h, \theta_0) \epsilon(k, \theta_0) \epsilon(h, \theta_0) \right\} \quad (10.42)$$

$$= \lim_{N \rightarrow \infty} \frac{1}{N} \sum_{k=1}^N \sum_{h=1}^N \psi(k, \theta_0) \psi^T(h, \theta_0) E \left\{ H_T(q) e_0(k) \cdot H_T(q) e_0(h) \right\} \quad (10.43)$$

$$= \lim_{N \rightarrow \infty} \frac{1}{N} \Psi^T(\theta_0, Z^N) C_\nu \Psi(\theta_0, Z^N) \quad (10.44)$$

where C_ν is given by

$$C_\nu = E \left\{ V V^T \right\}, \quad V = [\nu(1), \nu(2), \dots, \nu(N)] \quad (10.45)$$

with $\nu(k) = H_T(q) e_0(k)$. Thus the parameter covariance P_θ is given by

$$P_\theta = \lim_{N \rightarrow \infty} N \left(\Psi_o^T \Psi_o \right)^{-1} \Psi_o^T C_\nu \Psi_o \left(\Psi_o^T \Psi_o \right)^{-1} \quad (10.46)$$

with $\Psi_o = \Psi(\theta_o, Z^N)$. Then

$$\hat{P}_N = N (\Psi_N^T \Psi_N)^{-1} \Psi_N^T C_\nu \Psi_N (\Psi_N^T \Psi_N)^{-1} \quad (10.47)$$

with $\Psi_N = \Psi(\hat{\theta}_N, Z^N)$ will be a consistent estimate of the covariance P_θ . Notice that this is true even if the true noise filter $H_T(q)$ cannot be captured within the model set $H(q, \theta) = 1$. Thus we can obtain a consistent estimate of the parameter covariance provided the true system $G_T(q)$ can be described by our model set $G(q, \theta)$. This is an important property for OE models. Of course, in order to evaluate (10.47) the covariance matrix for the true noise $\nu(k)$ must be known. However, provided $G(q, \theta_0) = G_T(q)$ we have that $\epsilon(k, \theta_0) = \nu(k)$, see (10.35) on page 169. If we assume that $\nu(k)$ is a stationary stochastic process such that

$$E \{ \nu(k) \nu(h) \} = E \{ \nu(m) \nu(n) \} \quad \text{for } k - h = m - n \quad (10.48)$$

C_ν will be constant along the diagonal and all off-diagonals as well. Furthermore, we may estimate these diagonals from the prediction errors by averaging over all $\nu(i) \nu(j)$ for which $i - j = M$ with M constant. $M = 0$ then corresponds to the main diagonal, $M = 1$ to the first off-diagonal etc. The covariance estimate $R_N^\epsilon(\kappa)$ in (9.124) on page 155 used for model validation in Section 9.6.2 on page 155 is precisely what we need. Note, of course that C_ν is symmetric.

We may then replace C_ν by its estimate in (10.47) to obtain an estimate of the parameter covariance.

10.3 Fixed Denominator Models

Now we consider models which are linear in θ (fixed denominator models):

$$G(q, \theta) = \Lambda(q) \theta \quad (10.49)$$

with

$$\Lambda(q) = [\Lambda_1(q), \dots, \Lambda_n(q)] \quad (10.50)$$

$$\theta = [\theta_1, \dots, \theta_n]^T \quad (10.51)$$

$\Lambda_i(q)$ is known as the basis functions for $G(q, \theta)$. The optimal predictor in this case is

$$\hat{y}(k|\theta) = \Lambda(q) \theta u(k) = \phi(k) \theta \quad (10.52)$$

Clearly

$$\phi(k) = \Lambda(q) u(k) \quad (10.53)$$

is a deterministic sequence. Thus for fixed denominator models, the predictor is linear in θ and the regressor $\phi(k)$ is deterministic. With Y and Φ as before, see (10.16) and (10.17) on page 167, the least squares estimate of θ is given by

$$\hat{\theta}_N = (\Phi^T \Phi)^{-1} \Phi^T Y \quad (10.54)$$

The output vector Y may be written

$$Y = \begin{bmatrix} y(1) \\ \vdots \\ y(N) \end{bmatrix} = \begin{bmatrix} G_T(q)u(1) \\ \vdots \\ G_T(q)u(N) \end{bmatrix} + \begin{bmatrix} H_T(q)e_0(1) \\ \vdots \\ H_T(q)e_0(N) \end{bmatrix} \quad (10.55)$$

$$= G_T(q) \begin{bmatrix} u(1) \\ \vdots \\ u(N) \end{bmatrix} + \begin{bmatrix} \nu(1) \\ \vdots \\ \nu(N) \end{bmatrix} \quad (10.56)$$

$$= G_T(q)U + V \quad (10.57)$$

Thus

$$\hat{\theta}_N = (\Phi^T \Phi)^{-1} \Phi^T (G_T(q)U + V) \quad (10.58)$$

10.3.1 Variance of Fixed Denominator Parameter Estimate

Since Φ and $G_T(q)U$ are deterministic we may easily compute the expectation of $\hat{\theta}_N$:

$$E \{ \hat{\theta}_N \} = \theta^* = (\Phi^T \Phi)^{-1} \Phi^T G_T(q)U \quad (10.59)$$

Then

$$\tilde{\theta}_N = \hat{\theta}_N - \theta^* = (\Phi^T \Phi)^{-1} \Phi^T V \quad (10.60)$$

which gives us the covariance matrix for the parameter estimate

$$P_\theta = NE \{ \tilde{\theta}_N \tilde{\theta}_N^T \} = N (\Phi^T \Phi)^{-1} \Phi^T C_\nu \Phi (\Phi^T \Phi)^{-1} \quad (10.61)$$

where $C_\nu = E \{ VV^T \}$. Note that (10.61) is *not* an asymptotic expression like (10.46) on page 170. Thus the data estimate will be equal to the true covariance matrix for finite data. Furthermore this holds *regardless of the form of the true system* $G_T(q)$. That is, for fixed denominator models, a finite-data unbiased estimate of the parameter variance can be obtained *even in the case of undermodeling*. Then of course the parameter θ^* will not reflect the “true”

properties of $G_T(q)$. Thus when our main objective is to estimate the total model error, it is of little use that we can estimate P_θ . This will only provide the “variance” part of the total model error, see Section 13.1.1 on page 227.

If $G_T(q)$ can be represented within the model set ($G_T(q) = \Lambda(q)\theta_0$) then $\theta^* \rightarrow \theta_0$ for $N \rightarrow \infty$ and we may use (10.61) to map the parametric uncertainty into the frequency domain. Here we furthermore have the advantage that $G(q, \theta)$ is linear in θ so we need not to resort to Taylor approximations. Let

$$\tilde{g}(e^{j\omega T_s}) \triangleq \begin{bmatrix} \Re \left\{ G(e^{j\omega T_s}, \theta_0) - G(e^{j\omega T_s}, \hat{\theta}_N) \right\} \\ \Im \left\{ G(e^{j\omega T_s}, \theta_0) - G(e^{j\omega T_s}, \hat{\theta}_N) \right\} \end{bmatrix} \quad (10.62)$$

$$\Gamma(e^{j\omega T_s}) \triangleq \begin{bmatrix} \Re \left\{ \Lambda(e^{j\omega T_s}) \right\} & \Im \left\{ \Lambda(e^{j\omega T_s}) \right\} \end{bmatrix}^T \quad (10.63)$$

so that

$$\tilde{g}(e^{j\omega T_s}) = \Gamma(e^{j\omega T_s})(\theta_0 - \hat{\theta}_N). \quad (10.64)$$

Now $\sqrt{N}\tilde{g}(e^{j\omega T_s})$ will have asymptotic normal distribution for $N \rightarrow \infty$ with covariance $P_g(\omega)$:

$$\sqrt{N}\tilde{g}(e^{j\omega T_s}) \in \mathcal{N}(0, P_g(\omega)), \quad \text{for } N \rightarrow \infty \quad (10.65)$$

where the covariance matrix $P_g(\omega)$ is given by

$$P_g(\omega) = \lim_{N \rightarrow \infty} E \left\{ \sqrt{N}\tilde{g}(e^{j\omega T_s}) \tilde{g}^T(e^{j\omega T_s}) \sqrt{N} \right\} \quad (10.66)$$

$$= \lim_{N \rightarrow \infty} E \left\{ \Gamma(e^{j\omega T_s}) \sqrt{N}(\theta_0 - \hat{\theta}_N)(\theta_0 - \hat{\theta}_N)^T \sqrt{N} \Gamma^T(e^{j\omega T_s}) \right\} \quad (10.67)$$

$$= \Gamma(e^{j\omega T_s}) P_\theta \Gamma^T(e^{j\omega T_s}). \quad (10.68)$$

Thus the scalar

$$z(\omega) = N \tilde{g}^T(e^{j\omega T_s}) P_g^{-1}(\omega) \tilde{g}(e^{j\omega T_s}) \quad (10.69)$$

$$= \tilde{g}^T(e^{j\omega T_s}) \left[\Gamma(e^{j\omega T_s}) \frac{1}{N} P_\theta \Gamma^T(e^{j\omega T_s}) \right]^{-1} \tilde{g}(e^{j\omega T_s}) \quad (10.70)$$

will have χ^2 distribution with 2 degrees of freedom. Equation (10.70) may then be used to draw confidence ellipsis in the complex plane for the frequency response estimate $G(e^{j\omega T_s}, \hat{\theta}_N)$.

10.3.2 FIR Models

The most well-known fixed denominator model structure is probably the Finite Impulse Response (FIR) model:

$$G(q, \theta) = \sum_{k=1}^n g_k q^{-k} \quad (10.71)$$

The basis functions for the FIR model is q^{-k} , $k = 1, \dots, n$. Let $\mathcal{H}_2^*(\mathbf{C}, \mathbf{C})$ denote the Hilbert space of scalar functions $G(z)$ which are analytical in $|z| > 1$ (no unstable poles) and continuous in $|z| \geq 1$ (strictly proper). The scalar product on $\mathcal{H}_2^*(\mathbf{C}, \mathbf{C})$ is given as

$$\langle G, F \rangle = \frac{1}{2\pi j} \int_{-\pi}^{\pi} G^*(e^{-j\omega}) F(e^{-j\omega}) d\omega \quad (10.72)$$

$$= \frac{1}{2\pi j} \oint_{|z|=1} G^*(z) F(z) \frac{dz}{z} \quad (10.73)$$

where $G^*(z) = G(z^{-1})$. $\mathcal{H}_2^*(\mathbf{C}, \mathbf{C})$ is the space of all real rational stable strictly proper scalar discrete-time transfer functions and is the discrete-time counterpart of $\mathcal{H}_2(\mathbf{C}, \mathbf{C})$ introduced in Section 3.3.2 on page 27.

Before we proceed, let us review the concept of orthonormal basis.

Lemma 10.1 (Orthonormal Basis) *Let H be a Hilbert space. Then the set of elements $M = \{e_\alpha : \alpha \in A\}$ from H is called an orthonormal system if*

$$\langle e_\alpha, e_\beta \rangle = \delta_{\alpha\beta} \quad \text{for } \alpha, \beta \in A \quad (10.74)$$

where $\delta_{\alpha\beta}$ denotes the Kronecker delta, i.e. $\delta_{\alpha\alpha} = 1$, $\forall \alpha \in A$ and $\delta_{\alpha\beta} = 0$ for $\alpha \neq \beta$. An orthonormal system M is called an orthonormal basis of H if M is total in H which means that the smallest subspace of H that contains M is dense.

Example 10.1 (Orthonormal Basis) *The set of unit vectors $\{e_1, \dots, e_n\}$ is an orthonormal basis in \mathbf{R}^n . e_j is the vector with 1 at the j th place and zero otherwise.*

An important property of orthonormal basis functions is that if M is an orthonormal basis in H , then every element of H may be given as a linear combination of M .

It is now easy to show that the basis functions $\Lambda_k = e^{-j\omega T_s k}$ are orthonormal in

$\mathcal{H}_2^*(\mathbf{C}, \mathbf{C}^n);$

$$\langle \Lambda_k, \Lambda_l \rangle = \frac{1}{2\pi j} \int_{-\pi}^{\pi} e^{j\omega T_s k} e^{-j\omega T_s l} d\omega \quad (10.75)$$

$$= \frac{1}{2\pi j} \int_{-\pi}^{\pi} e^{j\omega T_s (k-l)} d\omega \quad (10.76)$$

$$= \delta_{kl} \quad (10.77)$$

Since $e^{-j\omega T_s k}$, $k = 1, 2, \dots$ form an orthonormal basis for functions in $\mathcal{H}_2^*(\mathbf{C}, \mathbf{C})$, then for $G(z) \in \mathcal{H}_2^*(\mathbf{C}, \mathbf{C})$ there exists a sequence such that

$$G(e^{j\omega T_s}) = \sum_{k=1}^{\infty} g_k e^{j\omega T_s k} \quad (10.78)$$

or equivalent

$$G(z) = \sum_{k=1}^{\infty} g_k z^{-k} \quad (10.79)$$

(10.79) is the well known relation between $G(z)$ and its impulse response g_k .

The orthonormality properties of the basis functions $\Lambda_k(q)$ ensure that the corresponding asymptotic covariance matrix for the regression vector $\phi(k)$:

$$R = \lim_{N \rightarrow \infty} \frac{1}{N} \sum_{k=1}^N \phi(k, \theta) \phi^T(k, \theta) \quad (10.80)$$

$$= \lim_{N \rightarrow \infty} \frac{1}{N} \Phi^T \Phi \quad (10.81)$$

has a certain (Toeplitz) structure, see [Wah94], which can be shown to improve the numerics in the least squares estimate of θ .

The above properties for FIR models are all quite well-known. It is probably less well-known that the FIR model structure is in some sense an optimal fixed denominator model structure *if the only a priori information we have about the system is that it is exponentially stable*. To see this we must introduce the so-called *n-width* of a set of transfer functions. The following definition is taken from [Wah94]:

Definition 10.1 (n-Width Measures) *Assume that we know that the transfer function $G(z)$ belongs to an a priori given bounded set $G(z) \in \mathcal{S}$. The n-width then measures the smallest approximation error for the worst possible system $G(z) \in \mathcal{S}$ using the best possible n-dimensional fixed denominator model set:*

$$d_n(\mathcal{S}; \mathcal{B}) = \inf_{\Phi_n \in M_n(\mathcal{B})} \sup_{G(z) \in \mathcal{S}} \inf_{G_n(z) \in \Phi_n} \|G(z) - G_n(z)\|_{\mathcal{B}} \quad (10.82)$$

where \mathcal{B} denotes some Banach space with norm B , e.g. \mathcal{H}_2 or \mathcal{H}_∞ . Φ_n is the n -dimensional linear subspace spanned by the basis functions $\{\Lambda_k\}$, $k = 1, \dots, n$. $M_n(\mathcal{B})$ denotes the collection of all such subspaces. If

$$d_n(\mathcal{S}; \mathcal{B}) = \sup_{G(z) \in \mathcal{S}} \inf_{G_n(z) \in \Phi_n^*} \|G(z) - G_n(z)\|_B \quad (10.83)$$

then Φ_n^* is called an **optimal** subspace for $d_n(\mathcal{S}; \mathcal{B})$.

Using the above definition we may now address the *optimal model set problem* for fixed denominator model structures. Now assume that the only a priori information about $G(z)$ is exponential stability. This means that $G(z)$ belongs to $\mathcal{S} = \mathcal{H}_{2,R}^*(\mathbf{C}, \mathbf{C})$, the Hardy space of real rational strictly proper stable scalar discrete-time transfer functions which are analytic outside the disc $|z| \leq R$, $R < 1$. Thus we know that the poles of $G(z)$ are all located within the disc $|z| \leq R$. The impulse response of $G(z)$ thus decreases at least as R^k . Then we have the following theorem from [Wah94]

Theorem 10.1 (n -Width of FIR Models) *The space Φ_n^* spanned by $\{z^{-1}, \dots, z^{-n}\}$ is an optimal n -dimensional subspace in the n -width sense for $\mathcal{H}_{2,R}^*(\mathbf{C}, \mathbf{C})$.*

Thus the FIR model structure is “optimal” if the a priori information is just exponential stability. The main drawback of the FIR model structure is that it may converge quite slowly if the true system has poles located closed to the unit circle; thus if R above is close to one such that the a priori information is “weak”. Then very high order models must be used. However, implementation, information and sensitivity aspects limit the allowable size of the model order n that can be tolerated in practice.

10.3.3 Laguerre Models

Using more appropriate basis functions than the delay operator q^{-1} we may dramatically reduce the number of parameter necessary for obtaining a useful estimate of $G_T(q)$. The problem is that the delay operator is not a suitable operator if the true system has poles closed to the unit circle because it has too short memory. Using operators with longer memory, the number of parameters necessary to describe useful approximations can be reduced. We will, however, for numerical purposes like to preserve the orthonormality properties of the basis functions and to maintain the asymptotic properties of the parameter estimate.

The Laguerre functions are a popular alternative to FIR models which comply

with the above. The discrete-time Laguerre models are defined by:

$$G(z, \theta) = \sum_{i=1}^n \Lambda_i(z) \theta_i \quad (10.84)$$

$$\Lambda_i(z) = L_i(z, a) = \frac{\sqrt{1-a^2}}{z-a} \left[\frac{1-az}{z-a} \right]^{i-1}, \quad a \in \mathbf{R}, |a| < 1, i = 1, \dots, n \quad (10.85)$$

It can be shown, see e.g. [NG94], that the Laguerre functions form an orthonormal basis for functions in $\mathcal{H}_2^*(\mathbf{C}, \mathbf{C})$. This means that if $G(z) \in \mathcal{H}_2^*(\mathbf{C}, \mathbf{C})$ then there exists a sequence $\{g_k\}$ such that

$$G(z) = \sum_{k=1}^{\infty} g_k L_k(z, a), \quad a \in \mathbf{R}, |a| < 1 \quad (10.86)$$

$$= \sum_{k=1}^{\infty} g_k \frac{\sqrt{1-a^2}}{z-a} \left[\frac{1-az}{z-a} \right]^{k-1}, \quad a \in \mathbf{R}, |a| < 1 \quad (10.87)$$

Notice the similarity with the FIR representation. For Laguerre models, however, the necessary number of basis functions $L_k(z, a)$ to obtain a useful estimate of $G(z)$ is much smaller than for the FIR models.

It can be shown that the Laguerre model structure is optimal in the n -width sense if a priori information about the dominating time constant of the system is available. This is a very common situation. We may obtain this knowledge from e.g. physical insight or step response experiments. Here we will first present the continuous-time results since they are more transparent.

Assume that the true system $G_T(s)$ is analytical outside the disc $|s + \alpha| \leq r$ in the left half s -plane with $0 < r < \alpha$. This corresponds to the situation where we know that the (dominating) poles of the system are located within $|s + \alpha| \leq r$, see Figure 10.1 on the following page. It can then be shown that the continuous-time Laguerre functions are the optimal fixed denominator model structure in the n -width sense. Again the following theorem is from [Wah94].

Theorem 10.2 (n -Width of Continuous-time Laguerre Models)

The space Φ_n^ spanned by the continuous-time Laguerre basis functions $\{L_1(s, a), \dots, L_n(s, a)\}$ with*

$$L_j(s, a) = \frac{\sqrt{2a}}{s+a} \left(\frac{s-a}{s+a} \right)^{j-1}, \quad j = 1, 2, \dots, n \quad (10.88)$$

and $a = \sqrt{\alpha^2 - r^2}$ is an optimal n -dimensional subspace in the n -width sense for functions $G(s) \in \mathcal{H}_2(\mathbf{C}, \mathbf{C})$ which are analytical outside the domain $|s + \alpha| \leq r$, $0 < r < \alpha$.

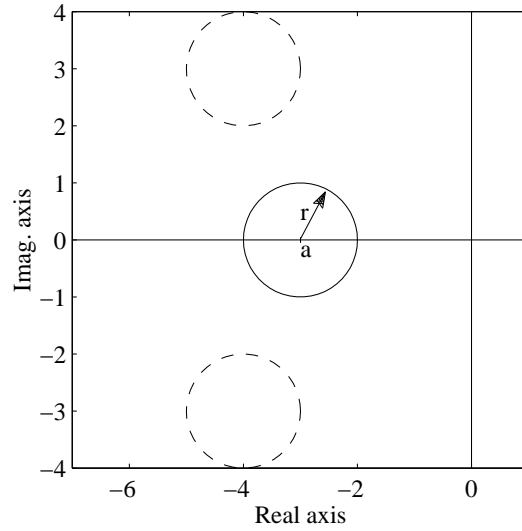


Figure 10.1: *A priori* information for Laguerre (solid) and Kautz (dashed) models.

Note that the optimal Laguerre pole a is smaller than the center pole α of the set $|s + \alpha| \leq r$. Thus the Laguerre pole should generally be chosen slightly faster than the dominant pole of the system to be approximated.

The corresponding discrete-time result is as follows [Wah94].

Theorem 10.3 (n -Width of Discrete-Time Laguerre Models) *The space Φ_n^* spanned by the discrete-time Laguerre basis function $\{L_1(z, a), \dots, L_n(z, a)\}$ with*

$$a = \frac{1}{2\alpha} \left(1 + \alpha^2 - r^2 + \sqrt{(1 + \alpha^2 - r^2)^2 - 4\alpha^2} \right) \quad (10.89)$$

is an optimal n -dimensional subspace in the n -width sense for functions $G(z) \in \mathcal{H}_2^(\mathbb{C}, \mathbb{C})$ which are analytic outside the domain $|z - \alpha| \leq r$, with $r > |\alpha| + 1$.*

The Laguerre model (10.87) on the page before can be represented by a *Laguerre Network*, see Figure 10.2 on the facing page. The structure is the same for continuous-time and discrete-time systems. Notice that the network consists of a single low-pass filter in series with several first order all-pass filters.

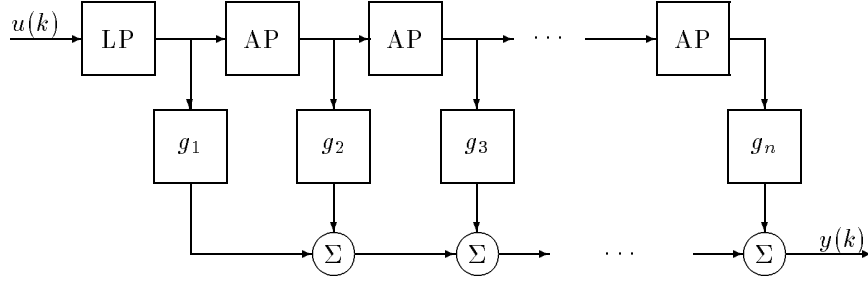


Figure 10.2: *Laguerre network. LP denotes a first order low-pass filter and AP denotes first order all-pass filters.*

The Laguerre functions provide useful approximations for well-damped systems with one dominating time constant. However for poorly damped systems the convergence will be slow since resonant poles occur in complex conjugate pairs. Furthermore systems with scattered poles cannot be well described. To obtain useful approximations for such systems we must use other basis functions, like e.g. the Kautz functions introduced in the next section.

10.3.4 Kautz Models

Assume that we know that the true continuous-time system $G_T(s)$ is resonant and that we know approximately the corresponding dominant mode. This is equivalent to assuming that the system is analytic outside the two regions shown in Figure 10.1 on the facing page. In order to determine which basis functions should be used when approximating resonant systems the methodology is to find a mapping which maps these regions onto $|s + \alpha| \leq r$ for which we know that the Laguerre functions are optimal. Then the Laguerre functions are mapped into the first domain and the result will be the desired basis functions for resonant systems. Because this mapping is two-to-one the procedure becomes somewhat technical and it will be beyond the scope of this work to treat it in detail. The interested reader may refer to [Wah94] and references therein. In [Wah94] it is shown that the continuous-time Laguerre functions map into the *Kautz functions*

defined by

$$\Psi_k(s, b, c) = \begin{cases} \frac{\sqrt{2bs}}{s^2 + bs + c} \left[\frac{s^2 - bs + c}{s^2 + bs + c} \right]^{\frac{k-1}{2}}, & k \text{ odd} \\ \frac{\sqrt{2bc}}{s^2 + bs + c} \left[\frac{s^2 - bs + c}{s^2 + bs + c} \right]^{\frac{k-2}{2}}, & k \text{ even} \end{cases} \quad (10.90)$$

$b > 0, c > 0, k = 1, 2, \dots$. The Kautz functions form an orthonormal basis for functions in $\mathcal{H}_2(\mathbf{C}, \mathbf{C})$. Furthermore the Kautz functions are optimal in the n -width sense for functions $G(s) \in \mathcal{H}_2(\mathbf{C}, \mathbf{C})$ which are analytic outside the domain $|(s^2 + \alpha s + c)/s| \leq r, r < \alpha$ since this set is mapped onto $|s + \alpha| \leq r$ by the transformation in question. $|(s^2 + \alpha s + c)/s| \leq r$ describes a rather complicated set; nevertheless it can capture a priori information about complex poles as well as multiple real ones. Formally we have the following theorem [Wah94].

Theorem 10.4 (n -Width of Continuous-time Kautz Models) *The space Φ_n^* spanned by the Kautz basis functions $\{\Psi_1(s, b, c), \dots, \Psi_n(s, b, c)\}$ with $b = \sqrt{\alpha^2 - r^2}$ is an optimal $2n$ -dimensional subspace in the n -width sense for functions $G(s) \in \mathcal{H}_2(\mathbf{C}, \mathbf{C})$, which are analytic outside the domain $|(s^2 + \alpha s + c)/s| \leq r, r < \alpha$.*

The discrete-time Kautz functions given by

$$\Psi_k(z, b, c) = \begin{cases} \frac{\sqrt{1-c^2}(z-b)}{z^2 + b(c-1)z - c} \left[\frac{-cz^2 + b(c-1)z + 1}{z^2 + b(c-1)z - c} \right]^{\frac{k-1}{2}}, & k \text{ odd} \\ \frac{\sqrt{(1-c^2)(1-b^2)}}{z^2 + b(c-1)z - c} \left[\frac{-cz^2 + b(c-1)z + 1}{z^2 + b(c-1)z - c} \right]^{\frac{k-2}{2}}, & k \text{ even} \end{cases} \quad (10.91)$$

with $-1 < b < 1, -1 < c < 1$ and $k = 1, 2, \dots$ form an orthonormal basis for functions in $\mathcal{H}_2^*(\mathbf{C}, \mathbf{C})$ such that any $G(z) \in \mathcal{H}_2^*(\mathbf{C}, \mathbf{C})$ may be written

$$G(z) = \sum_{k=1}^{\infty} g_k \Psi_k(z, b, c) \quad b, c \in \mathbf{R}, |b| < 1, |c| < 1 \quad (10.92)$$

Theorem 10.5 (n -Width of discrete-time Kautz Models) *The space Φ_n^* spanned by the discrete-time Kautz basis functions $\{\Psi_1(z, b, c), \dots, \Psi_n(z, b, c)\}$ with*

$$c = \frac{1}{2\alpha} \left(1 + \alpha^2 - r^2 + \sqrt{(1 + \alpha^2 - r^2)^2 - 4\alpha^2} \right) \quad (10.93)$$

is an optimal $2n$ -dimensional subspace in the n -width sense for functions $G(s) \in \mathcal{H}_2^*(\mathbf{C}, \mathbf{C})$, which are analytic outside the domain

$$\left| \frac{z(z-b)}{1-bz} - \alpha \right| \leq r \quad (10.94)$$

Assume we know that the dominating resonant mode in the true system is given approximately by the complex pair of poles β and β^* . Then the choice

$$b = \frac{\beta + \beta^*}{1 + \beta\beta^*}, \quad c = -\beta\beta^* \quad (10.95)$$

places the resonant mode of the Kautz filters close to that of the true system.

10.4 Combined Laguerre and Kautz Structures

Due to the linear properties of the Laguerre and Kautz model structures we can approximate systems with several possibly real and complex poles by cascading a number of Laguerre and Kautz filters. Such a general fixed denominator model structure can be written

$$G(q, \theta) = \Lambda(q)\theta \quad (10.96)$$

$$= \sum_{i=1}^{m^L} \sum_{k=1}^{n^{L_i}} L_k(q, a_i) \theta_k^{L_i} + \sum_{i=1}^{m^\Psi} \sum_{k=1}^{n^{\Psi_i}} \Psi_k(q, b_i, c_i) \theta_k^{\Psi_i} \quad (10.97)$$

10.5 Summary

The prediction error method was considered for some special cases. First the popular ARX model structure was investigated. An analytical expression for the parameter estimate could be obtained since the predictor for the ARX model is linear in θ . Unfortunately, the corresponding expression for the parameter covariance does not allow for a consistent data estimate unless in the case when *both the deterministic and stochastic part of the model* admit a perfect description of the true system. It is well known that if the ARX model admits a perfect description of the deterministic part $G(q, \theta)$ of the true system, if the same is *not* true for the stochastic part, then the parameter estimate for the deterministic part will be biased.

Next output error (OE) models were considered. The OE predictor is *not* linear in θ . Thus the parameter estimate $\hat{\theta}_N$ must be found using numerical search, using e.g. Marquardt's algorithm. On the other hand it was shown that the

expression for the parameter covariance P_θ was considerably simplified in the case where $G(q, \theta)$ admits a perfect description for the deterministic part of the true system *regardless of the true stochastic part*. A consistent estimate can then be obtained from the data.

Finally, fixed denominator models were considered. Models which are linear in the parameter vector have attracted much attention within the system identification community during the last 5 years. From a classical point of view it seems odd that the poles of the model is determined a priori and just the zeros estimated from the data. However, in many cases, very good a priori estimates of the dominating poles of the system can be obtained from e.g. step response tests. The predictor for fixed denominator models is linear in θ . Thus analytic expressions for the parameter estimate can be derived. Furthermore the regressors $\phi(k)$ are deterministic. This enables us to derive *non-asymptotic* expressions for the parameter covariance P_θ in the general case. Thus an unbiased estimate of the parameter estimate can be obtained *even in the case of undermodeling*. Of course, for “true” frequency domain error bounds we must require that the true system can be represented within the model set. Otherwise we will only obtain the variance part of the model error. Finite impulse response (FIR), Laguerre and Kautz model structures were then presented. Using n -width measures for optimality it was shown that the FIR model structure is an optimal fixed denominator model set if the only a priori information is exponential stability. However, usually we know more than that. If we know that the (dominating) poles of the system is located within a disc with radius r located at $(-a, 0)$ in the complex plane, then the Laguerre model structure becomes the optimal one in the n -width sense. Thus Laguerre models are useful in modeling well damped systems with one dominating time constant. For lightly damped systems or for systems with scattered poles, Kautz models provides useful descriptions.

Chapter 11

The Stochastic Embedding Approach

Contents

11.1 The Methodology	184
11.1.1 Necessary Assumptions	184
11.1.2 Model Formulation	185
11.1.3 Computing the Parameter Estimate	187
11.1.4 Variance of Parameter Estimate	188
11.1.5 Estimating the Model Error	189
11.1.6 Recapitulation	193
11.2 Estimating the Parameterizations of f_Δ and f_ν	194
11.2.1 Estimation Techniques	195
11.2.2 Choosing the Probability Distributions	196
11.2.3 Maximum Likelihood Estimation of ζ	197
11.3 Parameterizing the Covariances	198
11.3.1 Parameterizing the Noise Covariance C_ν	198
11.3.2 Parameterizing the Undermodeling Covariance C_η	199
11.3.3 Combined Covariance Structures	204
11.4 Summary	204
11.4.1 Remarks	205

In this chapter we will give an introduction to the stochastic embedding approach for estimation of frequency domain model error bounds. It is shown how the approach may be developed to construct a flexible framework for estimation of error bounds under different noise and undermodeling conditions. Furthermore quantitative properties of prior assumptions on the noise and the undermodeling may be estimated from current data. The main contribution of this work is to investigate and improve the qualitative prior assumptions regarding the covariance structures of the noise and undermodeling.

11.1 The Methodology

As discussed in the introduction on page 133 estimation of frequency domain model error bounds from a finite set of noisy data is a very difficult problem unless we assume that the true system can be represented within our model set. Some sort of a priori knowledge of the noise and the undermodeling will be required to obtain such bounds in the general case. The main paradigm of the stochastic embedding approach is to assume that the undermodeling is a realization of a stochastic process with known distribution. Henceforth the true transfer function of the system is assumed to be a realization of a stochastic process.

It is furthermore assumed that the transfer function for the true system may be decomposed into a parametric part $G(q, \theta_0)$ and a bias contribution $G_\Delta(q)$. Thus the frequency response of the true system is supposed given by:

$$G_T(e^{j\omega T_s}) = G(e^{j\omega T_s}, \theta_0) + G_\Delta(e^{j\omega T_s}) \quad (11.1)$$

We then assume that $G_\Delta(e^{j\omega T_s})$ is a realization of a zero mean stochastic process

$$E \{G_\Delta(e^{j\omega T_s})\} = 0 \quad (11.2)$$

$$\Rightarrow E \{G_T(e^{j\omega T_s})\} = G(e^{j\omega T_s}, \theta_0) \quad (11.3)$$

The expectation $E \{\cdot\}$ in Equation (11.2) and (11.3) means averaging over different realizations of the undermodeling. Of course, for any given system we will have just one realization and the undermodeling will be deterministic. However, the stochastic embedding of the undermodeling enables us to treat it within the same framework as the noise and to derive results which can be viewed as a natural extension of the classical results.

11.1.1 Necessary Assumptions

The following assumptions will be made:

1. The observed data are assumed to be generated by the linear system \mathcal{S} according to:

$$\mathcal{S} : y(k) = G_T(q)u(k) + H_T(q)e_0(k) \quad (11.4)$$

where $G_T(q)$ and $H_T(q)$ are strictly stable rational transfer functions, $e_0(k)$ is a zero mean i.i.d. (independent identically distributed) stochastic process, $u(k)$ is a quasi-stationary sequence (see [Lju87, pp 27]). Furthermore $u(k)$ and $e(k)$ are independent. Applying Equation (11.1) on the facing page we may write (11.4) as:

$$y(k) = G(q, \theta_0) u(k) + G_\Delta(q) u(k) + H(q) e_0(k) \quad (11.5)$$

2. The process noise $\nu(k) = H_T(q)e_0(k)$ is independent of the undermodeling described by $\delta(k) = G_\Delta(q) u(k)$.
3. The probability density function f_Δ for the zero mean stochastic process $\delta(k)$ can be parameterized as a function of a parameter vector β .
4. The probability density function f_ν for the process noise $\nu(k)$ can be parameterized as a function of a parameter vector γ .

Assumption 1 is more or less standard in system identification. Note that we have not restricted the distribution function for the noise to be Gaussian. Assumption 2 is obviously reasonable. From assumption 3 we now get:

$$f_\Delta = f_\Delta(G_\Delta, \beta) \quad (11.6)$$

and similar from 4:

$$f_\nu = f_\nu(H, \gamma) \quad (11.7)$$

11.1.2 Model Formulation

We will use fixed denominator modeling both for the parametric part $G(q, \theta)$ and the undermodeling $G_\Delta(q)$. In particular we will use a FIR model of order $L \leq N$ for $G_\Delta(q)$:

$$G_\Delta(q) = \sum_{k=1}^L \eta(k) q^{-k} \quad (11.8)$$

where $\eta(k)$ denotes the model error impulse response. Replacing q with $e^{j\omega T_s}$ we get the frequency response:

$$G_\Delta(e^{j\omega T_s}) = \Pi(e^{j\omega T_s}) \eta \quad (11.9)$$

with

$$\Pi(e^{j\omega T_s}) \triangleq [e^{-j\omega T_s}, e^{-2j\omega T_s}, \dots, e^{-Lj\omega T_s}] \quad (11.10)$$

$$\eta \triangleq [\eta(1), \eta(2), \dots, \eta(L)]^T \quad (11.11)$$

where T denotes transpose. We will use a general fixed denominator model for the parametric part $G(q, \theta)$:

$$G(e^{j\omega T_s}, \theta) = \Lambda(e^{j\omega T_s}) \theta \quad (11.12)$$

with

$$\Lambda(e^{j\omega T_s}) \triangleq [\Lambda_1(e^{j\omega T_s}), \Lambda_2(e^{j\omega T_s}), \dots, \Lambda_n(e^{j\omega T_s})] \quad (11.13)$$

where n is the order of the model. Hence the Laguerre and Kautz model structures introduced in Section 10.3 on page 171 will be valid model structures whereas the general polynomial model (9.1) on page 140 cannot readily be used.

We may now rewrite Equation (11.4) on the page before as:

$$y(k) = G_T(q)u(k) + H_T(q)e_0(k) \quad (11.14)$$

$$= G(q, \theta_0)u(k) + G_\Delta(q)u(k) + \nu(k) \quad (11.15)$$

$$= \Lambda(q)\theta_0 u(k) + \Pi(q)\eta u(k) + \nu(k) \quad (11.16)$$

$$= \phi^T(k)\theta_0 + \xi^T(k)\eta + \nu(k) \quad (11.17)$$

where

$$\phi^T(k) \triangleq \Lambda(q)u(k) = [\phi_1(k), \phi_2(k), \dots, \phi_n(k)] \quad (11.18)$$

$$\xi^T(k) \triangleq \Pi(q)u(k) = [u(k-1), u(k-2), \dots, u(k-L)] \quad (11.19)$$

Introducing:

$$Y \triangleq [y(1), y(2), \dots, y(N)]^T \quad (11.20)$$

$$V \triangleq [\nu(1), \nu(2), \dots, \nu(N)]^T \quad (11.21)$$

Equation (11.17) may be rewritten as:

$$Y = \begin{bmatrix} y(1) \\ y(2) \\ \vdots \\ y(N) \end{bmatrix} = \begin{bmatrix} \phi^T(1)\theta_0 \\ \phi^T(2)\theta_0 \\ \vdots \\ \phi^T(N)\theta_0 \end{bmatrix} + \begin{bmatrix} \xi^T(1)\eta \\ \xi^T(2)\eta \\ \vdots \\ \xi^T(N)\eta \end{bmatrix} + \begin{bmatrix} \nu(1) \\ \nu(2) \\ \vdots \\ \nu(N) \end{bmatrix} \quad (11.22)$$

$$= \Phi\theta_0 + X\eta + V \quad (11.23)$$

with Φ and X defined by:

$$\Phi \triangleq \begin{bmatrix} \phi_1(1) & \phi_2(1) & \cdots & \phi_n(1) \\ \phi_1(2) & \phi_2(2) & \cdots & \phi_n(2) \\ \vdots & \vdots & \ddots & \vdots \\ \phi_1(N) & \phi_2(N) & \cdots & \phi_n(N) \end{bmatrix} \quad (11.24)$$

$$X \triangleq \begin{bmatrix} \xi_1(1) & \xi_2(1) & \cdots & \xi_L(1) \\ \xi_1(2) & \xi_2(2) & \cdots & \xi_L(2) \\ \vdots & \vdots & \ddots & \vdots \\ \xi_1(N) & \xi_2(N) & \cdots & \xi_L(N) \end{bmatrix} \quad (11.25)$$

$$= \begin{bmatrix} u(1-1) & u(1-2) & \cdots & u(1-L) \\ u(2-1) & u(2-2) & \cdots & u(2-L) \\ \vdots & \vdots & \ddots & \vdots \\ u(N-1) & u(N-2) & \cdots & u(N-L) \end{bmatrix} \quad (11.26)$$

11.1.3 Computing the Parameter Estimate

Adopting a quadratic performance function for the estimation problem gives:

$$V_N(\theta, Z^N) = \sum_{k=1}^N (y(k) - \hat{y}(k|\theta))^2 \quad (11.27)$$

$$= \sum_{k=1}^N (y(k) - \phi^T(k)\theta)^2 \quad (11.28)$$

$$= (Y - \Phi\theta)^T (Y - \Phi\theta) \quad (11.29)$$

$$= Y^T Y - Y^T \Phi\theta - \theta^T \Phi^T Y + \theta^T \Phi^T \Phi\theta \quad (11.30)$$

The derivative of $V_N(\theta, Z^N)$ with respect to θ is henceforth given by:

$$V'_N(\theta, Z^N) = 0 - \frac{\partial}{\partial \theta} \{Y^T \Phi\theta\} - \frac{\partial}{\partial \theta} \{\theta^T \Phi^T Y\} + \frac{\partial}{\partial \theta} \{\theta^T \Phi^T \Phi\theta\} \quad (11.31)$$

$$= -\Phi^T Y - \Phi^T Y + \left(\Phi^T \Phi + (\Phi^T \Phi)^T\right) \theta \quad (11.32)$$

$$= -2\Phi^T Y + 2(\Phi^T \Phi) \theta \quad (11.33)$$

Minimizing the performance function gives the desired estimate of the parameter

vector θ as:

$$\hat{\theta}_N = \arg \min_{\theta} \{V_N(\theta, Z^N)\} \quad (11.34)$$

$$\Rightarrow \hat{\theta}_N = \arg_{\theta} \{V'_N(\theta, Z^N) = 0\} \quad (11.35)$$

$$\Leftrightarrow \Phi^T Y = (\Phi^T \Phi) \hat{\theta}_N \quad (11.36)$$

$$\Leftrightarrow \hat{\theta}_N = (\Phi^T \Phi)^{-1} \Phi^T Y \quad (11.37)$$

Equation (11.37) is the well known solution to the standard linear regression least-squares estimate of θ .

If the matrix $\Phi^T \Phi$ is ill-conditioned numerically more robust algorithms exists for computing the parameter estimate, e.g. through QR factorization, see Appendix F on page 313. However, as we noted in Section 10.3.2, see page 175, if we use orthonormal basis functions for $G(q, \theta)$ then $\Phi^T \Phi$ will asymptotically (for $N \rightarrow \infty$) have a Toeplitz structure which guarantees that the parameter estimate (11.37) will be well conditioned.

11.1.4 Variance of Parameter Estimate

In order to evaluate the covariance of the parameter estimate first introduce:

$$\Omega \triangleq (\Phi^T \Phi)^{-1} \Phi^T \quad (11.38)$$

to achieve:

$$\hat{\theta}_N = \Omega Y \quad (11.39)$$

$$= \Omega \Phi \theta_0 + \Omega X \eta + \Omega V \quad (11.40)$$

$$= (\Phi^T \Phi)^{-1} \Phi^T \Phi \theta_0 + \Omega X \eta + \Omega V \quad (11.41)$$

$$= \theta_0 + \Omega X \eta + \Omega V \quad (11.42)$$

equivalent to:

$$\hat{\theta}_N - \theta_0 = \Omega X \eta + \Omega V \quad (11.43)$$

The covariance of the parameter vector $\hat{\theta}_N$ with respect to the nominal value θ_0 is consequently given as:

$$\text{Cov}(\hat{\theta}_N - \theta_0) = E \left\{ \left(\hat{\theta}_N - \theta_0 \right) \left(\hat{\theta}_N - \theta_0 \right)^T \right\} \quad (11.44)$$

$$= E \left\{ (\Omega X \eta + \Omega V) (\Omega X \eta + \Omega V)^T \right\} \quad (11.45)$$

$$= E \left\{ \Omega (X \eta + V) (\eta^T X^T + V^T) \Omega^T \right\} \quad (11.46)$$

$$= E \left\{ \Omega (X \eta \eta^T X^T + X \eta V^T + V \eta^T X^T + V V^T) \Omega^T \right\} \quad (11.47)$$

$$= E \left\{ \Omega (X \eta \eta^T X^T + V V^T) \Omega^T \right\} \quad (11.48)$$

since η and V are assumed uncorrelated. Defining the covariance matrices for the noise C_ν and the undermodeling C_η as:

$$E \left\{ \eta \eta^T \right\} \triangleq C_\eta \quad (11.49)$$

$$E \left\{ V V^T \right\} \triangleq C_\nu \quad (11.50)$$

Equation (11.48) may be written as:

$$\text{Cov} \left(\hat{\theta}_N - \theta_0 \right) = \Omega \left[X C_\eta X^T + C_\nu \right] \Omega^T \quad (11.51)$$

$$= (\Phi \Phi^T)^{-1} \Phi^T \left[X C_\eta X^T + C_\nu \right] \Phi (\Phi^T \Phi)^{-1} \quad (11.52)$$

Equation (11.52) states that under the assumptions given the variance on the parameter estimate is a combination of a bias term ($\Omega X C_\eta X^T \Omega^T$) and a noise term ($\Omega C_\nu \Omega^T$). Compare with the classical expression for fixed denominator models (10.61) on page 172.

11.1.5 Estimating the Model Error

Combine Equation (11.1) on page 184, (11.9) on page 185 and (11.12) on page 186 to obtain:

$$G_T (e^{j\omega T_s}) = \Lambda \theta_0 + \Pi \eta \quad (11.53)$$

Furthermore substituting θ_0 with $\hat{\theta}_N$ in (11.12) on page 186 gives:

$$G \left(e^{j\omega T_s}, \hat{\theta}_N \right) = \Lambda \hat{\theta}_N \quad (11.54)$$

Combining Equation (11.53) and (11.54) we find that:

$$G_T (e^{j\omega T_s}) - G \left(e^{j\omega T_s}, \hat{\theta}_N \right) = \Lambda \left(\theta_0 - \hat{\theta}_N \right) + \Pi \eta \quad (11.55)$$

Combining this with Equation (11.43) on the facing page we achieve the key result:

$$G_T (e^{j\omega T_s}) - G \left(e^{j\omega T_s}, \hat{\theta}_N \right) = \Lambda (-\Omega X \eta - \Omega V) + \Pi \eta \quad (11.56)$$

$$= (\Pi - \Lambda \Omega X) \eta - \Lambda \Omega V \quad (11.57)$$

Equation (11.57) is a central result of the stochastic embedding approach. Π and Λ are known functions of the frequency ω whereas Ω and X are known functions of the input signals. Consequently, Equation (11.57) expresses the modeling error as a known linear combination of two independent random vectors η and V .

The expression (11.57) furthermore clearly separates the bias term $(\Pi - \Lambda\Omega X)\eta$ and the noise term $\Lambda\Omega V$. The bias term is especially interesting since it separates into an a priori term $\Pi\eta$, see Equation (11.9) on page 185, and a data induced correction term $\Lambda\Omega X\eta$, which compensate for the difference between θ_0 and $\hat{\theta}_N$, see also Equation (11.43) on page 188.

Also notice, that if $\hat{\theta}_N = \theta_0$ then:

$$G_T(e^{j\omega T_s}) - G(e^{j\omega T_s}, \hat{\theta}_N) = \Pi\eta, \quad \text{if } \hat{\theta}_N = \theta_0 \quad (11.58)$$

that is, our a priori estimate of $G_\Delta(e^{j\omega T_s})$ will not be changed as we will expect from Equation (11.1) on page 184 and the assumptions.

We will now investigate the second order properties of the modeling error. Introduce the following parameters:

$$\hat{\rho}_N \triangleq \begin{bmatrix} \hat{\theta}_N \\ 0 \end{bmatrix}, \quad \rho_0 \triangleq \begin{bmatrix} \theta_0 \\ \eta \end{bmatrix} \quad (11.59)$$

$$\Gamma(e^{j\omega T_s}) \triangleq \begin{bmatrix} \Re \left\{ \Lambda(e^{j\omega T_s}), \Pi(e^{j\omega T_s}) \right\} \\ \Im \left\{ \Lambda(e^{j\omega T_s}), \Pi(e^{j\omega T_s}) \right\} \end{bmatrix} \quad (11.60)$$

$$\tilde{g}(e^{j\omega T_s}) \triangleq \begin{bmatrix} \Re \left\{ G_T(e^{j\omega T_s}) - G(e^{j\omega T_s}, \hat{\theta}_N) \right\} \\ \Im \left\{ G_T(e^{j\omega T_s}) - G(e^{j\omega T_s}, \hat{\theta}_N) \right\} \end{bmatrix} \quad (11.61)$$

to obtain:

$$\Gamma(e^{j\omega T_s})(\rho_0 - \hat{\rho}_N) = \quad (11.62)$$

$$\begin{bmatrix} \Re \left\{ \Lambda_1 \cdots \Lambda_n, e^{-j\omega T_s} \cdots e^{-Lj\omega T_s} \right\} \\ \Im \left\{ \Lambda_1 \cdots \Lambda_n, e^{-j\omega T_s} \cdots e^{-Lj\omega T_s} \right\} \end{bmatrix} \begin{bmatrix} \theta_0(1) - \hat{\theta}_N(1) \\ \vdots \\ \theta_0(n) - \hat{\theta}_N(n) \\ \eta(1) \\ \vdots \\ \eta(L) \end{bmatrix} \quad (11.63)$$

$$= \begin{bmatrix} \Re \left\{ (\Lambda_1\theta_0(1) + \cdots + \Lambda_n\theta_0(n)) - (\Lambda_1\hat{\theta}_N(1) + \cdots + \Lambda_n\hat{\theta}_N(n)) \right. \\ \Im \left\{ (\Lambda_1\theta_0(1) + \cdots + \Lambda_n\theta_0(n)) - (\Lambda_1\hat{\theta}_N(1) - \cdots - \Lambda_n\hat{\theta}_N(n)) \right. \\ \left. + (e^{-j\omega T_s}\eta(1) + \cdots + e^{-Lj\omega T_s}\eta(L)) \right\} \\ \left. + (e^{-j\omega T_s}\eta(1) + \cdots + e^{-Lj\omega T_s}\eta(L)) \right\} \end{bmatrix} \quad (11.64)$$

$$= \begin{bmatrix} \Re e \left\{ G(e^{j\omega T_s}, \theta_0) - G(e^{j\omega T_s}, \hat{\theta}_N) + G_\Delta(e^{j\omega T_s}) \right\} \\ \Im m \left\{ G(e^{j\omega T_s}, \theta_0) - G(e^{j\omega T_s}, \hat{\theta}_N) + G_\Delta(e^{j\omega T_s}) \right\} \end{bmatrix} \quad (11.65)$$

$$= \begin{bmatrix} \Re e \left\{ G_T(e^{j\omega T_s}) - G(e^{j\omega T_s}, \hat{\theta}_N) \right\} \\ \Im m \left\{ G_T(e^{j\omega T_s}) - G(e^{j\omega T_s}, \hat{\theta}_N) \right\} \end{bmatrix} \quad (11.66)$$

$$= \tilde{g}(e^{j\omega T_s}) \quad (11.67)$$

From Equation (11.67) follows:

$$P_{\tilde{g}}(\omega) \triangleq E \left\{ \tilde{g}(e^{j\omega T_s}) \tilde{g}(e^{j\omega T_s})^T \right\} \quad (11.68)$$

$$= E \left\{ \Gamma(e^{j\omega T_s}) (\rho_0 - \hat{\rho}_N) (\rho_0 - \hat{\rho}_N)^T \Gamma^T(e^{j\omega T_s}) \right\} \quad (11.69)$$

$$= \Gamma(e^{j\omega T_s}) E \left\{ (\rho_0 - \hat{\rho}_N) (\rho_0 - \hat{\rho}_N)^T \right\} \Gamma^T(e^{j\omega T_s}) \quad (11.70)$$

$$= \Gamma(e^{j\omega T_s}) \Upsilon \Gamma^T(e^{j\omega T_s}) \quad (11.71)$$

Remembering that η and V are assumed uncorrelated, we obtain:

$$\Upsilon = E \left\{ (\rho_0 - \hat{\rho}_N) (\rho_0 - \hat{\rho}_N)^T \right\} \quad (11.72)$$

$$= E \left\{ \begin{bmatrix} \theta_0 - \hat{\theta}_N \\ \eta \end{bmatrix} \begin{bmatrix} \theta_0 - \hat{\theta}_N \\ \eta \end{bmatrix}^T \right\} \quad (11.73)$$

$$= E \left\{ \begin{bmatrix} -\Omega X \eta - \Omega V \\ \eta \end{bmatrix} \begin{bmatrix} (-\Omega X \eta - \Omega V)^T & \eta^T \end{bmatrix} \right\} \quad (11.74)$$

$$= E \left\{ \begin{bmatrix} \Omega(-X\eta - V)(-X\eta - V)^T \Omega^T & \Omega(-X\eta - V)\eta^T \\ \eta(-X\eta - V)^T \Omega^T & \eta\eta^T \end{bmatrix} \right\} \quad (11.75)$$

$$= E \left\{ \begin{bmatrix} \Omega(X\eta\eta^T X^T + VV^T) \Omega^T & -\Omega X\eta\eta^T \\ -\eta\eta^T X^T \Omega^T & \eta\eta^T \end{bmatrix} \right\} \quad (11.76)$$

$$= \begin{bmatrix} E \left\{ \Omega(X\eta\eta^T X^T + VV^T) \Omega^T \right\} & E \left\{ -\Omega X\eta\eta^T \right\} \\ E \left\{ -\eta\eta^T X^T \Omega^T \right\} & E \left\{ \eta\eta^T \right\} \end{bmatrix} \quad (11.77)$$

$$= \begin{bmatrix} \Omega(XC_\eta X^T + C_\nu) \Omega^T & -\Omega XC_\eta \\ -C_\eta X^T \Omega^T & C_\eta \end{bmatrix} \quad (11.78)$$

The second order properties of the total model error is then described by Equation (11.71) and (11.78). Once the distributions f_Δ and f_ν are determined (and the parameterizations of $C_\eta(\beta)$ and $C_\nu(\gamma)$ have been estimated) we may use (11.71) to map the uncertainty levels into the frequency domain.

We will now show how to find the magnitude expectation of the squared under-modeling (the total model error variance in the stochastic setting). We first show that it may be expressed as the trace of the covariance matrix $P_{\hat{g}}$:

$$\begin{aligned} E \left\{ \left| G(e^{j\omega T_s}, \hat{\theta}_N) - G_T(e^{j\omega T_s}) \right|^2 \right\} \\ = E \left\{ \left(G(e^{j\omega T_s}, \hat{\theta}_N) - G_T(e^{j\omega T_s}) \right) \left(G(e^{j\omega T_s}, \hat{\theta}_N) - G_T(e^{j\omega T_s}) \right)^* \right\} \end{aligned} \quad (11.79)$$

$$\begin{aligned} = E \left\{ \Re \left\{ G(e^{j\omega T_s}, \hat{\theta}_N) - G_T(e^{j\omega T_s}) \right\}^2 + \right. \\ \left. \Im \left\{ G(e^{j\omega T_s}, \hat{\theta}_N) - G_T(e^{j\omega T_s}) \right\}^2 \right\} \end{aligned} \quad (11.80)$$

$$= E \left\{ \tilde{g}_1^2(e^{j\omega T_s}) + \tilde{g}_2^2(e^{j\omega T_s}) \right\} \quad (11.81)$$

$$= \text{tr} \{ P_{\hat{g}}(\omega) \} \quad (11.82)$$

We may also express the undermodeling directly via Equation (11.57) on page 189 as:

$$\begin{aligned} E \left\{ \left| G(e^{j\omega T_s}, \hat{\theta}_N) - G_T(e^{j\omega T_s}) \right|^2 \right\} \\ = E \left\{ ((\Pi - \Lambda\Omega X) \eta - \Lambda\Omega V) ((\Pi - \Lambda\Omega X) \eta - \Lambda\Omega V)^* \right\} \end{aligned} \quad (11.83)$$

$$\begin{aligned} = E \left\{ (\Pi - \Lambda\Omega X) \eta \eta^T (\Pi - \Lambda\Omega X)^* + (\Pi - \Lambda\Omega X) \eta V^T \Omega^T \Lambda^* \right. \\ \left. - \Lambda\Omega V \eta^T (\Pi - \Lambda\Omega X)^* + \Lambda\Omega V V^T \Omega^T \Lambda^* \right\} \end{aligned} \quad (11.84)$$

$$= (\Pi - \Lambda\Omega X) E \{ \eta \eta^T \} (\Pi - \Lambda\Omega X)^* + 0 - 0 + \Lambda\Omega E \{ V V^T \} \Omega^T \Lambda^* \quad (11.85)$$

$$= (\Pi - \Lambda\Omega X) C_\eta (\Pi - \Lambda\Omega X)^* + \Lambda\Omega C_\nu \Omega^T \Lambda^* \quad (11.86)$$

Notice that in Equation (11.86) we have separated the contributions from the bias error and the variance error. Notice furthermore that in (11.86) and (11.71) on the preceding page everything but C_η and C_ν are uniquely determined from the parametric model structure and the input. Thus the total model error is shaped by the covariance matrices for the undermodeling and the noise. Remember that in the classical approach for fixed denominator models, see Section 10.3 on page 171, the model error was shaped by the noise covariance matrix in a similar manner.

The preliminary approach by Goodwin & Salgado [GS89b] – in which C_η and C_ν were assumed quantitatively given a priori – suffers from the fact that no input/output information was in fact used to estimate the model error! It consequently seems essential to obtain good estimates of C_η and C_ν from the available data.

11.1.6 Recapitulation

We have now demonstrated the main results of the stochastic embedding approach as proposed by Goodwin *et al.* Let us shortly recapitulate the key assumptions and results:

Main assumptions:

- We will describe the (deterministic) undermodeling of our process as one realization of a stochastic process. From this realization we will estimate the properties of the stochastic description.
- We assume that the true system $G_T(e^{j\omega T_s})$ may be decomposed as:

$$G_T(e^{j\omega T_s}) = G(e^{j\omega T_s}, \theta_0) + G_\Delta(e^{j\omega T_s})$$

where:

$$E\{G_\Delta(e^{j\omega T_s})\} = 0$$

and consequently:

$$E\{G_T(e^{j\omega T_s})\} = G(e^{j\omega T_s}, \theta_0)$$

where $E\{\cdot\}$ means expectation over different realizations of the stochastic process we associate with the undermodeling.

- The model $G(e^{j\omega T_s}, \theta_0)$ shall be linear in the parameter vector θ as e.g. are the class of Laguerre/Kautz models.

Main Results:

- The difference between the true system $G_T(e^{j\omega T_s})$ and the estimated model $G(e^{j\omega T_s}, \hat{\theta}_N)$ is given by:

$$G_T(e^{j\omega T_s}) - G(e^{j\omega T_s}, \hat{\theta}_N) = (\Pi - \Lambda\Omega X)\eta - \Lambda\Omega V$$

with symbols as defined above. This central result shows that under the stochastic embedding approach the modeling error may be expressed as a known linear combination of two independent random vectors η and V . Furthermore the expression separates the undermodeling from the noise contribution. The undermodeling contribution to the total model error $(\Pi - \Lambda\Omega X)\eta$ consists of two terms. $\Pi\eta$ is an a priori assumption of the undermodeling based on estimates of the impulse response η . $\Lambda\Omega X\eta$ is a data-induced correction term to this prior due to the shift from θ_0 to $\hat{\theta}_N$.

Furthermore:

$$E \left\{ \left| G(e^{j\omega T_s}, \hat{\theta}_N) - G_T(e^{j\omega T_s}) \right|^2 \right\} = (\Pi - \Lambda \Omega X) C_\eta (\Pi - \Lambda \Omega X)^* + \Lambda \Omega C_\nu \Omega^T \Lambda^*$$

In the above expression for the total model error variance the covariances C_ν and C_η are the only unknowns. If reasonable estimates of these matrices may be obtained and substituted in the above expression, estimates of the total model error and its contributions may be determined.

- With $\tilde{g}(e^{j\omega T_s})$ defined as in Section 11.1.5 we have:

$$\begin{aligned} E \{ \tilde{g}(e^{j\omega T_s}) \} &= 0 \\ E \{ \tilde{g}(e^{j\omega T_s}) \tilde{g}(e^{j\omega T_s})^T \} &\triangleq P_{\tilde{g}} = \Gamma(e^{j\omega T_s}) \Upsilon \Gamma(e^{j\omega T_s})^T \\ E \left\{ \left| G(e^{j\omega T_s}, \hat{\theta}_N) - G_T(e^{j\omega T_s}) \right|^2 \right\} &= \text{tr} \{ P_{\tilde{g}} \} \end{aligned}$$

Assumptions NOT made

- No assumptions have been made on the probability density functions for the undermodeling and the process noise other than that they may be parameterized as functions of β and γ .
- Also we have not limited us to consider special structures of the parametrization of these density functions. For the undermodeling this is equivalent to specifying the structure of undermodeling impulse response variance $E \{ \eta^2(k) \}$.

For the process noise, selection of parameterization structure amounts to specifying the necessary parameters for the chosen probability function.

11.2 Estimating the Parameterizations of f_Δ and f_ν

Having presented the central methodology, we now turn to specifying and estimating the parameterizations of the undermodeling and process noise.

11.2.1 Estimation Techniques

Goodwin *et al.* [GGN92] propose maximum likelihood methods in order to estimate the parameter vectors β and γ from the residuals vector ϵ defined by:

$$\epsilon \triangleq Y - \Phi \hat{\theta}_N \quad (11.87)$$

$$= Y - \Phi \Omega Y \quad (11.88)$$

$$= \left[I - \Phi (\Phi^T \Phi)^{-1} \Phi^T \right] Y \quad (11.89)$$

$$\triangleq P_\Phi Y \quad (11.90)$$

where P_Φ is a $N \times N$ matrix. However it is possible to show that the rank of P_Φ is only $N - p$ and hence ϵ will have a singular distribution and maximum likelihood methods will fail.

However we may transform ϵ into another coordinate system by:

$$\varpi \triangleq R^T \epsilon \quad (11.91)$$

$$= R^T Y - R^T \Phi \hat{\theta}_N \quad (11.92)$$

$$= R^T \Phi \theta_0 + R^T X \eta + R^T V - R^T \Phi \hat{\theta}_N \quad (11.93)$$

$$= R^T \Phi \left(\theta_0 - \hat{\theta}_N \right) + R^T X \eta + R^T V \quad (11.94)$$

If we choose a full rank ($N \times N - p$) transformation matrix R so that:

$$R^T \Phi = 0 \quad (11.95)$$

then

$$\varpi = R^T Y = R^T X \eta + R^T V \quad (11.96)$$

With R chosen as above the distribution on ϖ will be non-singular. Notice that the transformed data vector ϖ has only $N - p$ elements. Possible ways of choosing R is discussed in Section 11.2.3.1 on page 198.

From Equation (11.96), note that ϖ is the sum of two independent random vectors, η and V , whose probability density functions we have parameterized as functions of β and γ , see Equation (11.6) and (11.7) on page 185.

Now introduce the combined parameter vector ζ as:

$$\zeta \triangleq \begin{bmatrix} \beta \\ \gamma \end{bmatrix} \quad (11.97)$$

Then it will be possible to compute the likelihood function for the data vector ϖ given ζ and the inputs U under the given assumptions on the probability density

functions. The likelihood function will be denoted $\mathcal{L}(\varpi|U, \zeta)$. Maximizing the likelihood function will yield the desired estimate for the parameter vector ζ :

$$\hat{\zeta} = \arg \max_{\zeta} \mathcal{L}(\varpi|U, \zeta) \quad (11.98)$$

Notice that in the above procedure we have not narrowed the applicable class of probability density functions to be chosen.

11.2.2 Choosing the Probability Distributions

To proceed further we now have to make a specific choice of the assumed probability structure of the undermodeling and process noise. Assume that these are zero mean Gaussian distributed:

$$\eta \sim \mathcal{N}(0, C_\eta(\beta)) \quad (11.99)$$

$$V \sim \mathcal{N}(0, C_\nu(\gamma)) \quad (11.100)$$

with $C_\eta(\beta)$ being the parameterized covariance matrix for the impulse response of the undermodeling and $C_\nu(\gamma)$ the parameterized covariance matrix for the noise.

With these prior distributions on f_Δ and f_ν the parameter estimate $\hat{\theta}_N$ and $\tilde{g}(e^{j\omega T_s})$ will be Gaussian distributed as well:

$$\hat{\theta}_N \sim \mathcal{N}(\theta_0, P_\theta) \quad (11.101)$$

$$\tilde{g}(e^{j\omega T_s}) \sim \mathcal{N}(0, P_{\tilde{g}}) \quad (11.102)$$

Remember that this is still averaging over different realizations of a class of systems, from where the true system is just one realization. Consequently we will not generally expect $\hat{\theta}_N$ to converge against θ_0 for $N \rightarrow \infty$.

Equation (11.102) describes the assumed probability characteristics of the total model error for the class of systems defined. Since the true system is one such system it will constitute one event in the probability space assumed.

Since $\tilde{g}(e^{j\omega T_s})$ is zero mean Gaussian distributed with covariance $P_{\tilde{g}}$ the scalar $z(e^{j\omega T_s})$ given by:

$$z(e^{j\omega T_s}) = \tilde{g}(e^{j\omega T_s})^T P_{\tilde{g}}^{-1} \tilde{g}(e^{j\omega T_s}) \quad (11.103)$$

has χ^2 distribution with $\dim \tilde{g}(e^{j\omega T_s}) = 2$ degrees of freedom.

Equation (11.103) may thus be used to draw confidence ellipses in the complex plane for the frequency response estimate $G(e^{j\omega T_s}, \hat{\theta}_N)$ with respect to the class of true systems defined by Equation (11.1) on page 184.

The tractability of the results for the Gaussian assumptions on η and V motivates us to use the corresponding results in practice.

11.2.3 Maximum Likelihood Estimation of ζ

Equation (11.98) on the facing page may now be solved (numerically) under the given assumptions on the probability distributions and the structure of the covariance matrices. Unfortunately this may be a non-convex problem with multiple local maxima so we cannot guarantee to find the global maximum. The likelihood function of the $N - p$ data vector ϖ is equivalent to the probability density of ϖ . Since f_Δ and f_ν are assumed Gaussian the probability density of ϖ will be an $N - p$ dimensional Gaussian distribution with zero mean:

$$f(\varpi|U, \zeta) = \frac{1}{(2\pi)^{(N-p)/2}} \cdot \frac{1}{(\det \Sigma)^{1/2}} \cdot e^{-\frac{1}{2}\varpi^T \Sigma^{-1} \varpi} \quad (11.104)$$

where Σ is given by:

$$\Sigma \triangleq E \{ \varpi \varpi^T \} \quad (11.105)$$

$$= E \left\{ (R^T X \eta + R^T V) (R^T X \eta + R^T V)^T \right\} \quad (11.106)$$

$$= E \{ R^T X \eta \eta^T X^T R \} + E \{ R^T V V^T R \} \quad (11.107)$$

$$= R^T X C_\eta X^T R + R^T C_\nu R \quad (11.108)$$

with given parameterizations on C_η and C_ν . Maximizing the likelihood function is equivalent to maximizing the loglikelihood function. For computational purposes this is preferred. The loglikelihood function $\ell(\varpi|U, \zeta)$ is given by:

$$\ell(\varpi|U, \zeta) \triangleq \ln (f(\varpi|U, \zeta)) \quad (11.109)$$

$$= -\frac{N-p}{2} \ln(2\pi) - \frac{1}{2} \ln(\det \Sigma) - \frac{1}{2} \varpi^T \Sigma^{-1} \varpi \quad (11.110)$$

$$= -\frac{1}{2} \ln(\det \Sigma) - \frac{1}{2} \varpi^T \Sigma^{-1} \varpi + k \quad (11.111)$$

where $k = -\ln(2\pi)(N-p)/2$ is some constant. In Appendix G it is demonstrated how we may derive explicit expressions for the partial derivatives of $\ell(\varpi|U, \zeta)$ with respect to the elements of ζ and for the Hessian matrix. This enables us to construct numerical search algorithms for the maximum based on Marquardt's method. Such search procedures usually converge quickly and efficiently at least to a local maximum.

Assuming that the global maximum is found, it will now be possible to find the parameter vector ζ that maximizes the loglikelihood function for ϖ given the parameterizations on C_η and C_ν .

11.2.3.1 Choosing the Transformation R

The choice of R affect the singular value ratio¹ of the ϖ covariance matrix Σ . This is important since taking the loglikelihood of ϖ involves inversion of Σ , see Equation (11.111) on the page before. Consequently we must require that the singular value ratio of Σ is reasonably small. Furthermore since the determinant of Σ is the product of the eigenvalues, then if some of the eigenvalues are close to zero² then the determinant will be close to zero as well and we may have problems when taking the logarithm in Equation (11.111) on the preceding page. Consequently we will also require that the ratio of the largest eigenvalue of Σ to the smallest should be reasonably small.

We propose that R is obtained in either of the following two ways:

- as the orthonormal basis for P_Φ in (11.90) on page 195.
- through QR-factorization of Φ , see Appendix F.

Both these choices result in well balanced covariances Σ both with respect to eigenvalue and singular value ratios.

11.3 Parameterizing the Covariances

Parameterizing C_ν and C_η we may now estimate the parameters themselves as described in the previous section. Several parameterizations have been investigated.

11.3.1 Parameterizing the Noise Covariance C_ν

Two assumptions on the noise $\nu(k)$ have been investigated:

- $\nu(k)$ is assumed to be white measurement noise. This corresponds to $H(q) = 1$, see Equation (11.4) on page 185.
- $\nu(k)$ is assumed to be white noise filtered through a first order ARMA filter $H(q) = (1 + cq^{-1})/(1 + aq^{-1})$, see Equation (11.4).

¹The condition number.

²Relatively to the remaining eigenvalues.

11.3.1.1 White Noise Assumption

The white noise assumption on $\nu(k)$ is equivalent to specifying the covariance matrix for the noise as a diagonal matrix of the white noise variance σ_e^2 :

$$C_\nu(\gamma) = \sigma_e^2 \cdot I_N \quad (11.112)$$

where N is the number of measurements. The parameterization in (11.112) constitutes the simplest possible assumption on the noise, but may prove adequate in many applications.

11.3.1.2 Colored Noise Assumption

Assume that $\nu(k)$ is given by a first order ARMA model

$$\nu(k) = \frac{1 + cq^{-1}}{1 + aq^{-1}}e(k) \quad (11.113)$$

where $e(k) \in \mathcal{N}(0, \sigma_e^2)$ is white noise with variance σ_e^2 . It is then straightforward to show, see Appendix J on page 325 that the noise impulse response $h_\nu(k)$ will be given by:

$$h_\nu(k) = \begin{cases} 1 & , k = 0 \\ (-a)^{k-1}(-a + c) & , k > 0 \end{cases} \quad (11.114)$$

The corresponding noise covariance matrix $C_\nu(\gamma)$ will furthermore be given by:

$$C_\nu(i, j) = \sigma_e^2 \sum_{k=0}^{\infty} h_\nu(k)h_\nu(k + j - i) \quad (11.115)$$

$$= \begin{cases} \sigma_e^2 \left(1 + \frac{(c-a)^2}{1-a^2} \right) & , i = j \\ \frac{\sigma_e^2 (-a)^M (1 + c^2 - a * c - c/a)}{1-a^2} & , |j-i| = M \end{cases} \quad (11.116)$$

where $|\cdot|$ denotes absolute value. Other noise assumptions may be incorporated into $C_\nu(\gamma)$ e.g. if more detailed noise models are available. The computational labour for higher order noise descriptions may however be quite severe.

11.3.2 Parameterizing the Undermodeling Covariance C_η

3 different parameterizations of the undermodeling impulse response covariance have been investigated:

- A constant diagonal structure corresponding to a constant undermodeling impulse response variance.
- An exponential decaying diagonal structure corresponding to an exponentially decaying undermodeling impulse response variance.
- A non-diagonal structure corresponding to a 1st order undermodeling impulse response.

11.3.2.1 A Constant Diagonal Assumption

The simplest possible structure on the covariance matrix for the undermodeling impulse response would be a constant diagonal matrix:

$$C_\eta(\beta) = \alpha \cdot I_L \quad (11.117)$$

where L is the order of the undermodeling FIR description. The corresponding undermodeling impulse response variance is:

$$E \{ \eta^2(k) \} = \alpha \quad (11.118)$$

This corresponds for example to the assumption that 68,3% (1 standard deviation) of the undermodeling impulse responses will fall within the rectangle shown in Figure 11.1 on the facing page for $\sqrt{\alpha} = 5$ and $L = 25$.

Generally we would expect the undermodeling impulse response to decay with time. However the parameterization of C_η need not be a strict physical description. Equation (11.117) simply represents an unstructured description of the undermodeling.

Notice that the diagonal assumption on C_η causes the impulse response $\eta(k)$ to be mutually uncorrelated:

$$E \{ \eta(k) \eta(\tau) \} = 0 \quad \text{for } k \neq \tau \quad (11.119)$$

It is then easy to show that the initial estimate of the undermodeling is given by:

$$E \left\{ \left| G_\Delta(e^{j\omega T_s}) \right|^2 \right\} = \alpha \cdot L \quad (11.120)$$

Consequently the initial estimate of $\left| G_\Delta(e^{j\omega T_s}) \right|^2$ is a frequency domain stationary process. However, if the true system is strictly proper its frequency response will decay to zero at high frequencies and as a consequence, so should the absolute modeling error.

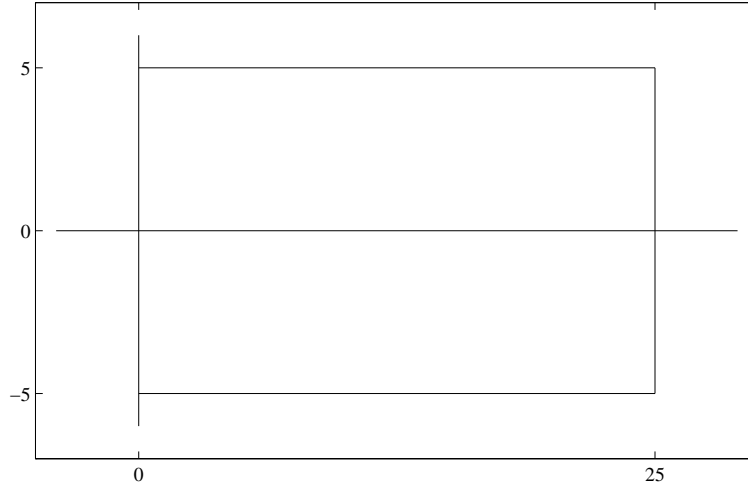


Figure 11.1: A *constant diagonal assumption on the undermodeling impulse response*. Shown are the one standard deviation borders for $\sqrt{\alpha} = 5$ and $L = 25$.

11.3.2.2 An Exponentially Decaying Assumption

Goodwin and co-workers [GGN92] proposes a diagonal structure on the covariance matrix for the undermodeling:

$$C_{\eta}(\beta) = \text{diag}_{1 \leq k \leq L} \alpha \lambda^k \quad (11.121)$$

Corresponding to the undermodeling impulse response variance:

$$E \{ \eta^2(k) \} = \alpha \lambda^k \quad (11.122)$$

This corresponds for example to the assumption that 68,3% (1 standard deviation) of the undermodeling impulse responses will fall within the rectangle shown in Figure 11.2 on the next page for $\sqrt{\alpha} = 5$, $\sqrt{\lambda} = 0.9$ and $L = 25$.

Compared with the constant undermodeling impulse response variance above we now have decaying properties on the undermodeling impulse response.

Notice however that the diagonal assumption on C_{η} still causes the impulse response $\eta(k)$ to be mutually uncorrelated:

$$E \{ \eta(k) \eta(\tau) \} = 0 \quad \text{for } k \neq \tau \quad (11.123)$$

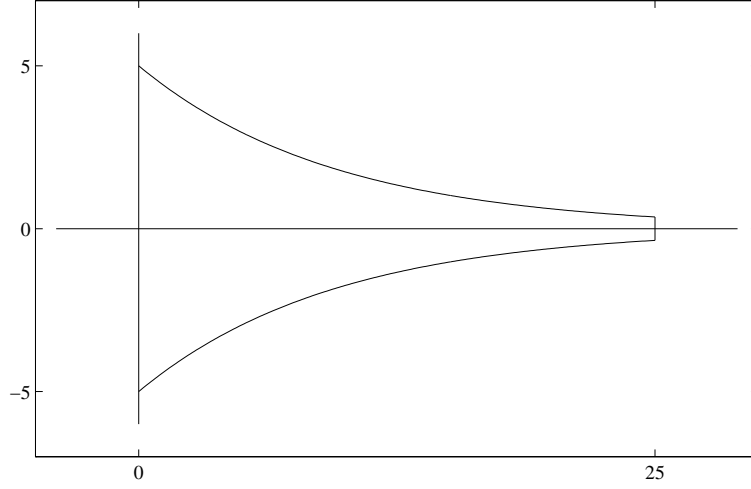


Figure 11.2: *A exponentially decaying assumption on the undermodeling impulse response. Shown are the one standard deviation borders for $\sqrt{\alpha} = 5$, $\sqrt{\lambda} = 0.9$ and $L = 25$.*

It is then easy to show that the initial estimate of the undermodeling is given by:

$$E \left\{ \left| G_{\Delta} (e^{j\omega T_s}) \right|^2 \right\} = \frac{\alpha\lambda}{1-\lambda} \quad (11.124)$$

Consequently the initial estimate of $\left| G_{\Delta} (e^{j\omega T_s}) \right|^2$ is still a frequency domain stationary process which is undesirable.

11.3.2.3 A Non-Diagonal Assumption

In order to obtain a frequency domain non-stationary initial estimate of $\left| G_{\Delta} (e^{j\omega T_s}) \right|^2$ we propose that the covariance matrix C_{η} may be parameterized as:

$$C_{\eta}(\beta) = [\alpha\lambda^0 \cdots \alpha\lambda^{L-1}]^T [\alpha\lambda^0 \cdots \alpha\lambda^{L-1}] \quad (11.125)$$

corresponding to a first order undermodeling impulse response η . Notice that the above C_{η} is singular. Thus the undermodeling impulse response $\{\eta(k)\}$ is a stochastic process with singular distribution and in fact of the form:

$$\eta(k) = a\lambda^{k-1} \quad (11.126)$$

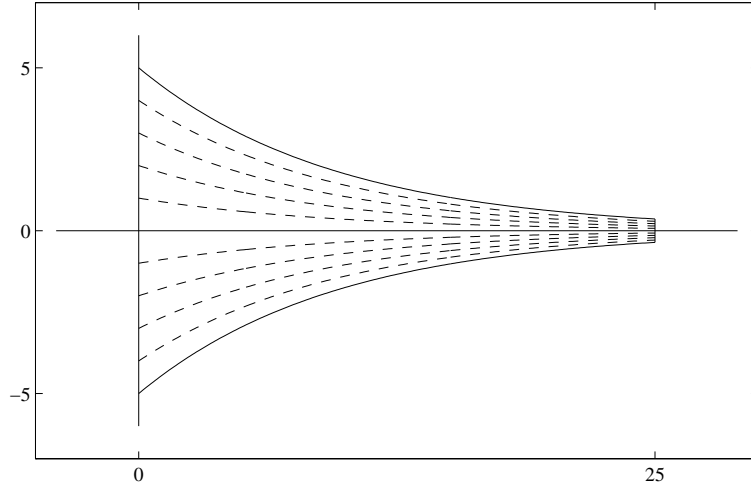


Figure 11.3: A first order decaying assumption on the undermodeling impulse response. Shown are the one standard deviation borders for $\alpha = 5$, $\lambda = 0.9$ and $L = 25$. The impulse response is smooth in precisely a first order fashion.

where $a \in \mathcal{N}(0, \alpha^2)$ and λ some fixed number. The covariance matrix for the stochastic process (11.126) on the facing page is namely given by:

$$C_\eta = E \left\{ [\eta(1), \eta(2), \dots, \eta(L)]^T [\eta(1), \eta(2), \dots, \eta(L)] \right\} \quad (11.127)$$

$$= E \left\{ [a\lambda^0, a\lambda^{-1}, \dots, a\lambda^{L-1}]^T [a\lambda^0, a\lambda^{-1}, \dots, a\lambda^{L-1}] \right\} \quad (11.128)$$

$$= E \left\{ a^2 [\lambda^0, \lambda^{-1}, \dots, \lambda^{L-1}]^T [\lambda^0, \lambda^{-1}, \dots, \lambda^{L-1}] \right\} \quad (11.129)$$

$$= E \{ a^2 \} [\lambda^0, \lambda^{-1}, \dots, \lambda^{L-1}]^T [\lambda^0, \lambda^{-1}, \dots, \lambda^{L-1}] \quad (11.130)$$

$$= \alpha^2 [\lambda^0, \lambda^{-1}, \dots, \lambda^{L-1}]^T [\lambda^0, \lambda^{-1}, \dots, \lambda^{L-1}] \quad (11.131)$$

which is the same as (11.125). Consequently every realization of η is smooth in precisely a first order fashion. This is a highly structured description of the undermodeling compared with the diagonal assumptions on $C_\eta(\beta)$. The parameterization (11.125) on the facing page corresponds for example to the assumption that 68,3% (1 standard deviation) of the undermodeling impulse responses will fall within the rectangle shown in Figure 11.3 for $\alpha = 5$, $\lambda = 0.9$ and $L = 25$.

The corresponding initial undermodeling estimate will then be given by:

$$E \left\{ |G_{\Delta}(e^{j\omega T_s})|^2 \right\} = \Pi(e^{j\omega T_s}) C_{\eta}(\beta) \Pi^T(e^{j\omega T_s}) \quad (11.132)$$

which is, in general, not frequency domain stationary. Notice that we have not increased the number of parameters.

11.3.3 Combined Covariance Structures

The different structures on the noise and undermodeling covariances may then be combined to provide 6 different parameterizations of the covariance matrices $C_{\nu}(\gamma)$ and $C_{\eta}(\beta)$.

11.4 Summary

The stochastic embedding approach for estimation of frequency domain model uncertainty was introduced. The main paradigm for the stochastic embedding approach is to assume that the undermodeling is a realization of a stochastic process. With this “technical” assumption we may extend the classical results on fixed denominator modeling to the case where no exact description of the true system exists within the model set. The expression for the parameter covariance matrix then contains two contributions: one due to the noise in the data set and one due to the undermodeling. We may furthermore derive an explicit expression for the total model error which nicely separates bias and variance contributions. In the expression for the frequency domain error bounds two covariance terms appear; one for the noise and one for the undermodeling impulse response. An estimate of these two covariances must be obtained in order to evaluate the frequency domain expression. Remember that for the classical fixed denominator approach we could quite easily obtain a non-parametric estimate of the noise covariance matrix C_{ν} from the model residuals. Unfortunately this is not the case now, since the residuals contain contributions both from the noise and the undermodeling. Instead a maximum likelihood approach is taken. If we parameterize the covariances the parameters themselves may then be estimated from the residuals. Unfortunately this approach is only tractable for small data series, see the remarks below. Two parameterizations for the noise were investigated, one corresponding to white noise and one corresponding to a first order ARMA noise model. Three parameterizations for the undermodeling were suggested corresponding to a constant undermodeling impulse response, an exponentially decaying undermodeling impulse response and finally a first order decaying undermodeling impulse response.

11.4.1 Remarks

We have only presented results for single-input single-output systems. We believe that the general stochastic embedding methodology can be straightforwardly extended to multivariable systems. However, the parameterization of the noise and undermodeling covariances and the maximum likelihood estimation of the parameters do not seem to readily fit into a multivariable framework.

The maximum likelihood estimation is also a severe bottleneck for large data series. The approach outlined here is only tractable for rather small data series (less than 300 measurements) because evaluation of the $N - p$ dimensional Gaussian distribution for the transformed residuals ϖ involves inversion of $N \times N$ matrices.

Chapter 12

Estimating Uncertainty using Stochastic Embedding

Contents

12.1 The True System	208
12.2 Error Bounds with a Classical Approach	210
12.3 Error bounds with Stochastic Embedding Approach	211
12.3.1 Case 1, A Constant Undermodeling Impulse Response	212
12.3.2 Case 2: An Exponentially Decaying Undermodeling Impulse Response	215
12.3.3 Case 3: A First Order Decaying Undermodeling Im- pulse Response.	219
12.4 Summary	222

In this chapter we will illustrate the stochastic embedding approach through a numerical example. We will estimate a second order Laguerre model from data generated by a third order system corrupted by white noise. Different parameterizations of the noise and undermodeling will then be investigated using monte-carlo experiments.

12.1 The True System

Suppose that the true system is given by:

$$G_T(s) = \frac{458}{(s+1)(s^2+30s+229)} \quad (12.1)$$

$G_T(s)$ is taken from the well-known paper by Rohrs *et al.* [RVAS85]. The system was sampled with sampling frequency 10 [Hz], the input sequence was a 0.4 [Hz] fundamental square wave and the output were corrupted by the white noise sequence:

$$\nu(k) \sim \mathcal{N}(0, 0.05) \quad (12.2)$$

200 samples were collected, 125 of which were used to get rid of initial condition effects. The last 75 samples were used for estimation. It is thus assumed that only a very limited data set is available for the identification procedure. A second order Laguerre model:

$$G(q, \theta) = \frac{\theta_1 q^{-1}}{1 + \xi q^{-1}} + \frac{\theta_2 q^{-1} (1 - \xi^{-1} q^{-1})}{(1 + \xi q^{-1})^2} \quad (12.3)$$

was fitted to the data. The Laguerre pole $-\xi$ was chosen as 0.85. The order of the FIR model for the undermodeling $G_\Delta(q)$ was chosen as $L = 20$.

The discrete-time equivalent of the true system assuming zero order holds on the input is:

$$G_T(q) = \frac{0.0370q^{-1} + 0.0717q^{-2} + 0.00785q^{-3}}{1 - 1.34q^{-1} + 0.446q^{-2} - 0.0450q^{-3}} \quad (12.4)$$

The discrete-time poles of the true system are consequently:

$$\begin{aligned} p_1 &= 0.905 \\ p_2 &= 0.219 + 0.0443j \\ p_2 &= 0.219 - 0.0443j \end{aligned} \quad (12.5)$$

The Laguerre pole is thus slightly faster than the dominant pole of the true system as usually recommended for Laguerre models.

The least squares estimate of θ averaging over 100.000 realizations of the noise was found as:

$$\theta^* \approx \hat{\theta}_{N,av} = \begin{bmatrix} 0.1079 \\ 0.0138 \end{bmatrix} \quad (12.6)$$

The estimated covariance matrix was

$$P_\theta = E \left\{ (\hat{\theta}_N - \theta^*)(\hat{\theta}_N - \theta^*)^T \right\} \quad (12.7)$$

$$= 10^{-4} \cdot \begin{bmatrix} 0.7366 & -0.0502 \\ -0.0502 & 0.0096 \end{bmatrix} \quad (12.8)$$

This corresponds nicely with the estimated covariance matrix for θ , given a fixed denominator model structure. Given the results in Section 10.3.1 \hat{P}_N is found as

$$\hat{P}_N = \Omega C_\nu \Omega^T \quad (12.9)$$

$$= 10^{-4} \cdot \begin{bmatrix} 0.7419 & -0.0505 \\ -0.0505 & 0.0096 \end{bmatrix} \quad (12.10)$$

Furthermore Ω is deterministic such that the covariance estimate (12.10) applies for any realizations of the noise. Note that \hat{P}_N is estimated from just 75 samples. Of course, we are cheating here since we assume that we know C_ν . However, we can use \hat{P}_N to evaluate the frequency domain uncertainty bounds obtained with a classic approach.

The distributions of the θ -estimate is shown in Figure 12.1. As seen the distributions correspond very nicely to the standard normal distribution as predicted by (9.33) on page 143.

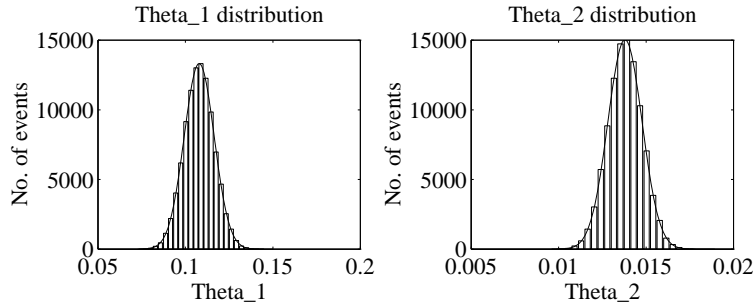


Figure 12.1: *Distribution of Laguerre model parameter estimates. Also shown are scaled normal distributions with computed mean and standard deviation.*

12.2 Error Bounds with a Classical Approach

Given a realization of the noise we may now compute frequency domain uncertainty ellipses around the estimated Nyquist. Since $G(q, \theta)$ is linear in θ we may write

$$G(q, \theta) = \Lambda(q)\theta \quad (12.11)$$

where $\Lambda(q)$ for the present example is given by

$$\Lambda(q) = \begin{bmatrix} \frac{q^{-1}}{1 + \xi q^{-1}} & \frac{q^{-1}(1 - \xi^{-1}q^{-1})}{1 + 2\xi q^{-1} + \xi^2 q^{-2}} \end{bmatrix} \quad (12.12)$$

Then $\tilde{g}(e^{j\omega T_s})$ defined as before

$$\tilde{g}(e^{j\omega T_s}) = \begin{bmatrix} \Re \left\{ G(e^{j\omega T_s}, \theta^*) - G(e^{j\omega T_s}, \hat{\theta}_N) \right\} \\ \Im \left\{ G(e^{j\omega T_s}, \theta^*) - G(e^{j\omega T_s}, \hat{\theta}_N) \right\} \end{bmatrix} \quad (12.13)$$

will be given by

$$\tilde{g}(e^{j\omega T_s}) = \Lambda(e^{j\omega T_s}) (\theta^* - \hat{\theta}_N) \quad (12.14)$$

Under our standard assumptions, $\tilde{g}(e^{j\omega T_s})$ will be normal distributed with covariance $P_{\tilde{g}}(\omega)$:

$$\tilde{g}(e^{j\omega T_s}) \in \mathcal{N}(0, P_{\tilde{g}}(\omega)) \quad (12.15)$$

where $P_{\tilde{g}}(\omega)$ is given by

$$P_{\tilde{g}}(\omega) = \Lambda(e^{j\omega T_s}) P_{\theta} \Lambda^T(e^{j\omega T_s}) \quad (12.16)$$

Thus the scalar

$$z(\omega) = \tilde{g}^T(e^{j\omega T_s}) [\Lambda(e^{j\omega T_s}) P_{\theta} \Lambda^T(e^{j\omega T_s})]^{-1} \tilde{g}(e^{j\omega T_s}) \quad (12.17)$$

will have χ^2 distribution with 2 degrees of freedom and may be used to draw confidence ellipses in the complex plane for the frequency response estimate $G(e^{j\omega T_s}, \hat{\theta}_N)$. Notice, however, that $G(q, \theta^*)$ does not represent the true system $G_T(q)$ due to undermodeling. Thus we will expect the estimated error bounds to be inaccurate.

Given a particular realization of the noise $\nu(k)$, the least squares estimate for θ was found as

$$\hat{\theta}_N = \begin{bmatrix} 0.1092 \\ 0.0143 \end{bmatrix} \quad (12.18)$$

In Figure 12.2 the true and predicted output is given. Furthermore, the true and estimated Nyquist are compared. Uncertainty ellipses corresponding to 2 standard deviations are shown superimposed on the estimated frequency response. Whilst the estimated uncertainty in the low frequency range corresponds well to the true Nyquist curve, notice how the correspondence vanishes in the high frequency area. If a controller design was based on the illustrated uncertainty estimates, the robustness to high frequency model uncertainty could very well be quite small.

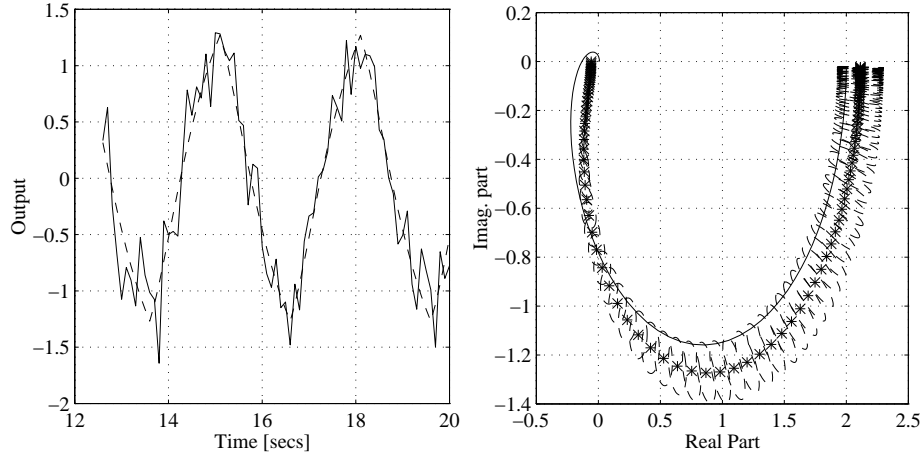


Figure 12.2: *Results from classical identification on Rohrs Counterexample. On the left are true and estimated output and on the right are true and estimated Nyquist with error bounds.*

In the next section we will use stochastic embedding of the bias in order to improve the classical error bounds.

12.3 Error bounds with Stochastic Embedding Approach

Estimating the total model error, the probability density functions for the noise and the undermodeling shall be identified. The parameterization of the noise was chosen as in (11.112) on page 199 corresponding to white measurement noise. The 3 different parameterizations of the undermodeling presented in Section 11.3.2

were investigated. The transformation matrix R was chosen through QR factorization of Φ as outlined in Section 11.2.3.1 on page 198. The loglikelihood function $\ell(\varpi|U, \zeta)$ was maximized using a Marquardt search algorithm.

12.3.1 Case 1, A Constant Undermodeling Impulse Response

First the undermodeling parameterization (11.117) on page 200 corresponding to a constant undermodeling impulse response variance will be investigated. The parameter vector ζ is consequently given by:

$$\zeta = \begin{bmatrix} \alpha \\ \sigma_e^2 \end{bmatrix} \quad (12.19)$$

1000 realizations of the process noise $\nu(k)$ were processed. 702 of the 1000 search procedures converged. The remainder mainly approached $[0, \sigma_e^2]$ corresponding to zero uncertainty¹.

The convergent estimates of ζ is displayed in Figure 12.3 together with the maximum values of $\ell(\varpi|U, \zeta)$.

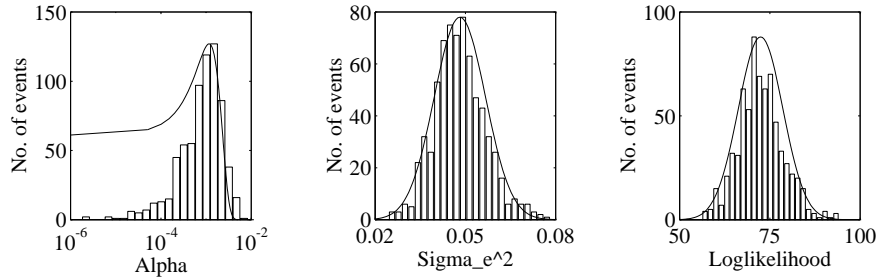


Figure 12.3: *Case 1: Montecarlo testing of the maximum likelihood estimation of ζ . 1000 realizations of $\nu(k)$ were investigated, 702 converged. Shown are histograms for α , σ_e^2 and $\max\{\ell(\varpi|U, \zeta)\}$ together with the corresponding scaled normal distributions.*

The mean value and standard deviation on ζ was estimated as:

$$\hat{\zeta}_N = \begin{bmatrix} 1.165 \cdot 10^{-3} \\ 4.816 \cdot 10^{-2} \end{bmatrix} \quad (12.20)$$

¹Notice that $\alpha < 0$ corresponds to a negative definite covariance matrix for the undermodeling. Consequently a lower bound of 10^{-10} was enforced on α .

$$\hat{\sigma}_\zeta = \begin{bmatrix} 0.963 \cdot 10^{-3} \\ 0.851 \cdot 10^{-2} \end{bmatrix} \quad (12.21)$$

In Figure 12.3 also scaled normal distributions corresponding to the estimated means and standard deviations are shown. We have not made any assumptions with regard to the distribution of ζ . However, if ζ is normal distributed, we would expect the estimation procedure to be in some sense “well-conditioned”. Notice that the α -estimate is not normal distributed whereas both σ_e^2 and the loglikelihood $\ell(\varpi|U, \zeta)$ corresponds well to a normal distribution. Notice also that an accurate estimate of the noise variance $\sigma_e^2 = 0.05$ is obtained. The loglikelihood mean was found to be:

$$\mu_{\max\{\ell(\varpi|U, \zeta)\}} = 72.43 \quad (12.22)$$

Now let us consider a particular realization of the noise. We will use the same realization as in Section 12.2 on page 210. The corresponding estimate of ζ was found as:

$$\hat{\zeta} = \begin{bmatrix} \alpha \\ \sigma_e^2 \end{bmatrix} = \begin{bmatrix} 2.365 \cdot 10^{-3} \\ 5.830 \cdot 10^{-2} \end{bmatrix} \quad (12.23)$$

Notice that this realization is representative with respect to ζ , see Figure 12.3 on the facing page.

The results of the uncertainty estimation is displayed in Figure 12.4 on the next page and 12.5 on page 215. Notice from Figure 12.4 that a reasonable uncertainty estimate is obtained through this simple parameterization of the noise and undermodeling. The uncertainty estimate is slightly conservative and with little phase information in the high frequency area. Small uncertainty is correctly predicted around the fundamental frequency of the square wave input. In Figure 12.5 the different contributions to the error estimate is shown. Recall from Equation (11.86) on page 192 that the total model error estimate is given by:

$$\begin{aligned} E \left\{ \left| G \left(e^{j\omega T_s}, \hat{\theta}_N \right) - G_T \left(e^{j\omega T_s} \right) \right|^2 \right\} \\ = (\Pi - \Lambda \Omega X) C_\eta (\Pi - \Lambda \Omega X)^* + \Lambda \Omega C_\nu \Omega^T \Lambda^* \end{aligned} \quad (12.24)$$

$$\begin{aligned} = \Pi C_\eta \Pi^* + \Lambda \Omega X C_\eta X^T \Omega^T \Lambda^* - \Lambda \Omega X C_\eta \Pi^* - \\ \Pi C_\eta X^T \Omega^T \Lambda^* + \Lambda \Omega C_\nu \Omega^T \Lambda^* \end{aligned} \quad (12.25)$$

The components of (12.25) will be denoted as follows:

- A priori estimate: $\Pi C_\eta \Pi^*$.
- Data induced term: $\Lambda \Omega X C_\eta X^T \Omega^T \Lambda^*$.

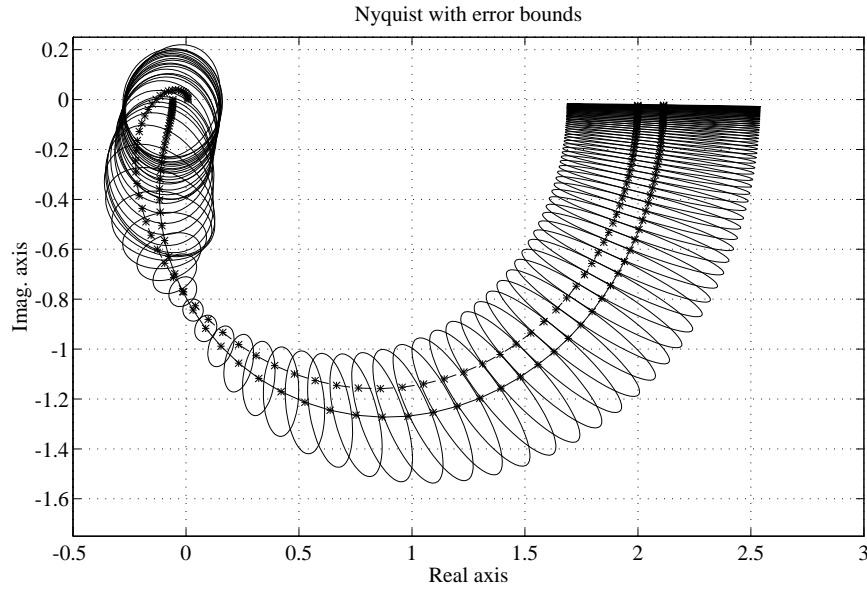


Figure 12.4: *Case 1: Nominal Nyquist (solid) with 1 std. deviation error bounds. Also shown is the true Nyquist (dashed). Each frequency point is marked (*) to provide insight in the quality of the uncertainty estimates.*

- Cross terms: $\Lambda \Omega X C_\eta \Pi^* + \Pi C_\eta X^T \Omega^T \Lambda^*$.
- Noise term: $\Lambda \Omega C_\nu \Omega^T \Lambda^*$.

From Figure 12.5 on the facing page the following observations may be made:

A priori estimate. The frequency response of the a priori estimate is independent of frequency. This is due to the simple parameterization of the undermodeling, see Section 11.3.2.1 on page 200. The total model error estimate converges to the a priori estimate as the frequency ω approaches the Nyquist frequency π/T_s .

Data induced and noise term. Both terms predicts smoothly decaying model error. Notice that even though the data seems rather noisy, see Figure 12.2 on page 211, the noise contribution to the total model error is very small compared with the bias terms.

Cross terms. These terms provide the “shaping” of the otherwise very smooth

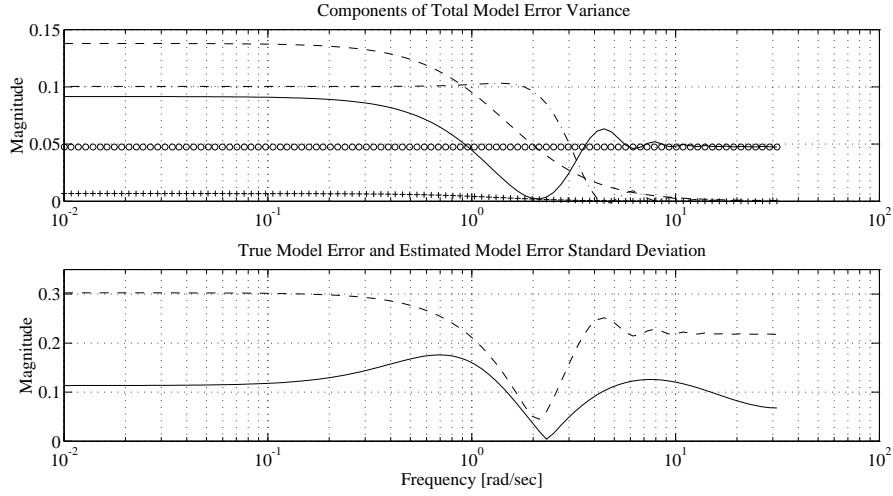


Figure 12.5: *Case 1: Total model error components and comparison with true model error. Upper: The total model error (solid), a priori estimate (o), data induced term (dashed), cross terms (dash-dotted) and noise term (+). Lower: True model error (solid) and estimated total model error standard deviation (dashed).*

error estimate. They represent a mixture of a priori information and data induced knowledge and seem to be somewhat difficult to interpret.

The comparison of the true model error magnitude with the estimated model error standard deviation provides another mean of assessing the performance of the uncertainty estimate. As seen from Figure 12.5 there is reasonable agreement between the true model error and the estimate although the error estimate is somewhat conservative.

12.3.2 Case 2: An Exponentially Decaying Undermodeling Impulse Response

Now the undermodeling parameterization (11.121) on page 201 corresponding to an exponentially decaying undermodeling impulse response variance will be investigated. The parameter vector ζ is consequently given by:

$$\zeta = \begin{bmatrix} \alpha \\ \lambda \\ \sigma_e^2 \end{bmatrix} \quad (12.26)$$

Again 1000 realizations of the noise $\nu(k)$ were processed. This time however, only 429 converged. The convergence hit-rate for this undermodeling parameterization is consequently considerably lower than for the constant undermodeling impulse response parameterization examined in the previous section. 241 realizations did not converge due to the lower bound on α , see footnote (1) on page 212. The remaining realizations diverged.

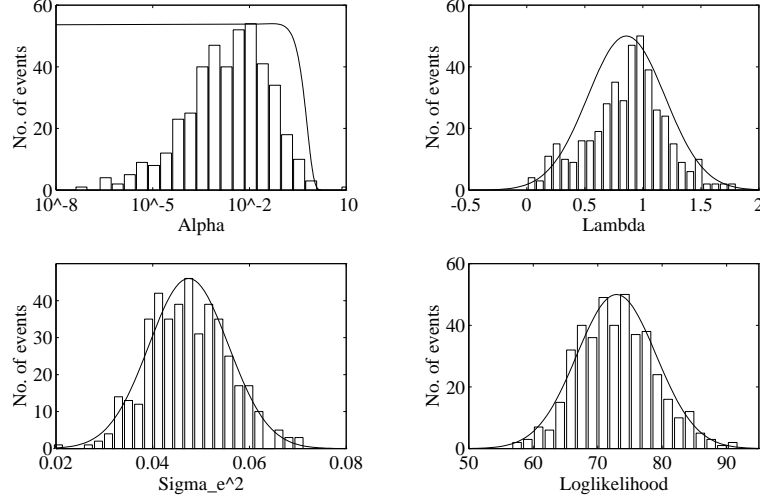


Figure 12.6: *Case 2: Montecarlo testing of the maximum likelihood estimation of ζ . 1000 realizations of $\nu(k)$ were investigated, 429 converged. Shown are histograms for α , λ , σ_e^2 and $\max\{\ell(\varpi|U, \zeta)\}$ together with the corresponding scaled normal distributions.*

The convergent estimates of ζ is displayed in Figure 12.6 together with the maximum values of $\ell(\varpi|U, \zeta)$. The mean value and standard deviation on ζ were estimated as:

$$\hat{\zeta}_N = \begin{bmatrix} 4.830 \cdot 10^{-2} \\ 8.581 \cdot 10^{-1} \\ 4.744 \cdot 10^{-2} \end{bmatrix} \quad (12.27)$$

$$\hat{\sigma}_\zeta = \begin{bmatrix} 41.12 \cdot 10^{-2} \\ 3.336 \cdot 10^{-1} \\ 0.824 \cdot 10^{-2} \end{bmatrix} \quad (12.28)$$

The corresponding normal distributions are also shown in Figure 12.6. Notice that approximately half of the realizations converged to $\lambda > 1$ corresponding to

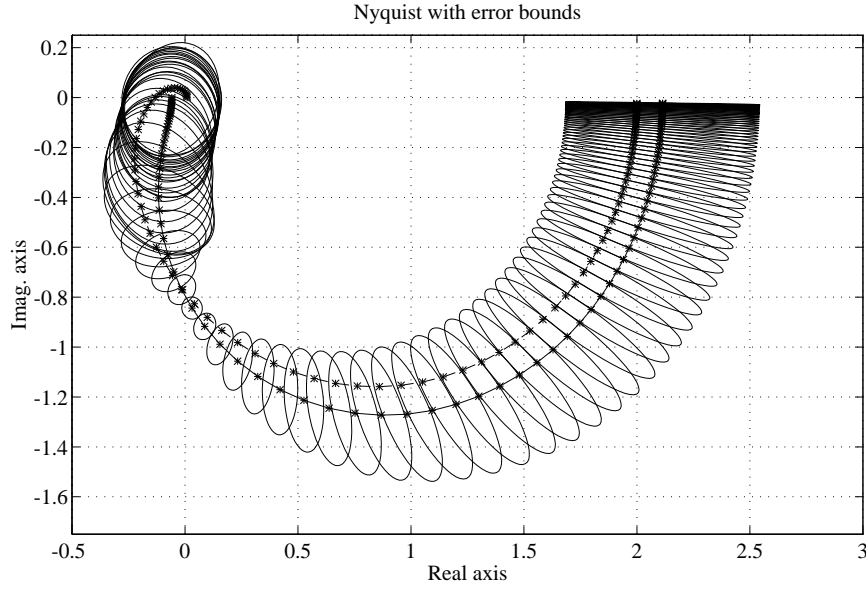


Figure 12.7: *Case 2: Nominal Nyquist (solid) with 1 std. deviation error bounds. Also shown is the true Nyquist (dashed). Each frequency point is marked (*) to provide insight in the quality of the uncertainty estimates.*

an exponentially rising undermodeling impulse response. This is equivalent to an unstable transfer function $G_{\Delta}(q)$ for an infinite impulse sequence. However since only 20 samples of the impulse response is used as approximation for $G_{\Delta}(q)$ this is generally not the case here.

Notice that the estimate of the noise variance σ_e^2 again corresponds nicely with the true value. The loglikelihood mean was found to be:

$$\mu_{\max\{\ell(\varpi|U,\zeta)\}} = 72.91 \quad (12.29)$$

that is, slightly better than for the undermodeling parameterization in Section 12.3.1 on page 212.

We now turn to the particular realization of the process noise introduced above. The corresponding estimate of ζ was determined as:

$$\hat{\zeta} = \begin{bmatrix} \alpha \\ \lambda \\ \sigma_e^2 \end{bmatrix} = \begin{bmatrix} 2.282 \cdot 10^{-3} \\ 1.0035 \\ 5.830 \cdot 10^{-2} \end{bmatrix} \quad (12.30)$$

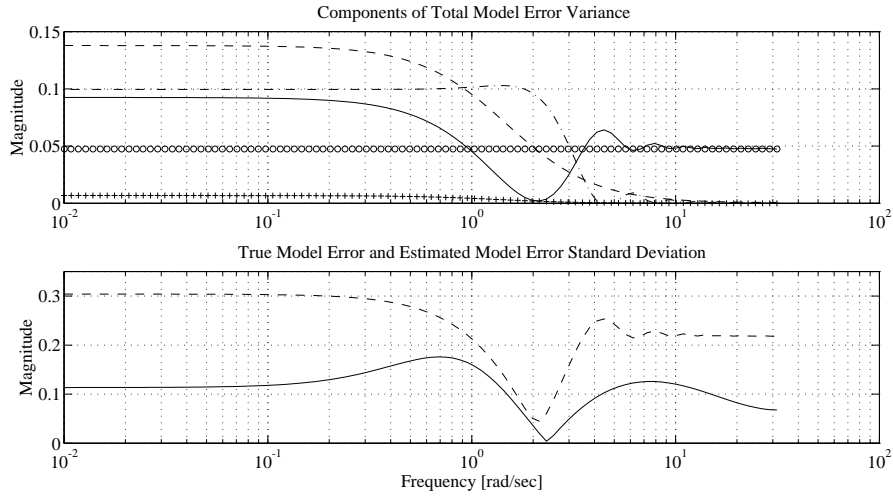


Figure 12.8: *Case 2: Total model error components and comparison with true model error. Upper: The total model error (solid), a priori estimate (o), data induced term (dashed), cross terms (dash-dotted) and noise term (+). Lower: True model error (solid) and estimated total model error standard deviation (dashed).*

The results of the uncertainty estimation is displayed in Figure 12.7 on the page before and 12.8. Notice that the uncertainty estimate presented in Figure 12.7 is almost exactly identical to the estimate in Section 12.3.1, see Figure 12.4 on page 214. This is not surprising since $\lambda \approx 1$ and the estimates of α and σ_e^2 are very similar, compare Equation (12.30) and (12.23).

The different components of the total model error, see Figure 12.8, are also almost identical with the results from Section 12.3.1 and hence the conclusions presented there also apply for the current parameterization of the undermodeling. The additional parameter λ introduced in the exponentially decaying parameterization of the undermodeling consequently is of little use in the current example. Furthermore the convergence rate of exponentially decaying parameterization of the undermodeling was rather poor compared with the simple constant parameterization introduced in Case 1.

12.3.3 Case 3: A First Order Decaying Undermodeling Impulse Response.

Finally the undermodeling parameterization (11.125) on page 202 corresponding to a 1st order decaying undermodeling impulse response will be investigated. The parameter vector is still given by (12.26) on page 215 and again 1000 realizations of the noise were processed. This time 773 of the realizations converged; the highest hit-rate of the three different undermodeling parameterizations. The remaining maximizations collided with the lower bound on α .

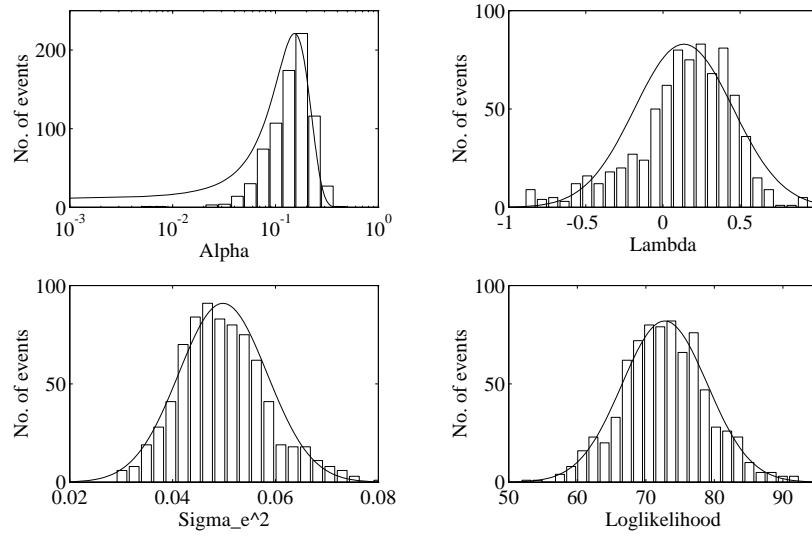


Figure 12.9: *Case 3: Montecarlo testing of the maximum likelihood estimation of ζ . 1000 realizations of $\nu(k)$ were investigated, 773 converged. Shown are histograms for α , λ , σ_e^2 and $\max\{\ell(\varpi|U, \zeta)\}$ together with the corresponding scaled normal distributions.*

The resulting estimates of ζ is displayed in Figure 12.9 together with the achieved loglikelihood of ϖ and the computed normal distributions. The mean and standard deviation of ζ were found as:

$$\hat{\zeta}_N = \begin{bmatrix} 1.533 \cdot 10^{-1} \\ 1.357 \cdot 10^{-1} \\ 4.979 \cdot 10^{-2} \end{bmatrix} \quad (12.31)$$

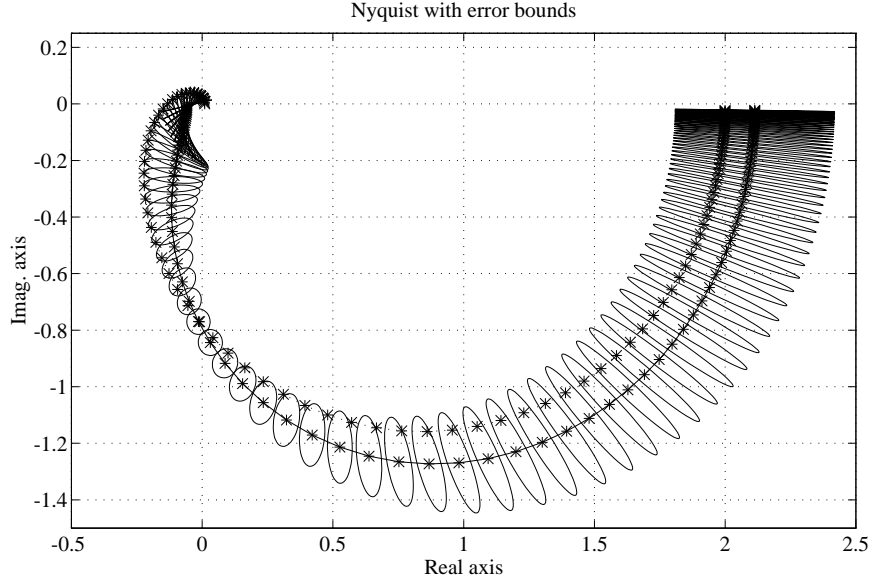


Figure 12.10: *Case 3: Nominal Nyquist (solid) with 1 std. deviation error bounds. Also shown is the true Nyquist (dashed). Each frequency point is marked (*) to provide insight in the quality of the uncertainty estimates.*

$$\hat{\sigma}_{\zeta} = \begin{bmatrix} 0.629 \cdot 10^{-1} \\ 3.193 \cdot 10^{-1} \\ 0.861 \cdot 10^{-2} \end{bmatrix} \quad (12.32)$$

Notice that the spread of λ is rather large, specifically λ takes negative values corresponding to that neighbor points in the undermodeling impulse response have different signs. This is a somewhat odd interpretation but does not violate our identification scheme since the covariance $C_{\eta}(\alpha, \lambda)$ is still positive definite.

Again a fine estimate of the noise covariance is obtained. The mean value of the obtainable loglikelihood was:

$$\mu_{\max\{\ell(\varpi|U, \zeta)\}} = 72.75 \quad (12.33)$$

that is, close to the means for the two other undermodeling parameterizations. It may consequently be concluded that level of the performance surfaces for the different parameterizations of the undermodeling are quite similar. For a given input-output realization, a considerable difference in the obtainable loglikelihood

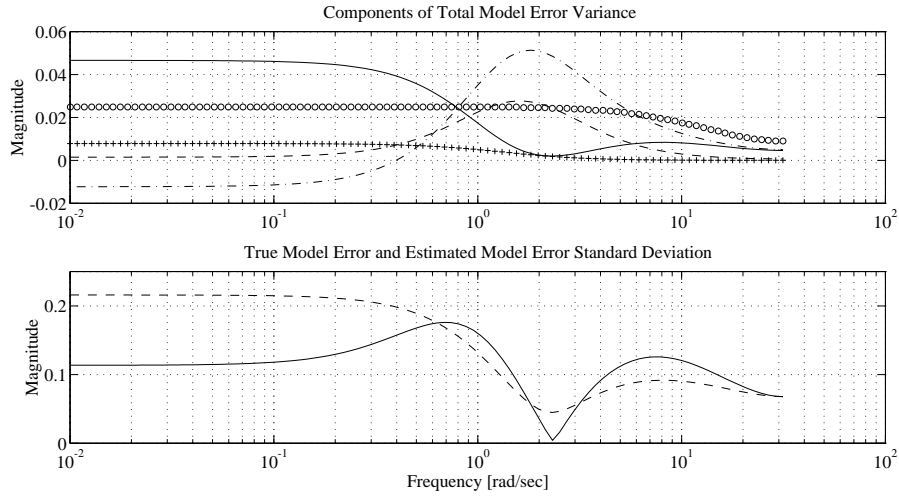


Figure 12.11: *Case 3: Total model error components and comparison with true model error. Upper: The total model error (solid), a priori estimate (o), data induced term (dashed), cross terms (dash-dotted) and noise term (+). Lower: True model error (solid) and estimated total model error standard deviation (dashed).*

may be used to distinguish and classify the goodness of different noise and undermodeling parameterizations.

The results of the uncertainty estimate for the particular realization discussed before is displayed in Figure 12.10 and 12.11. The corresponding estimate of ζ was found to be:

$$\hat{\zeta} = \begin{bmatrix} \alpha \\ \lambda \\ \sigma_e^2 \end{bmatrix} = \begin{bmatrix} 1.182 \cdot 10^{-1} \\ 2.523 \cdot 10^{-1} \\ 6.769 \cdot 10^{-2} \end{bmatrix} \quad (12.34)$$

Now the uncertainty estimate is considerably improved compared with the previous estimates. It is less conservative and the phase information of the error estimates have substantially improved. Furthermore notice from Figure 12.11 that the a priori estimate $\Pi C_\eta \Pi$ is now decaying with frequency. The data induced term $\Lambda \Omega X C_\eta X^T \Omega^T \Lambda^*$ is concentrated around the fundamental frequency of the input square wave, where the information in the data is large. The noise contribution is of approximately similar size as in connection with the previous undermodeling parameterizations. However the noise part of the total model error is now greater since the uncertainty estimate is less conservative.

12.4 Summary

Estimation of model uncertainty was performed for a second order Laguerre model applied in connection with a third order true system. From the above presented results the following conclusions were drawn:

- The estimated uncertainty regions using a classical approach and a second order Laguerre representation did not capture the true model uncertainty in the high frequency area.
- The estimated uncertainty regions using the stochastic embedding approach gave a fair indication of the model uncertainty, especially for the first order undermodeling impulse response parameterization.
- The maximum likelihood identification of the parameters in the noise and undermodeling covariance matrices converged for 70%, 43% and 77% of the noise realizations for the constant, exponentially decaying and 1st order decaying parameterizations of the undermodeling respectively. For the exponentially decaying parameterization, this is not satisfactory.
- The variance of the maximum likelihood estimate of ζ was rather high for all three parameterizations of the undermodeling.
- The covariance σ_e^2 of the measurement noise was accurately predicted for all three undermodeling parameterizations.
- The uncertainty around the fundamental frequency of the input square wave was correctly predicted to be small.

Generally speaking, the stochastic embedding method produced reliable uncertainty estimates, but the “robustness”² of the method seems somewhat poor. The problem is probably that the performance surface for the maximum likelihood estimate is rather shallow due to the small number of measurements. As noted in Section 11.4.1 on page 205 the maximum likelihood procedure unfortunately becomes intractable for large data series.

²By robustness we here mean the probability of finding the global maximum in the maximum likelihood search for ζ .

Part III

A Synergistic Control Systems Design Philosophy

Chapter 13

Combining System Identification and Robust Control

Contents

13.1 System Identification for Robust Control	226
13.1.1 Bias and Variance Errors	227
13.1.2 What Can We Do with Classical Techniques	227
13.1.3 The Stochastic Embedding Approach	230
13.1.4 Proposed Approach	231
13.2 Robust Control from System Identification	231
13.2.1 The \mathcal{H}_∞ Approach	232
13.2.2 The Complex μ Approach	235
13.2.3 The Mixed μ Approach	236
13.3 A Synergistic Approach to Identification Based Control	239
13.4 Summary	241

So far we have mainly considered robust control and system identification independently. This reflects the traditional segregation of the two fields within the automatic control community. In this part of the thesis we will suggest various schemes which combines the results from robust control presented in Part I with the results from system identification presented in Part II. The presentation will fall naturally into three parts. Section 13.1 summarizes the presented results on estimation of frequency domain model error bounds. Section 13.2 discusses how frequency domain uncertainty ellipses may be represented in a robust control framework and finally Section 13.3 addresses the question of posing an identification based robust control design strategy; the main result of this thesis. In the next chapter we will provide an example to illustrate the proposed design philosophy.

13.1 System Identification for Robust Control

When we use system identification for robust control we generally have two aims. The first aim, of course, is to obtain a useful description of the system. By the term useful we emphasize that this description is aimed at subsequent use for control design. Thus it need not be a very accurate detailed model which is valid throughout the entire physical envelope of the system. Rather it should be a reasonable simple model which is valid (that is, describes the real system as accurately as “necessary”) in the vicinity of the normal operating point of the system. The second aim using system identification for robust control is to get an estimate of the model quality. In fact, in many practical control designs, we would rather have a simple low-order model together with a quantification of the involved model uncertainty than a high-order very accurate model with very little uncertainty. The reason for this is that the order of the controller, using most modern control design methods, equals at least that of the generalized plant. Implementation of high-order controllers can be quite difficult, e.g. due to numerics, available memory etc.. Since we may often overbound the uncertainty of a simple model with a simple first or second order perturbation models, we can usually obtain low-order controllers for simple plant models.

Increasing performance demands will necessitate decreasing uncertainty levels and thus more accurate descriptions of the plant. Consequently it is in some sense the desired closed loop performance which determine the degree of accurateness with which we must know the plant. The robust control approach provides the designer with the opportunity of weighing out robustness and performance demands.

13.1.1 Bias and Variance Errors

Let us recapitulate what we mean by bias errors and variance errors. Decompose, at each frequency point, the total model error as

$$G_T(e^{j\omega T_s}) - G(e^{j\omega T_s}, \hat{\theta}_N) = G_T(e^{j\omega T_s}) - G(e^{j\omega T_s}, \theta^*) + G(e^{j\omega T_s}, \theta^*) - G(e^{j\omega T_s}, \hat{\theta}_N) \quad (13.1)$$

where θ^* denotes the asymptotic (for $N \rightarrow \infty$) estimate of θ as before. The first contribution $G_T(e^{j\omega T_s}) - G(e^{j\omega T_s}, \theta^*)$ is denoted the *bias error*. The bias error is a deterministic quantity. Clearly it is non-zero, at least at some frequencies, unless there exists a parameter vector θ^* such that $G_T(q) = G(q, \theta^*)$. If so $\theta_0 = \theta^*$ is denoted the true parameter vector. The second contribution $G(e^{j\omega T_s}, \theta^*) - G(e^{j\omega T_s}, \hat{\theta}_N)$ is denoted the *variance error*. The variance error is a random variable with respect to the probability space of the noise distribution. It vanishes when there is no noise or when the number of data tends to infinity.

13.1.2 What Can We Do with Classical Techniques

In Table 13.1 on the following page we have summarized some of the results on classical system identification presented in Chapter 9 and 10.

There is a few points we would like to emphasize:

- Local minima in the performance surface $V_N(\theta, Z^N)$ can be a severe problem if the parameter estimate cannot be found analytically, e.g. for the general PEM model and for output error (OE) models. This is of course especially true when the number of estimated parameters gets large. Various approaches can be made to circumvent this problem. The most obvious way is to repeat the minimization procedure (e.g. the Marquardt search) with different initial conditions. Alternatively, having determined a (local) minimum, we may step away from it again in such a way that the predictor is still stable and observe whether it will return to the same minimum. Different minima may of course be compared by the corresponding values of $V_N(\theta, Z^N)$.
- Clearly the data estimate \hat{P}_N of the parameter covariance matrix P_θ must be consistent: that is, converge for $N \rightarrow \infty$, if we are to obtain a proper estimate of the frequency domain model uncertainty $\tilde{g}(e^{j\omega T_s})$.
- To obtain a consistent estimate of the parameter covariance matrix P_θ for the general PEM structure we must assume that both the deterministic and the stochastic part of the true system can be represented within our

	Model structure				Fixed denominator
	PEM	ARX	OE		
Predictor	non-linear in θ	linear in θ	non-linear in θ		linear in θ
Least squares estimate	numeric	analytic	numeric		analytic
Regressor $\phi(k, \theta)$	stochastic	stochastic	deterministic		deterministic
Model gradient $\psi(k, \theta)$	stochastic	stochastic	deterministic		deterministic
\hat{P}_N consistent if	$G_T(q) = G(q, \theta_0)$ $H_T(q) = H(q, \theta_0)$	$G_T(q) = G(q, \theta_0)$ $H_T(q) = H(q, \theta_0)$	$G_T(q) = G(q, \theta_0)$		always
Expression for $\tilde{g}(e^{j\omega T_s})$	1st order Taylor	1st order Taylor	1st order Taylor		exact
Model validation	residuals $\epsilon(k, \hat{\theta}_N)$ = white noise ?	residuals $\epsilon(k, \hat{\theta}_N)$ = white noise ?	$u(k)$ and $\epsilon(k, \hat{\theta}_N)$ correlated ?		$u(k)$ and $\epsilon(k, \hat{\theta}_N)$ correlated ?

Table 13.1: Some properties of classical system identification techniques.

model set. Thus we need a complete description of the true system. Of course, due to e.g. non-linear effects this is often (always) impossible in practice. However, using high-order descriptions we can usually obtain a quite accurate model at least around a specified working point. This, however, implies that many parameters must be estimated in the identification procedure. In order to perform this estimation with adequate accuracy a large data set will be needed, usually several thousand measurements.

We can check the model quality by white noise analysis of the residuals $\{\epsilon(k, \hat{\theta}_N)\}$. However, as illustrated by the wind-turbine example in Section 9.6 on page 150, if we use high-order noise filters some parts of the output $y(k)$ which are truly due to the deterministic part of the system $G_T(q)$ may be explained by filtered white noise and thus represented in the noise filters. The residual tests were not capable of rejecting the hypothesis that the residuals were not white. This situation usually occur when the excitation in the input in the given frequency range is too small.

- The above applies for ARX models as well.
- With the output error model a consistent estimate of the covariance matrix P_θ can be obtained if the true deterministic system $G_T(q)$ can be represented within the model set $G(q, \theta)$. Thus we need not an exact description of the noise filter. The estimate for P_θ is then given by

$$\hat{P}_N = N (\Psi_N^T \Psi_N)^{-1} \Psi_N^T C_\nu \Psi_N (\Psi_N^T \Psi_N)^{-1} \quad (13.2)$$

where C_ν is the covariance matrix for the noise $\nu(k) = H_T(q)\epsilon(k)$ and $\Psi_N = \Psi(\hat{\theta}_N, Z^N)$ is the model gradient matrix, see Section 10.2.1 on page 170. Assuming that $\{\nu(k)\}$ is a stationary stochastic process we may estimate C_ν from the residuals as described on page 170. This makes the output error approach an appealing method for estimation of model uncertainty. One difficulty is that the parameter estimate $\hat{\theta}_N$ cannot be obtained analytically. Another problem might be that the uncertainty regions gets too large since we are not trying to use knowledge of the noise filter $H(q)$ to reduce the error bounds. However, this will partly be weighed out by the need for identifying additional parameters.

We may use cross-correlation analysis between the input $\{u(k)\}$ and the residuals $\{\epsilon(k, \hat{\theta}_N)\}$ to evaluate whether the structure on $G(q, \theta)$ is sufficient to describe the real system.

- With a fixed denominator model structure a consistent estimate of the parameter covariance P_θ can always be obtained since the estimate on page 172

$$\hat{P}_N = N (\Phi^T \Phi)^{-1} \Phi^T C_\nu \Phi (\Phi^T \Phi)^{-1} \quad (13.3)$$

will work even in the case of undermodeling and with finite data. Thus fixed denominator models seem an obvious choice for system identification for robust control. However, if $G_T(q) \neq G(q, \theta^*)$ then the parameter covariance will only reflect the variance part of the total model error, see (13.1) on page 227. Thus it must generally be assumed that the bias part of the error is zero; thus that the true deterministic system can be represented within the model set. From a traditional point of view this is unrealistic, even if the true system is stable and FDLTI, since we have a fixed denominator structure such that the poles of the system is determined prior to the identification procedure. However, if the basis functions $\Lambda_k(q)$, $k = 1, 2, \dots$ forms an orthonormal basis in $\mathcal{H}_2^*(\mathbf{C}, \mathbf{C})$, by taking the order n of the model high enough we can make the error arbitrarily small.

13.1.3 The Stochastic Embedding Approach

The stochastic embedding approach is treated in Chapter 11. The key idea is to treat the bias error as if it was a stochastic process. This is done by decomposing the true system as

$$G_T(q) = G(q, \theta_0) + G_\Delta(q) \quad (13.4)$$

and assuming that the undermodeling frequency response $G_\Delta(e^{j\omega T_s})$ is a realization of a stochastic process with zero mean

$$E \{G_\Delta(e^{j\omega T_s})\} = 0 \quad (13.5)$$

where $E \{\cdot\}$ means expectation over different realizations of the undermodeling. Then if we use a fixed denominator model structure for $G(q, \theta)$ we may extend the results reviewed above on fixed denominator models to the situation where undermodeling is present. The parameter covariance then becomes

$$P_\theta = N (\Phi^T \Phi)^{-1} \Phi^T (X C_\eta X^T + C_\nu) \Phi (\Phi^T \Phi)^{-1} \quad (13.6)$$

where X is given by (11.26) on page 187 and C_η is the covariance matrix for the undermodeling impulse response vector

$$C_\eta = E \{\eta \eta^T\} \quad (13.7)$$

Compare (13.3) and (13.6). It is seen that the noise contribution to the parameter covariance for the stochastic embedding approach equals the classical covariance result for the fixed denominator structure. However, (13.6) also contains a contribution from the bias. Assuming that the undermodeling impulse response is zero mean Gaussian distributed we may map the parameter covariance into the

frequency domain using a similar approach to the classical one with due attention to extra terms, see Section 11.2.2 on page 196.

As for the classical fixed denominator case we then need an estimate of the covariance matrices for the undermodeling C_η and noise C_ν . Again we will use the residuals to estimate C_ν and C_η . However, since we cannot readily separate the bias and variance contributions it becomes more complicated for the stochastic embedding approach. Fortunately, it turns out, that if we parameterize C_η and C_ν we may estimate the parameters through maximum likelihood methods. The drawback of this approach is that it is only numerically efficient for small data series (< 300 data points). Thus currently, the stochastic embedding approach is only tractable for small data series.

The stochastic embedding approach can be viewed as an extension of the classical results on fixed denominator model structures to the case where $G(q, \theta)$ cannot provide a correct description of the true system.

13.1.4 Proposed Approach

The approach we will propose for identification of frequency domain error bounds is twofold:

- If large data series are available it is recommended that the classical output error approach is used. Since we have a large number of measurements we may use quite high-order estimates $G(q, \theta)$ with reasonable little variance. A noise covariance estimate for computing the parameter covariance can be obtained from the residuals. Note that we will not obtain a parameterized model for the noise filter $H_T(q)$ in this case. If the main purpose of the subsequent control design is disturbance attenuation it is sometimes desirable to include an input weight on the noise (this is the weight denoted W_{p1} in Section 4.2 on page 36). The obvious choice for this weight is then (an approximation to) the estimated noise filter $H(q, \theta)$. In that case the general PEM approach could be an alternative.
- If small data series are available we recommend that the stochastic embedding approach is used to estimate the model error. Different parameterizations for the undermodeling and the noise covariances should be investigated.

13.2 Robust Control from System Identification

Regardless of the system identification approach taken, the results are (for scalar systems) a nominal model and a set of frequency domain uncertainty ellipses

around the nominal frequency response. The purpose of this section is to discuss how we may represent these uncertainty ellipses in a robust control framework. Generally we will represent the uncertain system as

$$G_T(z) = G(z, \hat{\theta}_N) + G_\Delta(z) \quad (13.8)$$

where $G_\Delta(z)$ is some unknown but norm bounded transfer function for the model uncertainty. We will thus consider the robust stability problem with a norm bounded additive uncertainty. The set-up can be viewed as in Figure 13.1 where the problem then is to determine the most suitable structure on $\Delta(z)$ and $N(z)$ such that an adequate formulation of the control problem is obtained.

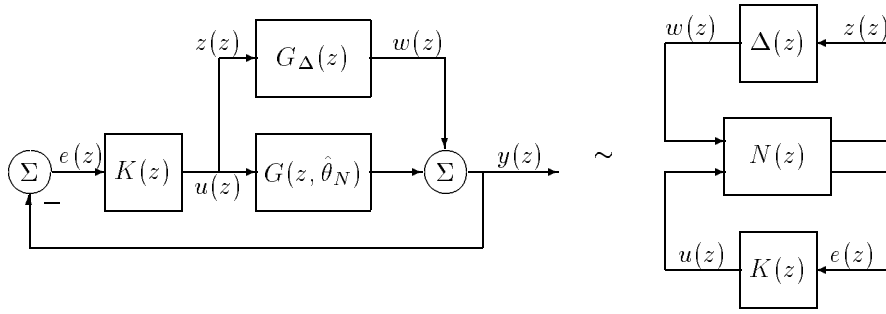


Figure 13.1: *Approximating estimated frequency domain uncertainty ellipses with a norm bounded perturbation set.*

13.2.1 The \mathcal{H}_∞ Approach

In the \mathcal{H}_∞ solution to the robust stability problem it is assumed that $\Delta(z)$ is an unstructured full complex block bounded in norm by $\bar{\sigma}(\Delta(e^{j\omega T_s})) \leq 1$. This means that we can represent uncertainty circles in the complex plane. In particular let

$$G_\Delta(z) = W_u(z)\Delta(z) \quad (13.9)$$

with

$$\Delta(z) = \delta^c \quad \delta^c \in \mathbf{C}, |\delta^c| \leq 1 \quad (13.10)$$

Then the uncertainty description will corresponds to frequency domain uncertainty circles with radius $|W_u(e^{j\omega T_s})|$ at each frequency ω . Consequently the

\mathcal{H}_∞ approach could be outlined as follows. Given the estimated frequency domain uncertainty ellipses, approximate each ellipse with a circumscribed circle. Fit a stable transfer function $W_u(z)$ to these circles such that

$$|W_u(e^{j\omega T_s})| \approx R(\omega) \quad (13.11)$$

where $R(\omega)$ denotes the radius of the circle evaluated at frequency ω . Construct the augmented system

$$N(z) = \begin{bmatrix} 0 & W_u(z) \\ -1 & -G(z, \hat{\theta}_N) \end{bmatrix} \quad (13.12)$$

and solve the optimal robust stability problem

$$K(z) = \arg \min_{K(z) \in \mathcal{K}_S} \|F_l(N(z), K(z))\|_\infty \quad (13.13)$$

for example by bilinear transformation to continuous-time. If the controller $K(z)$ achieves $\|F_l(N(z), K(z))\|_\infty < 1$, the system will be robustly stable.

13.2.1.1 Robust Performance

If we consider the robust performance problem rather than the robust stability problem we may formulate a 2×2 block problem as in Figure 13.2 on the following page with $N(z)$ given by

$$\begin{bmatrix} u'(z) \\ e'(z) \\ u'(z) \end{bmatrix} = N(z) \begin{bmatrix} r(z) \\ u(z) \end{bmatrix} = \begin{bmatrix} 0 & W_u(z) \\ W_p(z) & -W_p(z)G(z) \\ 1 & -G(z) \end{bmatrix} \begin{bmatrix} r(z) \\ u(z) \end{bmatrix} \quad (13.14)$$

It is then easy to show that

$$\begin{bmatrix} e'(z) \\ u'(z) \end{bmatrix} = F_l(N(z), K(z))r(z) = \begin{bmatrix} W_p(z)S(z) \\ W_u(z)M(z) \end{bmatrix} r(z) \quad (13.15)$$

where $W_p(z)$ is a sensitivity specification¹ and $S(z)$ and $M(z)$ are the sensitivity and control sensitivity respectively. Thus we can formulate an \mathcal{H}_∞ problem as

$$K(z) = \arg \min_{K(z) \in \mathcal{K}_S} \|F_l(N(z), K(z))\|_\infty \quad (13.16)$$

¹Note that we do not distinguish between the input and output sensitivity since they are identical for scalar systems.

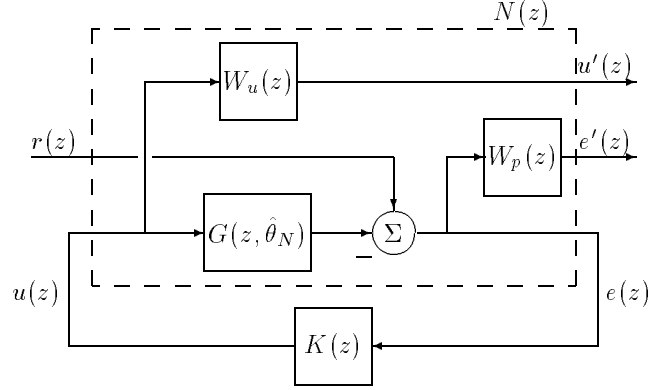


Figure 13.2: 2×2 block problem used for robust performance with \mathcal{H}_∞ approach.

For scalar systems it is easy to show that a *necessary and sufficient* condition for robust performance given an additive uncertainty and a sensitivity specification is

$$\sup_{\omega} (|W_p(e^{j\omega T_s}) S(e^{j\omega T_s})| + |W_u(e^{j\omega T_s}) M(e^{j\omega T_s})|) < 1 \quad (13.17)$$

Let us investigate how this corresponds to the \mathcal{H}_∞ solution. Omitting the dependency on ω we have

$$\bar{\sigma} \left(\begin{bmatrix} W_p S \\ W_u M \end{bmatrix} \right) = \sqrt{\lambda \left(\begin{bmatrix} W_p S \\ W_u M \end{bmatrix}^* \begin{bmatrix} W_p S \\ W_u M \end{bmatrix} \right)} \quad (13.18)$$

$$= \sqrt{|W_p S|^2 + |W_u M|^2} \quad (13.19)$$

$$= \begin{cases} \frac{1}{\sqrt{2}} (|W_p S| + |W_u M|) & , \text{ if } |W_p S| = |W_u M| \\ |W_p S| + |W_u M| & , \text{ if } |W_p S| = 0 \vee |W_u M| = 0 \end{cases} \quad (13.20)$$

Thus if we tighten our robust performance condition slightly to

$$\sup_{\omega} \bar{\sigma} \left(\begin{bmatrix} W_p S \\ W_u M \end{bmatrix} \right) < \frac{1}{\sqrt{2}} \quad (13.21)$$

we obtain in the above extreme cases

$$\| |W_p S| + |W_u M| \|_{\infty} < 1 \quad \text{if } |W_p S| = |W_u M| \quad (13.22)$$

$$\| |W_p S| + |W_u M| \|_{\infty} < \frac{1}{\sqrt{2}} \quad \text{if } |W_p S| = 0 \vee |W_u M| = 0 \quad (13.23)$$

and robust performance will thus be guaranteed. The \mathcal{H}_∞ solution will be non-conservative if the supremum is reached for $|W_p S| = |W_u M|$ and in general it will be conservative up to a factor $\sqrt{2}$. Compare with the multivariable results in Example 4.3 on page 52.

13.2.2 The Complex μ Approach

In the \mathcal{H}_∞ approach above two types of conservatism were introduced. Firstly, the frequency domain uncertainty ellipses were approximated by the circumscribed circle. If the ratio of the principal axis of a given ellipse is close to one, the ellipse will be “round” and may be quite accurately approximated by a circle. However if the principal axis ratio is much larger than one, the circle approximation will be potentially very conservative. Secondly, the “usual” \mathcal{H}_∞ conservatism in connection with robust performance problems cannot be avoided. However, for scalar systems the conservatism will be less than a factor $\sqrt{2}$ and for most designs it will in fact be quite small since the supremum for $|W_p S| + |W_u M|$ is usually obtained in the frequency area where $|W_p S| \approx |W_u M|$.

Let us now investigate what can be gained by a complex μ approach. We thus allow the perturbation set $\Delta(z)$ to be structured. However, only complex perturbations are allowed. The sad facts are then that this *does not* enhance our description of the uncertainty ellipses. Using a complex perturbation set we may still only describe circles in the complex plane. Thus for the robust stability problem, the complex μ approach reduce to a standard \mathcal{H}_∞ problem and nothing is gained.

13.2.2.1 Robust Performance

The robust performance problem may be addressed non-conservatively, since it may be formulated as a complex μ problem with the augmented perturbation block

$$\tilde{\Delta}(z) = \text{diag}\{\delta^c, \delta_p^c\}, \quad \delta^c, \delta_p^c \in \mathbf{C}, |\delta^c| \leq 1, |\delta_p^c| \leq 1 \quad (13.24)$$

The $N\Delta K$ formulation can then be given as in Figure 13.3 with $N(z)$ given by

$$N(z) = \begin{bmatrix} 0 & 0 & W_u(z) \\ -1 & 1 & -G(z, \hat{\theta}_N) \\ -W_p(z) & W_p(z) & -W_p(z)G(z, \hat{\theta}_N) \end{bmatrix} \quad (13.25)$$

The control problem is thus one of finding a controller which satisfies

$$K(z) = \arg \min_{K(z) \in \mathcal{K}_S} \left\| \mu_{\tilde{\Delta}}(F_l(N(z), K(z))) \right\|_\infty \quad (13.26)$$

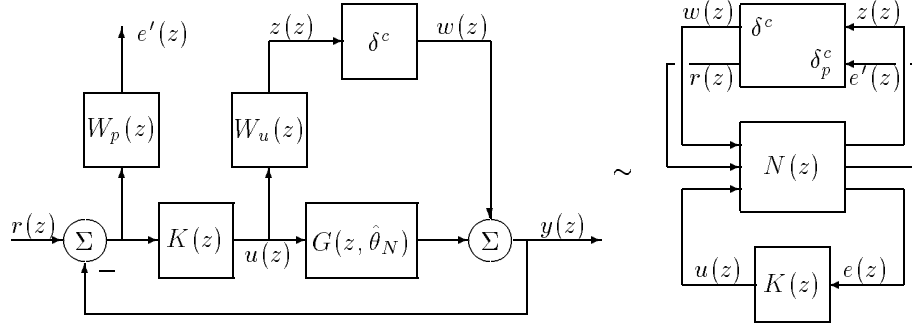


Figure 13.3: $N\Delta K$ framework used for robust performance with complex μ approach.

The optimal complex μ controller (13.26) on the preceding page can then be found using D - K iteration as outlined in Procedure 5.1 on page 79. If the controller obtains $\|\mu_{\hat{\Delta}}(F_l(N(z), K(z)))\|_{\infty} < 1$ the closed loop system has robust performance. Even though the robust performance problem may be specified without conservatism using a complex μ formulation, the enhancement in comparison with the \mathcal{H}_{∞} approach will be less than a factor $\sqrt{2}$. We find that the μ formulation is more natural due to the $N\Delta K$ framework. However, actual computation of the optimal complex μ controller is much more involved than the standard \mathcal{H}_{∞} solution. Furthermore the order of the controller is higher for the μ approach. The achievements using a complex μ approach over the standard \mathcal{H}_{∞} solution thus seems to be very marginal.

13.2.3 The Mixed μ Approach

As shown above, a structured, but purely complex perturbation set does not allow for an accurate description of the frequency domain uncertainty ellipses obtained from the system identification procedure. We will now show that using a mixed perturbation set with one real and one complex perturbation we may in fact construct an reasonable accurate approximation to the uncertainty ellipses. The conservatism will be bounded by a factor $4/\pi$.

The idea is as follows. In connection with the complex μ approach we noted that using a complex scalar perturbation we describe uncertainty circles in the frequency domain. If we combine this description with a real scalar perturbation we may thus describe a region in the complex plane constructed by successive circles placed along a straight line of some given length and some given angle.

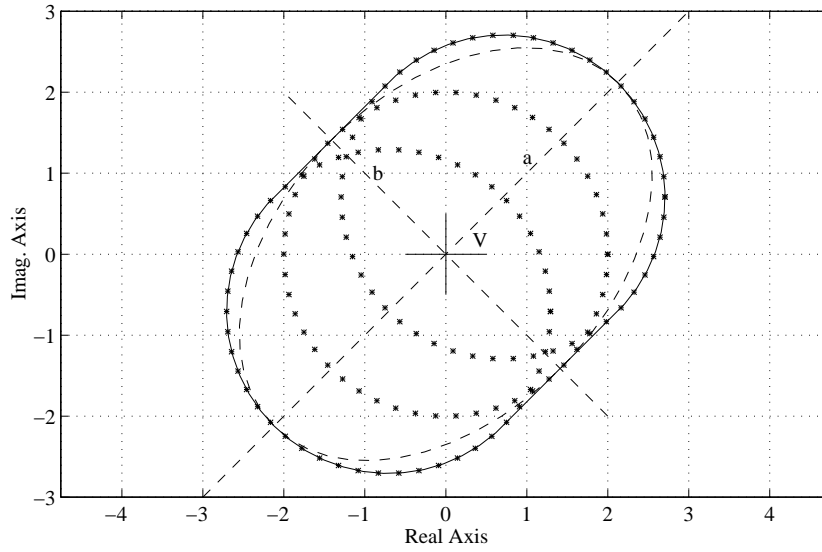


Figure 13.4: *Fitting an uncertainty ellipse (dashed) with a mixed perturbation set (solid). A , a and b denote the angle of rotation and major and minor principal axis of the ellipse respectively.*

We may then use this as an approximation for an ellipse, see Figure 13.4.

We will thus approximate the additive model uncertainty $G_{\Delta}(z)$ with the perturbation set

$$L(z) = W_{u,c}(z)\delta^c + W_{u,r}(z)\delta^r \quad (13.27)$$

where δ^c and δ^r are a complex respectively real perturbation:

$$\delta^c \in \mathbf{C}, \quad |\delta^c| \leq 1 \quad (13.28)$$

$$\delta^r \in \mathbf{R}, \quad -1 \leq \delta^r \leq 1 \quad (13.29)$$

and $W_{u,c}(z)$ and $W_{u,r}(z)$ are stable weighting functions. If A , a and b denote the angle of rotation and major and minor principal axis of the ellipse respectively the weighting functions $W_{u,c}(z)$ and $W_{u,r}(z)$ should be fitted to the ellipses in such a way that

$$|W_{u,c}(e^{j\omega T_s})| \approx b \quad (13.30)$$

$$|W_{u,r}(e^{j\omega T_s})| \approx a - b \quad (13.31)$$

$$\angle(W_{u,r}(e^{j\omega T_s})) \approx A \quad (13.32)$$

In Appendix K on page 329 it is shown how the relevant information about A , a and b can easily be extracted from the form matrix $P_{\hat{g}}(\omega)$ for the uncertainty ellipse. Notice that the weighting function $W_{u,r}(z)$ must be fitted both in amplitude and phase. This is not a trivial task. However, in the MATLAB *μ -Analysis and Synthesis Toolbox* the script file `fitsys.m` performs such a fit. The routine works for continuous-time transfer functions only but, of course, the result may be transformed into discrete-time time using e.g. a pre-warped Tustin approximation. The other weight $W_{u,c}(z)$ needs only to be fitted in magnitude².

The quality of the approximation assuming perfect realizations of the weighting functions can easily be checked by investigation of the ratio between the surface of the approximation and the surface of the ellipse:

$$\Gamma_A = \frac{A_L}{A_{ell}} \quad (13.33)$$

$$= \frac{4|W_{u,c}||W_{u,r}| + \pi|W_{u,c}|^2}{\pi|W_{u,c}|(|W_{u,r}| + |W_{u,c}|)} \quad (13.34)$$

$$= \frac{4|W_{u,r}| + \pi|W_{u,c}|}{\pi(|W_{u,r}| + |W_{u,c}|)} \quad (13.35)$$

For the two extremes $|W_{u,r}| = 0$ and $|W_{u,c}| = 0$ we obtain

$$|W_{u,r}| = 0 \Rightarrow A_L = A_{ell} \quad (13.36)$$

$$|W_{u,c}| = 0 \Rightarrow A_L = \frac{4}{\pi} A_{ell} \quad (13.37)$$

Thus for perfect realizations of the weightings

$$A_{ell} \leq A_L \leq 1.27 A_{ell} \quad (13.38)$$

13.2.3.1 Robust Performance

The robust performance problem may then be considered with the augmented perturbation block

$$\tilde{\Delta}(z) = \text{diag}\{\delta^c, \delta^r, \delta_p^c\}, \quad \delta^c, \delta_p^c \in \mathbf{C}, \delta^r \in \mathbf{R} \quad (13.39)$$

with $|\delta^c| \leq 1$, $|\delta_p^c| \leq 1$ and $-1 \leq \delta^r \leq 1$. The $N\Delta K$ formulation can be given as in Figure 13.5 on the facing page with $N(z)$ given by

$$N(z) = \begin{bmatrix} 0 & 0 & 0 & W_{u,c}(z) \\ 0 & 0 & 0 & W_{u,r}(z) \\ -1 & -1 & 1 & -G(z, \hat{\theta}_N) \\ -W_p(z) & -W_p(z) & W_p(z) & -W_p(z)G(z, \hat{\theta}_N) \end{bmatrix} \quad (13.40)$$

²`fitmag.m` from the μ toolbox may be used to perform the fit.

The optimal controller is thus given by

$$K(z) = \arg \min_{K(z) \in \mathcal{K}_S} \|\mu_{\hat{\Delta}}(F_l(N(z), K(z)))\|_{\infty} \quad (13.41)$$

No known solution to (13.41) exists but an approximation to the robust performance problem can be considered using μ - K iteration as outlined in Procedure 5.3 on page 86. If the final controller achieves $\|\mu_{\hat{\Delta}}(F_l(N(z), K(z)))\|_{\infty} < 1$ the closed loop system will have robust performance.

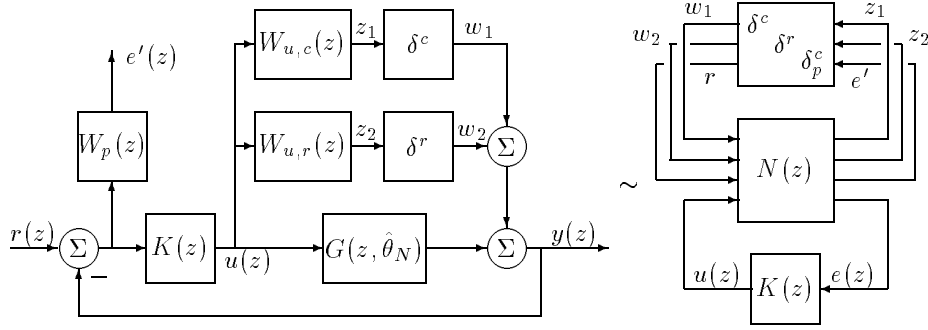


Figure 13.5: $N\Delta K$ formulation for robust performance problem with a mixed μ approach.

13.3 A Synergistic Approach to Identification Based Control

As shown above we can address the control problem with very little conservatism using a mixed μ approach. The price we must pay is a significant increase in the complexity of the solution, since we have to solve a mixed μ control problem. The optimal mixed μ controller will usually be of very high order and even though the number of controller states normally can be significantly reduced, the reduced controller will often have more states than the augmented plant. This may increase the costs of the actual implementation since, e.g. more memory will be needed in the process computer. Consequently, the increase in controller performance must be weighed out with the additional complexity of the control design and implementation. A sensible design methodology for system identification based robust control can thus be outlined as in Procedure 13.1.

Procedure 13.1 (A Synergistic Design Approach to Robust Control)

1. *Using either of the two proposed system identification methods outlined in Section 13.1.4 on page 231 estimate a nominal model $G(q, \hat{\theta}_N)$ and frequency domain uncertainty ellipses at a set of chosen frequency points ω . Thus if large data series are available use a classical approach. Use an output error model structure if a noise model is not important for the subsequent control design. If disturbance attenuation is of primary importance in the control design, use a more general model structure to obtain a noise model $H(q, \hat{\theta}_N)$ as well. If only small data sets are available, use the stochastic embedding paradigm to extend the classical results on fixed denominator models to the case with both bias and variance errors.*
2. *Design a \mathcal{H}_∞ optimal controller for the system using the approach outlined in Section 13.2.1 on page 232. Thus approximate the uncertainty ellipses determined in Step 1 with circumscribed circles. Then pose the 2×2 block problem shown in Figure 13.2 on page 234 where the stable uncertainty weight $W_u(z)$ has been fitted in magnitude to $R(\omega)$, the radius of the circle evaluated at frequency ω . Use a standard sensitivity specification for the performance weight $W_p(z)$. Of course more specialized performance requirements can be incorporated into the design. However, the \mathcal{H}_∞ solution may then become more conservative.*
3. *Evaluate the \mathcal{H}_∞ control design. Thus check for robust performance by (13.21) on page 234. Also check e.g. the open loop Nyquist with uncertainty ellipses, the transient response and any other performance demands in question. If these tests are passed satisfactorily, stop. If not, continue to Step 4.*
4. *Design a mixed μ optimal controller for the system using the approach outlined in Section 13.2.3 on page 236. Thus approximate the uncertainty ellipses with a mixed real and complex perturbation set and pose the control problem as in Figure 13.5 on the page before. The uncertainty weight $W_{u,r}(z)$ must be fitted in magnitude to the difference between the major and minor principal axis of the ellipses and in phase to the ellipses angle as indicated in Figure 13.4 on page 237. The uncertainty weight $W_{u,c}(z)$ must be fitted in magnitude to the minor principal axis of the ellipses. Use a standard sensitivity specification for the performance weight $W_p(z)$. If more specialized performance requirements should be incorporated into the design this can be done without conservatism as long as they can be specified within the $N\Delta K$ framework. Solve the control problem, e.g. using μ - K iteration as outlined in Procedure 5.3 on page 86.*
5. *Evaluate the control mixed μ design. Thus check for robust performance using $\mu_{\hat{\Delta}}(F_l(N(z), K(z)))$. Additional checks may be performed as in Step 3.*

Compare with the \mathcal{H}_∞ solution to assess any increase in performance obtained with the mixed μ approach. If the performance increase is significant and of importance in connection with the actual operation of the plant, select the mixed μ controller. If not, use the \mathcal{H}_∞ controller determined in Step 2 or redo the design with modified uncertainty and/or performance specifications. For example, a new set of plant measurements for the identification procedure may be needed to reduce the uncertainty level. Also the performance requirements perhaps must be reduced in order to fulfill the robust performance criterion.

6. *Finally, when necessary, use model reduction techniques to iteratively reduce the number of states in the controller until just before a significant increase in $\mu_{\hat{\Delta}}(F_l(N(z), K(z)))$ will occur.*

The above procedure is a central result of this thesis. It outlines a complete identification based robust control design approach for scalar systems. The extension to multivariable systems are straightforward with the exception of the following points. The stochastic embedding approach is only well developed for scalar systems. Furthermore the mapping of parametric uncertainty into the frequency domain for multivariable systems is not straightforward.

Of course, the design procedure need not be terminated in Step 3 even though the \mathcal{H}_∞ design is satisfactory. The mixed μ controller can be computed to investigate the possible increase in controller performance. Generally, if the uncertainty ellipses contain little phase information (are “round”) we will expect the \mathcal{H}_∞ design to have similar control performance to the mixed μ controller. On the other hand, if the ellipses are narrow we will generally expect the mixed μ design to be significantly superior to the \mathcal{H}_∞ design.

13.4 Summary

The combination of the results presented in Part I and Part II was addressed. At first, system identification for robust control was considered. A brief discussion of the classical techniques was given. Specifically we reviewed under which circumstances the data estimate \hat{P}_N of the parameter covariance matrix will be consistent. For the general PEM structure, the requirement is that the models for *both* the deterministic and stochastic part of the true system will admit an exact description. The same is true for the popular ARX model. However, for output error models, the parameter covariance estimate will be consistent even if the noise model ($H(q, \theta) = 1$) is inadequate. For fixed denominator models the parameter covariance estimate will be consistent even in the case of under-modeling, but then the corresponding frequency domain uncertainty regions will

represent the variance error only. The conclusion was that if large data sets are available, the classical output error approach may be applied if a disturbance model is unimportant in connection with the control design. We will then probably require the model order to be quite large in order to obtain residuals which are uncorrelated with the input signal. This could be impractical in connection with standard \mathcal{H}_∞ or μ design since the order of the controller will increase accordingly. Fixed order \mathcal{H}_∞ algorithms may be a solution to this problem. However, this has not been considered in this work.

If only short data series are available, the classical approach does not seem adequate. Then we propose that the stochastic embedding approach is used to estimate a fixed denominator model and corresponding frequency domain uncertainty ellipses. Different parameterizations of the noise and the undermodeling should be investigated.

Next, robust control from system identification was considered. For both the classical and the stochastic embedding approach the result is a nominal model and frequency domain uncertainty ellipses. Thus we need to synthesize a control design methodology which non-conservatively can capture these uncertainty templates. Here, three different design approaches were investigated: An \mathcal{H}_∞ approach, a complex μ approach and a mixed real and complex μ approach. It was illustrated how both \mathcal{H}_∞ and complex μ will allow only frequency domain uncertainty circles. With proper formulation of a mixed sensitivity problem, the conservatism in the \mathcal{H}_∞ approach compared with the complex μ approach can be bounded by $\sqrt{2}$. Since the design of the complex μ controller is considerably more involved and will result in a controller with more states, the \mathcal{H}_∞ design seems to be the most appropriate of the two. However, using a mixed μ approach we may obtain a quite accurate description of the uncertainty ellipses through a mixed perturbation set with one real and one complex scalar. The conservativeness in this description was bounded by $4/\pi = 1.27$. This approach furthermore has the advantage that more complicated performance measures may be included without conservatism.

Finally a synergistic system identification based robust control design algorithm was outlined. It was recommended that an initial \mathcal{H}_∞ design was applied and checked. If this design was not satisfactory, the mixed μ approach could be applied instead.

Chapter 14

Control of a Water Pump

Contents

14.1 Identification Procedure	244
14.1.1 Estimation of Model Uncertainty	246
14.1.2 Constructing A Norm Bounded Perturbation	249
14.2 Robust Control Design	252
14.2.1 Performance Specification	252
14.2.2 \mathcal{H}_∞ Design	254
14.2.3 Mixed μ Design	256
14.3 Summary	259

The purpose of this chapter is to provide an applications example of the proposed system identification based robust design approach, see Procedure 13.1 on page 239. The design procedure has been applied in control of a small domestic water supply system consisting of a centrifugal pump driven by a 840 Watt frequency modulated micro-computer controlled asynchronous type induction motor. The pump was a typical domestic water supply pump with a maximum capacity of approximately 3 m³/hr at 2.5 barg. A 3.5 liter (0.92 gallon) rubber membrane buffer tank was

placed in the outlet pipe from the pump. The size of the buffer tank is much smaller compared with more traditional domestic installations, where the volume of the buffer tank is usually around 60 liters (15.9 gallons). The small buffer tank makes it possible to design a very compact water supply unit which takes up much less space than a traditional system. On the other hand the small buffer tank increase the performance demands to the control system significantly, since the buffer tank have only very limited operating range. The traditional on/off control will then have unsatisfactory performance. Therefore, the electric motor has been equipped with frequency modulation in order to control the velocity of the pump. The input to the system was the frequency reference f_r [Hz] for the motor and the recorded output was the outlet water pressure φ [barg]. The system is sketched in Figure 14.1.

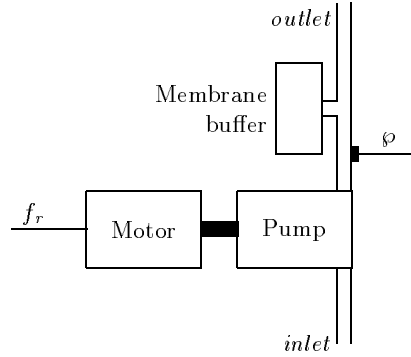


Figure 14.1: *The water supply system. The induction motor speed is controlled via the frequency f_r . Outlet water pressure φ is recorded as output.*

The data acquisition and control of the system were performed using an A/D,D/A data acquisition card and a 486 PC interface to the micro-computer.

14.1 Identification Procedure

The system was sampled with sampling frequency 50 Hz and the input used for identification was a 0.4 Hz fundamental square wave. 500 samples were collected, 300 of which were used to get rid of initial condition effects. The last 200 samples were used for identification. In Figure 14.2 on the facing page, the data sequence is shown. The working point of the system is given in Table 14.1.

	Pressure φ [barg]	Motor frequency f_r [Hz]	Flow Q [m ³ /hr]
Working point	2.33	90.7	0.90

Table 14.1: *Working point values for the data sequence used for estimation.*

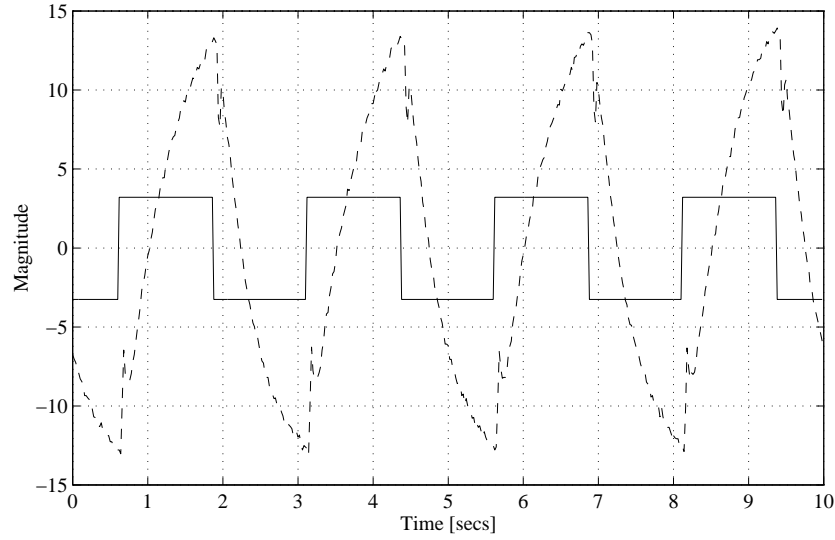


Figure 14.2: *Input/output sequence used for identification of pump system. Shown are working point deviations for the motor frequency reference f_r [Hz] (solid) and for the outlet water pressure p [0.01 barg].*

The system dynamics was dominated by a low frequency first order component with a time constant of approximately 1 sec. The low frequency component originates from the membrane buffer tank. Furthermore smaller high frequency components can also be identified from Figure 14.2. These originates mainly from the inertia in the induction motor and centrifugal pump.

A second order Laguerre model

$$G(q, \theta) = \frac{\theta_1 q^{-1}}{1 + \xi q^{-1}} + \frac{\theta_2 q^{-1} (1 - \xi^{-1} q^{-1})}{(1 + \xi q^{-1})^2} \quad (14.1)$$

was fitted to the data using a standard least squares estimate. The Laguerre pole $-\xi$ was chosen as 0.96, corresponding to a time constant $\tau \approx 0.5$ secs which is slightly faster than the dominating time constant of the true system. The least squares estimate of the parameter vector θ was found as

$$\hat{\theta}_N = \begin{bmatrix} 0.6845 \\ 0.1213 \end{bmatrix} \quad (14.2)$$

corresponding to a zero at $z = 0.9433$. In Figure 14.3 on the next page the true and simulated output is shown together with the estimated Nyquist. Here also

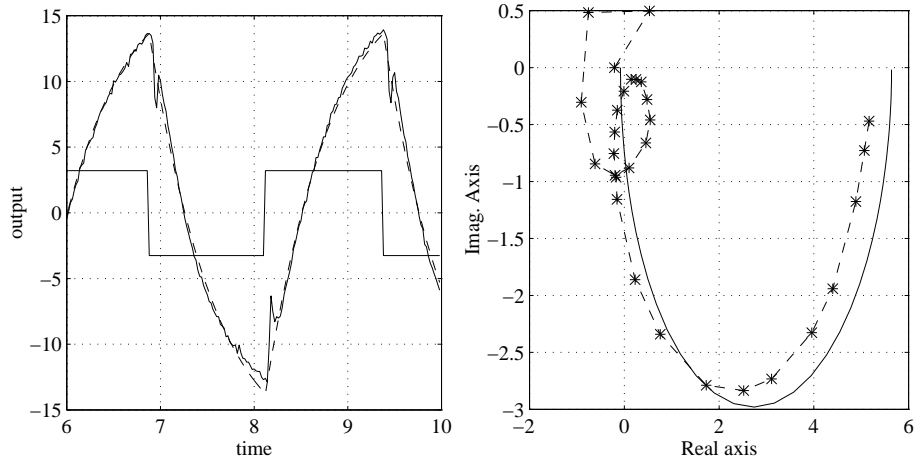


Figure 14.3: *True (solid) and simulated (dashed) output together with estimated Nyquist (solid) and measured discrete frequency points (*).*

measured discrete frequency point estimates are shown. These frequency point estimates were obtained from the true system by applying pure sines inputs at different frequencies and measuring the gain and phase shift in the output.

Notice how a fairly accurate estimate of the low frequency behavior of the pump system is obtained with the Laguerre model. However, in the high frequency range considerable deviations between the nominal Nyquist and the measured frequency points can be identified.

14.1.1 Estimation of Model Uncertainty

The stochastic embedding approach were used for estimating the model uncertainty. The order of the FIR model describing the undermodeling was chosen as $L = 50$. The following parameterizations for the noise and undermodeling covariance matrices were chosen

$$C_{\nu}^{i,j}(\gamma) = \begin{cases} \sigma_e^2 \left(1 + \frac{(c-a)^2}{1-a^2} \right) & , i = j \\ \frac{\sigma_e^2 (-a)^M (1 + c^2 - a * c - c/a)}{1-a^2} & , |j-i| = M \end{cases} \quad (14.3)$$

$$C_\eta(\beta) = \text{diag}_{1 \leq k \leq L} \alpha \lambda^k \quad (14.4)$$

corresponding to a first order ARMA noise model and an exponentially decaying undermodeling impulse response. Thus the combined parameter vector ζ for the covariances is given by

$$\zeta = \begin{bmatrix} \beta \\ \gamma \end{bmatrix} = \begin{bmatrix} \alpha \\ \lambda \\ a \\ c \\ \sigma_e^2 \end{bmatrix} \quad (14.5)$$

An estimate of ζ was found using the maximum likelihood approach outlined in Section 11.2.1 on page 195:

$$\hat{\zeta} = \arg \max_{\zeta} \mathcal{L}(\varpi|U, \zeta) \quad (14.6)$$

where U is the input vector and ϖ is the transformed residuals

$$\varpi = R^T \epsilon \quad (14.7)$$

The transformation matrix R ensures that the distribution on ϖ is non-singular. R was chosen through QR -factorization as described in Section 11.2.2 on page 196. The result of the maximum likelihood estimation is displayed in Figure 14.4 where the parameter tracks are shown together with the loglikelihood function.

The estimate of ζ was found as

$$\hat{\zeta} = \begin{bmatrix} \alpha \\ \lambda \\ a \\ c \\ \sigma_e^2 \end{bmatrix} = \begin{bmatrix} 0.3145 \\ 0.6264 \\ -0.9687 \\ -0.5095 \\ 0.0794 \end{bmatrix} \quad (14.8)$$

The covariance functions C_ν and C_η were then replaced by their corresponding estimates $C_\nu(\gamma)$ and $C_\eta(\beta)$ in the expression for $P_{\hat{g}}(\omega)$, see Equation (11.71) on page 191. A 90% confidence interval was chosen corresponding to the uncertainty ellipses shown in Figure 14.5 on the next page.

Generally the uncertainty ellipses provide a useful description of the model uncertainty. The uncertainty estimates seem rather conservative at low frequencies compared with the discrete frequency point estimates. This will, as we shall show later, limit the obtainable closed loop performance. The high frequency uncertainty ellipses nicely captures the rather large model uncertainty in the high frequency area. Furthermore, little uncertainty is predicted around the fundamental frequency of the square wave input. This also corresponds well with the measured frequency points.

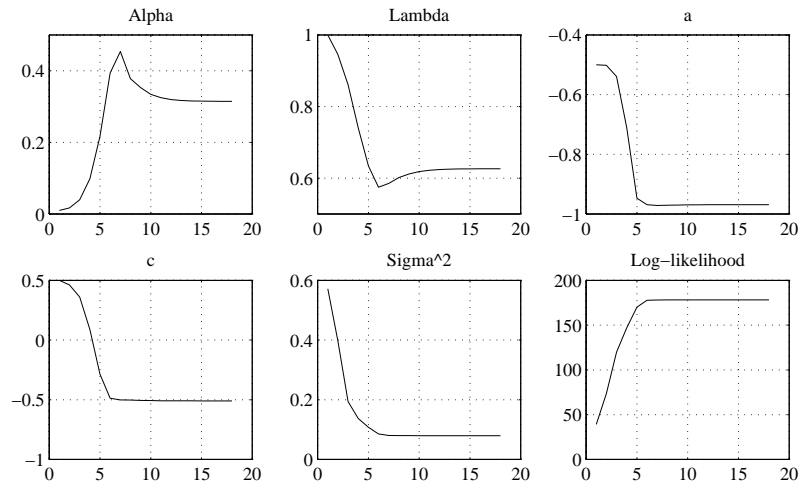


Figure 14.4: Results from the maximum likelihood estimation of ζ . Shown are parameter tracks for each parameter and the expiration of the log-likelihood function.

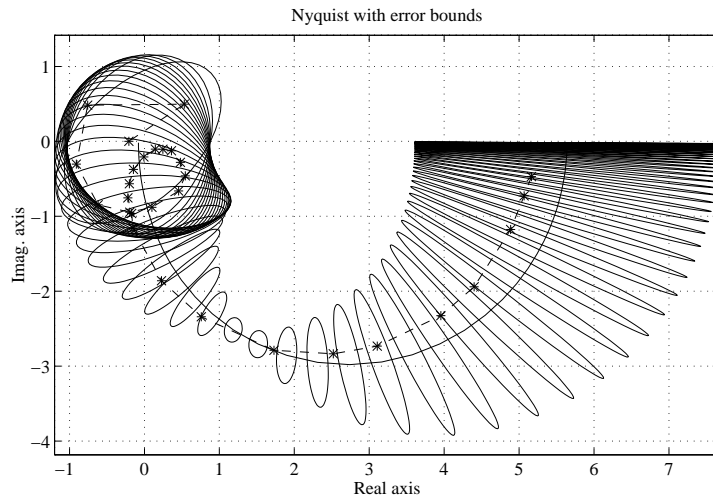


Figure 14.5: Nominal Nyquist with 90% uncertainty ellipses. Measured frequency response estimates also shown (*).

14.1.2 Constructing A Norm Bounded Perturbation

Now we will use the 90% confidence ellipses to construct a norm bounded additive uncertainty description as discussed in Section 13.2. As suggested in Procedure 13.1 on page 239 we will consider two design approaches, namely an \mathcal{H}_∞ design and a mixed μ design. We thus need two perturbation models; one based on a single complex perturbation corresponding to circumscribed circles and one based on a mixed perturbation set corresponding to the “oval” uncertainty region shown in Figure 13.4 on page 237.

14.1.2.1 A Single Complex Perturbation Model

Using the circumscribed circles as approximation to the estimated uncertainty circles the undermodeling $G_\Delta(z)$ is described as

$$G_\Delta(z) = W_u(z)\delta^c, \quad \delta^c \in \mathbf{C}, |\delta^c| \leq 1 \quad (14.9)$$

The weighting function $W_u(z)$ then must be fitted to the uncertainty ellipses in such a way that

$$|W_u(e^{j\omega T_s})| \approx R(\omega) \quad (14.10)$$

where $R(\omega)$ denotes the radius of the circumscribed ellipse. Clearly R equals the major principal axis a of the ellipse. A slightly modified version of the `sysfit.m` routine from the MATLAB *μ -Analysis and Synthesis Toolbox* [BDG⁺93] was used to perform the fit. A second order weighting function quite accurately matched $R(\omega)$. In Figure 14.6 on the following page some of the uncertainty ellipses are shown together with the frequency regions described by the perturbation model (14.9). Clearly, this perturbation model is rather conservative for narrow ellipses. However, the orientation of the ellipses are also important in assessing the conservatism. In the low frequency area, for example, it seems that the circumscribed circles are very conservative. However, since the sign of the gain is known, the low frequency uncertainty regions will not destabilize the closed loop plant. Furthermore, assume that we use a controller without pure integral action (finite real steady-state frequency response) and that our performance specification bounds the sensitivity function $S(z)$. A sensitivity specification corresponds to requiring that the open loop Nyquist $G(e^{j\omega T_s})K(e^{j\omega T_s})$ for each frequency ω remains outside a circle centered at the Nyquist point $(-1, 0)$ and with radius $|S_p^{-1}(e^{j\omega T_s})|$ where $S_p(z)$ denotes the upper bound on the sensitivity function. In this case, the low frequency uncertainty circles will *not* be conservative from a performance point of view since the distance from the open loop uncertainty circles/¹ and the open loop uncertainty ellipses to the Nyquist point will be approximately the same close to steady-state.

¹By open loop uncertainty we mean the plant uncertainty multiplied by the controller.

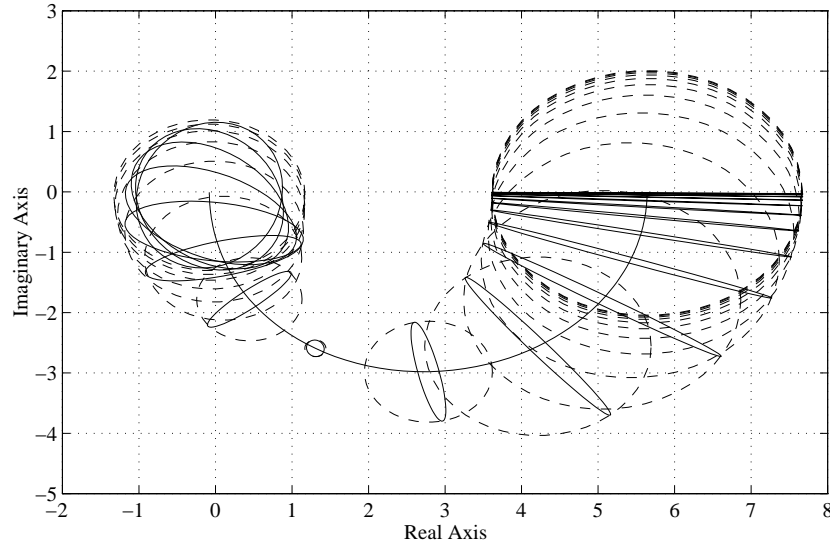


Figure 14.6: Comparison of uncertainty ellipses and perturbation model. \mathcal{H}_∞ approach

14.1.2.2 A Mixed Real and Complex Perturbation Model

Using ovals as approximation to the estimated uncertainty circles the undermodeling $G_\Delta(z)$ is described as

$$G_\Delta(z) = W_{u,c}(z)\delta^c + W_{u,r}(z)\delta^r, \quad \delta^c \in \mathbf{C}, \delta^r \in \mathbf{R}, |\delta^{c,r}| \leq 1 \quad (14.11)$$

The weighting functions $W_{u,c}(z)$ and $W_{u,r}(z)$ must be fitted to the uncertainty ellipses in such a way that

$$|W_{u,c}(e^{j\omega T_s})| \approx b \quad (14.12)$$

$$|W_{u,r}(e^{j\omega T_s})| \approx a - b \quad (14.13)$$

$$\angle(W_{u,r}(e^{j\omega T_s})) \approx A \quad (14.14)$$

where a and b denote major and minor principal axis respectively and A the angle of the ellipse. A third order weighting function was used for $W_{u,r}(z)$ and a fifth order weight for $W_{u,c}(z)$. The results of the fitting procedure is shown in

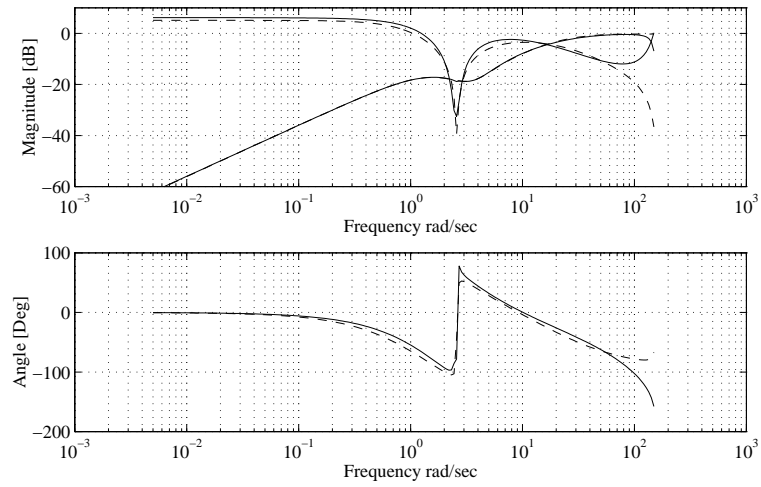


Figure 14.7: *Fitting weighting functions (dashed) to the principal axis and angles of the uncertainty ellipses*

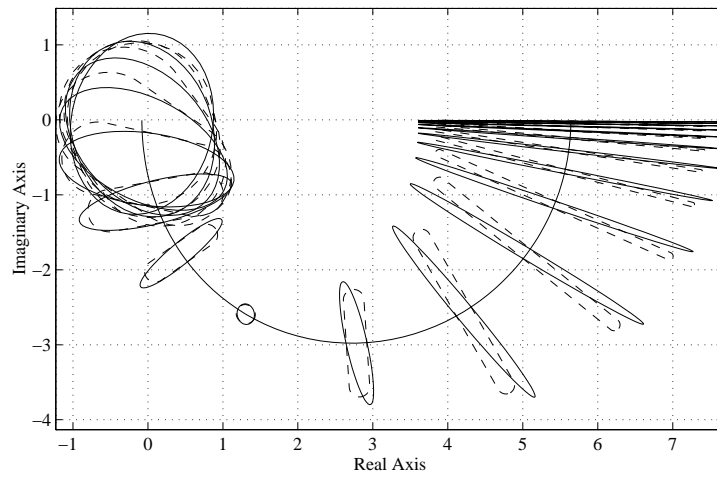


Figure 14.8: *Comparison of uncertainty ellipses (solid) and frequency domain regions described by the weights (dashed).*

Figure 14.7 and 14.8 on the preceding page. In Figure 14.7 a comparison is shown of the principal axis and angles extracted from the ellipses with the frequency response of the weighting functions according to Equation (14.12)–(14.14). Furthermore, in Figure 14.8 a comparison is made between the estimated ellipses and the frequency domain uncertainty regions corresponding to the weighting functions. It can be seen that with the given orders of the weighting functions a reasonable accurate fit is obtained.

The identification part of the design has then been completed. We obtained a 2nd order Laguerre model of the pump system and 90% confidence ellipses were estimated using the stochastic embedding approach. These uncertainty ellipses were then approximated with a purely complex perturbation set for \mathcal{H}_∞ design and a mixed real and complex perturbation set for mixed μ design.

14.2 Robust Control Design

We then turn to the controller design. First we will perform an \mathcal{H}_∞ design as outlined in Section 13.2.1 on page 232 and secondly a mixed μ control design will be made and compared with the \mathcal{H}_∞ design.

14.2.1 Performance Specification

We will consider the robust performance problem. Thus a performance specification must be constructed. There exists generally no explicit formalisms for obtaining such specifications. In this paper we have used time domain demands on the pump pressure response towards sudden changes in water flow Q , to formulate a maximum sensitivity bound. A standard step of $\Delta Q = 2/3 \text{ m}^3/\text{h}$ was used as the performance measure. The time domain demands on the outlet pressure $\varphi(t)$ given a standard step on $\Delta Q(t)$ were formulated as:

- maximum transient error: 0.4 bar,
- max 0.1 bar settling time: 2 sec,
- max stationary error: 0.1 bar.

These demands originates in design goals from a major Danish pump producer. It was observed that step disturbances on the flow ΔQ acted approximately through a first order system to d_φ , the disturbance on the outlet pressure. For a standard step $\Delta Q(s) = K_s s^{-1}$ with $K_s = 2/3$ we then have²:

$$d_{\varphi,step}(s) = \frac{K}{s + \tau^{-1}} \cdot \frac{K_s}{s} \quad (14.15)$$

²In order to make the approach more transparent we will carry out the derivation for a continuous-time system and simply transform the results to discrete-time.

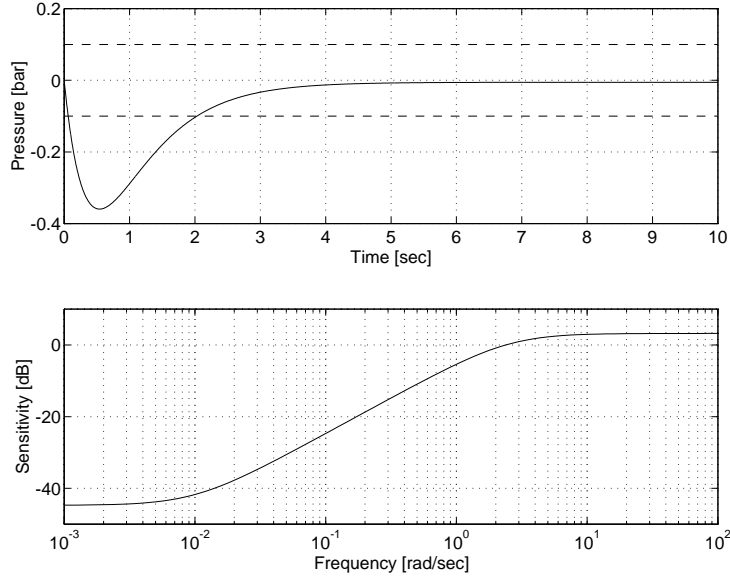


Figure 14.9: Time domain response $\varphi_{step}(t)$ (upper) corresponding to the chosen performance specification $S_p(z)$ (lower).

where K and τ are the gain and time constant of the first order filter respectively. $\tilde{K} = K K_s$ and τ were measured on the pump set-up as $\tilde{K} = 1.3 \text{ bar}/(\text{m}^3/\text{h})$ and $\tau = 0.75 \text{ sec}$.

Given a sensitivity specification $S(s) = \varphi(s)/d_p(s)$ the corresponding time domain response $\varphi_{step}(t)$ may then be computed. We will then use the heuristic assumption that our time demands will be fulfilled for a given compensated system having a sensitivity which falls below the specification for all frequencies. This is probably not guaranteed to be true for all systems, but it seems to work well in practice.

Here a first order discrete-time sensitivity specification was chosen:

$$S_p(z) = \frac{1.413z - 1.413}{z - 0.951} \quad (14.16)$$

As seen in Figure 14.9 the corresponding time domain response $\varphi_{step}(t)$ fulfill the stated demands.

The standard \mathcal{H}_∞ performance specification, see e.g. Theorem 5.3 on page 73, puts a unity bound on the transfer function from the normalized disturbances d' to the normalized errors e' . Letting $d' = d_p$ and $e' = W_p e_p$ we have the

performance specification:

$$\frac{e_p(z)}{d_p(z)} \leq S_p(z) \Rightarrow W_p(z) = S_p^{-1}(z) \quad (14.17)$$

14.2.2 \mathcal{H}_∞ Design

Let us then consider the \mathcal{H}_∞ control design. The control problem is then defined as the 2×2 block problem shown in Figure 13.2 on page 234. The optimal \mathcal{H}_∞ controller is given by

$$K(z) = \arg \min_{K(z) \in \mathcal{K}_S} \sup_{\omega} \bar{\sigma} (F_l(N(e^{j\omega T_s}), K(e^{j\omega T_s}))) \quad (14.18)$$

$N(z)$ is given by (13.14) on page 233 with $G(z)$ being the Laguerre model (14.1) on page 245. `dhfsyn.m` from the MATLAB μ toolbox was used to compute the optimal \mathcal{H}_∞ controller which achieved

$$\sup_{\omega} \bar{\sigma} (F_l(N(e^{j\omega T_s}), K(e^{j\omega T_s}))) = 0.775 \quad (14.19)$$

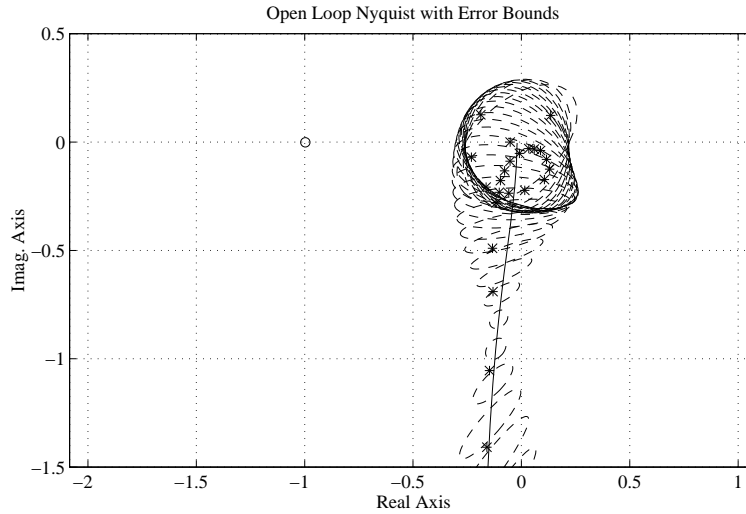


Figure 14.10: \mathcal{H}_∞ approach: Nominal Nyquist with error bounds. Shown are also the measured frequency response estimates multiplied by the controller.

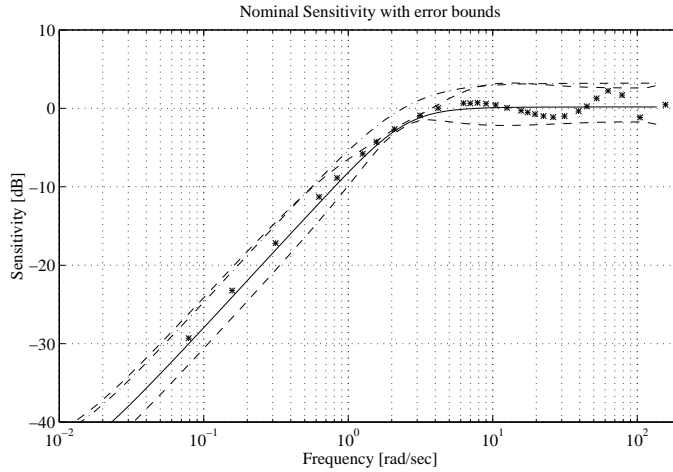


Figure 14.11: \mathcal{H}_∞ approach: Nominal sensitivity with error bounds. Shown are also the upper bound for the sensitivity function $S(e^{j\omega T_s})$ (dash-dotted) and the measured sensitivity estimates.

Remember that in order to guarantee robust performance the robust performance condition had to be strengthened to $1/\sqrt{2} = 0.707$. Thus the optimal \mathcal{H}_∞ did just miss guaranteed robust performance. In Figure 14.10 on the facing page and 14.11 we have checked for robust stability and nominal performance.

In Figure 14.10 the nominal Nyquist with open loop uncertainty ellipses are shown. In Appendix L on page 333 it is shown how the form matrix for an open loop ellipse is obtained. Furthermore, the discrete frequency points obtained by multiplying the measured plant frequency response with the controller are displayed. Since none of the uncertainty ellipses includes the Nyquist point $(-1, 0)$ we conclude that the system is robust stable.

In Figure 14.11 the nominal sensitivity function $S(z)$ is shown together with 90% confidence bounds. The error bounds on the sensitivity were calculated as the inverse of the minimum respectively maximum distance from the open loop uncertainty ellipses to the Nyquist point $(-1, 0)$. Also the upper bound on the sensitivity and a measured sensitivity estimate is shown. The latter was obtained by multiplying the measured discrete frequency point estimates by the controller, adding one and inverting. Note that the error bounds exceed the performance specification for frequencies below 0.5 rad/sec and around 10 rad/sec thus indicating a violation of the robust performance criteria. We may also check for robust

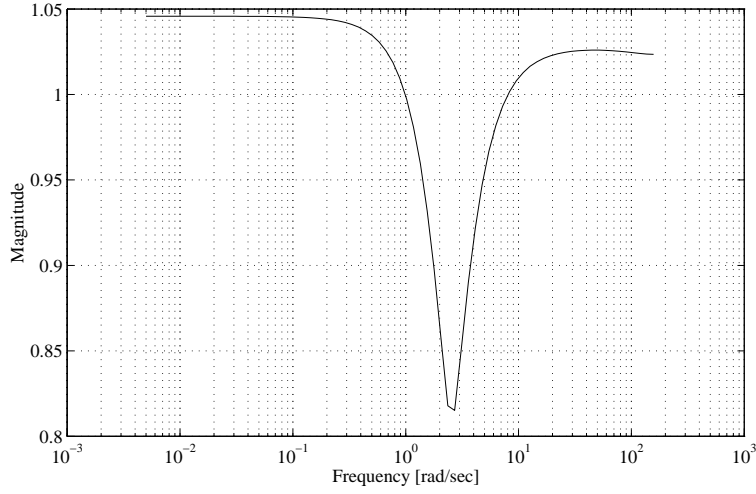


Figure 14.12: *Robust performance check for the \mathcal{H}_∞ controller. Shown are $|W_p(e^{j\omega T_s})S(e^{j\omega T_s})| + |W_u(e^{j\omega T_s})M(e^{j\omega T_s})|$ versus frequency ω .*

performance by Equation (13.17) on page 234. In Figure 14.12 we have plotted $|W_p(e^{j\omega T_s})S(e^{j\omega T_s})| + |W_u(e^{j\omega T_s})M(e^{j\omega T_s})|$ versus frequency ω . Note the correspondence between Figure 14.11 and 14.12. In the high frequency area the robust performance check in Figure 14.12 does not match the corresponding bounds on the sensitivity function in Figure 14.11. This is due to the conservativeness in the perturbation approximation and, possible, to imperfect realizations of the weighting functions.

Even though the \mathcal{H}_∞ design does not obtain robust performance, generally the design is quite satisfactory.

14.2.3 Mixed μ Design

Then let us turn to the mixed μ control design. The $N\Delta K$ formulation is thus given as in Figure 13.5 on page 239 with $N(z)$ given by (13.40) on page 238 and $G(z, \hat{\theta}_N)$ given by the Laguerre model (14.1) on page 245. The optimal mixed μ control problem is thus

$$K(z) = \arg \min_{K(z) \in \mathcal{K}_S} \sup_{\omega} \mu_{\tilde{\Delta}}(F_l(N(e^{j\omega T_s}), K(e^{j\omega T_s}))) \quad (14.20)$$

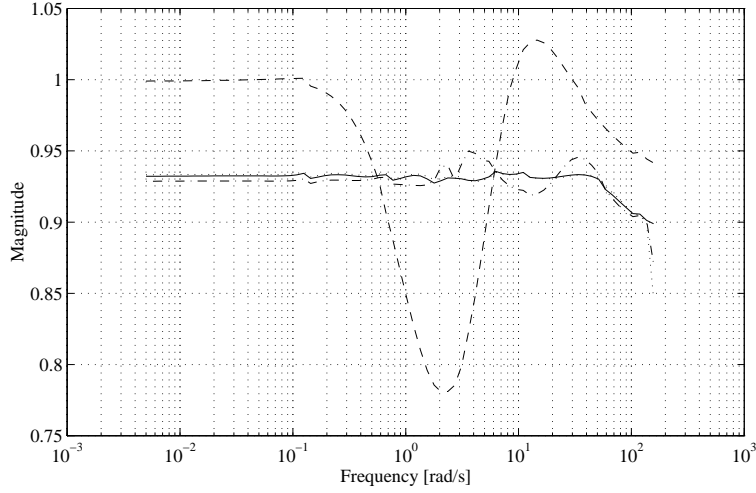


Figure 14.13: Result of μ - K iteration on the pump system. Shown are $\mu_{\tilde{\Delta}}(F_l(N(e^{j\omega T_s}), K(e^{j\omega T_s})))$ for 1st (dashed), 2nd (dash-dotted), 3rd (dotted) and 4th (solid) iteration.

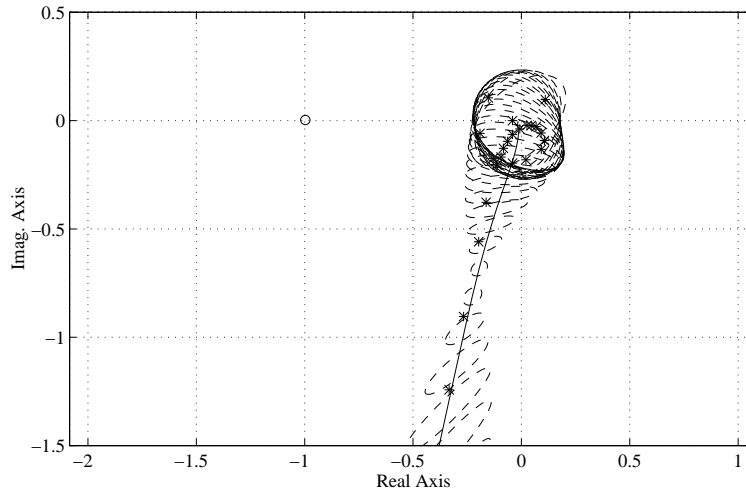
As noted several times, the above problem cannot be solved directly, since only upper and lower bounds for μ can be computed. Our approach here will be μ - K iteration as outlined in Procedure 5.3 on page 86. Of course the iteration will be performed in discrete-time³. The results of the μ - K iteration is shown in Figure 14.13 where the upper bound for $\mu_{\tilde{\Delta}}(F_l(N(e^{j\omega T_s}), K(e^{j\omega T_s})))$ is shown for each iteration. Furthermore some of the central variables in the iteration is tabulated in Table 14.2 on the next page. Note that the iteration converge quickly and that $\bar{\alpha} = 1$ and $\kappa = 1$ for each iteration.

Since $\mu_{\tilde{\Delta}}(F_l(N(e^{j\omega T_s}), K(e^{j\omega T_s})))$ peaks at 0.935 for the final full order controller robust performance was achieved. The final controller was of very high order (45) but it was possible to reduce the number of states down to 6 with very little increase in $\mu_{\tilde{\Delta}}(F_l(N(e^{j\omega T_s}), K(e^{j\omega T_s})))$, see Table 14.2 on the following page.

In Figure 14.14 and 14.15 on page 259 the nominal Nyquist with open loop uncertainty ellipses and the nominal sensitivity function with error bounds are

³The discrete-time μ - K iteration is identical to the continuous-time iteration with s and $j\omega$ replaced by z and $e^{j\omega T_s}$. Since some of the MATLAB μ toolbox routines can be applied only for continuous-time systems them, if they are used, some bilinear transformations from continuous-time to discrete-time must be employed.

Iteration No.	μ - K iteration				
	1	2	3	4	Red.
$\ \mu_{\Delta}(F_l(N(z), K(z)))\ _{\infty}$	1.028	0.950	0.935	0.935	0.936
$\sup_{\omega} \beta_i(\omega)$	0.114	0.0248	0.0133	0.0130	–
$\ F_l(P_i(z), K_i(z))\ _{\infty}$	1.302	1.031	0.966	0.935	–
$\inf_{\omega} \bar{\alpha}_i(\omega)$	1	1	1	1	–
κ	1	1	1	1	–

Table 14.2: Results from μ - K iteration on the pump system.Figure 14.14: μ approach: Nominal Nyquist with error bounds. Shown are also the measured frequency response estimates multiplied by the controller.

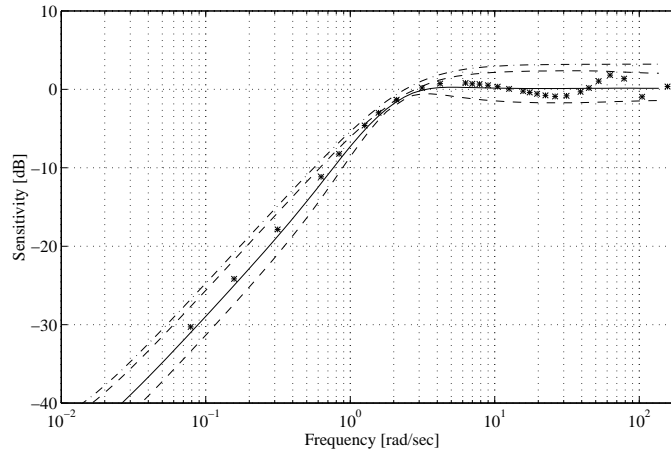


Figure 14.15: μ approach: Nominal sensitivity with error bounds. Shown are also the upper bound for the sensitivity function $S(e^{j\omega T_s})$ (dash-dotted) and the measured sensitivity estimates.

shown respectively. The reduced order controller has been used in computing the results given in both figures. In both plots we have furthermore included the measured frequency response estimates for comparison.

Compare Figure 14.14 and 14.15 with Figure 14.10 and 14.11 on page 255. From Figure 14.14 we conclude that the system is robustly stable since none of the uncertainty ellipses include the Nyquist point. In Figure 14.15, notice how smooth the mixed μ controller shapes the perturbed sensitivity function according to the performance specification.

Finally, in Figure 14.16 on the following page the results of implementing the sixth order controller on the pump system are shown. Here the system response to standard flow steps $\Delta Q = 2/3 \text{ m}^3/\text{hr}$ is investigated. As seen we quite easily comply with the demands given in Section 14.2.1 on page 252.

14.3 Summary

A robust control design for a domestic water supply unit was considered. The design methodology outlined in Procedure 13.1 on page 239 was applied to the system. A second order Laguerre model was identified and frequency domain

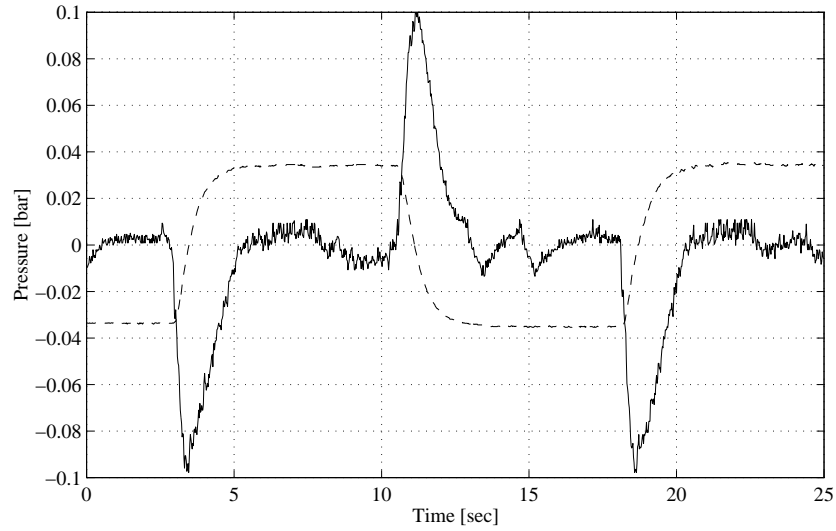


Figure 14.16: *Results from implementing the reduced order mixed μ controller on the pump system. Shown are the pressure response (solid) to standard flow steps (dashed)*

uncertainty ellipses were estimated using stochastic embedding of the bias. Discrete frequency response measurement obtained by applying pure sinusoids at the input verified the obtained uncertainty estimates. Two control designs were then performed; an \mathcal{H}_∞ design and a mixed μ design. Both designs produced satisfactory results even though the \mathcal{H}_∞ controller did not quite achieve robust performance. The mixed μ controller very smoothly shaped the closed loop sensitivity function such that the perturbed sensitivity fell below the performance specification. The mixed μ controller was of very high order (45). However it could be reduced down to sixth order with very little increase in μ . The sixth order controller was implemented on the system with satisfactory results.

Part IV

Conclusions

Chapter 15

Conclusions

Contents

15.1 Part I, Robust Control – Theory and Design	263
15.2 Part II, System Identification and Estimation of Model Error Bounds	268
15.3 Part III, A Synergistic Control Systems Design Methodology	269
15.4 Future Research	270

Now we will summarize the main results from the thesis. The main purpose of this work has been to develop a coherent design procedure for identification based robust control design.

15.1 Part I, Robust Control – Theory and Design

In Part I we presented the robust control design framework necessary for our approach. In Chapter 3 some of the important norms and spaces used in robust control design were discussed. It was shown how the familiar vector 1,2 and ∞ norms induce corresponding matrix norms. Furthermore the norm concept was

extended to operator norms or norms on sets of functions both in the time- and frequency domain. Of particular interest is the matrix 2-norm since we can use it to extend the classical Bode plot for scalar systems to multivariable frequency responses. Let e.g. $G(s)$ be a multivariable transfer function matrix. Then

$$\|G(j\omega)\|_2 = \sup_{u \in \mathbf{C}^n, u \neq 0} \frac{\|G(j\omega)u\|_2}{\|u\|_2} = \bar{\sigma}(G(j\omega)) \quad (15.1)$$

where $\|u\|_2$ is the usual Euclidean length of the vector u and $\bar{\sigma}(\cdot)$ denotes the maximum singular value. Thus the matrix 2-norm $\|G(j\omega)\|_2$ measures the maximum possible “gain” of $G(j\omega)$ in terms of the 2-norm of the input vector before and after multiplication by $G(j\omega)$. Performing a singular value decomposition, see Lemma 3.1 on page 19, of $G(j\omega)$ also the minimum singular value:

$$\underline{\sigma}(G(j\omega)) = \inf_{u \in \mathbf{C}^n, u \neq 0} \frac{\|G(j\omega)u\|_2}{\|u\|_2} \quad (15.2)$$

can be determined. Thus the gain of $G(j\omega)$ is bounded by its maximum and minimum singular values as the input vector varies over all possible directions. By plotting the singular values $\bar{\sigma}(G(j\omega))$ and $\underline{\sigma}(G(j\omega))$ for each frequency ω we obtain the multivariable generalization of the classical magnitude Bode plot. The peak of the singular value Bode plot equals the transfer function ∞ -norm:

$$\|G(s)\|_\infty = \sup_{\omega} \bar{\sigma}(G(j\omega)) \quad (15.3)$$

$\|G(s)\|_\infty$ thus measures the maximum possible gain of $G(j\omega)$ for all frequencies and all possible input directions. Another important interpretation of the transfer function ∞ -norm is that it also measures the maximum amplification of the input in terms of the *time-domain* operator 2-norm:

$$\|G(s)\|_\infty = \sup_{u(t) \in \mathbf{R}, u \neq 0} \frac{\|y(t)\|_2}{\|u(t)\|_2} \quad (15.4)$$

The space of all stable transfer functions for which (15.3) is finite is the Hardy space \mathcal{H}_∞ .

In Chapter 4, the “classical” \mathcal{H}_∞ control theory is reviewed. Robust control design is essentially a question of weighing out robustness and performance in an optimal way. In \mathcal{H}_∞ control design the uncertainty is assumed to be in the form of a single unstructured complex perturbation, e.g. like

$$G_T(s) = G(s) + \tilde{\Delta}(s) \quad (15.5)$$

where $G_T(s)$ and $G(s)$ denote the true system and nominal model respectively and $\tilde{\Delta}(s) \in \mathbf{C}^{m \times n}$ is some unknown perturbation which is bounded by its maximum singular value:

$$\bar{\sigma}(\tilde{\Delta}(j\omega)) \leq \ell(\omega) \quad (15.6)$$

Usually diagonal weighting matrices are introduced to normalize $\Delta(s)$ to norm one

$$\tilde{\Delta}(s) = W_{u2}(s)\Delta(s)W_{u1}(s) \quad (15.7)$$

where $\bar{\sigma}(\Delta(j\omega)) \leq 1$. There are two main reasons for picking such a perturbation model. First of all, it captures well the effects of high-frequency unmodeled dynamics, non-linearities, time-delays, etc. and secondly, it leads to tractable expressions for robust stability. In particular, using the Small Gain Theorem on page 44 it is straightforward to show, see Theorem 4.4 on page 44, that for the additive perturbation model (15.5) on the facing page, a necessary and sufficient condition for robust stability of the closed loop system is:

$$\bar{\sigma}(W_{u1}(j\omega)M(j\omega)W_{u2}(j\omega)) < 1 \quad \forall \omega \geq 0 \quad (15.8)$$

where $M(s) = K(s)(I + G(s)K(s))^{-1}$ is usually denoted the control sensitivity. It is a common mistake to believe that (15.8) is a conservative stability condition. This is *not* true. The condition (15.8) is tight such that there exists a perturbation $\Delta^*(s)$ with $\bar{\sigma}(\Delta^*(j\omega)) \leq 1$ for which the closed loop system becomes unstable unless (15.8) is satisfied. The conservatism in \mathcal{H}_∞ does not lie in the condition (15.8) but in the assumed structure of the perturbation. We will return to this shortly. Let us first, however, look at the performance measures in \mathcal{H}_∞ robust control. Generally in any control design, there are two main performance goals, namely command following (tracking problem) and disturbance attenuation (regulation problem). However, the tracking problem can to a large extent be considered by two-degree-of-freedom control concepts using a prefilter to improve the transient response of the system. Thus the performance demand for the feedback controller is mainly one of attenuating disturbances. A typical performance specification uses the output sensitivity function $S_o(s) = (I + G(s)K(s))^{-1}$. Since $S_o(s)$ is the transfer function matrix from disturbances on the output $y(s)$ to the control error $e(s)$ a performance demand can be written

$$\bar{\sigma}(W_{p2}(j\omega)S_o(j\omega)W_{p1}(j\omega)) \leq 1 \quad \forall \omega \geq 0 \quad (15.9)$$

where $W_{p1}(s)$ and $W_{p2}(s)$ are weighting functions, see Figure 4.3 on page 39. The input weight $W_{p1}(s)$ is used to transform the normalized input vector $\delta'(s)$ to the physical inputs $\delta(s) = W_{p1}(s)\delta'(s)$. The normalized inputs are assumed to belong to the bounded set

$$\mathcal{D}' = \left\{ \delta'(s) \left| \|\delta'\|_2 = \frac{1}{2\pi} \sqrt{\int_{-\infty}^{\infty} \delta(j\omega)^* \delta(j\omega) d\omega} \leq 1 \right. \right\} \quad (15.10)$$

The output weight $W_{p2}(s)$ is used to trade off the relative importance of the individual components of the control error $e(s)$ and to specify the attenuation level

across frequency. An important interpretation of the performance specification is that the time-domain 2-norm of the weighted control error $e'(t)$ will be bounded by $\|W_{p2}(s)S_o(s)W_{p1}(s)\|_\infty$:

$$\sup_{d'(s) \in \mathcal{D}'} \|e'(t)\|_2 = \sup_{d'(s) \in \mathcal{D}'} \sqrt{\int_0^\infty e'(t)^T e'(t) dt} = \|W_{p2}(s)S_o(s)W_{p1}(s)\|_\infty \quad (15.11)$$

If a controller is designed such that (15.9) on the preceding page is fulfilled, the closed loop system is said to have nominal performance. In Chapter 4 it is then shown how a 2×2 block problem may be posed both for the robust stability problem and for the nominal performance problem. For both control problems the optimal design problem will be of the form

$$K(s) = \arg \min_{K(s) \in \mathcal{K}_s} \|F_l(N(s), K(s))\|_\infty \quad (15.12)$$

where $N(s)$ is the augmented plant. (15.12) is the standard \mathcal{H}_∞ optimal control problem. An iterative state space solution with $K(s)$ having the same number of states as $N(s)$ were presented by Doyle, Glover, Khargonekar and Francis in 1988.

We may also consider robust stability and nominal performance simultaneously within the framework of the 2×2 block problem. However, often our main objective is robust performance, that is, our performance demands should be satisfied for all possible plants $G_T(s)$. Unfortunately as shown in Section 4.4 on page 49 nominal performance and robust stability does *not* necessarily imply robust performance. In fact, if the plant is ill-conditioned, robust performance can be arbitrarily poor even though we have robust stability and nominal performance. On the other hand, if the plant is well-conditioned, robust performance *cannot* be arbitrarily poor if we have robust stability and nominal performance. Generally, if an unstructured uncertainty description is tight, we believe that robust performance can be considered non-conservatively in the \mathcal{H}_∞ framework if a little care is taken when formulating the control problem, that is, when choosing the performance and uncertainty weights. We believe that the main problem with the \mathcal{H}_∞ approach is that we can only handle full complex perturbation blocks. Often much more detailed uncertainty descriptions will be available and they may consequently only be handled with conservatism in the \mathcal{H}_∞ framework.

Fortunately theory exists which can handle structured uncertainty in a non-conservative manner. Using the structured singular value μ we may address robust stability problem with mixed real and complex perturbation structures where the perturbation has a block diagonal structure. We thus can consider structured uncertainty which enters the nominal model in a linear fractional manner. The permitted perturbations in the μ framework are much more detailed than those permitted for \mathcal{H}_∞ problems. Using μ we can then derive necessary and

sufficient conditions for robust stability. Furthermore, the robust performance problem can be considered non-conservatively by augmenting the perturbation structure with a full complex perturbation block.

Very general control problems can be naturally formulated within the $N\Delta K$ framework introduced in Section 5.1.2 on page 71 and simple conditions for nominal performance, robust stability and robust performance can be given with μ .

Unfortunately, μ cannot be directly computed unless in some very restrictive special cases. This has naturally hampered the practical use of μ theory. However, reasonable tight upper and lower bounds for μ can be effectively computed and today commercially available hardware exists which support this. Thus from a control engineering point of view, the mathematical problems concerning μ are more or less insignificant. Of much greater importance is whether we can solve the optimal μ control problem:

$$K(s) = \arg \min_{K(s) \in \mathcal{K}_S} \|\mu_{\Delta}(F_l(N(s), K(s)))\|_{\infty} \quad (15.13)$$

Since we cannot normally compute μ it is clear that the problem (15.13) is not tractable. However, we may formulate the control problem in terms of the upper bound on μ instead. The upper bound problem is, however, also an yet unsolved problem. However, for purely complex perturbation sets, an approximation to μ synthesis can be made through a series of minimizations, first over the controller $K(s)$ and then over the scalings $D(\omega)$ involved in the upper bound. This procedure, known as *D-K iteration*, see Section 5.2.1 on page 78, seems to work quite well in practice even though the iteration cannot be guaranteed to converge. Thus for systems with purely complex perturbations a well-documented and software-supported design approach exists for optimal μ design.

Unfortunately the same is not true for mixed real and complex perturbation sets. During the past 5 years, the mixed μ synthesis problem has received considerable interest in the automatic control community. Peter Young [You93] was probably the first who presented a solution to this problem. However, the procedure outlined by Young, denoted *D,G-K iteration*, see Section 5.2.2 on page 80, is much more involved than *D-K iteration*. It involves a lot of spectral factorizations theory and unlike in *D-K iteration* the scaling matrices must be fitted both in phase and magnitude. Since the *G*-scalings are purely imaginary, this severely hampers the practical use of *D,G-K iteration*.

One of the major results of this thesis is a new approach for mixed real and complex μ synthesis. By sacrificing some of the convergence properties in *D,G-K iteration* we have obtained an iterative procedure denoted *μ -K iteration* where we only need to fit scaling matrices in magnitude.

In Chapter 6 a case study is performed in order to compare the results of the *D,G-K iteration* with our new approach. For this particular system it turns out,

that μ - K iteration performs 20% better in terms of achieved μ levels.

In Chapter 7 a complex μ design for an ASTOVL aircraft was performed. This particular system was very ill-conditioned so that a special performance weight had to be introduced. The final complex μ design gave significant improvement over the existing classical design.

15.2 Part II, System Identification and Estimation of Model Error Bounds

In Part II the problem of estimating a nominal model and frequency domain error bounds was considered. In robust control theory the uncertainty bounds are usually simply assumed given a priori. However, the determination of these bounds are by no means a trivial problem. It is therefore appealing to think that they may simply be estimated using system identification methods. However, as shown in Chapter 9, classical identification techniques will only produce consistent estimates of the model error provided the true system can be described by the chosen model structure. For the general model structure (9.1) on page 140, in order to obtain consistent estimates of the parameter covariance, we must require that both the deterministic and stochastic part of the true system can be described within our model set. In Chapter 10 different special cases are reviewed. In particular we notice that with an output error model structure we will obtain consistent estimates of the parameter covariance if the deterministic part of the true system can be represented within our model set regardless whether this goes for the stochastic part as well. Furthermore, using a fixed denominator model, we may obtain consistent estimates of the parameter covariance even in the case of undermodeling, that is, even though the true system cannot be represented within our model set. Since the least-squares parameter estimate for fixed denominator structures furthermore are analytical, there are strong motivations for using such model structures. During the last 5 years intensive research in fixed denominator model structures have been performed e.g. by Bo Wahlberg. Unfortunately, even though our parameter covariance estimates are consistent, if the true system cannot be represented within the model set, the frequency domain model error bounds will be misleading. Thus to obtain useful estimates of the frequency domain uncertainty with the classical approach we still need to assume that the true system can be represented within the model set.

Unfortunately this is often an inadequate assumption in connection with robust control, since we will like to have simple plant descriptions in order to avoid high order controllers. Consequently, the last decade have witnessed a growing awareness of that classical identification methods can not provide us with the frequency domain uncertainty bounds that we need for robust control design.

As a result, intensive research has been done on developing new techniques for estimation of model error bounds.

However, estimating of model error bounds from finite noisy data is a very difficult problem if the true system cannot be described within the model set. In that case, the model residuals will contain two parts; a deterministic part due to the undermodeling and a stochastic part due to the noise. However, the approach taken by most researchers has been to assume that either the noise is deterministic (unknown, but bounded in magnitude) nor that the undermodeling is stochastic (non-stationary and correlated with the input).

It is then well-known that some a priori knowledge of the noise and the undermodeling must be available in order to compute the model error bounds. However, as shown in Chapter 11, the *stochastic embedding approach* provides the opportunity of estimating the quantitative part of the necessary a priori knowledge. We feel that this makes the stochastic embedding approach superior to the other new approaches for estimation of model uncertainty. In Chapter 11 a thorough introduction to the stochastic embedding approach is provided. The main idea is to assume that the undermodeling is a realization of a zero mean stochastic process. We may then derive results for fixed denominator models which can be viewed as an extension to the classical results.

Our main contribution in this part of the thesis is investigation of new parameterizations for the covariance matrices for the noise and the undermodeling. In Chapter 12 a case study is performed where different parameterizations for the undermodeling are investigated. It is shown that we may obtain reasonable accurate estimates of the model error using the stochastic embedding approach.

15.3 Part III, A Synergistic Control Systems Design Methodology

Finally in Part III we have combined the results from Part I and Part II into a coherent design approach for identification based robust control design for scalar systems. If a large number of measurements are available we suggest that a classical output error approach is used for system identification. If only few measurements are available the stochastic embedding approach is suggested. In any case, the result will be a nominal model and frequency domain uncertainty ellipses.

It is then shown how a mixed perturbation set may be used to approximate the estimated uncertainty ellipses. The corresponding control problem will thus be a mixed μ problem. We suggest that μ - K iteration is applied in order to solve the control problem. A full step-by-step design procedure is outlined in Section 13.3

on page 239. This design procedure is the main result of the thesis. The design approach has been applied in control of a compact domestic water supply unit, see Chapter 14. The final mixed μ controller was implemented on the pump system with satisfactory results.

15.4 Future Research

The design methodology presented in this thesis can be applied only to scalar systems. However, modern design methods like \mathcal{H}_∞ and μ based synthesis algorithms have potential in particular for multivariable systems where the classical design methods become more “unpredictable”. The results presented on robust control design in Chapter 4 and Chapter 5 thus apply for multivariable systems in general. On the other hand, it seems that the emphasis in system identification has been placed mostly on scalar systems. It is possible to extend the classical PEM approach to multivariable systems without much difficulty. However, the asymptotic properties of the estimate seem not to have attracted much attention. One exception is the work by Zhu and co-workers, see e.g. [ZBE91]. These methods, however, are asymptotic not only in the number of data N , but also in the model order n . Thus the error bounds will only be valid for very high order models and for large data series. The stochastic embedding approach produce promising results for scalar systems. However, the maximum likelihood estimation of the covariance matrices for the noise and the undermodeling is only developed for scalar systems and only tractable for small data series.

In our future research on the subject we will try to extend the results presented on system identification in Chapter 9, 10 and 11 to multivariable systems.

Another area for future research is the proposed new algorithm for mixed real and complex μ synthesis, μ - K iteration. We established two necessary conditions for convergence of μ - K iteration. Firstly, the iteration must be monotonically non-increasing in the ∞ -norm of the augmented closed loop system $F_l(N_{D\Gamma_i}(s), K(s))$. Thus

$$\|F_l(N_{D\Gamma_i}(s), K_i(s))\|_\infty \leq \|F_l(N_{D\Gamma_{i-1}}(s), K_{i-1}(s))\|_\infty \quad \forall i \quad (15.14)$$

Secondly, the iteration must be monotonically non-increasing in the ∞ -norm of $\beta_i(\omega)$. Thus

$$\|\beta_i(\omega)\|_\infty \leq \|\beta_{i-1}(\omega)\|_\infty \quad \forall i \quad (15.15)$$

$\beta_i(\omega)$ is a measure of how well the augmented closed loop system approximates the mixed μ upper bound. We were able to prove the first of the two conditions above. We believe that we cannot always achieve the second condition. However, this is certainly an area which requires more research.

Bibliography

- [AA94] N. Amann and F. Allgöwer. μ -suboptimal design of a robustly performing controller for a chemical reactor. *Int. J. Control*, 59(3):665–687, 1994.
- [ATCP94] P. Andersen, S. Tøffner-Clausen, and T.S. Pedersen. Estimation of frequency domain model uncertainties with application to robust controller design. In *Proc. SYSID '94*, volume 3, pages 603–608, Copenhagen, Denmark, July 1994.
- [ÅW84] K.J. Åström and B. Wittenmark. *Computer Controlled Systems: Theory and Design*. Prentice-Hall Information and System Sciences Series. Prentice-Hall Inc., Englewood Cliffs, NJ, 1984.
- [ÅW89] K.J. Åström and B. Wittenmark. *Adaptive Control*. Number 09720 in Addison-Wesley Series in Electrical and Computer Engineering: Control Engineering. Addison-Wesley, 1989.
- [Bai92] J. Baillieul, editor. *IEEE Trans. Aut. Contr., Special Issue on System Identification for Robust Control*, volume 37, No. 7. IEEE Control Systems Society, July 1992.
- [BATC94] M. Blanke, P. Andersen, and S. Tøffner-Clausen. Modelling and uncertainty. Lecture Note for Young Researchers Week, Organized by the EURACO Network, Dublin R94-4064, Dept. of Control Engineering, Aalborg University, Frederik Bajers Vej 7, DK-9220 Aalborg Ø, Denmark, Aug. 1994.
- [BD92] T.C.P.M. Backx and A.A.H. Damen. Identification for the control of mimo industrial processes. *IEEE Trans. Aut. Contr.*, 37(7):980–986, July 1992.
- [BDG⁺93] G.J. Balas, J.C. Doyle, K. Glover, A. Packard, and R. Smith. *μ -Analysis and Synthesis Toolbox*. The MathWorks Inc., Natick, Mass., USA, 2nd edition, July 1993.

- [Ber94] B. Bernhardsson. The \mathcal{H}_∞ approach. In *EURACO Network: Robust and Adaptive Control Tutorial Workshop*, University of Dublin, Trinity College, 1994. Lecture 2.2.
- [BG94a] S. G. Breslin and M. J. Grimble. Multivariable control of an AS-TOVL aircraft. Part 1 : Analysis and design. Technical Report ICC/90/94, Industrial Control Centre, University of Strathclyde, 1994.
- [BG94b] S. G. Breslin and M. J. Grimble. Multivariable control of an AS-TOVL aircraft. Part 2 : MATLAB Toolbox. Technical Report ICC/91/94, Industrial Control Centre, University of Strathclyde, 1994.
- [BGFB94] S. Boyd, L. El Ghaoui, E. Feron, and V. Balakrishnan. *Linear Matrix Inequalities in System and Control Theory*. Number 15 in SIAM Studies in Applied Mathematics. Society for Industrial and Applied Mathematics, Philadelphia, Pennsylvania, 1994.
- [BGW90] R.R. Bitmead, M. Gevers, and V. Wertz. *Adaptive Optimal Control, The Thinking Man's GPC*. Prentice-Hall International Series in Systems and Control Engineering. Prentice Hall of Australia Pty Ltd, 1990.
- [BYM92] D.S. Bayard, Y. Yam, and E. Mettler. A criterion for joint optimization of identification and robust control. *IEEE Trans. Aut. Contr.*, 37(7):986–991, July 1992.
- [CS92] R.Y. Chiang and M.G. Safonov. *Robust Control Toolbox*. The MathWorks Inc., Natick, Mass., USA, Aug. 1992.
- [Dai90] R. Lane Dailey. Lecture notes for the workshop on \mathcal{H}_∞ and μ methods for robust control. American Control Conf., San Diego, California, May 1990.
- [dB93] A.C. den Brinker. Adaptive orthonormal filters. In *Proc. IFAC World Congress*, volume 5, pages 287–292, Sydney, Australia, July 1993.
- [DC85] J.C. Doyle and C.-C. Chu. Matrix interpolation and \mathcal{H}_∞ performance bounds. In *Proc. American Control Conf.*, pages 129–134, Boston, MA., 1985.
- [Dem88] J. Demmel. On structured singular values. In *Proc. American Control Conf.*, pages 2138–2143, Austin, Texas, Dec. 1988.

- [DGKF89] J.C. Doyle, K. Glover, P.P. Khargonekar, and B.A. Francis. State space solutions to standard \mathcal{H}_2 and \mathcal{H}_∞ control problems. *IEEE Trans. Aut. Contr.*, AC-34(8):831–847, 1989.
- [dMGG91] B. de Moor, M. Gevers, and G.C. Goodwin. Overbiased, underbiased and unbiased estimation of transfer functions. In *Proc. 9th IFAC/IFORS Symposium on System Identification and Parameter Estimation*, pages 946–951, Budapest, Hungary, July 1991.
- [Doy81a] J.C. Doyle. Limitations on achievable performance of multivariable feedback systems. AGARD Lectures Series No. 117 on Multivariable Analysis and Design Techniques, Sept. 1981.
- [Doy81b] J.C. Doyle. Multivariable design techniques based on singular value generalizations of classical control. AGARD Lectures Series on Multivariable Analysis and Design Techniques, Sept. 1981.
- [Doy82] J.C. Doyle. Analysis of feedback systems with structured uncertainties. In *IEE Proceedings*, volume 129, Part D, No. 6, pages 242–250, November 1982.
- [Doy85] J.C. Doyle. Structured uncertainty in control system design. In *Proc. 24th Conf. on Decision and Control*, pages 260–265, 1985.
- [DP87] J.C. Doyle and A. Packard. Uncertain multivariable systems from a state space perspective. In *Proc. American Control Conf.*, pages 2147–2152, Minneapolis, MN, 1987.
- [DPZ91] J.C. Doyle, A. Packard, and K. Zhou. Review of LFTs, LMIs and μ . In *Proc. 30th Conf. on Decision and Control*, pages 1227–1232, Brighton, England, December 1991. IEEE.
- [DS79] J.C. Doyle and G. Stein. Robustness with observers. *IEEE Trans. Aut. Contr.*, AC-24(4):607–611, August 1979.
- [DS81] J.C. Doyle and G. Stein. Multivariable feedback design: Concepts for a classical/modern synthesis. *IEEE Trans. Aut. Contr.*, AC-26(1):4–16, February 1981.
- [DV75] C.A. Desoer and M. Vidyasagar. *Feedback Systems: Input-Output Properties*. Academic Press, New York, 1975.
- [FD93] Y. Fu and G.A. Dumont. On determination of laquerre filter pole through step or impulse response data. In *Proc. IFAC World Congress*, volume 5, pages 303–307, Sydney, Australia, July 1993.

- [Fra87] B.A. Francis. *A Course in \mathcal{H}_∞ Control Theory*, volume 88 of *Lecture Notes in Control and Information Sciences*. Springer Verlag, Berlin, 1987.
- [Fre89a] J.S. Freudenberg. Analysis and design for ill-conditioned plants. part 1. lower bounds on the structured singular value. *Int. J. Control*, 49(3):851–871, 1989.
- [Fre89b] J.S. Freudenberg. Analysis and design for ill-conditioned plants. part 2. directionally uniform weightings and an example. *Int. J. Control*, 49(3):873–903, 1989.
- [FTD91] M.K.H. Fan, A.L. Tits, and J.C. Doyle. Robustness in the presence of mixed parametric uncertainty and unmodeled dynamics. *IEEE Trans. Aut. Contr.*, 36(1):25–38, Jan. 1991.
- [Gev91] M. Gevers. Connecting identification and robust control: A new challenge. In *Proc. IFAC Symposium on Identification and System Parameter Estimation*, Budapest, 1991. IFAC.
- [GGM91] G.C. Goodwin, M. Gevers, and D.Q. Mayne. Bias and variance distribution in transfer function estimation. In *Proc. 9th IFAC Symposium on Identification and System Parameter Estimation*, pages 952–957, Budapest, 1991. IFAC.
- [GGN90] G.C. Goodwin, M. Gevers, and B. Ninness. Optimal model order selection and estimation of model uncertainty for identification with finite data. Technical report, Louvain University, Belgium, 1990.
- [GGN91] G.C. Goodwin, M. Gevers, and B. Ninness. Optimal model order selection and estimation of model uncertainty for identification with finite data. In *Proc. 30th Conf. on Decision and Control*, pages 285–290, Brighton, England, December 1991. IEEE.
- [GGN92] G.C. Goodwin, M. Gevers, and B. Ninness. Quantifying the error in estimated transfer functions with application to model order selection. *IEEE Trans. Aut. Contr.*, 37(7):913–928, July 1992.
- [GJ88] M.J. Grimble and M.A. Johnson. *Optimal Control and Stochastic Estimation, Theory and Applications*, volume 1 and 2. John Wiley & Sons, 1988.
- [GK92] G. Gu and P.P. Khargonekar. Linear and nonlinear algorithms for identification in \mathcal{H}_∞ with error bounds. *IEEE Trans. Aut. Contr.*, 37(7):953–963, July 1992.

- [GM94] L. Giarre and M. Milanese. \mathcal{H}_∞ identification with mixed parametric and nonparametric models. In *Proc. SYSID '94*, volume 3, pages 255–259, Copenhagen, Denmark, July 1994. IFAC.
- [GNS90] G.C. Goodwin, B. Ninness, and M.E. Salgado. Quantification of uncertainty in estimation. In *Proc. American Control Conf.*, pages 2400–2405, San Diego, USA, May 1990.
- [Gri86] M.J. Grimble. Optimal \mathcal{H}_∞ robustness and the relationship to LQG design problems. *Int. J. Control*, 43(2):351–372, 1986.
- [Gri88] Micheal J. Grimble. Optimal \mathcal{H}_∞ multivariable robust controllers and the relationship to LQG design problems. *Int. J. Control*, 48(1):33–58, 1988.
- [Gri94] M.J. Grimble. *Robust Industrial Control*. Systems and Control Engineering. Prentice Hall, 1994.
- [GS89a] G.C. Goodwin and M.E. Salgado. Quantification of uncertainty in estimation using an embedding principle. In *Proc. American Control Conf.*, pages 1416–1421, Pittsburgh, PA, 1989.
- [GS89b] G.C. Goodwin and M.E. Salgado. A stochastic embedding approach for quantifying uncertainty in the estimation of restricted complexity models. *Int. J. Adaptive Control and Signal Processing*, 3(4):333–356, 1989.
- [GSM89] G.C. Goodwin, M.E. Salgado, and D.Q. Mayne. A bayesian approach to estimation with restricted complexity models. Technical report, Newcastle University, Dept. of Electrical & Computer Engineering, NSW 2308 Australia, 1989.
- [HdHB93] P.S.C. Heuberger, P.M.J. Van den Hof, and O.H. Bosgra. Modelling linear dynamical systems through generalized orthonormal basis functions. In *Proc. IFAC World Congress*, volume 5, pages 283–286, Sydney, Australia, July 1993.
- [Hja90] Håkon Hjalmarson. On estimation of model quality in system identification. Licentiate Thesis LIU-TEK-LIC-1990:51, Linköping University, Department of Electrical Engineering, S-581 83 Linköping, Sweden, October 1990.
- [Hja93] Håkon Hjalmarson. *Aspects on Incomplete Modeling in System Identification*. PhD thesis, Linköping University, Department of Electrical Engineering, S-581 83 Linköping, Sweden, 1993.

- [HJN91] A.J. Helmicki, C.A. Jakobson, and C.N. Nett. Control oriented system identification: A worst-case/deterministic approach in \mathcal{H}_∞ . *IEEE Trans. Aut. Contr.*, 36(10):1161–1176, October 1991.
- [HL90a] H. Hjalmarson and L. Ljung. How to estimate model uncertainty in the case of undermodelleing. In *Proc. Americal Control Conf.*, pages 323–324, San Diego, 1990.
- [HL90b] H. Hjalmarson and L. Ljung. How to estimate model uncertainty in the case of undermodelleing. LITH-ISY-I 1067, Linköping University, Department of Electrical Engineering, Marts 1990.
- [HL92] Håkon Hjalmarson and L. Ljung. Estimating model variance in case of undermodelling. *IEEE Trans. Aut. Contr.*, 37(7):1004–1008, july 1992.
- [HL94] H. Hjalmarson and L. Ljung. A unifying view of disturbances in identification. In *Proc. SYSID '94*, volume 2, pages 73–78, Copenhagen, Denmark, July 1994. IFAC.
- [Hol94] A.M. Holohan. A tutorial on mu-analysis. In *EURACO Network: Robust and Adaptive Control Tutorial Workshop*, University of Dublin, Trinity College, 1994. Lecture 2.5.
- [Irv91] J.P. Irving. Generic rigid aircraft model with multi-input, multi-output (mimo) control system for use in fcs design studies. Technical Report BAe-WAE-RP-RES-FCS-000462, British Aerospace, 1991.
- [Kal60] R.E. Kalman. Contributions to the theory of optimal control. *Bol. Soc. Mat. Mex.*, 5:102–119, 1960.
- [Kal64] R.E. Kalman. When is a linear control system optimal? *Journal of Basic Engineering (Trans. ASME D)*., 86:51–60, 1964.
- [KD88] K.Glover and J.C. Doyle. State-space formulae for all stabilizing controllers that satisfy an \mathcal{H}_∞ -norm bound and relations to risk sensitivity. *Systems & Control Letters*, 11(3):167–172, 1988.
- [KHN62] R.E. Kalman, Y.C. Ho, and K.S. Narendra. Controllability of linear dynamic systems. *Contributions to Differential Equations*, 1, 1962.
- [KK92] J.M. Krause and P.P. Khargonekar. A comparison of classical stochastic estimation and deterministic robust estimation. *IEEE Trans. Aut. Contr.*, 37(7):994–1000, Juli 1992.

- [KLB92] R.L. Kosut, M.K. Lau, and S.P. Boyd. Set-membership identification of systems with parametric and nonparametric uncertainty. *IEEE Trans. Aut. Contr.*, 37(7):929–941, July 1992.
- [Knu93] T. Knudsen. Systemidentifikation. Technical Report AUC-PROCES-U-93-4008, Institute of Electronic Systems, Aalborg University, Frederik Bajers Vej 7, DK-9220 Aalborg Ø, Denmark, Jan. 1993.
- [Kos93] R.L. Kosut. Determining model uncertainty of identified models for robust control design. In *Proc. IFAC World Congress*, volume 7, pages 373–376, Sydney, Australia, July 1993.
- [KR82] M. Knudsen and H. Rasmussen. Systemidentifikation. Technical Report R82-4, Institute of Electronic Systems, Aalborg University, Frederik Bajers Vej 7, DK-9220 Aalborg Ø, Denmark, 1982. Revised version, Jan. 1987.
- [Kwa85] H. Kwakernaak. Minimax frequency domain performance and robustness optimization of linear feedback systems. *IEEE Trans. Aut. Contr.*, AC-30(10):994–1004, 1985.
- [LBKF91] M.K. Lau, S.P. Boyd, R.L. Kosut, and G.F. Franklin. Robust control design for ellipsoidal plants set. In *Proc. 30th Conf. on Decision and Control*, pages 291–296, Brighton, England, December 1991. IEEE.
- [Lei89] W.E. Leithead. Control systems for wind turbines. *Wind Engineering*, 13(6):293–301, 1989.
- [Let81] N.A. Lethomaki. *Practical Robustness Measures in Multivariable Control System Analysis*. PhD thesis, Dept. of Electrical Eng. and Computer Science, Massachusetts Institute of Technology, Cambridge, MA, 1981.
- [Lit93] J. Little. *Control Systems Toolbox*. The MathWorks Inc., Natick, Mass., USA, 2nd edition, 1993.
- [Lju85] L. Ljung. Asymtotic variance expressions for identified black-box transfer function models. *IEEE Trans. Aut. Contr.*, AC-30(9):834–844, Sept. 1985.
- [Lju87] L. Ljung. *System Identification - Theory for the User*. Prentice Hall Inc., Englewood Cliffs NJ, 1987.

- [Lju89] L. Ljung. System identification in a noise free environment. In *Proc. Adaptive Systems in Control and Signal Processing*, pages 441–420, Glasgow, UK, 1989. IFAC.
- [Lju91] L. Ljung. A discussion of model accuracy in system identification. LiTH-ISY-I 1307, Linköping University, Department of Electrical Engineering, December 1991.
- [LPG93] J.-L. Lin, I. Postlethwaite, and D.-W. Gu. $\mu - K$ iteration: A new algorithm for μ -synthesis. *Automatica*, 29(1):219–224, 1993.
- [LW93] P. Lindskog and B. Wahlberg. Applications of kautz models in system identification. In *Proc. IFAC World Congress*, volume 5, pages 309–312, Sydney, Australia, July 1993.
- [LWH91] L. Ljung, B. Wahlberg, and H. Hjalmarsson. Model quality: The roles of prior knowledge and data information. In *Proc. of the 30th Conf. on Decision and Control*, pages 273–278, Brighton, England, December 1991. IEEE.
- [M91] P.M. Mäkilä. Laguerre methods and \mathcal{H}^∞ identification of continuous-time systems. *Int. J. Control*, 53(3):698–707, 1991.
- [Mac89] J.M. Maciejowski. *Multivariable Feedback Design*. Addison-Wesley Series in Electronic Systems Engineering. Addison-Wesley, 1989.
- [MPG94] P.M. Mäkilä, J.R. Partington, and T.K. Gustafsson. Robust identification. In *Proc. SYSID '94*, volume 1, pages 45–63, Copenhagen, Denmark, July 1994. IFAC.
- [MZ89] M. Morari and E. Zafiriou. *Robust Process Control*. Prentice-Hall Inc., 1989.
- [NG94] B. Ninness and G.C. Goodwin. Estimation of model quality. In *Proc. SYSID '94*, volume 1, pages 25–44, Copenhagen, Denmark, July 1994. IFAC.
- [Nih93] M.T. Nihtilä. Continuous-time order-recursive least-squares identification. In *Proc. IFAC World Congress*, volume 5, pages 299–302, Sydney, Australia, July 1993.
- [Nin93] B.M. Ninness. *Stochastic and Deterministic Modelling*. PhD thesis, University of Newcastle, New South Wales, Australia, Aug. 1993.

- [Nin94] B. Ninness. Orthonormal bases for geometric interpretation of the frequency response estimation problem. In *Proc. SYSID '94*, volume 3, pages 591–596, Copenhagen, Denmark, July 1994. IFAC.
- [NS91] M.P. Newlin and R.S. Smith. Model validation and a generalization of μ . In *Proc. 30th Conf. on Decision and Control*, pages 1257–1258, Brighton, England, December 1991. IEEE.
- [PB87] P.J. Parker and R.R. Bitmead. Adaptive frequency response identification. In *Proc. 26th Conf. on Decision and Control*, pages 348–353, Los Angeles, CA, Dec. 1987.
- [PD93] A. Packard and J.C. Doyle. The complex structured singular value. *Automatica*, 29(1):71–109, 1993.
- [PKKU94] A. Patra, U. Keuchel, U. Kiffmeier, and H. Unbehauen. Identification for robust control of an unstable plant. In *Proc. SYSID '94*, volume 3, pages 597–602, Copenhagen, Denmark, July 1994. IFAC.
- [PM94] J.R. Partington and P.M. Mäkilä. Analysis of linear methods for robust identification in ℓ_1 . In *Proc. SYSID '94*, volume 2, pages 79–84, Copenhagen, Denmark, July 1994. IFAC.
- [RI94] M.A. Rotea and T. Iwasaki. An alternative to the D-K iteration? In *Proc. American Control Conf.*, pages 53–55, Baltimore, Maryland, June 1994.
- [RVAS85] C.E. Rohrs, L. Valavani, M. Athans, and G. Stein. Robustness of continuous-time adaptive control algorithms in the presence of unmodeled dynamics. *IEEE Trans. Aut. Contr.*, AC-30(9):881–889, Sept. 1985.
- [SA87] G. Stein and M. Athans. The LQG/LTR procedure for multivariable feedback control design. *IEEE Trans. Aut. Contr.*, AC-32(2):105–114, February 1987.
- [Sch92] R.J.P. Schrama. Accurate identification for control: The necessity of an iterative scheme. *IEEE Trans. Aut. Contr.*, 37(7):991–994, July 1992.
- [SD89] R.S. Smith and J.C. Doyle. Model invalidation: A connection between robust control and identification. In *Proc. American Control Conf.*, pages 1435–1440, Pittsburg, PA, 1989.

- [SD90] R.S. Smith and J.C. Doyle. Towards a methodology for robust parameter identification. In *Proc. American Control Conf.*, pages 2394–2399, San Diego, USA, 1990.
- [SD91] G. Stein and J.C. Doyle. Beyond singular values and loop shapes. *Journal of Guidance, Control and Dynamics*, 14:5–16, Jan. 1991.
- [SD92] R.S. Smith and J.C. Doyle. Model validation: A connection between robust control and identification. *IEEE Trans. Aut. Contr.*, 37(7):942–952, July 1992.
- [SD93] R.S. Smith and J.C. Doyle. Closed loop relay estimation of uncertain bounds for robust control models. In *Proc. IFAC World Congress*, volume 9, pages 57–60, Sydney, Australia, July 1993.
- [SDMS87] R.S. Smith, J.C. Doyle, M. Morari, and A. Skjellum. A case study using μ : Laboratory process control problem. In *Proc. IFAC World Congress*, pages 403–415, Munich, Germany, 1987.
- [SLC89] M.G. Safonov, D.J.N. Limebeer, and R.Y. Chiang. Simplifying the \mathcal{H}_{∞} theory via loop-shifting, matrix-pencil and descriptor concepts. *Int. J. Control*, 50(6):2467–2488, 1989.
- [SMD88] S. Skogestad, M. Morari, and J.C. Doyle. Robust control of ill-conditioned plants: High-purity distillation. *IEEE Trans. Aut. Contr.*, 33(12):1092–1105, Dec. 1988.
- [Smi90] R.S. Smith. *Model Validation for Uncertain Systems*. PhD thesis, California Institute of Technology, 1990.
- [Smi93] R.S. Smith. Model validation for robust control: An experimental process control application. In *Proc. IFAC World Congress*, volume 9, pages 61–64, Sydney, Australia, July 1993.
- [sN94] K.J. ström and J. Nilsson. Analysis of a scheme for iterated identification and control. In *Proc. SYSID '94*, volume 2, pages 171–176, Copenhagen, Denmark, July 1994. IFAC.
- [SS89] T. Söderström and P. Stoica. *System Identification*. Prentice Hall International Series in System and Control Engineering. Prentice Hall, New York, 1989.
- [Sto92] A.A. Stoorvogel. *The \mathcal{H}_{∞} Control Problem: A State Space Approach*. Prentice Hall Inc., Englewood Cliffs NJ, 1992.
- [TC91] S. Tøffner-Clausen. Linear quadratic optimal design methods, theory & design. Master's thesis, Aalborg University, Institute of Electronic Systems, 1991.

- [TC95] S. Tøffner-Clausen. Identification for control: Quantification of uncertainty. In *Proc. Youth Automation Conference*, pages 155–159, Beijing, China, 1995. IFAC.
- [TCA93] S. Tøffner-Clausen and P. Andersen. Quantifying frequency domain model uncertainty in estimated transfer functions using a stochastic embedding approach. Research Report W1D-06-001, Reliability and Robustness in Industrial Process Control, Feb. 1993.
- [TCA94] S. Tøffner-Clausen and P. Andersen. Identification for control: Estimation of frequency domain model uncertainty. Research Report R94-4054, Aalborg University, Dept. of Control Eng., Frederik Bajers Vej 7, DK-9220 Aalborg, Denmark, Aug. 1994.
- [TCA95] S. Tøffner-Clausen and P. Andersen. μ -synthesis – a non-conservative methodology for design of controllers with robustness towards dynamic and parametric uncertainty. In *Proc. EURACO Workshop on Recent Results in Robust and Adaptive Control*, pages 269–303, Florence, Italy, September 1995.
- [TCABG95] S. Tøffner-Clausen, P. Andersen, S.G. Breslin, and M.J. Grimble. The application of μ -analysis and synthesis to the control of an ASTOVL aircraft. In *Proc. EURACO Workshop on Recent Results in Robust and Adaptive Control*, pages 304–322, Florence, Italy, September 1995.
- [TCASN94a] S. Tøffner-Clausen, P. Andersen, J. Stoustrup, and Hans Henrik Niemann. Estimated frequency domain model uncertainties used in robust controller design — a μ -approach. In *Proc. 3rd IEEE Conf. on Control Applications*, volume 3, pages 1585–1590, Glasgow, Scotland, Aug. 1994.
- [TCASN94b] S. Tøffner-Clausen, P. Andersen, J. Stoustrup, and H.H. Niemann. Estimated frequency domain model uncertainties used in robust controller design — a μ -approach. Poster Session, EURACO Young Researchers Week, Dublin, Aug. 1994.
- [TCASN95] S. Tøffner-Clausen, P. Andersen, J. Stoustrup, and H.H. Niemann. A new approach to μ -synthesis for mixed perturbation sets. In *Proc. 3rd European Control Conf.*, pages 147–152, Rome, Italy, 1995.
- [TCB95] S. Tøffner-Clausen and S.G. Breslin. Classical versus modern control design methods for safety critical control engineering

- practice. Technical Report ACT/CS08/95, Industrial Control Center, University of Strathclyde, 50 George Street, Glasgow G1 1QE, 1995.
- [vdHS94] P.M.J. van den Hof and R.J.P. Schrama. Identification and control – closed loop issues. In *Proc. SYSID '94*, volume 2, pages 1–13, Copenhagen, Denmark, July 1994. IFAC.
- [vdKvOvdB94] A.C. van der Klaauw, J.E.F. van Osch, and P.P.J. van den Bosch. Closed-loop identification methods for lq control design. In *Proc. SYSID '94*, volume 3, pages 609–613, Copenhagen, Denmark, July 1994. IFAC.
- [VH95] D.K. De Vries and P.M.J. Van Den Hof. Quantification of uncertainty in transfer function estimation: a mixed probabilistic – worst-case approach. *Automatica*, 31(4):543–557, 1995.
- [Wah87] B. Wahlberg. *On the Identification and Approximation of Linear Systems*. PhD thesis, Linköping University, Department of Electrical Engineering, Sweden, 1987.
- [Wah91a] B. Wahlberg. Identification of resonant systems using kautz filters. In *Proc. 30th Conf. on Decision and Control*, pages 2005–2010, Brighton, England, Dec. 1991.
- [Wah91b] B. Wahlberg. System identification using laquerre models. *IEEE Trans. Aut. Contr.*, 36(5):551–562, May 1991.
- [Wah94] B. Wahlberg. Laguerre and kautz models. In *Proc. SYSID '94*, volume 3, pages 1–12, Copenhagen, Denmark, July 1994. IFAC.
- [WBM89] C. Webb, H. Budman, and M. Morari. Identifying frequency domain uncertainty bounds for robust controller design - theory with application to a fixed-bed reactor. In *Proc. American Control Conf.*, pages 1528–1533, Pittsburg, PA, 1989.
- [WL90a] B. Wahlberg and L. Ljung. Hard frequency-domain model error bounds from least-squares like identification techniques. LITH-ISY-I 1144, Linköping University, Department of Electrical Engineering, Dec. 1990.
- [WL90b] B. Wahlberg and L. Ljung. On estimation of transfer function error bounds. LITH-ISY-I 1063, Linköping University, Department of Electrical Engineering, Feb. 1990.

- [WL91] B. Wahlberg and L. Ljung. On estimation of transfer function error bounds. LITH-ISY-I 1186, Linköping University, Department of Electrical Engineering, Feb. 1991.
- [WL92] B. Wahlberg and L. Ljung. Hard frequency-domain model error bounds from least-squares like identification techniques. *IEEE Trans. Aut. Contr.*, 37(7):900–912, July 1992.
- [YÅ94] P.M. Young and K.J. Åström. μ meets bode. In *Proc. American Control Conf.*, pages 1223–1227, Baltimore, Maryland, June 1994.
- [YND91] P.M. Young, M.P. Newlin, and J.C. Doyle. μ analysis with real parametric uncertainty. In *Proc. 30th IEEE Conf. on Decision and Control*, pages 1251–1256, Brighton, England, Dec. 1991.
- [YND92] P.M. Young, M.P. Newlin, and J.C. Doyle. Practical computation of the mixed μ problem. In *Proc. American Control Conf.*, volume 3, pages 2190–2194, Chicago, Illinois, June 1992.
- [You93] P.M. Young. *Robustness with Parametric and Dynamic Uncertainty*. PhD thesis, California Institute of Technology, Pasadena, California, May 1993.
- [You94] P.M. Young. Controller design with mixed uncertainties. In *Proc. American Control Conf.*, pages 2333–2337, Baltimore, Maryland, June 1994.
- [ZBE91] Y.C. Zhu, A.C.P.M. Backx, and P. Eykhoff. Multivariable process identification for robust control. EUT Report 91-E-249, Eindhoven University of Technology, Faculty of Electrical Engineering, Eindhoven, The Netherlands, Jan. 1991.
- [ZBG91] Z. Zang, R.L. Bitmead, and M. Gevers. \mathcal{H}_2 iterative model refinement and control robustness enhancement. In *Proc. 30th Conf. on Decision and Control*, pages 279–284, Brighton, England, December 1991. IEEE.

Part V

Appendices

Appendix A

Scaling and Loop Shifting for \mathcal{H}_∞

In this appendix the necessary scalings and loop shifting for transforming a general D state space matrix into the form required by Theorem 4.6 on page 56 will be given. The main idea is that these transformations do not change the ∞ -norm of the closed loop system. Let the general plant $N(s)$ be given by:

$$N(s) = \left[\begin{array}{c|cc} A & B_1 & B_2 \\ \hline C_1 & D_{11} & D_{12} \\ C_2 & D_{21} & D_{22} \end{array} \right] \quad (\text{A.1})$$

where $A \in \mathbf{R}^{n \times n}$, $B_1 \in \mathbf{R}^{n \times d}$, $B_2 \in \mathbf{R}^{n \times m}$, $C_1 \in \mathbf{R}^{e \times n}$, $C_2 \in \mathbf{R}^{r \times n}$, $D_{11} \in \mathbf{R}^{e \times d}$, $D_{12} \in \mathbf{R}^{e \times m}$, $D_{21} \in \mathbf{R}^{r \times d}$ and finally $D_{22} \in \mathbf{R}^{r \times m}$. Consequently n is the order of the generalized plant and the dimensions of the inputs d' and u and the outputs e' and y are given by:

$$d = \dim(d') \quad (\text{A.2})$$

$$m = \dim(u) \quad (\text{A.3})$$

$$e = \dim(e') \quad (\text{A.4})$$

$$r = \dim(y) \quad (\text{A.5})$$

It will be required that D_{12} is “tall” with full column rank and that D_{21} is “fat” with full row rank. This means that:

$$\text{rank}(D_{12}) = \dim(u) = m \quad (\text{A.6})$$

$$\text{rank}(D_{21}) = \dim(y) = r \quad (\text{A.7})$$

Now complete the following steps:

Step 1. Use the singular value decomposition (SVD) to factor D_{12} and D_{21} :

$$D_{12} = U_1 \begin{bmatrix} 0_{(e-m) \times m} \\ \Sigma_1 \end{bmatrix} V_1^T \quad (\text{A.8})$$

$$D_{21} = U_2 \begin{bmatrix} 0_{r \times (d-r)} & \Sigma_2 \end{bmatrix} V_2^T \quad (\text{A.9})$$

where $U_1 \in \mathbf{R}^{e \times e}$, $V_1 \in \mathbf{R}^{m \times m}$, $U_2 \in \mathbf{R}^{r \times r}$ and $V_2 \in \mathbf{R}^{d \times d}$ are unitary matrices and $\Sigma_1 \in \mathbf{R}^{m \times m}$ and $\Sigma_2 \in \mathbf{R}^{r \times r}$ are diagonal matrices of singular values. Notice that the above SVD is not in the standard format provided by e.g. MATLAB, so the columns of U_1 and the rows of V_2 may have to be rearranged to suit this format.

Step 2. Scale D_{11} and partition it into a block 2×2 matrix:

$$\tilde{D}_{11} = U_1^T D_{11} V_2 = \begin{bmatrix} \tilde{D}_{11_{11}} & \tilde{D}_{11_{12}} \\ \tilde{D}_{11_{21}} & \tilde{D}_{11_{22}} \end{bmatrix} \quad (\text{A.10})$$

where $\tilde{D}_{11} \in \mathbf{R}^{e \times d}$, $\tilde{D}_{11_{11}} \in \mathbf{R}^{(e-r) \times (d-m)}$, $\tilde{D}_{11_{12}} \in \mathbf{R}^{(e-r) \times m}$, $\tilde{D}_{11_{21}} \in \mathbf{R}^{r \times (d-m)}$ and $\tilde{D}_{11_{22}} \in \mathbf{R}^{r \times m}$.

Step 3. Let

$$K_\infty = - \left(\tilde{D}_{11_{22}} + \tilde{D}_{11_{21}} \left(\gamma^2 I - \tilde{D}_{11_{11}}^T \tilde{D}_{11_{11}} \right)^{-1} \tilde{D}_{11_{11}}^T \tilde{D}_{11_{12}} \right) \quad (\text{A.11})$$

such that $K_\infty \in \mathbf{R}^{r \times m}$.

Step 4. Calculate

$$\bar{D}_{11} = \tilde{D}_{11} + \begin{bmatrix} 0 & 0 \\ 0 & K_\infty \end{bmatrix} = \begin{bmatrix} \tilde{D}_{11_{11}} & \tilde{D}_{11_{12}} \\ \tilde{D}_{11_{21}} & \tilde{D}_{11_{22}} + K_\infty \end{bmatrix} \quad (\text{A.12})$$

and the transformation matrix

$$\Theta = \begin{bmatrix} \Theta_{11} & \Theta_{12} \\ \Theta_{21} & \Theta_{22} \end{bmatrix} \quad (\text{A.13})$$

$$= \begin{bmatrix} -\bar{D}_{11} & \left(I - \gamma^{-2} \bar{D}_{11} \bar{D}_{11}^T \right)^{1/2} \\ \left(I - \gamma^{-2} \bar{D}_{11}^T \bar{D}_{11} \right)^{1/2} & \gamma^{-2} \bar{D}_{11}^T \end{bmatrix} \quad (\text{A.14})$$

Step 5. Let

$$\tilde{D}_{12} = \Theta_{12}^{-1} \begin{bmatrix} 0 \\ I \end{bmatrix} \quad (\text{A.15})$$

$$\tilde{D}_{21} = \begin{bmatrix} 0 & I \end{bmatrix} \Theta_{21}^{-1} \quad (\text{A.16})$$

$$\tilde{D}_{22} = \begin{bmatrix} 0 & I \end{bmatrix} \Theta_{22} \Theta_{12}^{-2} \begin{bmatrix} 0 \\ I \end{bmatrix} \quad (\text{A.17})$$

denote the last m columns of Θ_{12}^{-1} , the last r rows of Θ_{21}^{-1} and the last $r \times m$ rows and columns of $\Theta_{22} \Theta_{12}^{-2}$ respectively.

Step 6. Use the singular value decomposition (SVD) to factor \tilde{D}_{12} and \tilde{D}_{21} :

$$\tilde{D}_{12} = U_3 \begin{bmatrix} 0_{(e-m) \times m} \\ \Sigma_3 \end{bmatrix} V_3^T \quad (\text{A.18})$$

$$\tilde{D}_{21} = U_4 \begin{bmatrix} 0_{r \times (d-r)} & \Sigma_4 \end{bmatrix} V_4^T \quad (\text{A.19})$$

where $U_3 \in \mathbf{R}^{e \times e}$, $V_3 \in \mathbf{R}^{m \times m}$, $U_4 \in \mathbf{R}^{r \times r}$ and $V_4 \in \mathbf{R}^{d \times d}$ are unitary matrices and $\Sigma_3 \in \mathbf{R}^{m \times m}$ and $\Sigma_4 \in \mathbf{R}^{r \times r}$ are diagonal matrices of singular values.

Step 7. Calculate the combined transformation above (T_1) and below (T_2) $N(s)$, see Figure A.1 on page 291.

$$T_1 = \begin{bmatrix} U_3^T \Theta_{11} V_4 & U_3^T \Theta_{12} U_1^T \\ V_2 \Theta_{21} V_4 & V_2 \Theta_{22} U_1^T \end{bmatrix} \quad (\text{A.20})$$

$$T_2 = \begin{bmatrix} T_{211} & T_{212} \\ T_{221} & T_{222} \end{bmatrix} \quad (\text{A.21})$$

where

$$T_{211} = V_1 \Sigma_1^{-1} K_\infty \Sigma_2^{-1} U_2^T (I - L_1)^{-1} \quad (\text{A.22})$$

$$T_{212} = V_1 \Sigma_1^{-1} (I - L_2)^{-1} V_3 \Sigma_3^{-1} \quad (\text{A.23})$$

$$T_{221} = \Sigma_4^{-1} U_4^T \Sigma_2^{-1} U_2^T (I - L_1)^{-1} \quad (\text{A.24})$$

$$T_{222} = -\Sigma_4^{-1} U_4^T \left[\Sigma_2^{-1} U_2^T D_{22} V_1 \Sigma_1^{-1} (I - L_2)^{-1} - \tilde{D}_{22} \right] V_3 \Sigma_3^{-1} \quad (\text{A.25})$$

$$L_1 = -D_{22} V_1 \Sigma_1^{-1} K_\infty \Sigma_2^{-1} U_2^T \quad (\text{A.26})$$

$$L_2 = -K_\infty \Sigma_2^{-1} U_2^T D_{22} V_1 \Sigma_1^{-1} \quad (\text{A.27})$$

Step 8. Form the transformed system:

$$\tilde{N}(s) = F_l(T_1, F_l(N(s), T_2)) \quad (\text{A.28})$$

The D state-space matrix of $\tilde{N}(s)$ can now be shown to satisfy:

$$D_{11} = 0 \quad (\text{A.29})$$

$$D_{12} = \begin{bmatrix} 0 \\ I \end{bmatrix} \quad (\text{A.30})$$

$$D_{21} = \begin{bmatrix} 0 & I \end{bmatrix} \quad (\text{A.31})$$

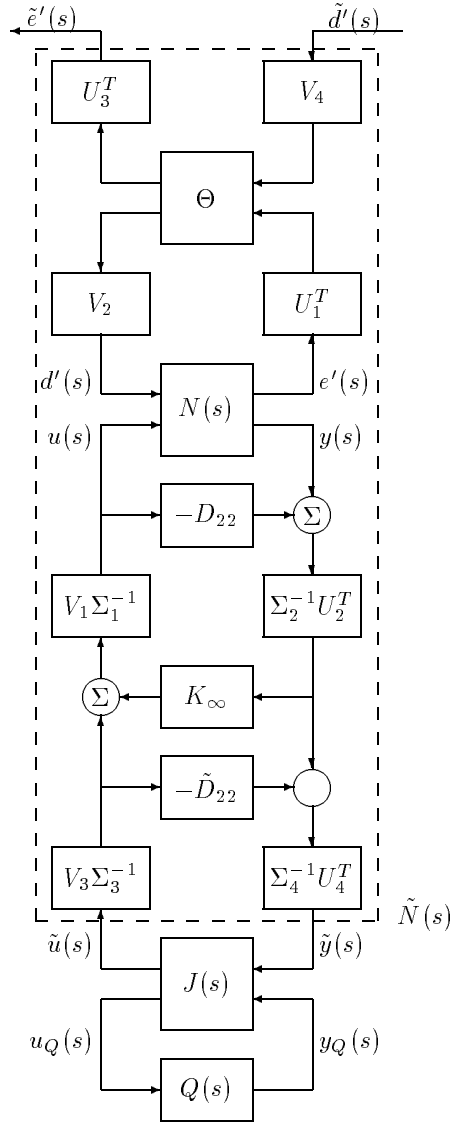
$$D_{22} = 0 \quad (\text{A.32})$$

Step 9. Compute the suboptimal \mathcal{H}_∞ controller $\tilde{K}(s)$ for the transformed system $\tilde{N}(s)$ and back-transform it to the original system $N(s)$. This is done via the linear fractional transformation:

$$K(s) = F_l(T_2, \tilde{K}(s)) \quad (\text{A.33})$$

Note that the transformation matrix T_1 is not needed to back-transform the controller.

The scalings and loop shifting operations described above is illustrated in block-diagram form in Figure A.1 on the facing page. Notice that since finding a optimal \mathcal{H}_∞ controller requires iteration on γ , for each iteration the scaling and loop shifting involving γ must be redone.

Figure A.1: *Scaling and loop shifting for \mathcal{H}_∞ suboptimal control.*

Appendix B

Convergence of μ - K Iteration

Here proof will be given for Lemma 5.1 on page 90. It will be shown that the minimizations:

$$K_i(s) = \arg \min_{K(s) \in \mathcal{K}_s} \sup_{\omega} \{ \bar{\sigma} (F_l (N_{D\Gamma_{i-1}}(j\omega), K(j\omega))) \} \quad (\text{B.1})$$

$$D_i^*(\omega) = \arg \min_{D \in \mathbf{D}} \bar{\sigma} (DF_l(N(j\omega), K_i(j\omega))D^{-1}), \quad \forall \omega \quad (\text{B.2})$$

from μ - K iteration are monotonically non-increasing in $\|F_l(N_{D\Gamma_i}, K_i)\|_{\infty}$. Given a controller $K_i(s)$ and scaling matrices $\Gamma_i(s)$ and $D_i(s)$ it is easy to show that:

$$\|F_l(N_{D\Gamma_i}(s), K_i(s))\|_{\infty} = \sup_{\omega} \bar{\sigma} (F_l (\Gamma_i(j\omega)D_i(j\omega)N(j\omega)D_i^{-1}(j\omega), K_i(j\omega))) \quad (\text{B.3})$$

$$= \sup_{\omega} |\gamma_i(j\omega)| \bar{\sigma} (F_l (D_i(j\omega)N(j\omega)D_i^{-1}(j\omega), K_i(j\omega))) \quad (\text{B.4})$$

Furthermore, assuming perfect realizations of the $\gamma_i(s)$ scalings, we have that

$$|\gamma_i(j\omega)| = (1 - \alpha_i)|\gamma_{i-1}(j\omega)| + \alpha_i \frac{\bar{\mu}_{\bar{\Delta}} (F_l (N(j\omega), K_i(j\omega)))}{\bar{\mu}_{\bar{\Delta}_e} (F_l (N(j\omega), K_i(j\omega)))} \quad (\text{B.5})$$

$$= |\gamma_{i-1}(j\omega)| \left(1 + \alpha_i \left(\frac{\bar{\mu}_{\bar{\Delta}} (F_l (N(j\omega), K_i(j\omega)))}{\bar{\mu}_{\bar{\Delta}_e} (F_l (N(j\omega), K_i(j\omega)))} \frac{1}{|\gamma_{i-1}(j\omega)|} - 1 \right) \right) \quad (\text{B.6})$$

$$= |\gamma_{i-1}(j\omega)| (1 + \alpha_i \beta_i(\omega)) \quad (\text{B.7})$$

Consequently:

$$\|F_l(N_{D\Gamma_i}(s), K_i(s))\|_\infty = \sup_\omega (1 + \alpha_i \beta_i(\omega)) |\gamma_{i-1}(j\omega)| \cdot \bar{\sigma}(F_l(D_i(j\omega)N(j\omega)D_i^{-1}(j\omega), K_i(j\omega))) \quad (\text{B.8})$$

In order to achieve a monotonically non-increasing algorithm it is thus required that

$$\sup_\omega (1 + \alpha_i \beta_i(\omega)) |\gamma_{i-1}(j\omega)| \bar{\sigma}(F_l(D_i(j\omega)N(j\omega)D_i^{-1}(j\omega), K_i(j\omega))) \leq \|F_l(N_{D\Gamma_{i-1}}(s), K_{i-1}(s))\|_\infty \quad (\text{B.9})$$

We now have the inequalities

$$\begin{aligned} & |\gamma_{i-1}(j\omega)| \bar{\sigma}(F_l(D_i(j\omega)N(j\omega)D_i^{-1}(j\omega), K_i(j\omega))) \\ & \leq |\gamma_{i-1}(j\omega)| \bar{\sigma}(F_l(D_{i-1}(j\omega)N(j\omega)D_{i-1}^{-1}(j\omega), K_i(j\omega))) \end{aligned} \quad (\text{B.10})$$

$$\leq \sup_\omega |\gamma_{i-1}(j\omega)| \bar{\sigma}(F_l(D_{i-1}(j\omega)N(j\omega)D_{i-1}^{-1}(j\omega), K_i(j\omega))) \quad (\text{B.11})$$

$$\leq \sup_\omega |\gamma_{i-1}(j\omega)| \bar{\sigma}(F_l(D_{i-1}(j\omega)N(j\omega)D_{i-1}^{-1}(j\omega), K_{i-1}(j\omega))) \quad (\text{B.12})$$

$$= \|F_l(N_{D\Gamma_{i-1}}(s), K_{i-1}(s))\|_\infty \quad (\text{B.13})$$

The first inequality follows from (B.2) on the preceding page with perfect realizations of the scalings $D_i(s)$. The last inequality follows from (B.1) on the page before. Since $\alpha_i \in [0; 1]$ and $\beta_i(\omega) \geq -1$ it then becomes clear from (B.10)-(B.13) and (B.8) that if $\beta_i(\omega) \leq 0, \forall \omega \geq 0$ then

$$\|F_l(N_{D\Gamma_i}(s), K_i(s))\|_\infty \leq \|F_l(N_{D\Gamma_{i-1}}(s), K_{i-1}(s))\|_\infty, \quad \sup_\omega \beta_i(\omega) \leq 0 \quad (\text{B.14})$$

and the algorithm will be monotonically non-increasing for all values of α_i . We may hence choose $\alpha_i = 1$. If $\beta_i(\omega) < 0, \forall \omega \geq 0$ it is thus guaranteed that the ∞ -norm $\|F_l(N_{D\Gamma_i}(s), K_i(s))\|_\infty$ will be reduced during the i 'th step of the iteration.

If $\beta_i(\omega) > 0$ for any frequency ω we must choose α so that (B.9) is fulfilled. Since the frequency at which the supremum is reached depends on α_i we must solve the inequality for all frequencies ω . Let $\bar{\alpha}_i$ denote the solution to (B.9) with inequality replaced with equality. It is easily verified that

$$\bar{\alpha}_i(\omega) = \left(\frac{\|F_l(N_{D\Gamma_{i-1}}(s), K_{i-1}(s))\|_\infty}{\bar{\sigma}(F_l(D_i(j\omega)N(j\omega)D_i^{-1}(j\omega), K_i(j\omega))) |\gamma_{i-1}(j\omega)|} - 1 \right) \frac{1}{\beta_i(\omega)} \quad (\text{B.15})$$

Thus if we choose α_i such that $\alpha_i \leq \min_\omega \bar{\alpha}_i(\omega)$ then (B.9) will be fulfilled and the algorithm will be monotonically non-increasing if $\alpha_i \geq 0$. From (B.10) we

have that

$$\begin{aligned} \|F_l(N_{D\Gamma_{i-1}}(s), K_{i-1}(s))\|_\infty \geq \\ \bar{\sigma} \left(F_l(D_i(j\omega)N(j\omega)D_i^{-1}(j\omega), K_i(j\omega)) \right) |\gamma_{i-1}(j\omega)| \end{aligned} \quad (\text{B.16})$$

where the equality holds only if $D_i(j\omega) = D_{i-1}(j\omega)$ and $K_i(j\omega) = K_{i-1}(j\omega)$ at the particular frequency at which the maximum is reached. Since $\beta_i(\omega) > 0$ it is then clear from (B.15) and (B.16) that $\alpha \geq 0$. If $\min_\omega \bar{\alpha}_i(\omega) > 0$ we may choose $\alpha_i > 0$ and it will be guaranteed that the ∞ -norm $\|F_l(N_{D\Gamma_i}(s), K_i(s))\|_\infty$ is reduced during the i 'th step of the iteration.

Appendix C

Rigid Body Model of ASTOVL Aircraft

In the following descriptions and numerical values are given for the rigid body aircraft model introduced in Chapter 7, see Figure 7.1 on page 107.

C.1 Flight Control Computer Hardware $G_c(s)$

The flight control computer and sample and hold delays are each represented by a first order Padé approximation in each input channel:

$$G_{fcc}(s) = \frac{-0.00725s + 1}{0.00725s + 1} \quad (C.1)$$

$$G_{s/h}(s) = \frac{-0.00208s + 1}{0.00417s + 1} \quad (C.2)$$

Furthermore, the input signals are converted into demands on the rear nozzle angle θ_R , forward thrust T_F and rear thrust T_R through a 3×3 transformation matrix T given by

$$T = \begin{bmatrix} -2.8610 \cdot 10^{-5} & 5.6070 \cdot 10^{-4} & -1.7920 \cdot 10^{-2} \\ 1.5120 \cdot 10^{-1} & -4.8362 \cdot 10^{-1} & -7.3830 \cdot 10^{-2} \\ -1.6560 \cdot 10^{-1} & -5.2706 \cdot 10^{-1} & 1.3958 \cdot 10^{-1} \end{bmatrix} \quad (C.3)$$

$G_c(s)$ is then given by

$$G_c(s) = G_{fcc}(s)G_{s/h}(s)I_3 \cdot T \quad (C.4)$$

C.2 Engine and Actuation Model $G_E(s)$

A block diagram representation of the engine and actuation model is given in Figure C.1. The thrust generated by the engine compressor is split into two parts, one part is ejected through the rear nozzle at a varying angle θ_R , to the horizontal, to produce a thrust T_F . The remaining thrust is directed to the forward nozzles where it can be augmented by plenum chamber burning before being ejected at a fixed angle θ_F , to produce the thrust T_F . The controller generates demands for rear nozzle actuator angle, and the magnitudes of the thrust ejected through the forward and rear nozzles.

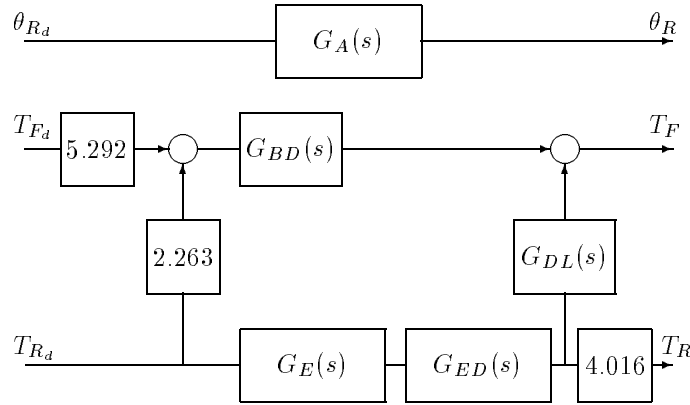


Figure C.1: *Engine and actuation system.*

The dynamics of the rear nozzle actuator are represented by a second order delay given by,

$$G_A = \frac{w_{n_A}^2}{s^2 + 2\zeta_A w_{n_A} s + w_{n_A}^2} \quad (C.5)$$

where $\zeta_A = 0.7$ and $w_{n_A} = 20.75$.

The plenum chamber burner delay is represented by a first order delay as,

$$G_{BD} = \frac{a_1}{1 + \tau_{BD}s} \quad (C.6)$$

where $a_1 = 0.1885$ and $\tau_{BD} = 0.06$.

The duct lag is also represented as a first order delay as,

$$G_{DL} = \frac{a_2}{1 + \tau_{DL}s} \quad (C.7)$$

where $a_2 = 1.713$ and $\tau_{DL} = 0.085$.

The engine time delay is approximated by a 2nd order Padé approximation as,

$$G_{ED} = \frac{1 - \frac{\tau_{ED}}{2}s + \frac{\tau_{ED}^2}{96}s^2}{1 + \frac{\tau_{ED}}{2}s + \frac{\tau_{ED}^2}{96}s^2} \quad (C.8)$$

where $\tau_{ED} = 0.125$.

The engine dynamics are represented by a second order transfer function as,

$$G_E = \frac{a_3 w_{n_E}^2}{s^2 + 2\zeta_E w_{n_E} s + w_{n_E}^2} \quad (C.9)$$

where $a_3 = 0.442$, $\zeta_E = 0.5$ and $w_{n_E} = 8.0$.

C.3 Force Transformation Matrix F_{mat}

The force transformation matrix resolves the forward and rear thrusts and the rear nozzle angle into an axial force, a normal force and a pitching moment. The relationship is:

$$\begin{bmatrix} X_F \\ Z_F \\ M \end{bmatrix} = F_{mat} \begin{bmatrix} \theta_R \\ T_F \\ T_R \end{bmatrix} \quad (C.10)$$

where F_{mat} is given by

$$F_{mat} = \frac{1}{\frac{1}{2}\rho V^2 S_{ref}} \frac{57.3}{2} \cdot \begin{bmatrix} -T_R \sin \theta_R & \cos \theta_F & \cos \theta_R \\ T_R \cos \theta_R & -\sin \theta_F & -\sin \theta_R \\ \frac{T_R(-z_R \sin \theta_R - x_R \cos \theta_R)}{l_T} & \frac{x_F \sin \theta_F + z_F \cos \theta_F}{l_T} & \frac{z_R \cos \theta_R - x_R \sin \theta_R}{l_T} \end{bmatrix} \quad (C.11)$$

where the parameters x_F , z_F , x_R and z_R denotes the position of the nozzles with respect to the center of gravity, S_{ref} is the wing area, ρ the air density, V the true air speed and finally l_T the tail arm.

Substitution of the numerical values for this flight condition and the scalings mentioned above yield the following matrix:

$$F_{mat} = 28.6499 \begin{bmatrix} -6.6210 \cdot 10^{-1} & 1.5700 \cdot 10^{-3} & 1.6800 \cdot 10^{-3} \\ -9.3520 \cdot 10^{-2} & -1.1900 \cdot 10^{-2} & -1.1880 \cdot 10^{-2} \\ -9.3050 \cdot 10^{-2} & 7.4100 \cdot 10^{-3} & -6.2900 \cdot 10^{-3} \end{bmatrix} \quad (C.12)$$

C.4 Rigid Aircraft Frame $G_A(s)$

The linearized equations of motion for the longitudinal dynamics of the rigid body aircraft flying at Mach 0.151, 100ft and 6° angle of attack are given by the following state-space equations :

$$\frac{d}{dt} \begin{bmatrix} u \\ w \\ \theta \\ q \end{bmatrix} = A \begin{bmatrix} u \\ w \\ \theta \\ q \end{bmatrix} + B \begin{bmatrix} X_{force} \\ Z_{force} \\ M \end{bmatrix} \quad (C.13)$$

$$\begin{bmatrix} q \\ \theta \\ h \\ a_x \end{bmatrix} = C \begin{bmatrix} u \\ w \\ \theta \\ q \end{bmatrix} + D \begin{bmatrix} X_{force} \\ Z_{force} \\ M \end{bmatrix} \quad (C.14)$$

where A, B, C and D are given by,

$$A = \begin{bmatrix} -0.0017 & 0.0413 & -5.3257 & -9.7565 \\ -0.0721 & -0.3393 & 49.5146 & -1.0097 \\ -0.0008 & 0.0138 & -0.2032 & 0.0009 \\ 0 & 0 & 1.0000 & 0 \end{bmatrix} \quad (C.15)$$

$$B = \begin{bmatrix} 0.2086 & -0.0005 & -0.0271 \\ -0.0005 & 0.2046 & 0.0139 \\ -0.0047 & 0.0023 & 0.1226 \\ 0 & 0 & 0 \end{bmatrix} \quad (C.16)$$

$$C = \begin{bmatrix} 0 & 0 & 57.2958 & 0 \\ 0 & 0 & 0 & 57.2958 \\ 0.1045 & -0.9945 & 0.1375 & 51.3791 \\ -0.0002 & 0.0045 & 0 & 0 \end{bmatrix} \quad (C.17)$$

$$D = \begin{bmatrix} 0 & 0 & 0 \\ 0 & 0 & 0 \\ 0 & 0 & 0 \\ 0.0212 & 0 & 0 \end{bmatrix} \quad (C.18)$$

C.5 Sensor Transfer Matrix $G_S(s)$

The delays in each sensor channel are represented by :

$$G_s(s) = \frac{1 - 0.005346s + 0.0001903s^2}{1 + 0.03082s + 0.0004942s^2} \quad (C.19)$$

In addition, anti-aliasing filters are included in the pitch rate and pitch attitude channels, given by :

$$G_{aa}(s) = \frac{1}{1 + 0.00398s + 0.0000158s^2} \quad (\text{C.20})$$

Thus $G_S(s)$ is given by

$$G_S(s) = \begin{bmatrix} G_s(s)G_{aa}(s) & 0 & 0 & 0 \\ 0 & G_s(s)G_{aa}(s) & 0 & 0 \\ 0 & 0 & G_s(s) & 0 \\ 0 & 0 & 0 & G_s(s) \end{bmatrix} \quad (\text{C.21})$$

Appendix D

Computing the Parameter Estimate $\hat{\theta}_N$

In this appendix a brief description of a general search algorithm for finding the parameter estimate $\hat{\theta}_N$ will be given. The algorithm is easy to implement in e.g. MATLAB. The search for $\hat{\theta}_N$ is considerably simplified for the special case where the predictor can be written as a linear expression in θ :

$$\hat{y}(k|\theta) = \phi^T(k)\theta \quad (\text{D.1})$$

where $\phi(k)$ is known as the state vector. An example of a model with linear predictor is the well-known ARX model structure

$$A(q)y(k) = B(q)u(k) + e(k) \quad (\text{D.2})$$

Notice that the ARX model corresponds to the general model (9.1) on page 140 with $F(q) = C(q) = D(q) = 1$. The ARX model predictor is thus given by

$$\hat{y}(k|\theta) = B(q)u(k) + (1 - A(q))y(k) = \phi^T(k)\theta \quad (\text{D.3})$$

for

$$\phi^T(k) = [-y(k-1), \dots, -y(k-n_a), u(k-1), \dots, u(k-n_b)] \quad (\text{D.4})$$

$$\theta^T = [a_1, \dots, a_{n_a}, b_1, \dots, b_{n_b}] \quad (\text{D.5})$$

A minimum for the criterion (9.10) on page 140 can now be computed from

$$V'_N(\hat{\theta}_N, Z^N) = 0 \quad (\text{D.6})$$

$$\Leftrightarrow -\frac{1}{N} \sum_{k=1}^N \psi(k, \hat{\theta}_N) \epsilon(k, \hat{\theta}_N) = 0 \quad (\text{D.7})$$

where the model gradient $\psi(k, \hat{\theta}_N)$ is given by

$$\psi(k, \hat{\theta}_N) = \frac{\partial \hat{y}(k|\hat{\theta}_N)}{\partial \theta} = \phi(k) \quad (\text{D.8})$$

Note that the model gradient for the ARX model structure is independent of the parameter vector θ . We then have:

$$-\frac{1}{N} \sum_{k=1}^N \phi(k)(y(k) - \phi^T(k)\hat{\theta}_N) = 0 \quad (\text{D.9})$$

$$\Leftrightarrow \sum_{k=1}^N \phi(k)\phi^T(k)\hat{\theta}_N = \sum_{k=1}^N \phi(k)y(k) \quad (\text{D.10})$$

$$\Leftrightarrow \hat{\theta}_N = \left[\sum_{k=1}^N \phi(k)\phi^T(k) \right]^{-1} \sum_{k=1}^N \phi(k)y(k) \quad (\text{D.11})$$

Consequently the expression for $\hat{\theta}_N$ is analytical provided $\sum_{k=1}^N \phi(k)\phi^T(k)$ is invertible. Since

$$V_N''(\theta, Z^N) = \frac{1}{N} \sum_{k=1}^N \phi(k)\phi^T(k) \quad (\text{D.12})$$

this is ensured if $V_N''(\hat{\theta}_N, Z^N)$ is positive definite.

In the general case, however, the predictor will not be linear in θ and we cannot derive analytical expressions for the parameter estimate $\hat{\theta}_N$. Instead we must use numerical search algorithms based on the gradient (9.14) and Hessian matrix (9.16) of the performance function. A popular search scheme is known as *Marquardt's algorithm*. The i 'th step in Marquardt's algorithm is

$$\theta_i = \theta_{i-1} - (V_N''(\theta_{i-1}, Z^N) + \rho_i I)^{-1} V_N'(\theta_{i-1}, Z^N) \quad (\text{D.13})$$

where I is a $n_a + n_b + n_f + n_c + n_d$ unity matrix and where ρ_i should be chosen as small as possible (to increase convergence speed) but so that $V_N(\theta_i, Z^N) < V_N(\theta_{i-1}, Z^N)$. Usually the approximation

$$V_N''(\theta, Z^N) \approx \frac{1}{N} \sum_{k=1}^N \phi(k, \theta)\phi^T(k, \theta) \quad (\text{D.14})$$

is used for the Hessian. The corresponding search scheme for (D.14) is sometimes denoted *Gauss-Newton's algorithm*, see [KR82].

D.1 Computation of $\phi(k, \theta)$ and $\psi(k, \theta)$

The remaining question is now how to efficiently compute the state vector $\phi(k, \theta)$ and the model gradient $\psi(k, \theta)$ for $1 \leq t \leq N$. For this purpose it proves convenient to write the predictor in the *pseudo-linear* form

$$\hat{y}(k|\theta) = \phi^T(k, \theta)\theta \quad (\text{D.15})$$

For the general predictor (9.8) on page 140, $\phi^T(k, \theta)$ can be found as follows. Rearrange (9.8) to get

$$C(q)F(q)\hat{y}(k|\theta) = F(q)[C(q) - D(q)A(q)]y(k) + D(q)B(q)u(k) \quad (\text{D.16})$$

$$\Leftrightarrow -C(q)F(q)[y(k) - \hat{y}(k|\theta)] = -F(q)D(q)A(q)y(k) + D(q)B(q)u(k) \quad (\text{D.17})$$

$$\Leftrightarrow \epsilon(k, \theta) = y(k) - \hat{y}(k|\theta) = \frac{D(q)}{C(q)} \left[A(q)y(k) - \frac{B(q)}{F(q)}u(k) \right] \quad (\text{D.18})$$

Now introduce

$$w(k, \theta) = \frac{B(q)}{F(q)}u(k), \quad v(k, \theta) = A(q)y(k) - w(k, \theta) \quad (\text{D.19})$$

to get

$$\epsilon(k, \theta) = \frac{D(q)}{C(q)}v(k, \theta) \quad (\text{D.20})$$

We now have:

$$w(k, \theta) = b_1u(k-1) + \dots + b_{n_b}u(k-n_b) - f_1w(k-1, \theta) - \dots - f_{n_f}w(k-n_f, \theta) \quad (\text{D.21})$$

$$v(k, \theta) = y(k) + a_1y(k-1) + \dots + a_{n_a}y(k-n_a) - b_1u(k-1) - \dots - b_{n_b}u(k-n_b) + f_1w(k-1, \theta) + \dots + f_{n_f}w(k-n_f, \theta) \quad (\text{D.22})$$

$$\begin{aligned} \epsilon(k, \theta) = & y(k) + a_1y(k-1) + \dots + a_{n_a}y(k-n_a) - b_1u(k-1) - \dots - \\ & - b_{n_b}u(k-n_b) + f_1w(k-1, \theta) + \dots + f_{n_f}w(k-n_f, \theta) + \\ & + d_1v(k-1, \theta) + \dots + d_{n_d}v(k-n_d, \theta) - c_1\epsilon(k-1, \theta) - \dots - \\ & - c_{n_c}\epsilon(k-n_c, \theta) \end{aligned} \quad (\text{D.23})$$

and may write the predictor as

$$\hat{y}(k|\theta) = y(k) - \epsilon(k, \theta) = -(\epsilon(k, \theta) - y(k)) \quad (\text{D.24})$$

$$\begin{aligned} = & -a_1y(k-1) - \dots - a_{n_a}y(k-n_a) + b_1u(k-1) + \dots + b_{n_b}u(k-n_b) - \\ & - f_1w(k-1, \theta) - \dots - f_{n_f}w(k-n_f, \theta) + c_1\epsilon(k-1, \theta) + \dots + \\ & + c_{n_c}\epsilon(k-n_c, \theta) - d_1v(k-1, \theta) - \dots - d_{n_d}v(k-n_d, \theta) \end{aligned} \quad (\text{D.25})$$

$$= \phi^T(k, \theta)\theta \quad (\text{D.26})$$

with

$$\begin{aligned} \phi^T(k, \theta) = & [-y(k-1), \dots, -y(k-n_a), u(k-1), \dots, u(k-n_b), \\ & -w(k-1, \theta), \dots, -w(k-n_f, \theta), \epsilon(k-1, \theta), \dots, \epsilon(k-n_c, \theta), \\ & -v(k-1, \theta), \dots, -v(k-n_d, \theta)] \end{aligned} \quad (\text{D.27})$$

and θ given by (9.9) on page 140. From (D.26) on the preceding page a convenient expression for the *predicted output vector*

$$\hat{Y}(\theta, Z^N) = [\hat{y}(k_s|\theta), \hat{y}(k_s+1|\theta), \dots, \hat{y}(N|\theta)]^T \quad (\text{D.28})$$

can be derived. k_s is given by

$$k_s = \max\{n_a, n_b, n_f, n_c, n_d\} + 1 \quad (\text{D.29})$$

We thus do not start the prediction until the state vector $\phi(k, \theta)$ is filled with measurements. Now let $\Phi(\theta, Z^N)$ be given by

$$\begin{aligned} \Phi(\theta, Z^N) = & \begin{bmatrix} -y(k_s-1) & -y(k_s) & -y(k_s+1) & \cdots & -y(N-1) \\ \vdots & \vdots & \vdots & \vdots & \vdots \\ -y(k_s-n_a) & -y(k_s-n_a+1) & -y(k_s-n_a+2) & \cdots & -y(N-n_a) \\ u(k_s-1) & u(k_s) & u(k_s+1) & \cdots & u(N-1) \\ \vdots & \vdots & \vdots & \vdots & \vdots \\ u(k_s-n_b) & u(k_s-n_b+1) & u(k_s-n_b+2) & \cdots & u(N-n_b) \\ -w(k_s-1, \theta) & -w(k_s, \theta) & -w(k_s+1, \theta) & \cdots & -w(N-1, \theta) \\ \vdots & \vdots & \vdots & \vdots & \vdots \\ -w(k_s-n_f, \theta) & -w(k_s-n_f+1, \theta) & -w(k_s-n_f+2, \theta) & \cdots & -w(N-n_f, \theta) \\ \epsilon(k_s-1, \theta) & \epsilon(k_s, \theta) & \epsilon(k_s+1, \theta) & \cdots & \epsilon(N-1, \theta) \\ \vdots & \vdots & \vdots & \vdots & \vdots \\ \epsilon(k_s-n_c, \theta) & \epsilon(k_s-n_c+1, \theta) & \epsilon(k_s-n_c+2, \theta) & \cdots & \epsilon(N-n_c, \theta) \\ -v(k_s-1, \theta) & -v(k_s, \theta) & -v(k_s+1, \theta) & \cdots & -v(N-1, \theta) \\ \vdots & \vdots & \vdots & \vdots & \vdots \\ -v(k_s-n_d, \theta) & -v(k_s-n_d+1, \theta) & -v(k_s-n_d+2, \theta) & \cdots & -v(N-n_d, \theta) \end{bmatrix} \end{aligned} \quad (\text{D.30})$$

Then it is easy to see that

$$\hat{Y}(\theta, Z^N) = \Phi^T(\theta, Z^N)\theta \quad (\text{D.31})$$

$$E(\theta, Z^N) = Y - \hat{Y}(\theta, Z^N) \quad (\text{D.32})$$

$$V_N(\theta, Z^N) = \frac{1}{N - k_s} \frac{1}{2} E^T(\theta, Z^N) E(\theta, Z^N) \quad (\text{D.33})$$

where the prediction error vector $E(\theta, Z^N)$ is given by

$$E(\theta, Z^N) = [\epsilon(k_s, \theta), \epsilon(k_s + 1, \theta), \dots, \epsilon(N, \theta)]^T \quad (\text{D.34})$$

The above expression for $\hat{Y}(\theta, Z^N)$, $E(\theta, Z^N)$ and $V_N(\theta, Z^N)$ can be easily and efficiently implemented in MATLAB, see Appendix E on page 311.

Let us now return to the computation of the model gradient $\psi(k, \theta)$. From Equation (D.26) on page 305 we have

$$\psi(k, \theta) = \frac{\partial \hat{y}(k|\theta)}{\partial \theta} = \phi(k, \theta) + \frac{\partial \phi^T(k, \theta)}{\partial \theta} \theta \quad (\text{D.35})$$

$$= \left[\frac{\partial \hat{y}(k|\theta)}{\partial a_1}, \dots, \frac{\partial \hat{y}(k|\theta)}{\partial a_{n_a}}, \frac{\partial \hat{y}(k|\theta)}{\partial b_1}, \dots, \frac{\partial \hat{y}(k|\theta)}{\partial b_{n_b}}, \frac{\partial \hat{y}(k|\theta)}{\partial f_1}, \dots, \frac{\partial \hat{y}(k|\theta)}{\partial f_{n_f}}, \right. \\ \left. \frac{\partial \hat{y}(k|\theta)}{\partial c_1}, \dots, \frac{\partial \hat{y}(k|\theta)}{\partial c_{n_c}}, \frac{\partial \hat{y}(k|\theta)}{\partial d_1}, \dots, \frac{\partial \hat{y}(k|\theta)}{\partial d_{n_d}} \right]^T \quad (\text{D.36})$$

Let us derive an expression for the derivative $\psi_i(k, \theta) = \partial \hat{y}(k|\theta) / \partial a_i$ where $1 \leq i \leq n_a$:

$$\psi_i(k, \theta) = \frac{\partial \hat{y}(k|\theta)}{\partial a_i} = \phi_i(k, \theta) + \frac{\partial \phi^T(k, \theta)}{\partial a_i} \theta = -y(k-i) + \frac{\partial \phi^T(k, \theta)}{\partial a_i} \theta \quad (\text{D.37})$$

where

$$\frac{\partial \phi^T(k, \theta)}{\partial a_i} = \left[-\frac{\partial y(k-1)}{\partial a_i}, \dots, -\frac{\partial y(k-n_a)}{\partial a_i}, \frac{\partial u(k-1)}{\partial a_i}, \dots, \frac{\partial u(k-n_b)}{\partial a_i}, \right. \\ \left. -\frac{\partial w(k-1, \theta)}{\partial a_i}, \dots, -\frac{\partial w(k-n_f, \theta)}{\partial a_i}, \frac{\partial \epsilon(k-1, \theta)}{\partial a_i}, \dots, \frac{\partial \epsilon(k-n_c, \theta)}{\partial a_i}, \right. \\ \left. -\frac{\partial v(k-1, \theta)}{\partial a_i}, \dots, -\frac{\partial v(k-n_d, \theta)}{\partial a_i} \right] \quad (\text{D.38})$$

$$= \left[0, \dots, 0, -\frac{\partial \hat{y}(k-1|\theta)}{\partial a_i}, \dots, -\frac{\partial \hat{y}(k-n_c|\theta)}{\partial a_i}, -y(k-1-i), \dots, \right. \\ \left. -y(k-n_d-i) \right] \quad (\text{D.39})$$

since $\epsilon(k, \theta) = y(k) - \hat{y}(k|\theta)$ and

$$v(k) = y(k) + a_1 y(k-1) + \dots + a_{n_a} y(k-n_a) - w(k, \theta) \quad (\text{D.40})$$

Notice that $w(k, \theta)$ is independent of a_i . We then have

$$\frac{\partial \hat{y}(k|\theta)}{\partial a_i} = -y(k-i) - c_1 \frac{\partial \hat{y}(k-1|\theta)}{\partial a_i} - \dots - c_{n_c} \frac{\partial \hat{y}(k-n_c|\theta)}{\partial a_i} - \\ d_1 y(k-1-i) - \dots - d_{n_d} y(k-n_d-i) \quad (\text{D.41})$$

Thus

$$\left[1 + c_1 q^{-1} + \cdots + c_{n_c} q^{-n_c}\right] \frac{\partial \hat{y}(k|\theta)}{\partial a_i} = \left[1 + d_1 q^{-1} + \cdots + d_{n_d} q^{-n_d}\right] y(k-i) \quad (\text{D.42})$$

and

$$\psi_i(k, \theta) = \frac{\partial \hat{y}(k|\theta)}{\partial a_i} = -\frac{D(q)}{C(q)} y(k-i) = \frac{D(q)}{C(q)} \phi_i(k, \theta) \quad (\text{D.43})$$

If $[\psi_1(k, \theta), \dots, \psi_{n_a}(k, \theta)]^T$ and $[\phi_1(k, \theta), \dots, \phi_{n_a}(k, \theta)]^T$ are denoted $\psi_A(k, \theta)$ and $\phi_A(k, \theta)$ respectively we may write

$$\psi_A(k, \theta) = \frac{D(q)}{C(q)} \phi_A(k, \theta) \quad (\text{D.44})$$

The first n_a elements of the model gradient $\psi(k, \theta)$ is consequently found by filtering of the first n_a elements of the state vector $\phi(k, \theta)$ with the filter $D(q)/C(q)$. Unlike for the ARMAX model structure

$$A(q)y(k) = B(q)u(k) + C(q)\epsilon(k) \quad (\text{D.45})$$

where it can be shown, see e.g. [Knu93], that

$$\psi(k, \theta) = \frac{1}{C(q)} \phi(k, \theta) \quad (\text{D.46})$$

the filters for the general model structure are not equal for the different “parts” of $\phi(k, \theta)$. Using similar arguments as above it is straightforward to show that

$$\psi_{n_a+i}(k, \theta) = \frac{\partial \hat{y}(k|\theta)}{\partial b_i} = \frac{D(q)}{F(q)C(q)} u(k-i) = \frac{D(q)}{F(q)C(q)} \phi_{n_a+i}(k, \theta) \quad (\text{D.47})$$

$$\begin{aligned} \psi_{n_a+n_b+i}(k, \theta) &= \frac{\partial \hat{y}(k|\theta)}{\partial f_i} = -\frac{D(q)}{F(q)C(q)} w(k-i, \theta) = \\ &= \frac{D(q)}{F(q)C(q)} \phi_{n_a+n_b+i}(k, \theta) \end{aligned} \quad (\text{D.48})$$

$$\begin{aligned} \psi_{n_a+n_b+n_c+i}(k, \theta) &= \frac{\partial \hat{y}(k|\theta)}{\partial c_i} = \frac{1}{C(q)} \epsilon(k-i, \theta) \\ &= \frac{1}{C(q)} \phi_{n_a+n_b+n_c+i}(k, \theta) \end{aligned} \quad (\text{D.49})$$

$$\begin{aligned}\psi_{n_a+n_b+n_f+n_c+i}(k, \theta) &= \frac{\partial \hat{y}(k|\theta)}{\partial d_i} = -\frac{1}{C(q)}v(k-i, \theta) \\ &= \frac{1}{C(q)}\phi_{n_a+n_b+n_f+n_c+i}(k, \theta)\end{aligned}\quad (\text{D.50})$$

Thus with

$$\phi_{BF}(k, \theta) = [\phi_{n_a+1}, \dots, \phi_{n_a+n_b+n_f}(k, \theta)]^T \quad (\text{D.51})$$

$$\phi_{CD}(k, \theta) = [\phi_{n_a+n_b+n_f+1}, \dots, \phi_{n_a+n_b+n_f+n_c+n_d}(k, \theta)]^T \quad (\text{D.52})$$

the model gradient can be written

$$\psi(k, \theta) = \begin{bmatrix} \frac{D(q)}{C(q)}\phi_A(k, \theta) \\ \frac{D(q)}{F(q)C(q)}\phi_{BF}(k, \theta) \\ \frac{1}{C(q)}\phi_{CD}(k, \theta) \end{bmatrix} \quad (\text{D.53})$$

Notice that for the special case of the ARMAX model structure ($D(q) = F(q) = 1$) the general expression for $\psi(k, \theta)$ (D.53) reduce to (D.46) on the facing page.

In order to find a convenient expression for the gradient $V'_N(\theta, Z^N)$ and the Hessian $V''_N(\theta, Z^N)$ introduce

$$y_f(k) = -\frac{D(q)}{C(q)}y(k) \quad (\text{D.54})$$

$$u_f(k) = \frac{D(q)}{F(q)C(q)}u(k) \quad (\text{D.55})$$

$$w_f(k, \theta) = -\frac{D(q)}{F(q)C(q)}w(k, \theta) \quad (\text{D.56})$$

$$\epsilon_f(k, \theta) = \frac{1}{C(q)}\epsilon(k, \theta) \quad (\text{D.57})$$

$$v_f(k, \theta) = -\frac{1}{C(q)}v(k, \theta) \quad (\text{D.58})$$

and

$$\Psi(\theta, Z^N) = \begin{bmatrix} -y_f(k_s-1) & -y_f(k_s) & -y_f(k_s+1) & \cdots & -y_f(N-1) \\ \vdots & \vdots & \vdots & \vdots & \vdots \\ -y_f(k_s-n_a) & -y_f(k_s-n_a+1) & -y_f(k_s-n_a+2) & \cdots & -y_f(N-n_a) \\ u_f(k_s-1) & u_f(k_s) & u_f(k_s+1) & \cdots & u_f(N-1) \\ \vdots & \vdots & \vdots & \vdots & \vdots \\ u_f(k_s-n_b) & u_f(k_s-n_b+1) & u_f(k_s-n_b+2) & \cdots & u_f(N-n_b) \\ -w_f(k_s-1, \theta) & -w_f(k_s, \theta) & -w_f(k_s+1, \theta) & \cdots & -w_f(N-1, \theta) \\ \vdots & \vdots & \vdots & \vdots & \vdots \\ -w_f(k_s-n_f, \theta) & -w_f(k_s-n_f+1, \theta) & -w_f(k_s-n_f+2, \theta) & \cdots & -w_f(N-n_f, \theta) \\ \epsilon_f(k_s-1, \theta) & \epsilon_f(k_s, \theta) & \epsilon_f(k_s+1, \theta) & \cdots & \epsilon_f(N-1, \theta) \\ \vdots & \vdots & \vdots & \vdots & \vdots \\ \epsilon_f(k_s-n_c, \theta) & \epsilon_f(k_s-n_c+1, \theta) & \epsilon_f(k_s-n_c+2, \theta) & \cdots & \epsilon_f(N-n_c, \theta) \\ -v_f(k_s-1, \theta) & -v_f(k_s, \theta) & -v_f(k_s+1, \theta) & \cdots & -v_f(N-1, \theta) \\ \vdots & \vdots & \vdots & \vdots & \vdots \\ -v_f(k_s-n_d, \theta) & -v_f(k_s-n_d+1, \theta) & -v_f(k_s-n_d+2, \theta) & \cdots & -v_f(N-n_d, \theta) \end{bmatrix}$$

Then it is easily checked that

$$V'_N(\theta, Z^N) = -\frac{1}{N-k_s} \Psi(\theta, Z^N) E(\theta, Z^N) \quad (\text{D.59})$$

$$V''_N(\theta, Z^N) \approx \frac{1}{N-k_s} \sum_{k=k_s}^N \psi(k, \theta) \psi^T(k, \theta) = \frac{1}{N-k_s} \Psi(\theta, Z^N) \Psi^T(\theta, Z^N) \quad (\text{D.60})$$

The above expressions for $V'_N(\theta, Z^N)$ and $V''_N(\theta, Z^N)$ can be easily and efficiently implemented in MATLAB, see Appendix E on the facing page.

Having determined computable expressions for the criterion function $V_N(\theta, Z^N)$ and its first and second derivatives we may construct simple and effective search algorithms based on Marquardt's iteration scheme. If we want to get rid of initial condition effects using delayed start of the criterion function, simply replace k_s with $N_1 \geq k_s$ in (D.33), (D.59) and (D.60) and let

$$E(\theta, Z^N) = [\epsilon(N_1, \theta), \epsilon(N_1+1, \theta), \dots, \epsilon(N, \theta)]^T. \quad (\text{D.61})$$

Appendix E

A MATLAB Function for Computing $\Phi(\theta)$ and $\Psi(\theta)$

The following is an example of how the expressions for $\Phi(\theta)$ and $\Psi(\theta)$ derived in Appendix D may be efficiently implemented into MATLAB.

```
function [FI,PSI] = mk_signals(theta,nn,U,Y)
% [FI,PSI] = mk_signals(theta,nn,U,Y,) creates
% the state vector matrix FI and the model gradient
% matrix PSI from the parameter vector theta,
% nn=[na,nb,nf,nc,nd], input vector U and output
% vector Y.

% S. Toffner-Clausen, Last revised: 95.02.21
% Copyright (c) by the authors
% All Rights Reserved.

N = length(U);
ks = max(nn)+1;
na=nn(1);nb=nn(2);nf=nn(3);nc=nn(4);nd=nn(5);
ns = sum(nn);
Ns = N-ks+1;
PSI = zeros(ns,Ns);           % allocating space for PSI
FI = zeros(ns,Ns);           % allocating space for FI
jj = ks:N;
A = [1 theta(1:na)'];         % A polynomial
B = theta(na+1:na+nb)';       % B polynomial
```

```

F = [1 theta(na+nb+1:na+nb+nf)'];           % F polynomial
C = [1 theta(na+nb+nf+1:na+nb+nf+nc)'];     % C polynomial
D = [1 theta(na+nb+nf+nc+1:ns)'];           % D polynomial
w = filter([0 B],F,U');                     % use filter.m for fast
v = filter(A,1,Y')-w;                       % computation of signals
e = filter(D,C,v);
yf = filter(-D,C,Y');
uf = filter(D,conv(F,C),U');
wf = filter(-D,conv(F,C),w);
ef = filter(1,C,e);
vf = filter(-1,C,v);
for i = 1:na                                % computing FI and PSI
    FI(i,:) = -Y(jj-i)';
    PSI(i,:) = yf(jj-i);
end;
for i = 1:nb
    FI(na+i,:) = U(jj-i)';
    PSI(na+i,:) = uf(jj-i);
end;
for i = 1:nf
    FI(na+nb+i,:) = -w(jj-i);
    PSI(na+nb+i,:) = wf(jj-i);
end;
for i = 1:nc
    FI(na+nb+nf+i,:) = e(jj-i);
    PSI(na+nb+nf+i,:) = ef(jj-i);
end;
for i = 1:nd
    FI(na+nb+nf+nc+i,:) = -v(jj-i);
    PSI(na+nb+nf+nc+i,:) = vf(jj-i);
end;

```

Appendix F

Computing the θ Estimate through QR Factorization

Recall the performance function for the least squares parameter estimate given as Equation (11.29) on page 187:

$$V_N(\theta, Z^N) = (Y - \Phi\theta)^T (Y - \Phi\theta) \quad (\text{F.1})$$

$$= \|Y - \Phi\theta\|_2^2 \quad (\text{F.2})$$

where $\|\cdot\|_2$ is the usual Euclidean norm. Given an $(N \times N)$ orthonormal matrix T^1 the performance function $V_N(\theta, Z^N)$ is clearly not affected by the *orthonormal transformation*:

$$V_N(\theta, Z^N) = \|T(Y - \Phi\theta)\|_2^2 \quad (\text{F.3})$$

Now choose T such that:

$$T\Phi = \begin{bmatrix} Q \\ 0 \end{bmatrix} \quad (\text{F.4})$$

where Q is an $(n \times n)$ upper triangular matrix, where n is the order of the parametric model.

Now rewrite Equation (F.4) as:

$$T^T T\Phi = T^T \begin{bmatrix} Q \\ 0 \end{bmatrix} \quad (\text{F.5})$$

$$\Leftrightarrow \Phi = T^T \begin{bmatrix} Q \\ 0 \end{bmatrix} \quad (\text{F.6})$$

¹An orthonormal matrix T satisfies $T^T T = I$.

Equation (F.6) on the preceding page is known as the *QR Factorization* of Φ . QR factorizations is easily performed in e.g. MATLAB.

Having determined a T and Q according to (F.6) introduce:

$$TY = \begin{bmatrix} \vartheta \\ \varrho \end{bmatrix} \quad (\text{F.7})$$

where ϑ is a n vector and ϱ is a $N - n$ vector. Inserting (F.4) and (F.7) into (F.3) it is easily seen that:

$$V_N(\theta, Z^N) = \left\| \begin{bmatrix} \vartheta \\ \varrho \end{bmatrix} - \begin{bmatrix} Q \\ 0 \end{bmatrix} \theta \right\|_2^2 \quad (\text{F.8})$$

$$= \left\| \begin{bmatrix} \vartheta - Q\theta \\ \varrho \end{bmatrix} \right\|_2^2 \quad (\text{F.9})$$

$$= \|\vartheta - Q\theta\|_2^2 + \|\varrho\|_2^2 \quad (\text{F.10})$$

The performance criterion given by (F.10) is clearly minimized for:

$$Q\hat{\theta}_N = \vartheta \quad (\text{F.11})$$

$$\Leftrightarrow \hat{\theta}_N = Q^{-1}\vartheta \quad (\text{F.12})$$

The minimum of $V_N(\theta, Z^N)$ is then:

$$V_N(\hat{\theta}_N, Z^N) = \|\varrho\|_2^2 \quad (\text{F.13})$$

Notice that from (F.4) on the page before it follows that:

$$Q^T Q = \Phi^T T^T T \Phi = \Phi^T \Phi = \mathcal{R}(N) \quad (\text{F.14})$$

where $\mathcal{R}(N)$ is the coefficient matrix for the non-transformed estimation problem, see Equation (11.37) on page 188. It can now be shown that the ratio between the smallest and largest eigenvalue of Q is the square root of that of $\mathcal{R}(N)$, see [Lju87, pp 276]. Consequently the inversion of Q is better conditioned than the conversion of $\Phi^T \Phi$ and the parameter estimate given by Equation (F.12) has superior numerical properties than the estimate given by (11.37) on page 188.

F.1 Transforming the Residuals

When applying maximum likelihood estimation on the parameter vector ζ the residuals ϵ shall be transformed into a non-singular distribution:

$$\varpi = R^T \epsilon \quad (\text{F.15})$$

where ϖ has non singular distribution. The choice of R affects the condition number of the covariance matrix Σ for ϖ . Since the numerical solution to the maximum likelihood estimate involves inversion of Σ this should be well conditioned. Inspired by the above QR factorization we suggest that R is chosen as:

$$R^T = \kappa \tilde{T} \tag{F.16}$$

where κ is a scalar scaling factor and \tilde{T} is the last $(N - p)$ columns of T found by the QR factorization above.

This particular transformation yielded very nice numerical properties of the maximum likelihood estimate. κ scales the numerical value of the loglikelihood function.

Appendix G

First and Second Order Derivatives of $\ell(\varpi|U, \zeta)$

It will now be demonstrated how one may derive explicit expressions for the partial derivatives of the loglikelihood function $\ell(\varpi|U, \zeta)$ with respect to ζ . Knowledge of these derivatives enables us to construct the *Fisher Information Matrix* given by:

$$M \triangleq E \left\{ \left[\frac{\partial \ell}{\partial \zeta} \right] \left[\frac{\partial \ell}{\partial \zeta} \right]^T \right\} = -E \left\{ \frac{\partial^2 \ell}{\partial \zeta^2} \right\} \quad (\text{G.1})$$

$$\Rightarrow [M_\zeta]_{ij} = E \left\{ \frac{\partial \ell}{\partial \zeta_i} \cdot \frac{\partial \ell}{\partial \zeta_j} \right\} \quad (\text{G.2})$$

Remember that the Hessian matrix H is given as:

$$H = \frac{\partial^2 \ell}{\partial \zeta^2} \quad (\text{G.3})$$

so that:

$$M = -E \{H\} \quad (\text{G.4})$$

Thus Fishers Information Matrix is the estimated Hessian.

G.1 Partial First Order Derivatives of $\ell(\varpi|U, \zeta)$

Recall Equation (11.111) on page 197:

$$\ell(\varpi|U, \zeta) = -\frac{1}{2} \ln(\det \Sigma) - \frac{1}{2} \varpi^T \Sigma^{-1} \varpi + k \quad (\text{G.5})$$

where Σ is given by:

$$\Sigma = R^T X C_\eta X^T R + R^T C_\nu R \quad (\text{G.6})$$

In order to evaluate the partial derivatives we need the following two Lemma's:

Lemma G.1 *Consider an invertible square matrix Σ parameterized by a set of scalars $\{\zeta_1, \dots, \zeta_n\}$. The partial derivative of $\ln \det(\Sigma)$ with respect to one of the parameterizing constants ζ_i may be written:*

$$\frac{\partial \ln \det(\Sigma)}{\partial \zeta_i} = \text{tr} \left\{ \Sigma^{-1} \frac{\partial \Sigma}{\partial \zeta_i} \right\} \quad (\text{G.7})$$

Lemma G.2 *Consider a matrix Σ as above. The partial derivative of Σ^{-1} with respect to ζ_i may be written:*

$$\frac{\partial \Sigma^{-1}}{\partial \zeta_i} = -\Sigma^{-1} \frac{\partial \Sigma}{\partial \zeta_i} \Sigma^{-1} \quad (\text{G.8})$$

The proofs of these Lemma's are straightforward and may be found in [GGN92]. Applying the Lemma's to Equation (G.5) one obtain:

$$\frac{\partial \ell(\varpi|U, \zeta)}{\partial \zeta_i} = -\frac{1}{2} \frac{\partial}{\partial \zeta_i} \{ \ln \det \Sigma \} - \frac{1}{2} \varpi^T \frac{\partial}{\partial \zeta_i} \{ \Sigma^{-1} \} \varpi + 0 \quad (\text{G.9})$$

$$= -\frac{1}{2} \text{tr} \left\{ \Sigma^{-1} \frac{\partial \Sigma}{\partial \zeta_i} \right\} + \frac{1}{2} \varpi^T \Sigma^{-1} \frac{\partial \Sigma}{\partial \zeta_i} \Sigma^{-1} \varpi \quad (\text{G.10})$$

$$= -\frac{1}{2} \text{tr} \left\{ \Sigma^{-1} \left(R^T X \frac{\partial C_\eta}{\partial \zeta_i} X^T R + R^T \frac{\partial C_\nu}{\partial \zeta_i} R \right) \right\} \\ + \frac{1}{2} \varpi^T \Sigma^{-1} \left(R^T X \frac{\partial C_\eta}{\partial \zeta_i} X^T R + R^T \frac{\partial C_\nu}{\partial \zeta_i} R \right) \Sigma^{-1} \varpi \quad (\text{G.11})$$

When the parameterizations of the covariance matrices $C_\eta(\beta)$ and $C_\nu(\gamma)$ have been chosen the corresponding partial derivatives with respect to each element in ζ may then be determined, and from (G.11) the partial derivatives of $\ell(\varpi|U, \zeta)$ can be found.

G.2 Partial Second Order Derivatives of $\ell(\varpi|U, \zeta)$

Applying Equation (G.2) with (G.11) will yield the desired expression for the *Fisher Information Matrix*. In [GGN92] it is shown that the Fisher Matrix can be written:

$$[M_\zeta]_{ij} = E \left\{ \frac{\partial \ell}{\partial \zeta_i} \cdot \frac{\partial \ell}{\partial \zeta_j} \right\} \quad (\text{G.12})$$

$$= \frac{1}{2} \text{tr} \left\{ \Sigma^{-1} \frac{\partial \Sigma}{\partial \zeta_i} \Sigma^{-1} \frac{\partial \Sigma}{\partial \zeta_j} \right\} \quad (\text{G.13})$$

$$= \frac{1}{2} \text{tr} \left\{ \Sigma^{-1} \left(R^T X \frac{\partial C_\eta}{\partial \zeta_i} X^T R + R^T \frac{\partial C_\nu}{\partial \zeta_i} R \right) \cdot \right. \\ \left. \Sigma^{-1} \left(R^T X \frac{\partial C_\eta}{\partial \zeta_j} X^T R + R^T \frac{\partial C_\nu}{\partial \zeta_j} R \right) \right\} \quad (\text{G.14})$$

We may then use (G.14) to obtain an estimate of the Hessian matrix. With the first and second order partial derivatives we may then construct powerful search algorithms for the maximum of the loglikelihood function.

The partial derivatives of the noise covariance for the investigated parameterizations is presented in Appendix H on page 321. The results for the undermodeling is given in Appendix I on page 323.

Appendix H

Partial Derivatives of the Noise Covariance

The partial derivatives of the noise covariance matrix for the different assumptions on the covariance structure will be derived. The partial derivatives is used to compute the gradient and Fisher for the loglikelihood function of the transformed residuals ϖ when searching for the maximum of the loglikelihood function.

Two different parameterization of the noise covariance has been investigated:

$$C_{\nu_1} = \sigma_e^2 \cdot I_N \quad (\text{H.1})$$

$$C_{\nu_2}(i, j) = \begin{cases} \sigma_e^2 \left(1 + \frac{(c-a)^2}{1-a^2} \right) & , i = j \\ \frac{\sigma_e^2 (-a)^M (1 + c^2 - a * c - c/a)}{1-a^2} & , |j-i| = M \end{cases} \quad (\text{H.2})$$

For C_{ν_1} the obvious solution is:

$$\frac{\partial C_{\nu_1}}{\partial \sigma_e^2} = I_N \quad (\text{H.3})$$

For C_{ν_2} a few hand calculations yield the following three derivatives:

$$\frac{\partial C_{\nu_2}(i, j)}{\partial a} = \begin{cases} \sigma_e^2 \left(\frac{2a(c-a)^2 - 2(c-a)(1-a^2)}{(1-a^2)^2} \right) & , i = j \\ \left(\frac{\sigma_e^2 (-a)^M [(1+c^2 - a*c - c/a)(M + (2-M)a^2) + (a-a^3)(c/a^2 - c)]}{a(1-a^2)^2} \right) & , |j - i| = M \end{cases} \quad (\text{H.4})$$

$$\frac{\partial C_{\nu_2}(i, j)}{\partial c} = \begin{cases} \sigma_e^2 \left(\frac{2(c-a)}{1-a^2} \right) & , i = j \\ \sigma_e^2 \left(\frac{(-a)^M (2c - a - a^{-1})}{1-a^2} \right) & , |j - i| = M \end{cases} \quad (\text{H.5})$$

$$\frac{\partial C_{\nu_2}(i, j)}{\partial \sigma_e^2} = \begin{cases} \left(1 + \frac{(c-a)^2}{1-a^2} \right) & , i = j \\ \left(\frac{(-a)^M (1+c^2 - ac - c/a)}{1-a^2} \right) & , |j - i| = M \end{cases} \quad (\text{H.6})$$

Appendix I

Partial Derivatives of the Undermodeling Covariance

The partial derivatives of the undermodeling impulse response covariance matrix for the different assumptions on the covariance structure will be derived. The partial derivatives is used to compute the gradient and Fisher for the loglikelihood function of the transformed residuals ϖ when searching for the maximum of the loglikelihood function.

Three different parameterization of the undermodeling covariance has been investigated:

$$C_{\eta_1} = \alpha \cdot I_L \quad (I.1)$$

$$C_{\eta_2} = \text{diag}_{1 \leq k \leq L} \{ \alpha \lambda^k \} \quad (I.2)$$

$$C_{\eta_3} = [\alpha \lambda^0 \dots \alpha \lambda^{L-1}]^T [\alpha \lambda^0 \dots \alpha \lambda^{L-1}] \quad (I.3)$$

The partial derivatives are easily found as:

$$\frac{\partial C_{\eta_1}}{\partial \alpha} = I_L \quad (I.4)$$

$$\frac{\partial C_{\eta_2}}{\partial \alpha} = \text{diag}_{1 \leq k \leq L} \lambda^k \quad (I.5)$$

$$\frac{\partial C_{\eta_2}}{\partial \lambda} = \text{diag}_{1 \leq k \leq L} \alpha k \lambda^{k-1} \quad (I.6)$$

$$\frac{\partial C_{\eta_3}}{\partial \alpha} = 2\alpha [\lambda^0 \dots \lambda^{L-1}]^T [\lambda^0 \dots \lambda^{L-1}] \quad (I.7)$$

$$\frac{\partial C_{\eta_3}}{\partial \lambda} = \alpha^2 \begin{bmatrix} 0 & 1 & \cdots & (L-1)\lambda^{L-2} \\ 1 & 2\lambda & \cdots & L\lambda^{L-1} \\ \vdots & \vdots & \ddots & \vdots \\ (L-1)\lambda^{L-2} & L\lambda^{L-1} & \cdots & 2(L-1)\lambda^{2L-3} \end{bmatrix} \quad (1.8)$$

Appendix J

ARMA(1) Noise Covariance Matrix

Assume that the process noise $\nu(k)$ is given by the ARMA(1) description:

$$\nu(k) = H(q) = \frac{1 + cq^{-1}}{1 + aq^{-1}}e(k) \quad (\text{J.1})$$

where $e(k)$ is white noise with variance σ_e^2 . If $h_\nu(k)$ is the impulse response of $H(q)$ we may write $\nu(k)$ as:

$$\nu(k) = \sum_{\kappa=0}^{\infty} h_\nu(\kappa)e(k - \kappa) \quad (\text{J.2})$$

The (i, j) 'th element of the covariance C_ν is then defined by:

$$C_\nu(i, j) \triangleq E \{ \nu(i)\nu(j) \} \quad (\text{J.3})$$

$$= E \left\{ \sum_{\kappa=0}^{\infty} h_\nu(\kappa)e(i - \kappa) \sum_{\lambda=0}^{\infty} h_\nu(\lambda)e(j - \lambda) \right\} \quad (\text{J.4})$$

$$= E \left\{ \sum_{\kappa=0}^{\infty} \sum_{\lambda=0}^{\infty} h_\nu(\kappa)h_\nu(\lambda)e(i - \kappa)e(j - \lambda) \right\} \quad (\text{J.5})$$

Now since:

$$E \{ e(i - \kappa)e(j - \lambda) \} = 0 \quad (i - \kappa) \neq (j - \lambda) \quad (\text{J.6})$$

$$E \{ e(i - \kappa)e(j - \lambda) \} = \sigma_e^2 \quad (i - \kappa) = (j - \lambda) \quad (\text{J.7})$$

we may write the covariance as:

$$C_\nu(i, j) = \sigma_e^2 \sum_{\kappa=0}^{\infty} h_\nu(\kappa) h_\nu(\kappa + j - i) \quad (\text{J.8})$$

Given the ARMA(1) noise description (J.1) on the page before we may write the difference equation for $\nu(k)$ as:

$$\nu(k) = -a\nu(k-1) + e(k) + ce(k-1) \quad (\text{J.9})$$

The impulse response $h_\nu(k)$ is then obtained by setting $e(k) = \delta_0(k)$:

$$h_\nu(0) = 1 \quad (\text{J.10})$$

$$h_\nu(1) = -a + c \quad (\text{J.11})$$

$$h_\nu(2) = -a(-a + c) \quad (\text{J.12})$$

$$h_\nu(3) = (-a)^2(-a + c) \quad (\text{J.13})$$

$$h_\nu(n) = (-a)^{n-1}(-a + c) \quad (\text{J.14})$$

or:

$$h_\nu(k) = \begin{cases} 1 & , k = 0 \\ (-a)^{k-1}(-a + c) & , k > 0 \end{cases} \quad (\text{J.15})$$

We may now compute the (i, j) 'th element of C_ν as follows:

$$C_\nu(i, j) = \sigma_e^2 \left(1 + \sum_{\kappa=1}^{\infty} ((-a)^{\kappa-1}(-a + c))^2 \right) \quad j-i=0 \quad (\text{J.16})$$

$$= \sigma_e^2 \left(1 + (-a + c)^2 \sum_{\kappa=1}^{\infty} ((-a)^2)^{\kappa-1} \right) \quad j-i=0 \quad (\text{J.17})$$

$$= \sigma_e^2 \left(1 + (-a + c)^2 \frac{1}{1 - a^2} \right) \quad j-i=0 \quad (\text{J.18})$$

$$C_\nu(i, j) = \sigma_e^2 \left((-a + c) + \sum_{\kappa=1}^{\infty} (-a)^{\kappa-1}(-a + c)(-a)^\kappa(-a + c) \right) \quad j-i=1 \quad (\text{J.19})$$

$$= \sigma_e^2 \left((-a + c) + (-a + c)^2(-a)^1 \sum_{\kappa=1}^{\infty} ((-a)^2)^{\kappa-1} \right) \quad j-i=1 \quad (\text{J.20})$$

$$= \sigma_e^2 \left((-a + c) + (-a + c)^2(-a)^1 \frac{1}{1 - a^2} \right) \quad j-i=1 \quad (\text{J.21})$$

$$C_\nu(i, j) = \sigma_e^2 \left((-a)^{M-1}(-a+c) + \sum_{\kappa=1}^{\infty} (-a)^{\kappa-1}(-a+c)(-a)^{\kappa-1+M}(-a+c) \right) \quad j-i=M \quad (\text{J.22})$$

$$= \sigma_e^2 \left((-a)^{M-1}(-a+c) + (-a+c)^2(-a)^M \sum_{\kappa=1}^{\infty} ((-a)^2)^{\kappa-1} \right) \quad j-i=M \quad (\text{J.23})$$

$$= \sigma_e^2 \left((-a)^{M-1}(-a+c) + (-a+c)^2(-a)^M \frac{1}{1-a^2} \right) \quad j-i=M \quad (\text{J.24})$$

for $M > 0$. However since C_ν is symmetric we may generalize the above expressions. A little rearranging then gives:

$$C_\nu(i, j) = \begin{cases} \sigma_e^2 \left(1 + \frac{(c-a)^2}{1-a^2} \right) & , j = i \\ \sigma_e^2 \left((-a)^M \frac{1+c^2-ac-c/a}{1-a^2} \right) & , |j-i| = M \end{cases} \quad (\text{J.25})$$

where $|\cdot|$ denotes absolute value.

Appendix K

Extracting Principal Axis from Form Matrix

Here it will shown how the principal axis and the angle of an ellipse with form matrix P can be extracted from the form matrix. Let the ellipse in Figure K.1 on the following page with major and minor principal axis a and b respectively and angle A be given by the ellipse equation

$$x^T P^{-1} x = 1 \quad (\text{K.1})$$

In order to find the major and minor principal axis and the angle we perform an eigenvalue decomposition of the form matrix P^{-1} :

$$P^{-1} = V D V^{-1} \quad (\text{K.2})$$

where $D = \text{diag}\{\lambda_1, \lambda_2\}$ is a diagonal vector of eigenvalues and V is a 2-by-2 matrix whose columns are the corresponding eigenvectors. We may then write

$$x^T V D V^{-1} x = 1 \quad (\text{K.3})$$

$$\Rightarrow x^T V D^{\frac{1}{2}} D^{\frac{1}{2}} V^{-1} x = 1 \quad (\text{K.4})$$

$$\Rightarrow y^T y = 1 \quad (\text{K.5})$$

with

$$y = D^{\frac{1}{2}} V^{-1} x \quad (\text{K.6})$$

$$\Rightarrow x = \left(D^{\frac{1}{2}} V^{-1} \right)^{-1} y \quad (\text{K.7})$$

$$\Leftrightarrow x = V D^{-\frac{1}{2}} y \quad (\text{K.8})$$

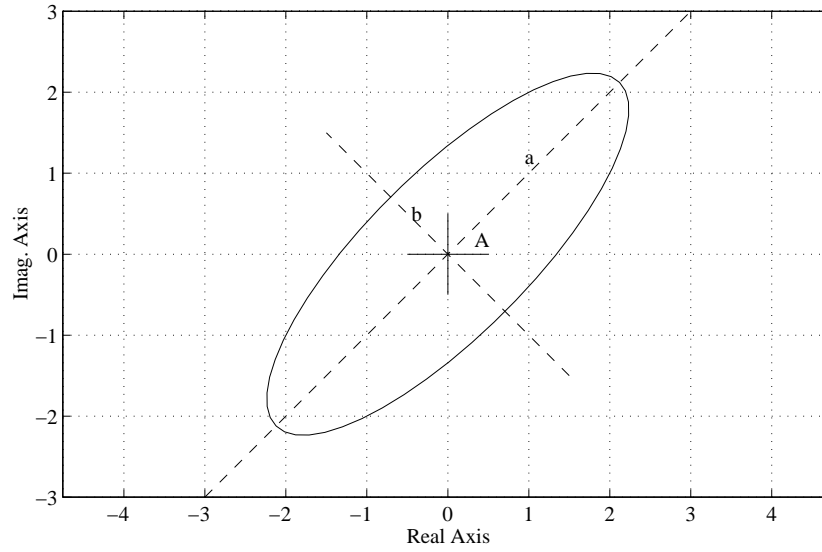


Figure K.1: *Ellipse with major and minor principal axis a and b respectively and angle A .*

Thus the ellipse given by (K.2) on the page before can be seen as the circle (K.5) on the preceding page transformed by

$$x = V D^{-\frac{1}{2}} y \quad (\text{K.9})$$

For $V = I_2$ we obtain

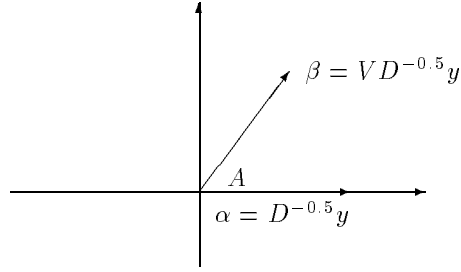
$$\begin{bmatrix} x_1 \\ x_2 \end{bmatrix} = \begin{bmatrix} \lambda_1^{-\frac{1}{2}} & 0 \\ 0 & \lambda_2^{-\frac{1}{2}} \end{bmatrix} \begin{bmatrix} y_1 \\ y_2 \end{bmatrix} \quad (\text{K.10})$$

$$\Leftrightarrow x_1 = \frac{1}{\sqrt{\lambda_1}} y_1, \quad x_2 = \frac{1}{\sqrt{\lambda_2}} y_2 \quad (\text{K.11})$$

corresponding to a pure scaling in the $y_1 - y_2$ plane. Assuming that the eigenvalue decomposition has been ordered such that $\lambda_1 \leq \lambda_2$ the major and minor principal axis are given by

$$a = \frac{1}{\sqrt{\lambda_1}}, \quad b = \frac{1}{\sqrt{\lambda_2}} \quad (\text{K.12})$$

The eigenvector matrix V performs a rotation of the scaled circle, see Figure K.2 on the facing page.

Figure K.2: *Rotation of ellipse.*

Then it is easy to check that β in Figure K.2 may be written as the following transformation of α

$$\beta = R\alpha, \quad R = \begin{bmatrix} \cos(A) & -\sin(A) \\ \sin(A) & \cos(A) \end{bmatrix} \quad (\text{K.13})$$

Thus the angle A of the ellipse is given by the solution to the equation

$$V = \begin{bmatrix} \cos(A) & -\sin(A) \\ \sin(A) & \cos(A) \end{bmatrix} \quad (\text{K.14})$$

The solution in degrees can then be determined as follows

- First quadrant:

$$\left. \begin{array}{l} \cos(A) \geq 0 \\ \sin(A) \geq 0 \end{array} \right\} \Rightarrow \left. \begin{array}{l} V_{11} \geq 0 \\ V_{21} \geq 0 \end{array} \right\} \Rightarrow A = \arccos(V_{11}) \frac{180}{\pi} \quad (\text{K.15})$$

- Second quadrant:

$$\left. \begin{array}{l} \cos(A) < 0 \\ \sin(A) \geq 0 \end{array} \right\} \Rightarrow \left. \begin{array}{l} V_{11} < 0 \\ V_{21} \geq 0 \end{array} \right\} \Rightarrow A = \arccos(V_{11}) \frac{180}{\pi} \quad (\text{K.16})$$

- Third quadrant:

$$\left. \begin{array}{l} \cos(A) < 0 \\ \sin(A) < 0 \end{array} \right\} \Rightarrow \left. \begin{array}{l} V_{11} < 0 \\ V_{21} < 0 \end{array} \right\} \Rightarrow A = 360^\circ - \arccos(V_{11}) \frac{180}{\pi} \quad (\text{K.17})$$

- Fourth quadrant:

$$\left. \begin{array}{l} \cos(A) \geq 0 \\ \sin(A) < 0 \end{array} \right\} \Rightarrow \left. \begin{array}{l} V_{11} \geq 0 \\ V_{21} < 0 \end{array} \right\} \Rightarrow A = 360^\circ - \arccos(V_{11}) \frac{180}{\pi} \quad (\text{K.18})$$

Appendix L

Determining Open Loop Uncertainty Ellipses

The open loop Nyquist $G(e^{j\omega T_s})K(e^{j\omega T_s})$ with estimated error bounds can be quite useful in assessing the robustness of the closed loop system. Clearly, provided the plant is stable, a necessary and sufficient condition for closed loop stability is that none of the open loop uncertainty ellipses include the Nyquist point $(-1, 0)$. In this appendix we will show how the form matrices for the open loop uncertainty ellipses are determined from the plant uncertainty ellipses and the controller.

Clearly the open loop uncertainty ellipse at frequency ω is centered at the nominal open loop Nyquist $G(e^{j\omega T_s})K(e^{j\omega T_s})$. The ellipse is amplified by $|K(e^{j\omega T_s})|$ and rotated $\angle(K(e^{j\omega T_s}))$ degrees in comparison with the plant uncertainty ellipse at that frequency. We wish to determine the transformation matrix R which must be multiplied onto the form matrix $P_{\tilde{g}}$ for the plant uncertainty ellipse to obtain the form matrix for the open loop ellipse P_{ol} . Let the plant uncertainty ellipse at frequency ω be given by

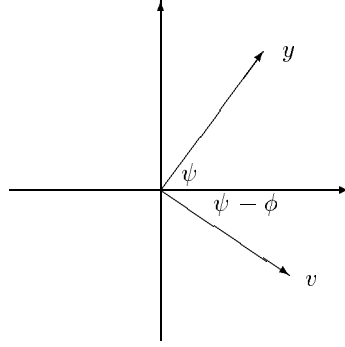
$$z = x^T P_{\tilde{g}}^{-1} x \quad (\text{L.1})$$

Then let us start by considering the two vectors y and v given in Figure L.1 on the following page.

Let $|y| = |v|$ and let y and v be given by

$$y = \begin{bmatrix} y_1 \\ y_2 \end{bmatrix} = \begin{bmatrix} |y| \cos(\psi) \\ |y| \sin(\psi) \end{bmatrix} \quad (\text{L.2})$$

$$v = \begin{bmatrix} v_1 \\ v_2 \end{bmatrix} = \begin{bmatrix} |v| \cos(\psi - \phi) \\ |v| \sin(\psi - \phi) \end{bmatrix} \quad (\text{L.3})$$

Figure L.1: Rotating the vector y ϕ degrees.

Thus v is the vector y rotated ϕ deg. Let us determine the transformation matrix R which performs this rotation. Thus:

$$v = Ry \quad (\text{L.4})$$

$$\Rightarrow \begin{bmatrix} |v| \cos(\psi - \phi) \\ |v| \sin(\psi - \phi) \end{bmatrix} = R \begin{bmatrix} |y| \cos(\psi) \\ |y| \sin(\psi) \end{bmatrix} \quad (\text{L.5})$$

$$\Rightarrow \begin{bmatrix} \cos(\psi - \phi) \\ \sin(\psi - \phi) \end{bmatrix} = \begin{bmatrix} R_{11} & R_{12} \\ R_{21} & R_{22} \end{bmatrix} \begin{bmatrix} \cos(\psi) \\ \sin(\psi) \end{bmatrix} \quad (\text{L.6})$$

$$\Rightarrow \begin{cases} \cos(\psi - \phi) = R_{11} \cos(\psi) + R_{12} \sin(\psi) \\ \sin(\psi - \phi) = R_{21} \cos(\psi) + R_{22} \sin(\psi) \end{cases} \quad (\text{L.7})$$

The equations (L.7) are fulfilled for the transformation matrix R given by

$$R = \begin{bmatrix} \cos(-\phi) & -\sin(-\phi) \\ \sin(-\phi) & \cos(-\phi) \end{bmatrix} \quad (\text{L.8})$$

Note that ϕ in Figure L.1 was a negative rotation. If we use standard sign convention for ϕ , the transformation matrix R becomes

$$R = \begin{bmatrix} \cos(\phi) & -\sin(\phi) \\ \sin(\phi) & \cos(\phi) \end{bmatrix} \quad (\text{L.9})$$

If $|v| = k|y|$, the result is

$$v = kRy \quad (\text{L.10})$$

with R given by (L.8).

Then let us consider the ellipse equation for $z = 1$:

$$x^T P_{\tilde{g}}^{-1} x = 1 \quad (\text{L.11})$$

$$\Rightarrow x^T V D V^{-1} x = 1 \quad (\text{L.12})$$

$$\Rightarrow x^T V D^{\frac{1}{2}} D^{\frac{1}{2}} V^{-1} x = 1 \quad (\text{L.13})$$

$$\Rightarrow \bar{z}^T \bar{z} = 1 \quad (\text{L.14})$$

Here $P_{\tilde{g}} = V D V^{-1}$ is the eigenvalue decomposition of the form matrix and \bar{z} is obviously given by $\bar{z} = D^{\frac{1}{2}} V^{-1} x$. (L.14) is the equation for a circle. Consequently, a point \bar{z}' on a circle can be transformed to a point x' on the ellipse with form matrix $P_{\tilde{g}} = V D V^{-1}$ via

$$x' = \left(D^{\frac{1}{2}} V^{-1} \right)^{-1} \bar{z}' = V D^{-\frac{1}{2}} \bar{z}' \quad (\text{L.15})$$

Then a point y' on the open loop ellipse amplified by k and rotated by ϕ is given by the transformation (L.10) on the facing page:

$$y' = k R x' = k R V D^{-\frac{1}{2}} \bar{z}' \quad (\text{L.16})$$

$$\Rightarrow \bar{z}' = \left(k R V D^{-\frac{1}{2}} \right)^{-1} y' = \frac{1}{k} D^{\frac{1}{2}} V^{-1} R^{-1} y' \quad (\text{L.17})$$

and

$$\bar{z}^T \bar{z} = 1 \quad (\text{L.18})$$

$$\Rightarrow \frac{1}{k^2} y^T \left(D^{\frac{1}{2}} V^{-1} R^{-1} \right)^T \left(D^{\frac{1}{2}} V^{-1} R^{-1} \right) y = 1 \quad (\text{L.19})$$

$$\Rightarrow \frac{1}{k^2} y^T R^{-T} V D^{\frac{1}{2}} D^{\frac{1}{2}} V^{-1} R^{-1} y = 1 \quad (\text{L.20})$$

$$\Rightarrow \frac{1}{k^2} y^T R^{-T} P_{\tilde{g}}^{-1} R^{-1} y = 1 \quad (\text{L.21})$$

$$\Rightarrow y^T P_{ol}^{-1} y = 1 \quad (\text{L.22})$$

where P_{ol} is given by

$$P_{ol} = k^2 R P_{\tilde{g}} R^T \quad (\text{L.23})$$

which is the desired transformation for $k = |K(e^{j\omega T_s})|$ and $\phi = \angle(K(e^{j\omega T_s}))$.

